UNIVERSITY OF OKLAHOMA

GRADUATE COLLEGE

MODELING AND FORMULATION OF MICROEMULSIONS: THE NET-AVERAGE CURVATURE MODEL AND THE COMBINED LINKER EFFECT

A Dissertation

SUBMITTED TO THE GRADUATE FACULTY

In partial fulfillment of the requirements for the

degree of

Doctor of Philosophy

By

Edgar Acosta
Norman, Oklahoma
2004

Downloaded from SHAREOK. Persistent Handle URL: https://hdl.handle.net/11244/695

UMI Number: 3120034

INFORMATION TO USERS

The quality of this reproduction is dependent upon the quality of the copy submitted. Broken or indistinct print, colored or poor quality illustrations and photographs, print bleed-through, substandard margins, and improper alignment can adversely affect reproduction.

In the unlikely event that the author did not send a complete manuscript and there are missing pages, these will be noted. Also, if unauthorized copyright material had to be removed, a note will indicate the deletion.

UMI®

UMI Microform 3120034

Copyright 2004 by ProQuest Information and Learning Company.

All rights reserved. This microform edition is protected against unauthorized copying under Title 17, United States Code.

ProQuest Information and Learning Company
300 North Zeeb Road
P.O. Box 1346
Ann Arbor, MI 48106-1346

©Copyright by Edgar Acosta 2004
All Rights Reserved.

MODELING AND FORMULATION OF MICROEMULSIONS: THE NET-AVERAGE CURVATURE MODEL AND THE COMBINED LINKER EFFECT

A Dissertation

APROVED FOR THE

SCHOOL OF CHEMICAL ENGINEERING AND

MATERIALS SCIENCE

BY

Prof. Jeffrey H. Harwell.

Prof. David A. Sabatini

Prof. John F. Scamehorn

Prof. Tohren C. Kibbey

Prof. Hirotaka Uchiyama

DEDICATION

This dissertation is dedicated to my daughter Michelle, my wife Yasmin, my parents Edgar Nicolas and Virginia, my brother Jose and my sisters Ana and Luslene.

ACKNOWLEDGMENTS

I would like to express my gratitude to my advisor Dr. Jeffrey Harwell for his advice, support, and encouragement. His vision of the important issues and opportunities in colloid science and technology has served as a north for the research efforts presented in this work. I am also in great debt to my coadvisor Dr. David Sabatini, who has become a mentor and an example for my academic and personal life. His support has allowed me to explore new areas and techniques such as low-toxicity microemulsion systems and neutron scattering techniques. Thanks to the support of both Drs. Sabatini and Harwell I have been able to present this work in numerous conferences in the United States and abroad. I am also grateful to Dr. John Scamehorn for his advice and teachings on colloid science and the world of industrial applications of surfactant science. My appreciation also to Drs. Hirotaka Uchiyama and Tohren Kibbey for their participation as committee members and their valuable comments. I am thankful to Dr. Brian Grady for his advice and help in carrying out the neutron scattering experiments and Dr. Jeffrey Childs for his guidance and friendship during my first years of my doctoral studies.

I want to express my appreciation to the Institute for Applied Surfactant Research (IASR), the U. S. Environmental Protection Agency (USEPA), and the Integrated Petroleum Environmental Consortium (IPEC) for contributing to the economical support of this work and to the National Institute of Standards and Technology (NIST) center for neutron research for facilitating the neutron scattering experiments.

My appreciation also to my colleagues Mrs. Erika Szekeres, Mrs. Melissa Le, Mrs. Do Phuong Mai, Mrs. Thu Nguyen, Mr. Marshall McDaniel, Mr. Daniel Gallo, Mr.

Doan Tuan, Mr. Anand Upadhyaya, Mrs. Aranya Fungawadsdi, Dr. Chantra Tocompou, Dr. Napaporn Komesvarakul whose help and encouragement have been essential to this work.

I want to acknowledge the assistance of the staff of both Civil Engineering and Enviromental Science department and the Chemical Engineering and Materials Science department with all administrative matters of this work.

Thanks to my wife Yasmin and daughter Michelle for their support, understanding, patience, love and for giving me a home in a foreign land that has become a second home country for us.

Thanks to God for leading me into a path where I have found all these wonderful people, for the health and wisdom to make the right choices, and the opportunities that He has put in my path.

TABLE OF CONTENTS.

Page

ACKNOWLEDGMENTS iv

TABLE OF CONTENTS vii

LIST OF TABLES ix

LIST OF FIGURES xi

PREFACE xvii

CHAPTER 1. Overview 1
References 7

CHAPTER 2. A Net-Average Curvature Model for Solubilization and Supersolubilization in Surfactant Microemulsions 9
Abstract 9
Introduction 10
Model Basis 11
Experimental Procedures 16
Results and Discussion 19
Net-average curvature model 28
Net-average curvature model: solubilization curves 34
Net-average curvature model: phase volumes 36
Net-average curvature model: microemulsion droplet size 38
Net-average curvature model: interfacial tension 42
Conclusions 47
References 48

CHAPTER 3. Net-average curvature model of microemulsions: predictions and measurements using small angle neutron scattering, dynamic light scattering and NMR techniques 54
Abstract 54
Introduction 56
Experimental section 63
Results and Discussion 68
Conclusions 93
References 95

CHAPTER 4. Coalescence and Solubilization Kinetics in Linker-Modified Microemulsions and Related Systems 100
Abstract 100
Introduction 101
Experimental section 108
Results and Discussion 111
Conclusions 132
References 133

CHAPTER 5. Linker-Modified Microemulsions for a Variety of Oils and Surfactants 138
Abstract 138
Introduction 139
Experimental procedures 146
Results and Discussion 150
Literature 171

CHAPTER 6. Self-Assembly in Linker-Modified Microemulsions 175
Abstract 175
Introduction 176
Materials and Methods 180
Results and Discussion 183
Summary 213
Literature 215

CHAPTER 7. Linker-based Non-toxic Microemulsions 219
Abstract 219
Introduction 220
Experimental Procedures 228
Results and Discussion 230
Conclusions 254
Literature 255

CHAPTER 8. Conclusions 263

APPENDIX 1. Modeling Microemulsion Solubilization and Interfacial Tension: The Net-average Curvature Model 268

APPENDIX 2. Turbidity curves used to determine the kinetics of coalescence in linker microemulsions (Chapter 4) 283

APPENDIX 3. Small Angle Neutron Scattering Studies of Linker-Modified Toluene Microemulsions 293

LIST OF TABLES

Table 2.1. Selected properties and molecular structure of oils studied..... 17

Table 2.2. Chemical structure and area per molecule of surfactant studied..... 18

Table 2.3. Optimum salinity and characteristic length at optimum formulation for selected series..... 25

Table 2.4. Length parameter "L" used in the net-average curvature model for different microemulsion systems. using the Huh equation 42

Table 3.1. Microemulsion composition for the system hydrogenated water - sodium dihexyl sulfosuccinate (SDHS) - toluene and sodium chloride as electrolyte..... 64

Table 3.2. Contrast match series used in SANS studies..... 66

Table 3.3 Microemulsion composition for water - sodium dodecyl sulfate - butanol - toluene systems with sodium chloride as electrolyte..... 67

Table 3.4. Small angle neutron scattering (SANS) morphology parameters for SDHS - toluene microemulsions 72

Table 4.1. Optimum formulation of Type III formulations and electrical conductivity of corresponding bicontinuous middle phase microemulsion and excess aqueous phase..... 112

Table 4.2. Optimum middle phase (Type III) viscosity, concentrations of SMDNS and dodecanol, and percentage of SMDNS in the middle phase microemulsion..... 120

Table 5.1a. Properties of the oils formulated in microemulsions..... 147

Table 5.1b. Properties of the amphiphilic molecules..... 147

Table 5.2. Properties of optimum middle phase microemulsions - formulation..... 152

Table 5.3. Properties of optimum middle phase microemulsions - characteristic length, interfacial rigidity, viscosity and partition of linkers..... 159

Table 6.1a. Properties of the oils formulated in microemulsions..... 180

Table 6.1b. Properties of the amphiphilic molecules..... 181

Table 6.2. Interfacial concentrations of surfactant and linkers for selected systems in Figures 6.10 through 6.13..... 203

Table 7.1. Selected properties for lecithin (surfactant), sorbitan monoleate (lipophilic linker) and hexyl polyglucoside (hydrophilic linker)..... 226

Table 7.2. Selected properties of the oils used in this study..... 226

Table 7.3. Characterization of hexyl polyglucoside as a hydrophilic linker using SDHS (0.10M) as surfactant..... 232

LIST OF FIGURES

Figure 1.1 Number of publications per year containing the keyword "microemulsion"..... 1

Figure 1.2. Number of publications using microemulsions in selected applications..... 2

Figure 2.1: Oil droplet suspended in water..... 12

Figure 2.2a. Curvature model in trichloroethylene microemulsions..... 22

Figure 2.2b. Curvature model in limonene microemulsions..... 24

Figure 2.2c. Curvature model in styrene microemulsions..... 26

Figure 2.3. Curvature models in trichloroethylene microemulsions..... 33

Figure 2.4. Solubilization diagram for SDS- pentanol – hexane microemulsions. 35

Figure 2.5. Volume fraction diagram for TCE-enriched mixture of chlorinated solvents microemulsion with sodium dihexyl sulfosuccinate and 2-propanol..... 37

Figure 2.6a. Droplet size of paraffin – aromatic oil with nonyl orthoxylene sulfonate microemulsions..... 39

Figure 2.6b. Droplet size of paraffin – aromatic oil with dodecyl orthoxylene sulfonate microemulsions..... 40

Figure 2.7. Interfacial tension of paraffin – aromatic oil / dodecyl orthoxylene sulfonate microemulsions at 23°C..... 44

Figure 2.8. Interfacial tension of trichloroethylene / sodium dihexyl sulfosuccinate microemulsions at 27°C..... 45

Figure 3.1. Equivalent spherical droplet radius based on solubilization data and the corresponding net-average curvature model fit. Part A corresponds to the sodium dihexyl sulfosuccinate (SDHS) - toluene system. Part B corresponds to SDS-butanol-toluene data from Guering and Lindman..... 70

Figure 3.2. Scattering curves for the SDHS-toluene microemulsion systems with oil/water contrast. Part A corresponds to Type I systems, part B to bicontinuous Type III systems and part C to Type II microemulsion systems. The solid lines represent the scattering model fit described in Table 3.4. The shaded areas in the schematic represent the deutrated phase..... 73

Figure 3.3. Scattering curves for the SDHS-toluene microemulsion systems with film contrast. Part A corresponds to Type I systems, part B to bicontinuous Type III systems and part C to Type II microemulsion systems. The solid lines represent the scattering model fit described in Table 3.4. The shaded areas in the schematic represent the deutrated phase..... 79

Figure 3.4. Equivalent spherical radius for SDHS-toluene microemulsion systems as calculated from the morphologies obtained from the SANS studies, the solubilization studies and the predicted from the net-average curvature model..... 83

Figure 3.5. Porod plot for oil/water contrast experiments for Type I microemulsion formulated with 4% aqueous concentration of SDHS..... 85

Figure 3.6. Modification of the net-average curvature model to account for changes in area per molecule of the surfactant. Part A indicates the area per molecule as a function of electrolyte concentration. Part B presents the projected area per molecule of the surfactant a_S for different curvatures. Part C presents the modified radii predicted by the net-average curvature model after modifying for surfactant area per molecule..... 88

Figure 3.7. Comparison of the radius of gyration of Type I and II microemulsions determined by dynamic light scattering (DLS) with the equivalent spherical radius determined from SANS data and the net-average curvature model..... 90

Figure 3.8. Relative self-diffusion coefficients (D/Do) for toluene and water for the toluene - SDS - butanol systems. Data points from Lindman et al. Lines were estimated by combining the net-average curvature model and Equations 9 and 10..... 92

Figure 4.1a. Solubilization mechanism based on oil exchange between droplets and micelles after a soft collision..... 104

Figure 4.1b. Solubilization mechanism based on surfactant adsorption/liquid crystal formation followed by oil uptake and collective desorption of surfactant and oil..... 104

Figure 4.1c. Solubilization mechanism based on molecules of oil dissolved in water before being dissolved in micelles..... 105

Figure 4.2. Schematic of the turbidity meter designed to study the kinetics of coalescence of macroemulsion and solubilization of microemulsions. Test tubes illustrate the relationship between the equilibrium middle phase microemulsion, the corresponding macroemulsion produced upon shaking and the intermediate states that occur in between..... 110

Figure 4.3. Phase diagram of TCE-SDHS microemulsions with and without lipophilic linker (0.09M dodecanol) or hydrophilic linker (0.09M SMDNS). The centerline of each system corresponds to the optimum middle phase microemulsion (equal volumes of oil and water in the middle phase) for a given scan @ 27°C..... 113

Figure 4.4a. Turbidity curves during coalescence of macroemulsions made from optimum middle phase TCE microemulsions, and excess TCE and aqueous phase with different linker combinations @ 27 °C, [SDHS] = 0.103 M..... 115

Figure 4.4b. Inverse turbidity curves during coalescence of macroemulsions made from optimum middle phase TCE microemulsions and excess TCE and aqueous phases at different linker combinations @ 27 °C, [SDHS] = 0.103 M..... 115

Figure 4.5. Coalescence kinetic constant (k_c) for macroemulsions made from optimum middle phase microemulsions and excess TCE and aqueous phases at different linker concentrations @ 27 °C, [SDHS] = 0.103 M..... 119

Figure 4.6. Microscopic lattice model of an optimum bicontinuos microemulsion showing the surfactant dynamic membrane and the characteristic length (ξ)..... 123

Figure 4.7. Characteristic length (ξ) of optimum middle phase TCE microemulsions at different linker concentrations @ 27 °C, [SDHS] = 0.103 M..... 125

Figure 4.8. Interfacial tension of optimum middle phase TCE microemulsions at different linker concentrations @ 27 °C, [SDHS] = 0.103 M..... 126

Figure 4.9. Interfacial rigidity (E_r) of optimum middle phase TCE microemulsions at different linker concentrations @ 27 °C, [SDHS] = 0.103 M..... 127

Figure 4.10. Correlation between characteristic length (ξ) and interfacial rigidity (E_r). White line represents the DeGennes correlation using α=35Å..... 129

Figure 4.11. Correlation between coalescence constant (kc) and interfacial rigidity (Er)..... 130

Figure 4.12. Turbidity curves during solubilization of 250 μl of TCE injected into 5ml of SDHS solution to form a type I microemulsion @ 27 °C, [SDHS] = 0.103 M..... 131

Figure 5.1. Phase behavior of microemulsions with SDHS and tetrachloroethylene showing Winsor phases (Type I-III-II) and corresponding interfacial tension and solubilization..... 140

Figure 5.2. Schematic of the linker effect, showing the surfactant, lipophilic, and hydrophilic linker at the oil/water interface..... 142

Figure 5.3. Interfacial tension and characteristic length of the microemulsions as a function of EACN and surfactant series..... 154

Figure 5.4. Interfacial rigidity (Er) and SMDNS/oleyl mole ratio in middle phase as a function of oil EACN and surfactant series..... 156

Figure 5.5. Turbidity versus time for coalescence of middle phase for SDHS microemulsion with different oils..... 158

Figure 5.6. Partition of linkers into the middle phase as a function of oil EACN (see equations 5 & 6 for definitions)..... 158

Figure 5.7. Turbidity versus time for coalescence of middle phase for AOT microemulsion with different oils..... 164

Figure 5.8a. Hexadecane column study with AOT + linker formulation..... 167

Figure 5.8b. Motor oil column study with AOT + linker formulation..... 167

Figure 5.9a. Detergency performance of linker formulation for hexadecane on cotton: detergent alone, detergent plus commercial pretreatment, detergent plus linker formulation..... 170

Figure 5.9b. Detergency performance of linker formulation for motor oil on cotton: detergent alone, detergent plus commercial pretreatment, detergent plus linker formulation..... 170

Figure 6.1. Schematic of the linker effect. The lipophilic linker and the hydrophilic linker self-assemble to act as a surfactant at the interface..... 177

Figure 6.2. "Fish" phase diagrams for (A) SDHS-TCE microemulsion, (B) SDHS-PCE microemulsions. The roman numerals indicate the different types of microemulsion systems. The solid lines represent the phase transitions and the dotted lines indicate the optimum middle phase microemulsion..... 185

Figure 6.3. Optimum electrolyte concentration for SDHS-alone microemulsions with TCE and PCE..... 188

Figure 6.4. Interfacial tension versus SDHS concentration at constant NaCl concentration (TCE-1.35%NaCl and PCE-5.0%NaCl). Black circles correspond to the interfacial tension of the SDHS solution and PCE. Black diamonds correspond to the SDHS-TCE system..... 188

Figure 6.5. "Fish" phase diagrams for (A) SDHS-TCE microemulsion, and (B) SDHS-PCE microemulsions. All systems contained 0.09M of SMDNS and 0.09M of dodecanol. The solid lines represent the phase transitions and the dotted line indicate the optimum middle phase microemulsion..... 192

Figure 6.6 Optimum electrolyte concentration for SDHS microemulsions formulated with 0.09M SMDNS and 0.09M dodecanol; and with TCE and PCE as oil phases..... 194

Figure 6.7. Interfacial tension and composition of SDHS microemulsions of PCE and TCE at 0.09M of SMDNS and 0.09M of dodecanol. Part (A) Interfacial tension between the excess oil and water phases as a function of SDHS concentration at optimum formulation. Part (B) SDHS aqueous concentration at optimum formulation, the dotted line indicates the initial aqueous concentration of SDHS..... 196

Figure 6.8. Percentage of SMDNS adsorption and dodecanol segregation expressed as thickness of dodecanol-rich palisade layer for the SDHS-linker optimum formulation (dotted line) systems presented in Figures 6.5a (TCE) and 6.5b (PCE)..... 200

Figure 6.9. Characteristic length of SDHS optimum middle phase microemulsions for TCE and PCE with and without linkers (0.09 M SMDNS and 0.09 M dodecanol)..... 201

Figure 6.10. Dodecanol segregation expressed as molecules segregates per nm^2 of interfacial area as a function of the concentration of dodecanol in the bulk excess oil phase for TCE (part A) and PCE (part B) at different initial concentration of SMDNS and 0.103 M (4 g/100ml) of SDHS..... 205

Figure 6.11. SMDNS percentage middle phase adsorption as a function of the concentration of dodecanol in the bulk excess oil phase for TCE (part A) and PCE (part B) at different initial concentration of SMDNS and 0.103 M (4 g/100ml) of SDHS... 207

Figure 6.12. Relative increase in characteristic length of microemulsion systems (ξ) with the segregation of dodecanol for TCE (triangles) and PCE (circles)..... 208

Figure 6.13. Dodecanol segregation for TCE (triangles) and PCE (circles) with 0.104M SDHS and 0.09M of each SMDNS and dodecanol as a function of relative electrolyte concentration..... 209

Figure 6.14. "Fish" phase diagrams for SDHS-alone TCE microemulsion (thick lines), and a mixture of constant ratio of 10 molar parts of SDHS to 9 SMDNS to 9 dodecanol (C12OH) (thin lines)..... 211

Figure 6.15. Interfacial tension SDHS microemulsions of TCE without linkers (solid dots) and with linkers at constant molar ratio SDHS(10)/SMDNS(9)/C12OH(9) (open dots) as a function of SDHS concentration..... 213

Figure 7.1. Schematic of the linker effect using non-toxic surfactant lecithin, exemplified by phosphatiyl choline dialkyl. Hexyl polyglucoside is shown as hydrophilic linker and sorbitol monoleate as lipophilic linker..... 225

Figure 7.2. Interfacial tension of isopropyl myristate/ hexyl polyglucoside solutions as a function of hexyl polyglucoside concentration at 300K and 0.9 g NaCl/100 ml. 233

Figure 7.3. Phase behavior study of linker-based isopropyl myristate microemulsion formulated with 4% w/v Lecithin, 4% w/v sorbitol monoleate, 0.9%w/v NaCl. Oil to aqueous solution volume ratio =1/1..... 235

Figure 7.4. Phase map for IPM microemulsions prepared with sorbitol monoleate to lectihin weight ratio = 1/1 at 300K and 0.9 % w/v NaCl. 236

Figure 7.5. Characterization of isopropyl myristate microemulsion prepared with 4% lecithin, 4% sorbitol monoleate, 0.9% w/v NaCl 239

Figure 7.6. Interfacial tension of IPM microemulsion formulated with 4% lectihin, 4% sorbitol monoleate and varying concentration of hexyl polyglucoside. 240

Figure 7.7. Phase maps for IPM microemulsions prepared with sorbitol monoleate to lectihin weight ratio = 1/1 at different temperatures (10°C, 27°C, 40°C) and 0.9 % w/v NaCl. 242

Figure 7.8. Phase maps for IPM microemulsions prepared with sorbitol monoleate to lectihin weight ratio = 1/1 at 300K and at two levels of electrolyte: 0.9 % and 4% w/v NaCl. 242

Figure 7.9. Phase maps for IPM microemulsions prepared with sorbitol monoleate to lectihin weight ratio = 1/1 at 300K, at 0.9 % w/v NaCl and at three different levels of pH (3.5, 6.5 and 10.7). 244

Figure 7.10. Phase maps for IPM microemulsions prepared with two different ratios of sorbitol monoleate (Span 80) to lectihin weight ratio (1/1 and 2/1) at 300K, at 0.9 % w/v NaCl..... 245

Figure 7.11. Formulation of linker lecithin microemulsion with a wide variety of oils, indicating the hexyl polyglucoside (AG-6) to lectihin ratio to achieve a single phase microemulsion and the minimum amount of lecithin required to form a single phase microemulsion..... 247

Figure 7.12. Properties of linker lecithin microemulsion with a wide variety of oils, indicating the characteristic length and interfacial tension of the microemulsions whose formulation is described in Figure 7.11..... 250

PREFACE

Microemulsions are phases that contain both oil and water which coextist in thermodynamic equilibrium due to the presence of surfactant films that segregate at the oil - water interface. These systems can be used in numerous applications, including enhanced oil recovery, remediation of oil-impacted aquifers, nanoparticle synthesis, drug and cosmetic delivery and cleaning systems. The thermodynamic properties of microemulsions are dictated by the properties of the surfactant membrane such as curvature, characteristic length and rigidity. The goal of this work was to understand the role of surfactant, linker molecules and formulation conditions (e.g. electrolyte concentration, temperature, additive to surfactant ratios, etc.) on the curvature, characteristic length and rigidity of surfactant membranes in microemulsions. Chapters 2 and 3 describe a critical scaling model of surfactant membrane curvature called the net-average curvature that was able to reproduce the phase behavior of surfactant systems, including solubilization, droplet size, phase transitions, phase volumes and interfacial tensions. Three important parameters are essential to this model: the extended length of the surfactant tail, the characteristic length, and the interfacial rigidity. Chapter 4 studies the effect of adding hydrophilic and lipophilic linkers on the characteristic length of microemulsion systems, and how the interfacial rigidity influences the dynamic behavior of microemulsions. Chapter 5 extends the concept of linker formulations for a wide variety of oils and studies the performance of these systems in oil removal from porous media and from textiles. Chapter 6 attempts to elucidate how hydrophilic and lipophilic linkers self-assemble at the surfactant membrane. Chapter 7 studies how to use linker

molecules to formulate non-toxic microemulsion systems. Chapter 8 provides a summary of the results and conclusions obtained in this research.

CHAPTER I

Overview

Microemulsions are optically isotropic phases containing oil and water domains in thermodynamic equilibrium due to the presence of a surfactant membrane present at the oil/water interface. The discovery of these systems dates back to 1943 with the initial observations of Schulman who produced microemulsion phases upon addition of medium chain alcohols to soap emulsions (1). A more detailed historical overview of microemulsions is available elsewhere (2).

It is interesting to note that searching the database SciFinder® with "microemulsion" as a keyword retrieved over 10 thousand references. To put this number in perspective, using the keyword "carbon nanotube" retrieved just below 10 thousand references. It is thus clear that microemulsions are of great interest. Figure 1.1 presents the number of publications on the topic of microemulsions for each year between 1943 to 2003, where is clear that the level of interest in microemulsions continues to grow.

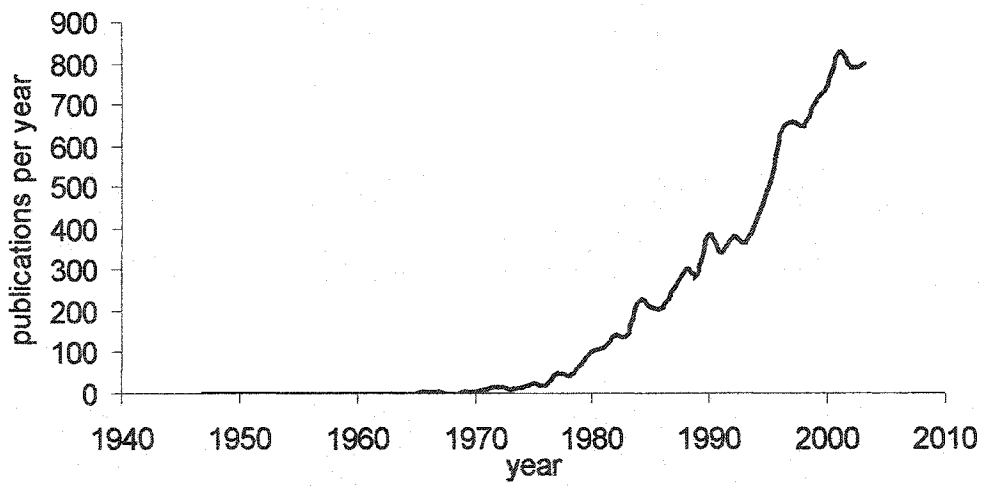

Figure 1.1 Number of publications per year containing the keyword "microemulsion"

While the SciFinder® database does not have a complete account for articles before 1960, it is clear from Figure 1.1 that during the latter part of the 1970s, microemulsions became an important subject of research, especially due to the interest in using these systems to promote the displacement of crude oil from reservoirs as a tertiary oil recovery method. While this particular application of microemulsions has yet to be economically viable and widely implemented, the initial research and characterization of these systems during the late 1970s and 1980s gave way to the use of microemulsions in a number of other applications. Figure 1.2 illustrates the different applications of microemulsions in terms of the number of publications in each microemulsion-related application between 1943 and 2003.

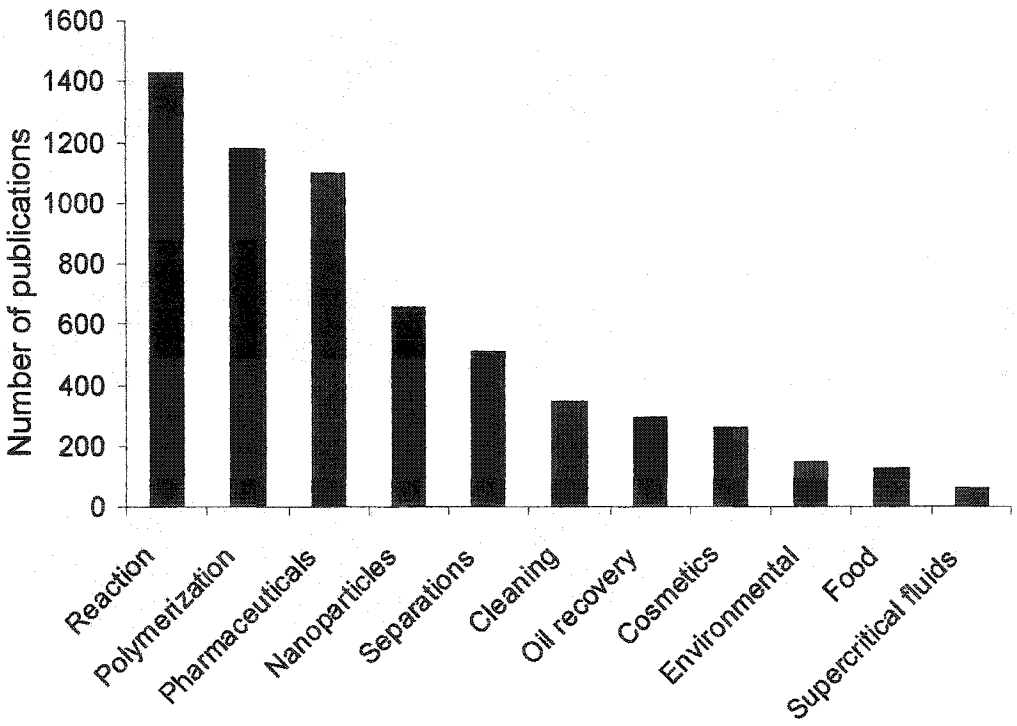

Figure 1.2. Number of publications using microemulsions in selected applications.

Most of the applications in Figure 1.2 take advantage of the nanoscale size of the oil and/or water domain in microemulsions either as a reaction medium, including polymerization, to aiding in the transport of pharmaceuticals through biological membranes, and producing nanoparticles, etc. In addition to the nanoscale size of microemulsions, another important property is the ability of surfactants to reduce the interfacial tension between the microemulsion phase and excess water and/or excess oil phases. Such low interfacial tension allows the displacement of oil trapped in porous media, which is essential in enhanced oil recovery, cleaning formulations and environmental remediation applications.

The advance of microemulsion technologies has been hindered in great part by two factors, the difficulty of formulating microemulsions and the lack of a unified model to predict the thermodynamic equilibrium of microemulsion systems. While a unified theory or model microemulsion of thermodynamics does not yet exist, it has been somewhat agreed that the equilibrium of microemulsions is dictated by the properties of the surfactant membrane that stabilizes the oil and water domains (3,4,5).

As will be discussed later in this work, surfactant membrane properties depend on the relative interactions between the surfactant molecules with several components: themselves, oil and water molecules, and the cosurfactants and additives present in the formulation. In previous research, we have introduced the use of combined hydrophilic and lipophilic linker molecules to formulate microemulsions with chlorinated hydrocarbons (6,7,8). These molecules can enhance the molecular interaction between the surfactant and oil (lipophilic linker) and surfactant and water (hydrophilic linker),

thus modifying important membrane properties that improvemed the solubilization capacity of these formulations and, in some cases, produced shorter equilibration times while avoiding the use of medium chain alcohols to obtain clear isotropic microemulsion phases. In addition to these exceptional properties, the co-addition of both lipophilic and hydrophilic linkers was able to act as pseudo-surfactant that could replace a fraction of the original surfactant and still retain the same level of solubilization in the system.

These earlier results demanded additional studies to understand how these linker molecules affected the surfactant membrane properties, such as curvature, thickness, rigidity. This work aims to understand the role of surfactant, linker molecules and formulation conditions (e.g. electrolyte concentration, temperature, additive to surfactant ratios, etc.) on surfactant membranes properties.

This dissertation is organized in two main blocks, (i) modeling of microemulsion phase behavior and (ii)microemulsion formulation with linker molecules. Chapters 2 and 3 focus on microemulsion modeling. Chapter 2 introduces the net-average curvature model of microemulsions as a critical scaling model that relates the net curvature of the surfactant membrane as an expression of the surfactant affinity (or chemical potential) difference (SAD) of being dissolved in water and in oil phase. In this approach the critical point is assumed to be the point of net-zero curvature or optimum formulation. The main parameters that rule the phase behavior of microemulsions are the distance (expressed in SAD terms) to the critical point, the characteristic length of the microemulsion system at critical point, the extended length of the surfactant and the interfacial rigidity of the surfactant membrane. This contribution has appeared in

Langmuir (9). Chapter 2 reports on the use of the net-average curvature model to reproduce bulk properties of microemulsions such as composition, phase volumes, phase transitions and interfacial tensions, in Chapter 3 the model is tested against the morphology of microemulsion aggregates investigated using small angle neutron scattering (SANS) along with dynamic light scattering and pulse-gradient NMR technique. In addition to these contributions Appendix 1 shows how to use the net-average curvature model to reproduce the phase behavior of non-ionic surfactant microemulsions, which has been published in the proceedings of topical conferences of the AIChE 2002 national meeting.

Chapter 4 describes the impact of hydrophilic and lipophilic linkers on the characteristic length and the interfacial rigidity of microemulsion systems. In addition this chapter describes the role of the interfacial rigidity in determining the dynamic aspects of microemulsions. In short, the addition of hydrophilic linkers reduces the characteristic length of microemulsion systems, and reduces the interfacial rigidity, which in turn reduces the activation energy and thus accelerates the dynamics of microemulsion systems. This contribution has appeared in Langmuir (10).

Chapter 5 extends the concept of linker formulations for a wide variety of oils, showing that the use of combined linkers can produce microemulsion systems that would otherwise not be possible to obtain using combinations of simple surfactants and medium chain alchols. Successful formulations with oils as hydrophobic as motor oil are shown and employed to study the performance of these systems in oil removal from porous

media and textiles. This contribution has appeared in the Journal of Surfactant and Detergents (11).

Chapter 6 attempts to elucidate how hydrophilic and lipophilic linker molecules segregate at the surfactant membrane. A series of microemulsion phase maps and interfacial tension studies are presented with the objective of investigating how the self-assembly of hydrophilic and lipophilic linkers occurs. While a molecular mechanism for this interaction could not be drawn from the data, the self-assembly of these linker molecules requires the presence of a minimum surfactant concentration necessary to produce middle phase microemulsions using linker molecules. This contribution has been accepted to the Journal of Colloids and Interface Science.

Chapter 7 builds on the finding of Chapter 5 by extending the combined linker approach to the formulation of non-toxic microemulsions using lecithin as the surfactant, and non-toxic, biocompatible linkers. The objective of this work is to produce formulations that can be used in pharmaceutical and cosmetic formulations, as well as environmentally friendly cleaning products.

Finally, Chapter 8 presents some concluding remarks and an outlook on the potential impact of the findings of this work.

Appendix 2 compiles the coalescence curves of emulsions that form after shaking middle phase microemulsions formulated with a variety of linker formulations. The coalescence kinetics constants are reported in chapter 4. Appendix 3 summarizes the small angle neutron scattering studies of linker-based microemulsions and comments regarding how the SANS morphology supports the earlier findings of Chapter 4. Finally,

the latter references in this section record related work in which the author was involved that do not appear as a part of this dissertation (12,13,14,15,16,17)

References.

[1] Hoar, T. P.; Schulman, J. H. Transparent water-in-oil dispersions: the oleopathic hydro-micelle. *Nature.* **1943**, 152 , 102-3.

[2] Lindman, B. ; Friberg. S. E. *In Handbook of Microemulsion Science and Technology.* Kumar, P., Mittal, K.L. Marcel Dekker, New York, 1999. p 1-12

[3] Promod Kumar and K.L. Mittal, Editors. *Handbook of Microemulsion Science and Technology*. Marcel Dekker, Inc., New York, 1999

[4] Gelbart, W. M., Ben-Shaul, A. and Roux, D. Editors. *Micelles, Membranes, Microemulsions and Monolayers.* Springer-Verlag, New York, 1994, p 395-426

[5] Helfrich, W. Elastic properties of lipid bilayers. Theory and possible experiments. *Z. Natureforsch.* **1973**, 28c, 693

[6] Uchiyama, H.; Acosta, E.; Tran, S.; Sabatini, D. A.; Harwell, J. H. Supersolubilization in Chlorinated Hydrocarbon Microemulsions: Solubilization Enhancement by Lipophilic and Hydrophilic Linkers. *Ind. Eng. Chem. Res.* **2000**, 39(8), 2704-2708

[7] Acosta, E.; Uchiyama, H.; Sabatini, D. A.; Harwell, J. H. The role of hydrophilic linkers. *J. Surfact. Deterg.* **2002**, 5(2), 151-157.

[8] Acosta, E.; Tran, S.; Uchiyama, H.; Sabatini, D. A.; Harwell, J. H. Formulating Chlorinated Hydrocarbon Microemulsions Using Linker Molecules. *Environ. Sci. Technol.* **2002**, 36(21), 4618-4624.

[9] Acosta, E.; Szekeres, E.; Sabatini, D. A.; Harwell, J. H. Net-Average Curvature Model for Solubilization and Supersolubilization in Surfactant Microemulsions. *Langmuir.* **2003**, 19(1), 186-195.

[10] Acosta, E. J.; Le, M. A.; Harwell, J. H.; Sabatini, D. A. Coalescence and Solubilization Kinetics in Linker-Modified Microemulsions and Related Systems. *Langmuir* **2003**, 19(3), 566-574.

[11] Acosta, E.; Mai, P.; Harwell, J. H.; Sabatini, David A. Linker-modified microemulsions for a variety of oils and surfactants. *J. Surfactants Detergents* **2003**, 6(4), 353-363.

[12] Childs J., Acosta E., Scamehorn J. F and Sabatini D. A, Surfactant-Enhanced Treatment of Oil-Based Drill Cuttings. Submitted to Journal of Energy Resources and Technology (JERT) journal, March 2003

[13] Jeffrey D. Childs, Edgar Acosta, Robert Knox, Jeffrey H. Harwell, and David A. Sabatini. Improving the Extraction of Tetrachloroethylene from Soil Columns using Surfactant Gradient Systems. Accepted by J. Cont. Hydrol. September 2003.

[14] Sabatini, David A.; Acosta, Edgar J.; Harwell, Jeffrey H. Linker molecules in surfactant mixtures. *Curr. Opin. Colloid Interface Sci.* **2003**, 8(4,5), 316-326

[15] Doan, T.; Acosta, E.; Scamehorn, J. F.; Sabatini, D. A. Formulating middle-phase microemulsions using mixed anionic and cationic surfactant systems. *J. Surfactants Detergents.* **2003**, 6(3), 215-224.

[16] Tongcumpou, C.; Acosta, E. J.; Quencer, L. B.; Joseph, A. F.; Scamehorn, J. F.; Sabatini, D. A.; Chavadej, S.; Yanumet, N. Microemulsion formation and detergency with oily soils: II. Detergency formulation and performance. Journal of Surfactants and Detergents (2003), 6(3), 205-214.

[17] Tongcumpou, C.; Acosta, E. J.; Quencer, L. B.; Joseph, A. F.; Scamehorn, J. F.; Sabatini, D. A.; Chavadej, S.; Yanumet, N. Microemulsion formation and detergency with oily soils: I. Phase behavior and interfacial tension. Journal of Surfactants and Detergents (2003), 6(3), 191-203.

CHAPTER 2

A Net-Average Curvature Model for Solubilization and Supersolubilization in Surfactant Microemulsions[§]

Abstract

In this work, we propose a mathematical model to reproduce the solubilization, equivalent droplet radius, interfacial tension and phase transitions of anionic surfactant microemulsions by scaling the curvature of the surfactant membranes to the electrolyte concentration required to obtain an optimum microemulsion formulation. At optimum formulation, equal amounts of oil and water are co-solubilized in a bicontinuous media that has a zero net curvature. Our first modeling approach is to use a single curvature term (inverse of an equivalent spherical droplet ratio) which proves to be inadequate as the system transitions to a bicontinuous microemulsion (supersolubilization), where the micelles become swollen and are no longer spherical. Later we introduce two curvature terms (net and average curvature) to interpret bicontinuous microemulsion behavior. The scaling constant (L), which has a length scale, was obtained for sodium dihexyl sulfosuccinate microemulsions with styrene, trichloroethylene and limonene. This scaling constant (L) is shown to be independent of the oil type, temperature, surfactant or additive concentration. We use this net-average curvature model to reproduce selected

[§] This chapter or portions thereof has been published previously in Langmuir under the title "Net-Average Curvature Model for Solubilization and Supersolubilization in Surfactant Microemulsions ", Langmuir 2003, 19, 186-195. The current version has been formatted for this dissertation.

published data. We also compare the scaling constant (L) for the different microemulsion systems studied, finding that this parameter is proportional to the length of the extended tail of the surfactant, and reflects the surfactant solubilization potential. Additionally, the model was modified to account for palisade micellar solubilization. Finally, we introduce the interfacial rigidity concept to reproduce the interfacial tension of these systems.

Keywords: microemulsion, curvature, model, scaling, interfacial, tension, solubilization.

Introduction

Surfactant micelles can increase the overall aqueous "solubility" of oils by one or two orders of magnitude compared to their molecular solubility. During solubilization in micelles, polar solutes can accumulate close to the micelle surface, amphiphiles in the palisade layer, and non-polar oils in the hydrophobic core of the micelle (1-4).

The maximum micellar solubilization may be quantified by the micellar solubilization ratio (MSR). The MSR is small for oils with a large molar volume. For any particular oil, an apparent maximum MSR is found when the hydrophilic/lipophilic balance of the surfactant (HLB) fits that of the oil (5,6).

Microemulsion supersolubilization is an extension of the micellar solubilization concept, where reductions in the micelle curvature allows increased oil solubilization in the core of these "swollen" micelles. The solubilization capacity of these swollen micelles can be, on average, up to one order of magnitude higher than regular micelle solubilization (7-10). The increased solubilization capacity in supersolubilization makes

this approach attractive for many applications, including hard surface cleaners, aqueous-based solvents, detergency, surfactant remediation of oil contaminated sites, emulsion polymerization, etc.

Despite its economical benefits and numerous applications, microemulsion supersolubilization has received only limited attention. In this paper, we introduce a thermodynamic model for microemulsion supersolubilization based on curvature and scaling law arguments. While most of the supersolubilization occurs in the core of the micelle, palisade layer solubilization is introduced to the model to link supersolubilization with the more traditional micellar solubilization and to reproduce interfacial tension data.

Model basis

Excess free energy of an oil droplet:

Consider an oil droplet of radius R with water/oil interfacial tension (γ_o) and molar volume (v_o) suspended in water, as shown in Figure 2.1. The excess free energy (G_E) of the droplet relative to bulk oil is:

$$G_E = 4\pi R_d^{\,2}\gamma_o \qquad \text{Eq. 1}$$

When averaged per mol of oil present in the droplet, the chemical potential (μ) of transferring a molecule from the bulk oil phase (b) to the droplet (d) is obtained as follows:

$$\mu_{o,d} - \mu_{o,b} = \frac{4\pi R_d^{\,2}\gamma_0}{\frac{4}{3}\pi R_d^{\,3}\frac{1}{\upsilon_o}} = \frac{3\gamma_o v_o}{R_d} \qquad \text{Eq. 2}$$

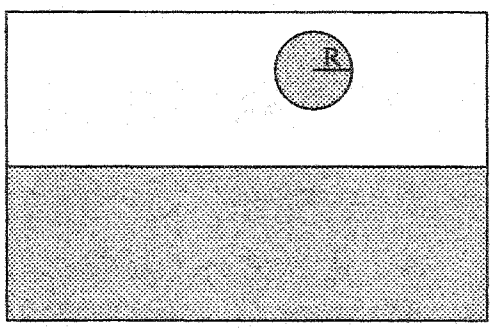

Figure 2.1: Oil droplet suspended in water.

For this spherical configuration, $1/R_d$ is equivalent to the curvature (H). Eq. 2 provides the thermodynamic basis of the Ostwald- Ripening model of coalescence and is an equivalent form of the Kelvin equation (11).

In order to obtain a thermodynamically stable emulsion (a microemulsion) of a certain radius R_d, Ostwald ripening must be avoided (11). Therefore, the excess free energy provided by Eq. 2 has to be neutralized by the adsorption of surfactant at the oil/water interface.

Currently, a model does not exist that clearly describes this stabilization based on molecular interactions. There are phenomenological models based on curvature rigidities, and there are molecular thermodynamic approaches that use Monte Carlo simulations to reproduce the essence of the phase diagram. These approaches have been summarized in recent publications (12-14).

Another modeling approach proposed in the literature is based on geometrical considerations of micelles, swollen micelles and bicontinuous microemulsions together with molecular interactions (10, 15-17). These models more closely represent the actual

system, but their relative complexity and their need for multiple adjustable parameters make the models unsuitable for modeling actual processes involving microemulsions (surfactant enhanced oil recovery, surfactant enhanced remediation, detergency, etc).

A practical approach for describing microemulsion systems is that proposed by Salager et al., based on the surfactant affinity difference (SAD) equation (18-20), which for ionic surfactants is as follows:

$$SAD^{\#} = \frac{SAD}{RT} = -\ln S + K \times ACN + f(A) - \sigma + a_t(T - T_{ref}) \qquad \text{Eq. 3}$$

where $SAD^{\#}$ is the dimensionless surfactant affinity difference, R is the universal gas constant, T is the absolute temperature, S is the electrolyte concentration, K is a constant for a given surfactant (ranging from 0.1 to 0.2), and ACN is the alkane carbon number of the oil (for non-hydrocarbon it becomes EACN equivalent-ACN). The parameter f(A) is a function of the alcohol/cosurfactant concentration, σ is a parameter that is a function of surfactant, a_t is a constant , ~ 0.01 when temperature is in Celsius, T_{ref} is a reference temperature.

The SAD is the free energy required to transfer a surfactant molecule from the water phase to the oil phase: $\frac{SAD}{RT} = \ln\frac{C^w}{C^o} = \frac{\mu_s^{*o} - \mu_s^{*w}}{RT}$, where C^w and C^o are the surfactant monomer concentration in water and oil phases respectively, μ^{*o}_s and μ^{*o}_s are the standard chemical potential of the surfactant in the water and oil phases respectively (18-20). We propose here that while SAD focuses on the chemical potential difference of the surfactant under different formulation variables, it is related to the chemical potential difference due to changes in the curvature of the droplets predicted by the Kelvin

equation (equation 2). Similarly, Kalbanov and Strey (21,22) have scaled the surfactant curvature of micelles and swollen micelles to the optimal formulation using the same form of the variables as in the SAD equation.

Based on these preliminary observations, in this paper we generalize the SAD correlation by hypothesizing that the curvature "H" changes proportionally to the $SAD^{\#}$:

$$H \propto SAD^{\#} \Rightarrow H = C \times \left[-\ln S + K \times ACN + f(A) - \sigma + a_t (T - T_{ref}) \right] \qquad \text{Eq.4}$$

where "C" is a proportionality constant. At optimum formulation, the SAD and the interfacial curvature are "zero". The salinity or electrolyte concentration at this condition is called the optimum salinity, S*, as given by Eq. 3:

$$\ln S^* = -K \times ACN - f(A) + \sigma - a_t (T - T_{ref}) \qquad \text{Eq. 5}$$

Substituting Eq. 5 in Eq. 4 we have:

$$H = C \times SAD^{\#} = C \times \left[\ln \frac{S^*}{S} \right] \qquad \text{Eq. 6}$$

In equation 6, when the electrolyte concentration (S) is less than the electrolyte concentration to obtain optimum middle phase microemulsions (S*), the term (S*/S) is greater than one and its logarithm is positive. According to our convention, this positive curvature signs this corresponds to droplets of oil in water. When the electrolyte concentration is equal to the optimum value (S*), then the S*/S has a value of one and its logarithm is zero. In this case the net-curvature is zero, which corresponds to a bicontinuous microemulsion, as we will discuss later. When the S>S* the logarithm is negative and corresponds to the formation of water droplets suspended in oil continuous media (Type II microemulsion)

If the curvature is taken as the inverse of the radius of a spherical droplet, then:

$$R_d = \frac{1}{C \ln\left[\frac{S^*}{S}\right]} = \frac{L}{\ln\left[\frac{S^*}{S}\right]} \qquad \text{Eq.7}$$

where L is the proportionality constant (with length units). Here as the electrolyte concentration increases towards the optimum electrolyte (S*), the curvature reduces which in turn results in swollen micelles. When the electrolyte concentration (S) is equal to the optimum electrolyte concentration (S*), this radius goes to infinity. However, this is not the real behavior because the entropy (as discussed later) will limit the length scale of the oil and water domains and lead to formation of the bicontinuous phase.

In more general terms,

$$R_d = \frac{1}{C \times SAD^{\#}} = \frac{L}{\Delta\mu^*_s} \qquad \text{Eq. 8}$$

where $\Delta\mu^*_s$ is the non-dimensional excess chemical potential of the surfactant referenced to a flat interface (optimum formulation). This type of expression has been previously found using scaling theory. According to this approach, the correlation length (ξ) is (23):

$$\xi = \frac{\xi_o}{\left|(\Delta\mu^*_s)\right|^n} \qquad \text{Eq. 9}$$

Huang and Kim (24) scaled the hydrodynamic radius (R_h) of oil in water microemulsions finding that "n" is 0.75. Dorshow et al. (25) found "n" to be approximately 1.13. In this work the value of "n" is assumed to be 1 based on the hypothesis that the curvature (H) is proportional to the $SAD^{\#}$, as discussed earlier.

In summary, we propose a semi-empirical scaling model where the curvature of the surfactant membrane (H) is scaled using the nondimensional surfactant affinity difference ($SAD^{\#}$) which reflects the chemical potential difference of transferring the surfactant molecule from the water to the oil phase. By comparing the expressions of the Kelvin equation and the $SAD^{\#}$ equation we propose that the scaling exponent "n" has a value of 1.

Experimental procedures.

Materials

The following chemicals were obtained from Aldrich (Milwaukee, WI) at the concentrations shown and were used without further purification: trichloroethylene (TCE, 99%+), limonene (99+), styrene (99%), n-dodecanol (98+%), sodium chloride (99%+), oleic acid (98%) and sodium hydroxide (99%). The surfactant sodium dihexyl sulfosuccinate (80% wt. solution in water) was purchased from Aldrich Chemicals (Fluka brand). Sodium mono and dimethyl naphthalene sulfonate (SMDNS, 95%) was supplied by CKWitco (Houston, TX). Table 2.1 shows the molecular structure, density (ρ_o), molecular weight and equivalent alkane number (EACN) of the oils considered in this work. Table 2.2 shows the molecular weight, critical micelle concentration (CMC), area per molecule (a_i) and chemical structure for the surfactants employed.

Table 2.1. Selected properties and molecular structure of oils studied.

Oil	Chemical Structure	Density (q/ml)	EACN	Mol Weight
Limonene (Lim)	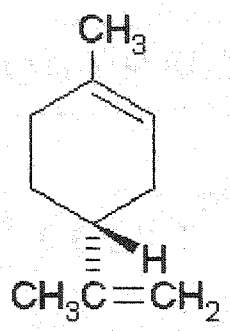	0.84	~ 6	136
Styrene (Sty)	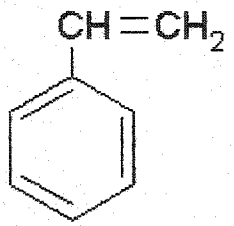	0.91	~ 3	104
Trichloroethylene (TCE)	$Cl_2C{=}CHCl$	1.46	-3.81	131
Hexane (Hx)	$CH_3(CH_2)_4CH_3$	0.66	6	86

Table 2.2. Chemical structure and area per molecule of surfactant studied.

Chemical name	Molecular Weight g/mol	CMC Mol/L	Area per molecule, Å^2	Chemical structure
Sodium dihexyl sulfosuccinate (SDHS)	389	0.014[a,b]	100[a,b]	$(CH_3(CH_2)_5OOCCH)_2(SO_3Na)$
Sodium mono and dimethyl naphthalene sulfonate (SMDNS)	251	>0.01[b]	90[b]	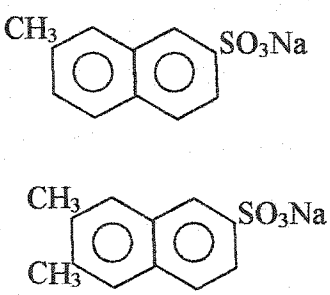
Sodium dodecyl sulfate (SDS)	288	0.008[a]	60[a]	$CH_3(CH_2)_{11}SO_4Na$
1-Pentanol (C5OH)	88		30[c]	$CH_3(CH_2)_4OH$
1- Dodecanol (C12OH)	186		--	$CH_3(CH_2)_{11}OH$

(a) From Rosen (35)
(b) From Acosta et al (27).
(c) From Rosen (35) using C8E1 as surrogate.

Methods.

Phase behavior studies were performed using equal volumes of aqueous solution and oil (5 mL each). Electrolyte scans were performed by varying the sodium chloride concentration at constant temperature, additive content (alcohols, acids, hydrotropes, etc), and pressure (1 atm). Test tubes were placed in a water bath at 27°C, shaken once a day for three days, and left to equilibrate for two weeks. The phase volumes were determined

by measuring the levels of each phase in the test tube. The concentrations of TCE, styrene and SMDNS were measured using a Shimadzu HPLC equipped with a C18 column and UV Waters detector set at 225 nm. Limonene concentrations were measured by gas chromatography using a Varian 3300 with FID detector and a SPB20 capillary column with programmed temperature. Sodium dihexyl sulfosuccinate was measured using a Dionex ion chromatography system with a NS1 column.

Interfacial tensions were measured using a Model 500 University of Texas spinning drop interfacial tensiometer, injecting 1 to 5 μl of the equilibrated middle phase in a 300 μl tube filled with the excess denser phase from the 10-ml microemulsion sample tube.

Results and discussion

The hypothesis to be tested in this work is that the equivalent radius (R_d) of a swollen micelle in supersolubilization can be obtained by scaling the curvature ($H=1/R_d$) to the SAD[#]. Specifically, we hypothesize that for ionic surfactants this scaling can be performed using a non-dimensional electrolyte concentration ($\ln(S^*/S)$). This hypothesis is summarized by Eq. 7. To test this hypothesis, the equivalent radius of the solubilized oil is plotted versus the inverse of the dimensionless electrolyte concentration ($1/\ln(S^*/S)$).

The first task in this endeavor is to convert oil concentrations measured by chromatography to an equivalent radius, using:

$$R = \frac{3V_o}{As} \qquad \text{Eq. 10}$$

where the volume of the solubilized oil (V_o, $Å^3$) can be calculated based on the concentration of the oil (C_0, mg/L) in the aqueous micellar solution (i.e. for a 5 ml initial aqueous solution):

$$V_o = \frac{5 \times 10^{18} C_o}{\rho_o (1 - \frac{10^{-6} C_o}{\rho_o})} \qquad \text{Eq. 11}$$

And the interfacial area (As, $Å^2$) is given by:

$$As = \sum_i 5 \times 10^{-3} Cs_i \times 6.023 \times 10^{23} \times a_i \qquad \text{Eq. 12}$$

where Cs_I is the molar concentration of surfactant or cosurfactant added to 5 ml aqueous solution, and a_I is the interfacial area per molecule of the surfactant.

We have made several assumptions in estimating the equivalent radius using the procedure specified. The first assumption is that the area per molecule of the surfactant (a_i, which is obtained using the Gibbs equation to interpret surface or interfacial tension curves of flat interfaces) is constant and corresponds to the area of contact between the surfactant and oil (the effect of electrolyte on the area will be discussed later). Second, we assume that all the surfactant is present in the aqueous solution and associated in micelles. Third, we assume that the aggregates are spheres and exist in a continuous water phase.

The first assumption, that the surfactant area per molecule (a_i) determines the interfacial area, has been the subject of discussion in the literature (10). Ruckenstein and Nagarajan (10) have considered that the surfactant has three particular areas, one being the area of contact with the water, another being the area of contact with oil, and the third

being the area at the "neck" of the surfactant. According to their approach (which we use in this work), the area in contact with the water decreases as the curvature of the micelle decreases due, for example, to increased levels in electrolyte concentration. At the same time, as the area in contact with the oil increases and the neck area remains constant, eventually the cone-shape of the surfactant packed in micelles goes through a cylinder shape (flat curvature) at high enough electrolyte concentration; at this point all the areas are equal. The area calculated based on the Gibbs adsorption model is actually the neck area because, when compared to the scale of the surfactant molecules, the macroscopic interface appears flat. This assumption neglects the volumes of the head and tail of the surfactant, which is not significant when the solubilization is sufficient and surpasses the volumes of these portions of the surfactant molecules. In future versions of this model, we will consider this effect in producing phase diagrams of highly concentrated surfactant solutions (30% of surfactant or more)

The assumption that all the surfactant is in aqueous micelles is largely valid in oil/water microemulsions when no cosolvent is added and when the CMC is small relative to the surfactant concentration. The assumption of spherical droplets may be the most inaccurate. Close to the Winsor type I to III phase transition, micelles assume a worm-like configuration, in which even water continuity is no longer valid (12,13,23).

Figure 2.2a is a plot of oil droplet radius (R_d), as defined by Eq. 10, versus $1/\ln(S^*/S)$ for trichloroethylene microemulsions. Series "S" represents a system with surfactant (sodium dihexyl sulfosuccinate 0.103 M) alone. Series "S+LL" represents a system with surfactant (sodium dihexyl sulfosuccinate 0.103 M) and dodecanol (0.09 M)

used as a lipophilic linker (26). Series "S+HL" represents surfactant and SMDNS (0.09 M) used as hydrophilic linker (26,27). Series "S+LL+HL" corresponds to surfactant and 0.09 M of each linker.

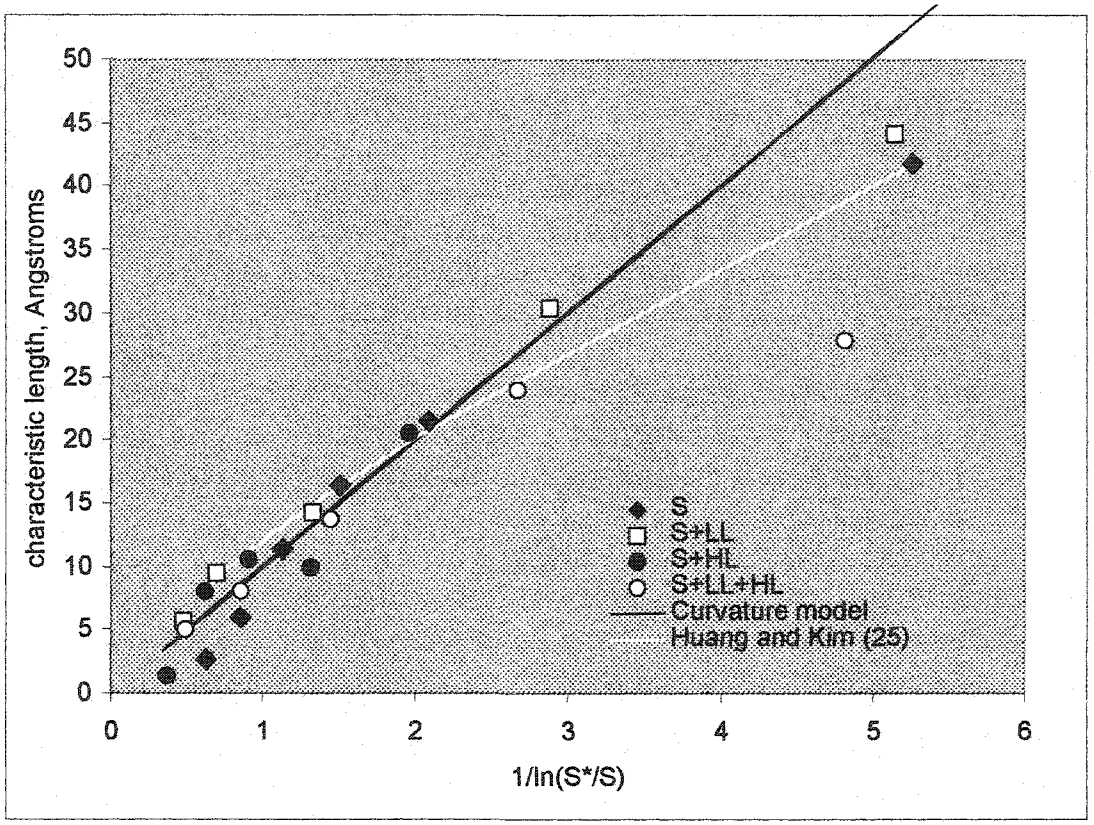

Figure 2.2a. Curvature model in trichloroethylene microemulsions.

Figure 2.2a shows the curvature model (Eq. 7) drawn using L= 10 Å. As seen, the model fits well for values of "1/ln(S*/S)" less than 3. As values of 1/ln(S*/S) increase, the solution approaches the bicontinuous phase. The disparity between the data and model at higher values of 1/ln(S*/S) was expected due to the breakdown of the spherical micelle droplet assumption. The data helps to establish the range of salinity over which this approach is valid. The Huang and Kim approximation (n=0.75) is also plotted in

Figure 2.2a, in which case L = 12 Å. This model seems to be more suitable closer to the bicontinuous transition.

One interesting feature of Figure 2.2a is that the model constant L seems to work for all combinations of surfactant and additives (linkers). This is an encouraging result since most of the time microemulsions are obtained by mixing a series of additives with the main surfactant.

One question that remains is "what is the physical meaning of L=10 Å?", and, even more important, "how is this value affected by different oils, temperatures, surfactant concentration, or surfactant type?".

Figure 2.2b shows the equivalent oil droplet radius model versus the modified salinity scale (1/ln(S*/S)) for limonene microemulsions. The difference from trichloroethylene microemulsions is that limonene is a more hydrophobic oil (EACN of TCE is –3.81 vs. 6 for limonene, see Table 2.1) with higher optimum salinity (S*, see Table 2.3) and lower solubilization (ξ^*, see Table 2.3). As seen in Figure 2.2b, these differences do not appear to impact how well the curvature model fits the data, which has also been constructed using L=10 Å. In this case, using the Huang and Kim exponent (n=0.75) with L=12 Å seems to overestimate the solubilization in the lower range of salinity.

The results with limonene in Figure 2.2b reinforce the fact that the curvature model is valid in the medium range of electrolyte concentration ($0<1/\ln(S^*/S)<3$). The fact that the same constant (L=10 Å for the proposed model and L=12 Å using the Huang

and Kim exponent) can be used for different oils is also encouraging from the modeling point of view.

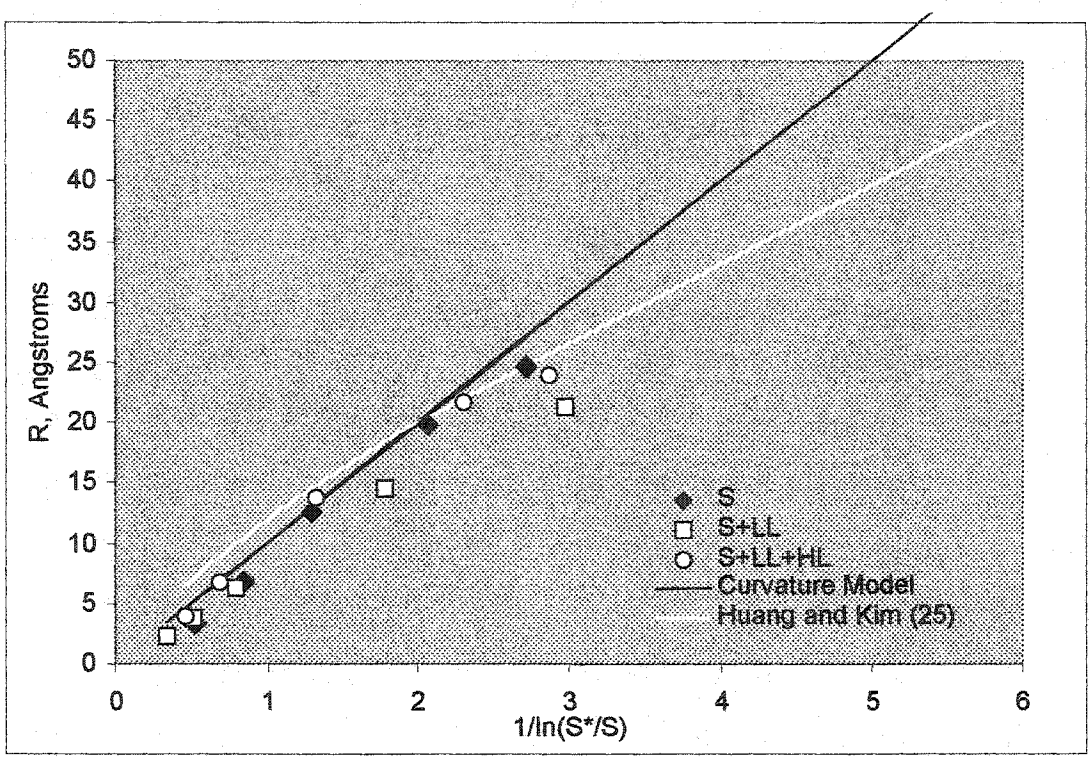

Figure 2.2b. Curvature model in limonene microemulsions

The curvature model was also tested for styrene microemulsions at different surfactant concentrations and temperatures. The solubilization results are presented in Figure 2.2c. The data in Figure 2.2c represents surfactant only results (S, sodium dihexyl sulfosuccinate) at different concentrations and temperatures (either 25°C or 60°C), as indicated in each series. The proposed curvature model (n=1) and the model using the Huang and Kim exponent (n=0.75), are plotted using the same length parameter (L), as above.

Table 2.3. Optimum salinity and characteristic length at optimum formulation for selected series.

Formulation	Optimum salinity (S*), %NaCl	Characteristic length (ξ^*) at optimum formulation, Å
0.1 M SDHS – TCE, 27°C	1.25	99
0.1 M SDHS + 0.09 M C12OH – TCE, 27°C	0.85	146
0.1 M SDHS + 0.09 M SMDNS – TCE, 27°C	3.0	70
0.1 M SDHS + 0.09 M C12OH + 0.09 M SMDNS – TCE, 27°C	1.6	103
0.1 M SDHS – Lim, 27°C	6.4	44
0.1 M SDHS + 0.09 M C12OH – Lim, 27°C	3.5	
0.1 M SDHS + 0.09 M SMDNS + 0.09 M C12OH – Lim, 27°C	8.5	
0.05 M SDHS - Sty, 25°C	3.7	
0.1 M SDHS - Sty, 25°C	3.5	
0.2 M SDHS - Sty, 25°C	3.1	
0.05 M SDHS - Sty, 60°C	5.2	
0.1 M SDHS - Sty, 60°C	4.8	
0.2 M SDHS - Sty, 60°C	4.3	
1.6% wt. SDS + 2.4% wt. C5OH – Hx	5.65	415

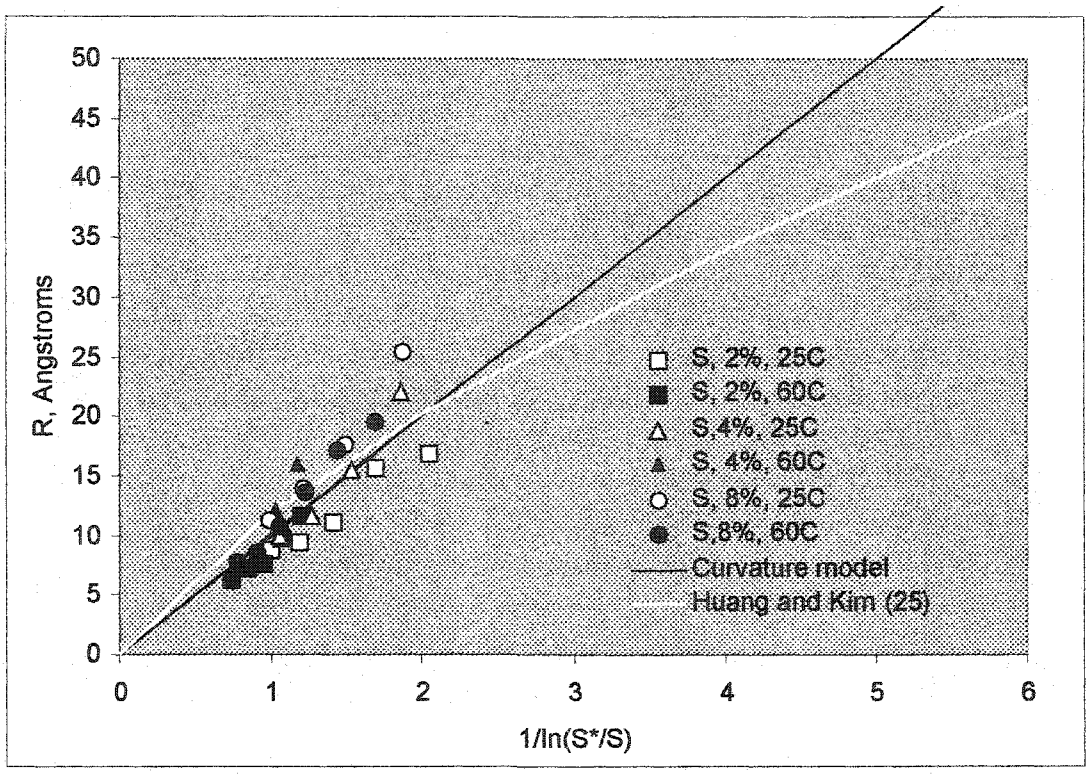

Figure 2.2c. Curvature model in styrene microemulsions

From Figure 2.2c, the data is rather scattered along both models and they seem to follow the trend even at different surfactant concentrations and temperatures. Unfortunately there is no data at or above a value of 3 (1/ln(S*/S)) for these systems, which prevents us from confirming whether the model is valid under these conditions. According to the data in Figure 2.2c, the length parameter is not a function of surfactant concentration or temperature, at least in the 25°C to 60°C range.

Thus, the curvature model is observed to apply independent of oil type, additives, surfactant concentration and temperature. The model appears to be valid for dimensionless electrolyte (1/ln(S*/S)) values of 3 or less for our formulations (W/O ratio = 5ml/5ml). By using the Huang and Kim exponent (n=0.75), the data seem to fit closer

in the vicinity of the bicontinuous transition. It is worth noting that for "1/ln(S*/S)" of 3 or greater these systems show a "bluish" color, which evidences the presence of large oil droplets concentrated enough to scatter the blue light.

The value of the constant L seems to be independent of the variables studied in Figures 2.2a, 2.2b and 2.2c. While L could be a function of the surfactant type, we have not yet considered this effect. Since the constant L seems to be associated with the solubilization ability of each surfactant, for a given electrolyte concentration (expressed as 1/ln(S*/S)), a higher L value would mean higher solubilization of the oil.

The simple curvature model, using the proposed exponent (n=1) or the Huang and Kim exponent (n=0.75), breaks down under certain limiting conditions. With no added salt the total electrolyte concentration is low (only the unbounded counterion) and both models tend to underpredict the radius of the oil. Later in this paper we give an example of trichloroethylene and sodium dihexyl sulfosuccinate (SDHS) microemulsion where this effect is numerically illustrated and we introduce palisade layer solubilization in addition to core solubilization (accounted by the curvature model) to reproduce solubilization at low electrolyte concentration. Another problem with this initial curvature model is that at the optimum salinity (S*) the radius is predicted to be infinite, which is also not true. At optimum solubilization, the characteristic length (or correlation length) has a finite value (ξ^*). In the next section we will revisit the simple curvature model based on these observations.

Net - average curvature model

One of the main disadvantages of the simple curvature model is the assumption of medium continuity. In Type I or Type II microemulsions, where either water or oil is the continuum media, the scaled curvature (equations 8 and 9) was easily identified with the inverse radius of an equivalent spherical droplet, as discussed before. When we approach a bicontinuous media (type III microemulsion) there are no clear domains of oil and water, but irregular channels of both phases that are interconnected in an intricate three-dimensional network, as indicated by electrical conductivity, NMR-self diffusion coefficient studies and scattering techniques (28). Because of the irregularity of these systems, it is difficult to identify a physical structure and a corresponding scaled curvature. Another approach to this problem is to consider the average local orthogonal curvatures of the surfactant membrane (c_1,c_2) which are in the mechanical interpretation of surfactant membranes by Helfrich (29):

$$\frac{dG}{dA} = \frac{K}{2}(c_1 + c_2 - 2c_0)^2 + \underline{\mathbf{k}}c_1c_2 \qquad \text{Eq. 13}$$

where dG is the change in surface free energy, dA is the change in interfacial area, K is the bending elasticity modulus of the system (energy units), $\underline{\mathbf{k}}$ is the Gaussian or saddle splay modulus, and c_1 and c_2 are the orthogonal curvatures of the surfactant membrane. The value of c_0 corresponds to the preferred curvature (no tension). Kegel et al. have used this approach to generate a thermodynamic theory of droplet-type microemulsions (Type I or II) based on the spherical droplet approach (as we consider in this work) (30). Kegel et al. were unable to reproduce bicontinuous (Type III) microemulsions due to the lack of a regular structure to which they could assign the orthogonal curvatures (c_1 and c_2) (30).

While the approach of Helfrich, as further developed by Kegel et al., is based on a thermodynamic analysis of the bending energies of the surfactant membrane, our approach differs by relying on scaling theory. However, both approaches fail to deliver an appropriate model for bicontinuous microemulsions due to the disordered state of these systems.

As in any disordered media, we propose the use of statistics to describe the curvature of the surfactant membranes in bicontinuous phases. Specifically we assume that bicontinuous middle phases are composed of oil and water droplets coexisting at the same time, and with oil and water radii as considered above (R_o, R_w). Based on these radii we propose a net curvature that will describe the curvature of the surfactant membrane itself and an average curvature to describe the size of the oil and water regions within the bicontinuous phase:

The average curvature is defined as:

$$H_a = \frac{1}{2}\left(\left|\frac{1}{R_o}\right| + \left|\frac{1}{R_w}\right|\right) = \frac{1}{\xi} \qquad \text{Eq. 14}$$

And the net curvature as:

$$H_n = \left|\frac{1}{R_o}\right| - \left|\frac{1}{R_w}\right| = \frac{1}{L}\ln\left(\frac{S^*}{S}\right) \qquad \text{Eq. 15}$$

Equation 14 gives rise to an expression used to calculate the "correlation or characteristic length" of De Gennes (ξ) (31). R_w is obtained using Eq. 10, but replacing the oil volume ($V_o=\varphi_o \times V$) by the volume of the aqueous phase ($V_w=\varphi_w \times V$). By introducing these terms, equation 14 becomes:

$$\xi = \frac{6 * \varphi_o \varphi_w V}{As} \qquad \text{Eq. 16}$$

where φ_o and φ_w correspond to the volume fraction of oil and water in the microemulsion phase and V is the volume of the microemulsion phase. In obtaining equation 16, the volume of the surfactant is neglected so that $\varphi_o + \varphi_w = 1$. The characteristic or correlation length that can be calculated using equation 16 have been corroborated by X-ray, neutron scattering and dynamic light scattering techniques (31). Here we used measured solubilization values of oil, water and surfactant (as determined by liquid and gas chromatography, see method section) to obtain the different parameters indicated used in equation 16. One important parameter in this model is the characteristic length at optimum formulation (ξ^*) which we obtain by applying equation 16 to the optimum middle phase microemulsion. While this parameter, as explained below, is dictated by the molecular interactions taking place in the oil and water side of the interface, no model exist that can predetermine this value. Rather, it has to be obtained from phase behavior studies, as described in this work. We hope that future efforts will identify models capable of determining ξ^* based on molecular considerations alone.

As indicated above, the net curvature (equation 15) describes the curvature of the surfactant membrane itself, which is scaled to the $SAD^{\#}$ as in equation 6. In this case, a net curvature of zero at optimum formulation results not from an infinite curvature radius, but rather from the coexistence of finite curvatures of opposite signs. The sign convention is taken so that an oil droplet in continuous water will have a positive value and the curvature of a water droplet in aqueous system will have a negative value.

Equations 15 and 16 can be solved to reproduce the phase behavior of Type I-III-II microemulsion phases. In type I microemulsions the SAD is positive, and oil droplets are present with a certain radius (R_o). We can calculate a fictitious water droplet radius (even when the microemulsion is continuous in water) based on the volume of water and the aqueous surfactant concentration using equations 10 through 12 (R_w). Using R_w we can calculate for R_o using equation 15. For most Type I microemulsions the radius of water will be so large compared to the radius of the oil droplet that the net curvature will take the form of the simple curvature model. If the oil droplet size increases near the size of the fictitious water radius, this water radius acts as a correction factor for the deviation from the spherical droplet assumption. The more important role of the fictitious water radius in Type I microemulsions is its use in calculating the average curvature (equation 14). As we explained before, this curvature is the inverse of the correlation length of the surfactant membrane. The maximum correlation length or optimum characteristic length (ξ^*) is the maximum distance that a molecule of oil or water can be separated from the surfactant membrane (oil/water interface) and still interact with the surfactant membrane. In other words this is the length at which the molecular interaction energy between the oil or water molecule with the interface becomes equal to the molecular entropy (K_BT) (31-33). When the inverse of the average curvature (ξ) is equal to the optimum characteristic length (ξ^*) then the microemulsion no longer retains the water continuity, and gives way to a bicontinuous phase to ensure that all the molecules are separated from the interface a maximum of ξ^*. The same is true for the Type II-III microemulsion phase transition. In other words, the fictitious radius of water (or oil) in Type I (or Type II) microemulsion

serves mainly as a benchmark point for the transition towards the bicontinuous microemulsion (Type III).

The transition described above from a Type I towards Type III microemulsion can be summarized by indicating that in droplet-containing microemulsions (Type I or II) the size of those droplets is controlled by the curvature of the surfactant membrane (equations 6 through 9) while in bicontinuous microemulsion this size is controlled by the entropy which disperses the interaction forces between the water or oil molecules and the surfactant adsorbed at the oil/water interface. These effects are always recognized in the microemulsion literature and are considered in the solution of equations 14 and 15 (17, 30-32). Next we will describe the details of the solution of this modified net-average curvature model for our systems and systems reported in the literature.

To solve the net curvature model (Eq. 15) for type I microemulsions, R_w has to be calculated using equation 10 with V_w as the initial aqueous solution volume (5ml for the data considered in Figures 2.2 and 2.3). Figure 2.3 presents the same set of data presented in Figure 2.2a but includes the prediction from the net-average curvature model. Figure 2.3 shows that the net-average curvature model follows very closely the simple curvature model using the exponent n=1 at values of "1/ln(S*/S)" of 3 and lower, but for larger values, it agrees better with the Kim and Huang expression.

Hypothetically the net curvature model could be used throughout the phase transition from oil in water microemulsion (type I) to bicontinuous (type III) to water in oil microemulsion (type II). For type I (or type II) microemulsions the radius of water,

Rw (or oil, Ro) is fixed by the volume of brine (or oil) initially added to the solution. The radius of oil (or water) can be found by using equation 15.

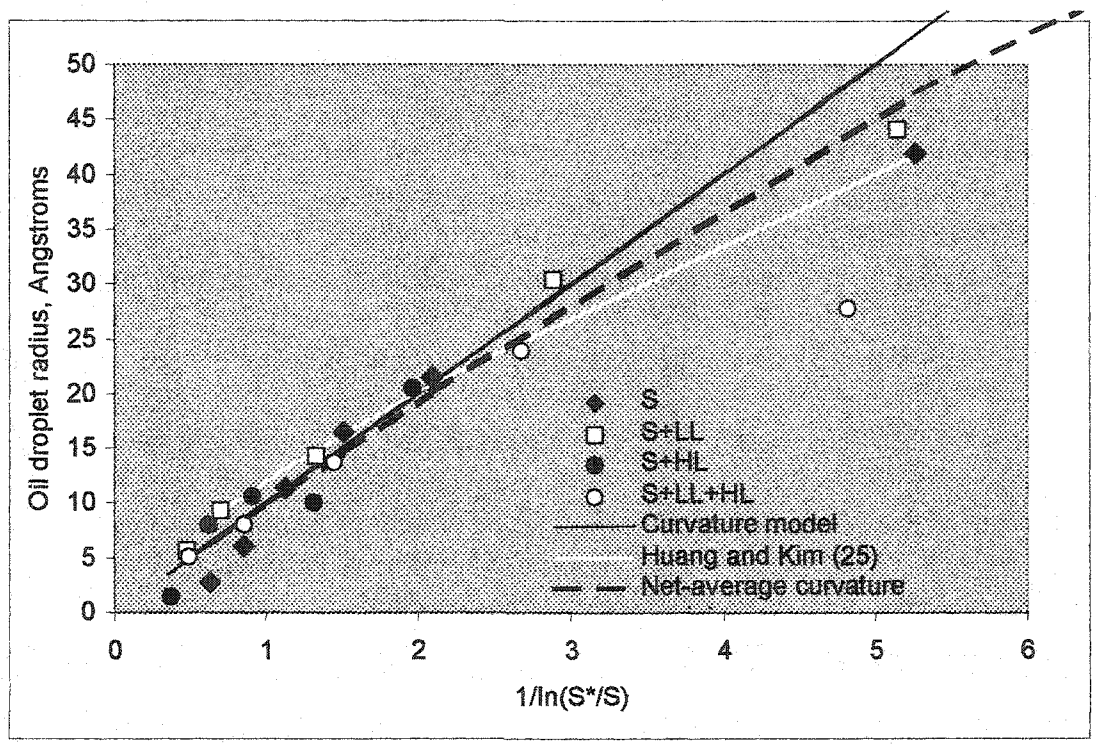

Figure 2.3. Curvature models in trichloroethylene microemulsions

The problem of using this model for middle phase (bicontinuous) microemulsions is that the volume of oil and water are not the same as initially added. Therefore, no radius of oil or water can be used to solve equation 15. In this case it is useful to utilize the correlation length concept in the De Gennes critical theory of polymers (31). According to this concept, any polymer chains separated by a distance less than ξ_k are rigidly bonded. In microemulsions, this critical length corresponds to ξ^*, and is the maximum length scale at which any oil or water can be correlated to the surfactant membrane. To solve the model for bicontinuous microemulsions, the average curvature is

equated to this value. Then equations 14 and 15 are simultaneously solved for Ro and Rw.

Net – Average model: Solubilization curves

Using the procedure described above, the solubilization diagram for hexane – sodium dodecyl sulfate (SDS) - pentanol was modeled and compared to the experimental values presented in the literature (23, 34). The optimum salinity (S*=5.67 % NaCl), the salinity window (5.4%NaCl – 5.8%NaCl), and the solubilization parameter at optimum (SP*=25 ml hexane / ml of surfactant + alcohol), were obtained from the literature. This particular system has 60 parts of pentanol per 40 parts of SDS. The value of ξ^* was calculated using equation 15 and the resulting SP* value. It was assumed that the pentanol has an area per molecule at the interface of 30 $Å^2$ (based on C8E1, as in Rosen (35)) and that all of it is adsorbed at the interface. SDS area per molecule was assumed to be 60 $Å^2$ (35). The calculation results in $\xi^* = 415$ Å.

The length constant in equation 15 was adjusted to fit the salinity window, with the resulting value being L= 20 Å. Figure 2.4 presents the data and the model predictions for SDS – pentanol – hexane solubilization diagram from the literature (23,34). The model reproduced the data fairly well, considering that only one parameter was adjusted (L=20 Å). The radius of the oil droplets (SPo) seems to be underestimated, possibly due to the assumption that the alcohol is completely adsorbed at the interface throughout the salinity scan. This assumption is suspect due to the partition effects of pentanol in excess water and oil. Even considering the likelihood of this source of error, the net-average

curvature model effectively reproduces the phase transition of the SDS-hexanol-hexane system.

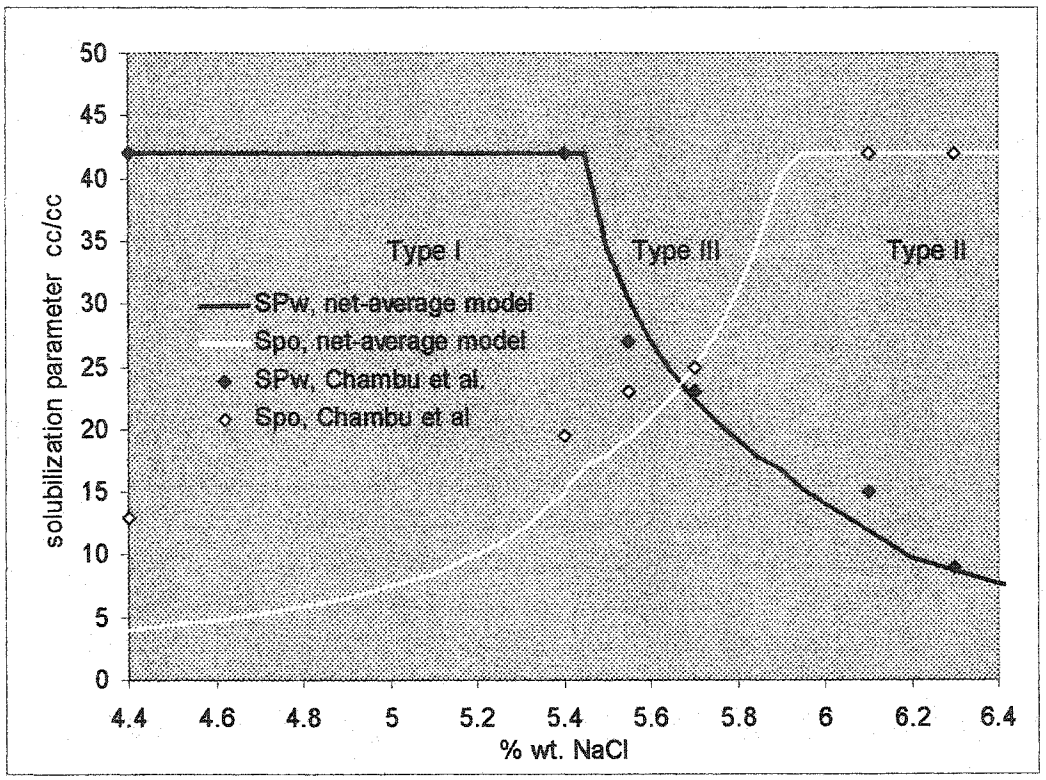

Figure 2.4. Solubilization diagram for SDS- pentanol – hexane microemulsions. Data points after Chambu et al found in reference 34.

Thus, to our knowledge, our net – average curvature model is the first to successfully reproduce the phase behavior and solubilization diagrams of real microemulsions systems from type I to type III to type II. By contrast, other models based on scaling laws, including the Huang and Kim approach, break down in the vicinity of the bicontinuous phase transition.

Earlier we posed the question whether the L constant depends on the surfactant structure. This question seems to be partially answered by the fact that L = 20 Å in SDS microemulsions. Sodium dodecyl sulfate (SDS) has a linear 12-carbon tail and it has an

extended length of about 18 Å. Sodium dihexyl sulfosuccinate has two 6-carbon tails to make a total of 12 carbons but the extended length is the same as a 6-carbon tail ~ 9 Å. For the latter case, L would be10 Å . From this discussion it can be inferred that the L factor represents the solubilization capacity of the surfactant, which seems to scale to the extended length of the surfactant tail.

Net – Average model: Phase volumes

As indicated above, the net-average curvature model can also be used to reproduce the volumes of the different phases (phase behavior or phase volume diagrams). The following example corresponds to a microemulsion system studied by Dwarakanath et al. (36).

Dwarakanath et al. (36) studied the phase behavior of a 2-ml trichloroethylene-enriched solvent mixture microemulsion with 2-ml of 8% (0.204 M) sodium dihexyl sulfosuccinate and 4% 2-propanol at temperatures ranging from 12°C to 23°C. The phase volumes after equilibration were registered and presented as volume fractions (based on 4-ml total) as a function of normalized electrolyte concentration (S/S*). Figure 2.5 presents selected data at 12°C and 23°C.

The net-average curvature model was used to reproduce the phase behavior. The procedure to calculate the radius of water and oil (R_w, R_o) for the different types of microemulsions was as described above. The "L" parameter was taken as 10 Å, as determined above for sodium dihexyl sulfosuccinate surfactant. In this calculation, it was assumed that the interfacial area, As, was provided by the surfactant (100 $Å^2$/molecule) and by the alcohol (2-propanol, 30 $Å^2$/molecule). The characteristic length at optimum

formulation (ξ^*) was calculated using equation 16 considering the phase volumes reported by Dwarakanath et al (36). For both temperatures, the characteristic length (ξ^*) is approximately 51 Å. The volumes of the different phases were calculated using equation 10 based on the radius of oil and water.

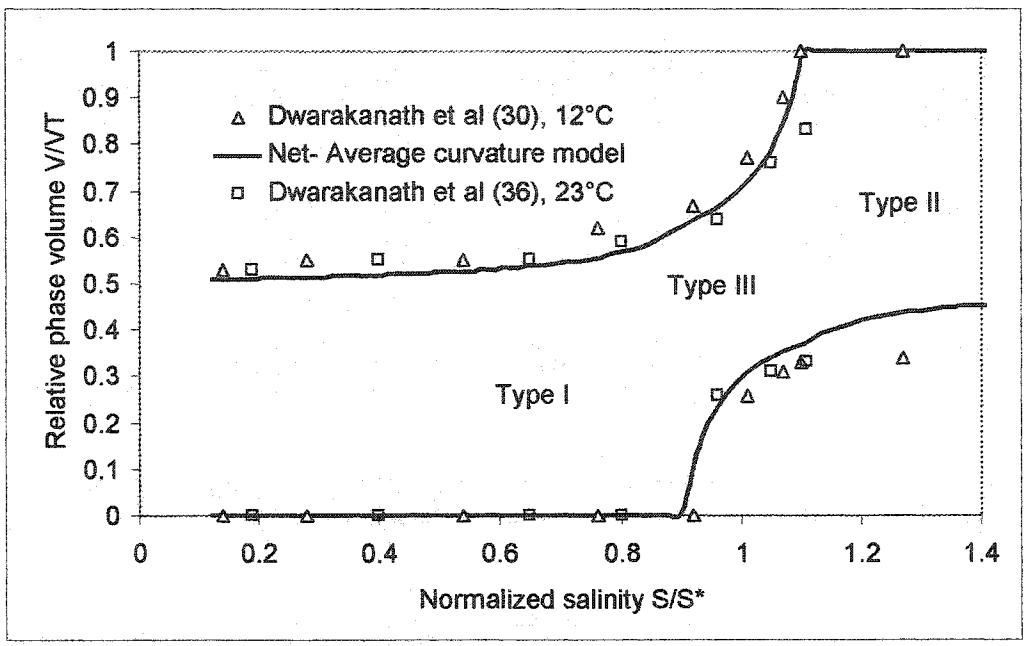

Figure 2.5. Volume fraction diagram for TCE-enriched mixture of chlorinated solvents microemulsion with sodium dihexyl sulfosuccinate and 2-propanol.

Figure 2.5 shows the phase volumes as calculated from the model. In general, the net-average model traces the phase behavior observed for the system. In this case, the length parameter, L= 10 Å, was used to reproduce data at temperatures as low as 12°C. This reinforces the previous observation for styrene microemulsions, where we observed that the length constant is not a function of temperature, at least in the range studied (12°C – 60°C) here.

Net – Average model: microemulsion droplet size

In the two previous case studies (23,34,36) we have used the net - average model to reproduce solubilization and phase volumes diagrams and compared them to actual data. In one additional application of the model we will estimate the droplet size for paraffin and aromatic oil microemulsions, using the data from Hwan et al. (37).

Hwan et al. (37) studied the drop size distribution of a paraffin + aromatic oil mixture (simulating a crude oil) with a 5% surfactant + alcohol mixture. They used nonyl (C9) and dodecyl (C12) orthoxylene sulfonate surfactants (37% by volume) and tertiary amyl alcohol (63% by volume). The droplet size distribution of oil and water were calculated based on the sedimentation rates measured using the ultracentrifugation technique. The solubilization and interfacial tension curves of these systems were previously obtained by Healy et al. (38).

The net-average curvature model was fitted to this data, using the solubilization curves obtained by Healy et al (38) (and reproduced by Hwan et al. (37)). For both surfactants (nonyl and dodecyl tails) the area per molecule was assumed to be 55 $Å^2$, similar to alkylbenzene sulfonate surfactants (35). The tert-amyl alcohol was also considered in the calculation of the total interfacial area "As". As previously assumed for the case of the tert-amyl alcohol, the area per molecule was assumed to be 30 $Å^2$. The procedure of fitting the model was the same as for the case of the SDS- pentanol-hexane microemulsion.

Under the above conditions, the characteristic lengths of the nonyl and dodecyl orthoxylene sulfonate microemulsions were 55 Å and 106 Å respectively. The length parameter "L" was 20 Å for the nonyl tail surfactant and 30 Å for the dodecyl tail.

Figures 2.6a and 2.6b present the radius of the droplets measured by Hwan et al (37), the radius calculated by the Hwan's model, the radius obtained from the net – average curvature model and the droplet radius calculated from the solubilization data. Figures 2.6a and 2.6b show that the droplet radius obtained from the net-average droplet follow the trend of the droplet size measured but has considerably lower values. In both cases, the droplet radius calculated (including the area per molecule of the alcohol) using the solubilization agrees with the values calculated using the net-average model.

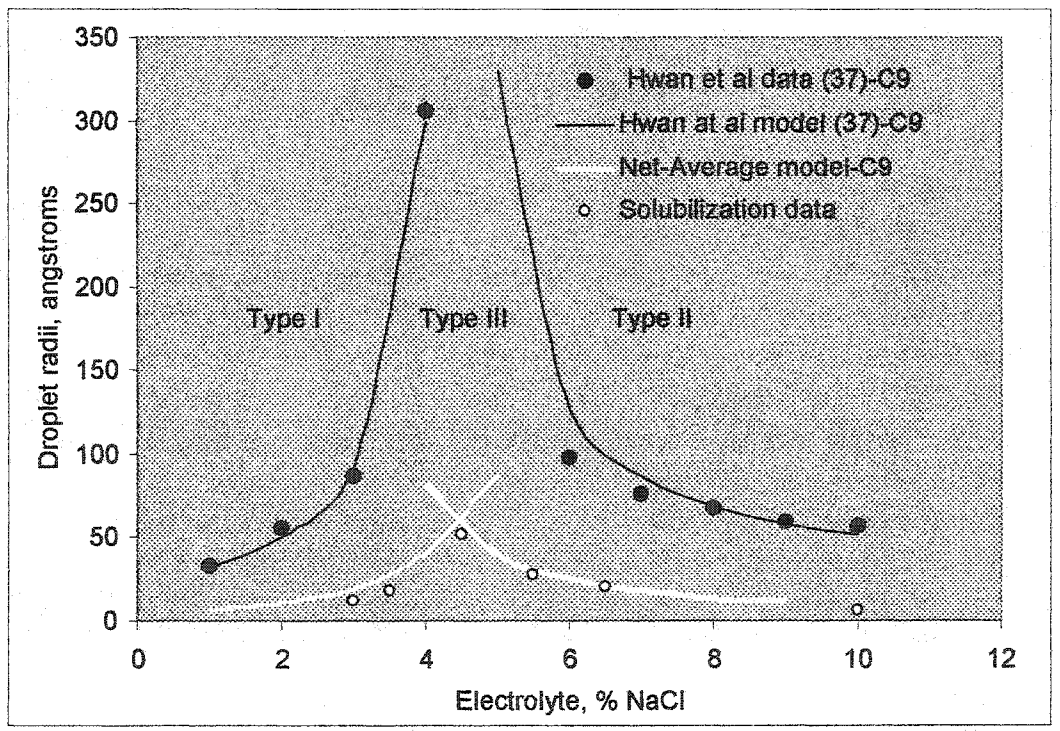

Figure 2.6a. Droplet size of paraffin – aromatic oil with nonyl orthoxylene sulfonate microemulsions.

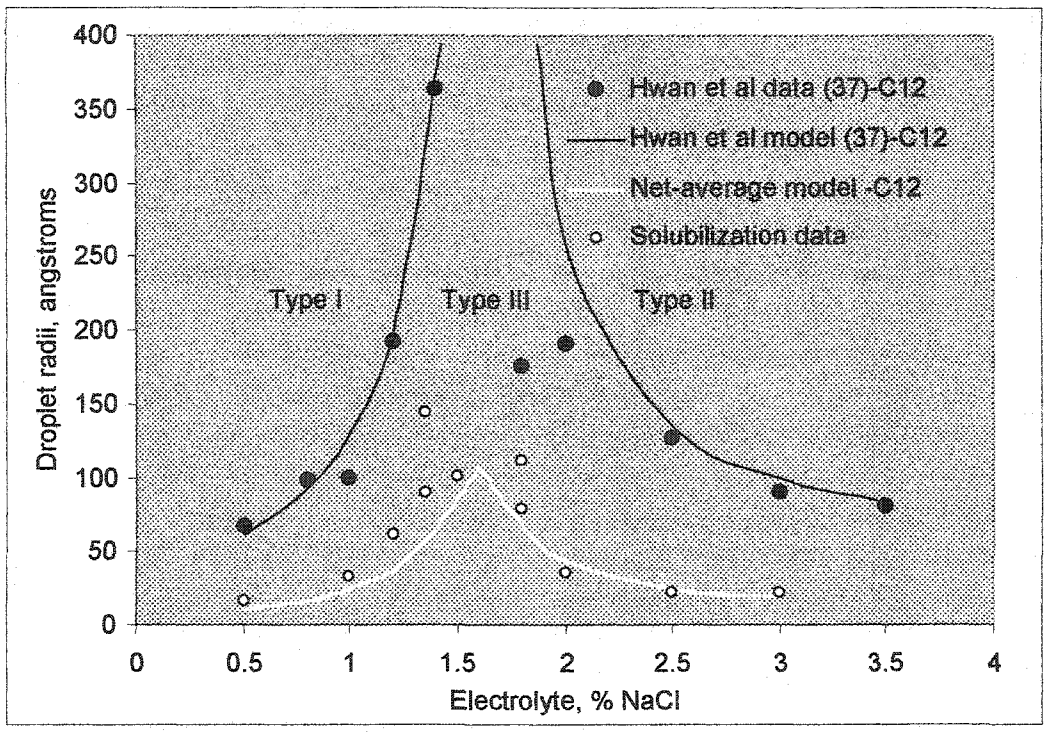

Figure 2.6b. Droplet size of paraffin – aromatic oil with dodecyl orthoxylene sulfonate microemulsions.

The reason for the discrepancy between the net-average curvature model and the Hwan et al. data (37) was somewhat expected because the net-average curvature model only calculates the radius of an equivalent sphere (i.e. internal micelle core), neglecting the volume of the surfactant and alcohol. The radius measured by ultracentrifugation is the hydrodynamic radius of the micelle, which might include hydration of the counterion crown, and for swollen micelles, most likely the real shape is worm-like which increases the hydrodynamic radius as compared to the spherical shape.

Figures 2.6a and 2.6b also present the results of a model proposed by Hwan et al. (37). This model is based on geometrical considerations of the area of the surfactant at the interface. The model reduces to:

$$R = \frac{\delta}{\left(1 - \frac{k_o^{-1}}{k^{-1}}\right)} = \frac{\delta}{\left(1 - \sqrt{\frac{S}{S*}}\right)} \qquad \text{Eq. 17}$$

Where k^{-1} is the Debye length of the ionic surfactant at certain salinity (S) and k^{-1}_0 is the Debye length at the optimum salinity (S*), and R, S and S* are the same as used in equation 7. The parameter δ is the extended length of the surfactant tail. By plotting $1/\ln(S*/S)$ versus $1/(1-(S/S*)^{0.5})$, it can be shown that equations 17 and 7 are linearly correlated. Based on the linear relationship between these equations, it can be deduced that the length parameter "L" is, indeed, a value that scales to the extended length of the surfactant, as the initial results suggested.

Table 2.4 summarizes the length parameter (L) and the extended tail length (δ) used for the different microemulsion systems studied. For the data evaluated, the relation between "L" and "δ" is directly proportional. It is important to recall that when an alcohol cosurfactant ($C_3 - C_8$) is present, the contribution of the alcohol to the interfacial area (As) has to be accounted for. When the previous step is omitted, the length parameter increases and the correlation to the extended length is no longer valid.

Table 2.4. Length parameter "L" used in the net-average curvature model for different microemulsion systems.

Surfactant	Length parameter, "L",Å	Extended length, "δ",Å	Systems
Sodium dihexyl sulfosuccinate alone and in combination with 2-propanol, dodecanol or sodium mono and dimethyl naphthalene sulfonate.	10	9	Trichloroethylene Limonene Styrene Solvent mixture (36)
Sodium dodecyl sulfate in combination with pentanol	20	18	Hexane
Nonyl orthoxylene sulfonate in combination with tert-amyl alcohol	20	17 (37)	Paraffin – Aromatic mixture (37,38)
Dodecyl orthoxylene sulfonate in combination with tert-amyl alcohol	30	27(37)	Paraffin – Aromatic mixture (37,38)

Net – Average model: Interfacial tension

In the previous sections, the net-average curvature model was used to reproduce solubilization data, phase volumes and the droplet sizes of oils in different microemulsion systems. Another physical parameter, the interfacial tension, is the subject of this section. Since interfacial tension does not appear in the net-average model, assessing this parameter required integrating additional equations and models, as previously proposed in the literature.

One of the most common approaches for modeling the interfacial tension in microemulsions makes use of the Helfrich equation of surface free energy of amphiphile membranes (29) explained before.

De Gennes and Taupin (31) have further developed the Helfrich equation into an interfacial tension expression:

$$\gamma \propto \frac{K}{2R^2} \qquad \text{Eq. 18}$$

The value of "K" is somewhat difficult to measure or estimate. Techniques such as electrical birefringence, ellipsometry and interfacial tension measurements have given a wide range of results for the same system (39).

Here, we propose an analogous but somewhat different approach which makes use of the surface energy expression for a spherical droplet, as shown in equation 1. In equation 1, the interfacial tension considered is the bare oil/water interfacial tension. In the following equation (equation 19), we consider the interfacial tension measured when the surfactant is present at a given electrolyte concentration, and where the surface free energy provided by the self-assembly to stabilize the oil "droplet" solubilized is noted as "E_r" or interfacial rigidity:

$$\gamma = \frac{E_r}{4\pi R^2} \qquad \text{Eq. 19}$$

By comparing equations 18 and 19, one can deduce that E_r is proportional to the rigidity constant ($E_r \sim 2\pi K$). To estimate the interfacial tension, solubilization data is used to find the radius (R) of the oil and water droplets. The value of E_r are fitted to

match experimental data. Figures 2.7 and 2.8 show the interfacial tension curves of the dodecyl orthoxylene surfactant + paraffin/aromatic oil system and for the sodium dihexyl sulfosuccinate + trichloroethylene system respectively. Both figures show, in log – log scale, the interfacial tension of the phase containing the surfactant (type I, III or II) with the excess phase (oil or water) as a function of the electrolyte concentration.

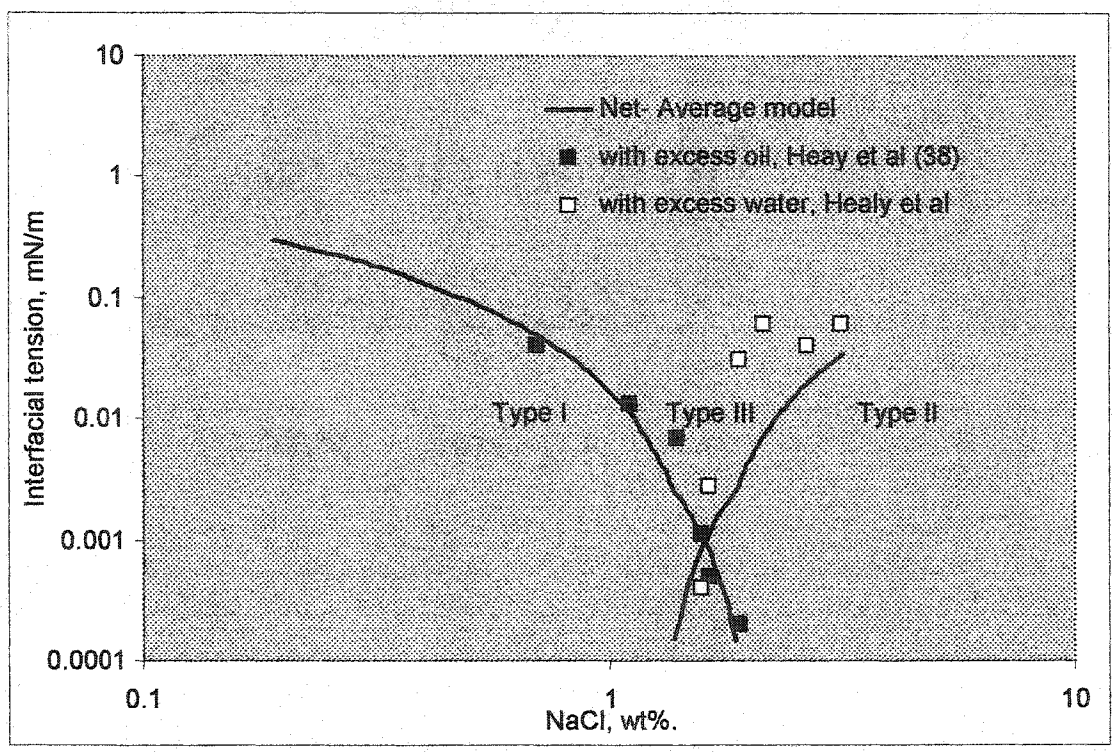

Figure 2.7. Interfacial tension of paraffin – aromatic oil / dodecyl orthoxylene sulfonate microemulsions at 23°C, data points from Healy et al (38).

The black solid curve in Figures 2.7 and 2.8 was constructed using the net-average model and equation 19. For the system in Figure 2.7, "Er" was set to 0.33 k_BT (Boltzmann energy units at 300K). For the system in Figure 2.8, "Er" was set to 1.0 k_BT.

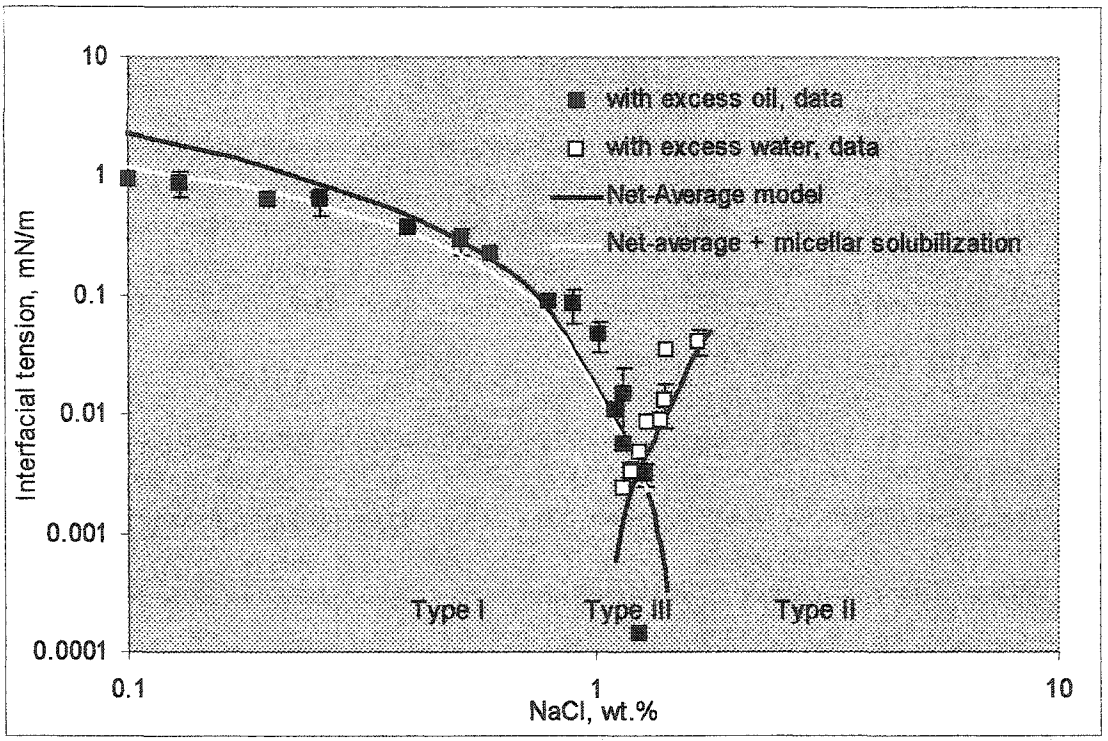

Figure 2.8. Interfacial tension of trichloroethylene / sodium dihexyl sulfosuccinate microemulsions at 27°C.

In general, the net-average model reproduces the experimental data in both cases. For the case of the oil-in-water (type II) microemulsions in Figure 2.7 several points are almost one order of magnitude higher than the value estimated by the model. The rest of the data show good agreement.

The values of "E_r" obtained for both systems are within the range of the values of the bending modulus, "K", reported in the literature (39). For the limonene – sodium dihexyl sulfosuccinate system (not shown here) the value of "E_r" also was found to be 1.0 k_BT. Certain additives, especially short chain cosurfactants, such as tert-amyl alcohol, help to reduce the interfacial rigidity, "E_r". In an upcoming publication, the effect of

additives on the interfacial rigidity and the concomitant effect in the kinetics aspects of coalescence and solubilization will be further developed.

Despite the overall agreement between the net-average model and experimental data, the model has one significant flaw, which is evidenced in Figure 2.8: it tends to over-predict the interfacial tension at low electrolyte concentration. The reason is simple; at low electrolyte concentration the predicted radius (R_o) tends toward zero, and therefore the interfacial tension predicted by equation 19 increases rapidly.

When the simple curvature model was discussed at the beginning of this paper, it was pointed out that the model could not be used to assess simple micellar solubilization because it did not account for the palisade layer solubilization that is so important in this case. In order to account for palisade layer solubilization one more term has to be added to the oil droplet radius, as follows:

$$R_m = R_o + R_p \qquad \text{Eq.20}$$

where R_o is the radius of the oil calculated using the net-average model, R_p is the equivalent radius of the oil solubilized in the palisade layer, and R_m is the modified radius of the oil that accounts for palisade layer solubilization.

The value of R_m is used in equation 19 to calculate the interfacial tension instead of R_o. The white solid line in Figure 2.8 was constructed by introducing this modification, using R_p 1.5 Å. This value of R_p corresponds to a 5000 mg/L of trichloroethylene (TCE) solubilized in a 0.1 M solution of sodium dihexyl sulfosuccinate. When there is no added electrolyte (NaCl), the solubilization of TCE in this surfactant solution was measured as 15000 ± 2000 mg/L. The presence of the surfactant alone

introduces a certain concentration of free sodium (CMC, equivalent to 0.07% NaCl) that accounts for approximately 9500 mg/L (using the net average model). Thus, when the palisade (R_p) and core (R_o) solubilization are added up, one obtains the total micellar solubilization.

While R_p is very important to assess micellar solubilization, it is negligible in the supersolubilization region where the core solubilization (R_o) is at least one order of magnitude higher, and is approaching the solubilization seen in Winsor III microemulsions.

Conclusions

The initial objective of this work was to generate a mathematical model that could reproduce the solubilization behavior in microemulsions systems including the supersolubilization region (i.e., Type I to III transition region). By combining the Kelvin equation of surface energy, the empirical surfactant affinity difference equation and scaling law principles, a simple curvature model was generated.

This simple curvature model used one adjustable length parameter, which was shown to be proportional to the extended length of the surfactant hydrophobic tail, and to be representative of the solubilization capacity of the surfactant. This model was further modified to account for bicontinuous phases. In this case, the coexistence of oil and water droplets and the curvature of the system was described using a net curvature and an average curvature. The latter was shown to be equivalent to the characteristic length of microemulsions.

This net-average curvature model was tested for different microemulsion systems, and it was able to reproduce the experimental solubilization curves, phase volume diagrams, and droplet sizes. Later, introducing an interfacial rigidity concept (E_r, that is shown to be equivalent to the surfactant membrane elastic modulus of microemulsions) we could also reproduce the interfacial tension of these systems.

References.

1. Smith, George A.; Christian, Sherril D.; Tucker, Edwin E.; Scamehorn, John F. Use of the semi-equilibrium dialysis method in studying the thermodynamics of solubilization of organic compounds in surfactant micelles. System n-hexadecylpyridinium chloride-phenol-water *J. Solution Chem.* **1986**, 15(6), 519-529.

2. Smith, George A.; Christian, Sherril D.; Tucker, Edwin E.; Scamehorn, John F. Group contribution model for predicting the solubilization of organic solutes by surfactant micelles. *Langmuir.* **1987**, 3(4), 598-9.

3. Tucker, Edwin E.; Christian, Sherril D. Solubilization of benzene by aqueous sodium octylsulfate: effect of added sodium chloride. *J. Colloid Interface Sci.* **1985**, 104(2), 562-8

4. Rouse, Joseph D.; Sabatini, David A.; Deeds, Neil E.; Brown, R. Eric; Harwell, Jeffrey H. Micellar Solubilization of Unsaturated Hydrocarbon Concentrations As Evaluated by Semiequilibrium Dialysis. *Environ. Sci. Technol.* **1995**, 29(10), 2484.

5. Shinoda, Kozo; Kunieda, Hironobu. Conditions to produce so-called microemulsions. Factors to increase the mutual solubility of oil and water by solubilizer. *J. Colloid Interface Sci.* **1973**, 42(2), 381-7.

6. Diallo, Mamadou S.; Abriola, Linda M.; Weber, Walter J., Jr. Solubilization of Nonaqueous Phase Liquid Hydrocarbons in Micellar Solutions of Dodecyl Alcohol Ethoxylates. *Environ. Sci. Technol.* **1994**, 28(11), 1829-37.

7. Wu, Bin; Harwell, Jeffrey H.; Sabatini, David A.; Bailey, Jason D. Alcohol-free diphenyl oxide disulfonate middle-phase microemulsion systems. *J. Surfactants Deterg.* **2000**, 3(4), 465-474.

8. Pope, G. A.; Wade W. H. Lessons from enhanced oil recovery research for surfactant-enhanced aquifer remediation. *In Surfactant-Enhanced Subsurface Remediation.* Harwell, J.H. and Sabatini, D.A. Eds. ACS Symposium Series 594, Washington, DC, 1995, pp. 142-160.

9. Dwarakanath, V.; Kostarelos, K.; Pope, Gary A.; Shotts, Doug; Wade, William H. Anionic surfactant remediation of soil columns contaminated by nonaqueous phase liquids. *J. Contam. Hydrol.* **1999**, 38(4), 465-488.

10. Nagarajan, R.; Ruckenstein, E. Molecular theory of microemulsions. *Langmuir* **2000**, 16(16), 6400.

11. Binks, Bernard P. *Modern Aspects of Emulsion Science*. Royal Society of Chemistry (publisher), Cambridge, UK **1998**, 1-55.

12. Promod Kumar and K.L. Mittal, Editors. *Handbook of Microemulsion Science and Technology*. Marcel Dekker, Inc., New York, 1999.

13. Gompper, Gerhard; Schick, Michael. In *Micelles, Membranes, Microemulsions and Monolayers*. Gelbart, W. M., Ben-Shaul, A. and Roux, D. Eds.; Springer-Verlag, New York, 1994, p 395-426.

14. Davis, H. T. *Statistical Mechanics of Phases, Interfaces and Thin Films*. VCH publishers, New York (1996), 712 pp.

15. Ruckenstein, E.; Krishnan, R. The equilibrium radius of microemulsions formed with ionic surfactants. *J. Colloid Interface Sci.* **1980**, 75(2), 476-92.

16. Huh, Chun. Interfacial tensions and solubilizing ability of a microemulsion phase that coexists with oil and brine. *J. Colloid Interface Sci.* **1979**, 71(2), 408-26.

17. Safran, S. A. In *Micelles, Membranes, Microemulsions and Monolayers*. Gelbart, W. M., Ben-Shaul, A. and Roux, D. Eds.; Springer-Verlag, New York, 1994, p 427-84.

18. Salager, J.L.; Antón R.E. *In Handbook of Microemulsion Science and Technology*. Kumar, P., Mittal, K.L. Marcel Dekker, New York, 1999. p 247-280

19. Salager, J. L.; Marquez, N.; Graciaa, A. and Lachaise J. Partitioning of Ethoxylated Octylphenol Surfactants in Microemulsion-Oil-Water Systems: Influence of Temperature and Relation between Partitioning Coefficient and Physicochemical Formulation. *Langmuir* **2000**, 16, 5534

20. Marquez, N.; Anton, R. E.; Graciaa, A. ; Lachaise J. and Salager J. L. Partitioning of ethoxylated alkylphenol surfactants in microemulsion-oil-water systems. *Colloids Surf. A* **1995**, 100, 225

21. Strey, R. Microemulsion microstructure and interfacial curvature. *Colloid Polym. Sci.* **1994**, 272(8), 1005-19.

22. Kabalnov, Alexey S. *Modern Aspects of Emulsion Science*. Royal Society of Chemistry (publisher), Cambridge, UK **1998**, 205-260.

23. Bourrel, M. and Schecter R. *Microemulsions and related systems*. Marcell Dekker Inc. New York, 1988.

24. Huang, John S.; Kim, Mahn Won. Critical scaling behavior of microemulsion systems. *Soc. Pet. Eng. J.* **1984**, 24(2), 197-202.

25. Dorshow, R.; Briggs, J.; Bunton, C. A.; Nicoli, D. F. Dynamic light scattering from cetyltrimethylammonium bromide micelles. Intermicellar interactions at low ionic strengths. *J. Phys. Chem.* **1982**, 86(13), 2388-95.

26. Uchiyama, Hirotaka; Acosta, Edgar; Tran, San; Sabatini, David A.; Harwell, Jeffrey H. Supersolubilization in Chlorinated Hydrocarbon Microemulsions: Solubilization Enhancement by Lipophilic and Hydrophilic Linkers. *Ind. Eng. Chem. Res.* **2000**, 39(8), 2704-2708

27. Acosta, Edgar; Uchiyama, Hirotaka; Sabatini, David A.; Harwell, Jeffrey H. The role of hydrophilic linkers. *J. Surfact. Deterg.* **2002**, 5(2), 151-157.

28. Ezrahi, S. Aserin, A. and Garti, N. *In Handbook of Microemulsion Science and Technology*. Kumar, P., Mittal, K.L. Marcel Dekker, New York, 1999. p 247-280

29. Helfrich, W. Elastic properties of lipid bilayers. Theory and possible experiments. *Z. Natureforsch.* **1973**, 28c, 693

30. Kegel, W. K.; Overbeek, T. G. and Lekkerkerker H. N. W. *In Handbook of Microemulsion Science and Technology*. Kumar, P., Mittal, K.L. Marcel Dekker, New York, 1999. p 13-44

31. De Gennes, P.G. and Taupin C. Microemulsions and the flexibility of oil/water interfaces. *J. Chem Phys.* **1982**, 86, 2284.

32. De Gennes, P.G. Polymers at an interface; a simplified view. *Adv. Colloid Interface Science*. 27, 189-209.

33. Israelachvili J. N. *Intermolecular and Surface Forces*. 2nd ed., Academic Press, New York, 1992

34. Bourrel, M. and Chambu, C. The rules for achieving high solubilization of brine and oil by amphiphilic molecules. *J. Soc. Pet. Eng.* **1983**, 23, 327.

35. Rosen, M.J. *Surfactants and interfacial phenomena*. 2nd. Ed. John Wiley & Sons, New York, 1989, pp 431

36. Dwarakanath, V.; Pope, Gary A. Surfactant Phase Behavior with Field Degreasing Solvent. *Environ. Sci. Technol.* **2000**, 34, 4842-4848

37. Hwan, Rei-Nan; Miller C.A.; Fort, T. Determination of microemulsion phase continuity and drop size by ultracentrifugation. *J. Colloid Interface Sci.* **1979**, 68(2), 221-234.

38. Healy, R. N.; Reed, R. L.; Stenmark, D. G. Multiphase microemulsion systems. *J. Soc. Pet. Eng.* **1976**, 16, 147-160.

39. Langevin, Dominique; Meunier, Jacques. In *Micelles, Membranes, Microemulsions and Monolayers*. Gelbart, W. M., Ben-Shaul, A. and Roux, D. Eds.; Springer-Verlag, New York, 1994, p 485-515.

CHAPTER 3

Net-average curvature model of microemulsions: predictions and measurements using small angle neutron scattering, dynamic light scattering and NMR techniques.

Abstract

Previously we introduced the net-average curvature model of microemulsions to model the solubilization capacity, phase transitions, phase volumes and interfacial tensions of microemulsion systems. The model was based on a simple critical scaling approach of the net curvature of surfactant membranes. The net-average curvature model was based on certain premises: e.g., the area per surfactant molecule is a constant value, that virtual oil and water spherical droplets occur in the phases, and that virtual oil and water droplets coexist in bicontinuous microemulsions with a constant characteristic length. This work seeks to obtain direct insight into the nanoscale environment of microemulsions through the use of small angle neutron scattering (SANS), dynamic light scattering (DLS) and nuclear magnetic resonance (NMR), and to compare the microemulsion morphology with that predicted by the net-average curvature model. Neutron scattering and dynamic light scattering experiments were performed on toluene microemulsions formulated with the surfactant sodium dihexyl sulfosuccinate (SDHS), while the NMR data was extracted from literature data on toluene microemulsions formulated with sodium dodecyl sulfate (SDS) and butanol. The SANS scattering

patterns, which were obtained for systems with increasing electrolyte concentration, show that as Type I microemulsion aggregates increase in size they pass from a spherical shape into a cylindrical shape. The trend of increasing size with electrolyte concentration is consistent between the DLS and SANS measurements and the net-average curvature model prediction. The net-average curvature model was able to predict the characteristic length of bicontinuous microemulsions but not the exact size of droplet-type microemulsions. Further investigation of the area per surfactant molecule using a Porod analysis reveals that for droplet type microemulsions the area of the surfactant per molecule projected in the interior of the micelle, or reverse micelle, varies as a function of electrolyte. In addition, this variation is within the limits of the minimum area for head/tail packing and the area per molecule predicted by the Gibbs adsorption model applied to surface and interfacial tension data. The net-average curvature model was used to predict the self-diffusion coefficient of bicontinuous and droplet-type microemulsions and these values are in agreement with literature data for the toluene-SDS+butanol system. After analyzing all the experimental evidence we conclude that the net-average curvature model reproduces the trends shown by the SANS, DLS and NMR data. When modified to account for the non-constant surfactant area per molecule, the model predictions agree with the size of the aggregates obtained by SANS and DLS measurements.

Key words: microemulsion, solubilization, SANS, NMR, DLS, scattering, model.

Introduction

The net-average curvature model.

Recently we have introduced the net-average curvature model to predict the solubilization capacity, phase transitions, phase volumes and interfacial tension of microemulsion systems (1). The net-average curvature model uses a critical scaling approach to predict the size of the microemulsion aggregates (1,2):

$$\xi = \frac{\xi_o}{\left|(\Delta\mu^*_s)\right|^n} \qquad \text{Eq. 1}$$

where ξ is a length parameter related to the radius of the oil solubilized in type I microemulsions, ξ_0 is a length constant, n is the scaling exponent, and $\Delta\mu^*_S$ is the difference in chemical potential between the actual thermodynamic state and the "critical" point. The appropriate length scale (ξ) to be used in Equation 1 was found to be the inverse of the net curvature of the surfactant membrane ($1/H_N$). This net curvature was calculated based on the assumption of the coexistence of virtual oil and water spherical droplets:

$$H_N = \left|H_O\right| - \left|H_W\right| = \frac{1}{R_o} - \frac{1}{R_w} \qquad \text{Eq. 2}$$

where R_o and R_w are the radii of oil and water virtual droplets. Equation 2 supposes that the net curvature is positive for Type I (micelles) microemulsions and negative for Type II (reverse micelles). Bicontinuous microemulsions have a near zero curvature.

The chemical potential difference ($\Delta\mu^*_S$) in Equation 1 corresponds to the free energy change per unit of surfactant molecule that is required to change the membrane

curvature from a given curvature value to the critical curvature point. The critical curvature point was selected as the point where the net curvature is flat (i.e. Hn=0). At this condition the microemulsion system contains equal amounts of oil and water, and the properties of these bicontinuous system are in between the properties of the oil and water.

We proposed to use the surfactant affinity difference (SAD) concept to account for the chemical potential difference ($\Delta\mu^*$). The SAD for ionic surfactant systems as introduced by Salager et al. (3,4,5), is as follows:

$$SAD^{\#} = \frac{SAD}{RT} = \frac{\mu_o^s - \mu_w^s}{RT} = -\ln S + K \times ACN + f(A) - \sigma + a_t(T - T_{ref}) \qquad \text{Eq. 3}$$

where $SAD^{\#}$ is the dimensionless form of SAD, R is the ideal gas constant, T is the absolute temperature of the system, the term $\mu^s_o - \mu^s_w$ is the chemical potential difference for transferring the surfactant molecule from the aqueous to the oil phase, S is the electrolyte concentration, K is a constant for a given surfactant (ranging from 0.1 to 0.2), and ACN is the alkane carbon number of the oil (for non-hydrocarbon ACN becomes EACN; equivalent-ACN). The parameter f(A) is a function of the alcohol/cosurfactant concentration, σ is a parameter that is a function of surfactant, a_t is a constant , (~ 0.01 when temperature is in Celsius), and T_{ref} is a reference temperature.

Equation 3 reaches the value of zero at "optimum formulation" which corresponds to the critical curvature point where, for a given oil, surfactant and water system, the bicontinuous microemulsion contains the same amount of oil and water and the net curvature of the surfactant membrane is flat. The electrolyte concentration that can achieve this critical condition is called the optimum salinity (S*). By introducing this

concept into Equation 3 and combining with Equation 1 and 2, and using a scaling exponent of 1 (n=1) selected from dimensional analysis using the Kelvin equation (1), we obtain:

$$H_N = \frac{1}{R_O} - \frac{1}{R_W} = \frac{SAD^{\#}}{\xi_0} = \frac{1}{\xi_0} \times \left[\ln \frac{S^*}{S} \right] \qquad \text{Eq. 4}$$

According to Equation 4 the aggregate size grows as the system approaches the critical curvature point. We introduce the average curvature equation as a means to obtain the average aggregate size and restrict their growth to a certain optimum characteristic length (ξ^*). This value, analogous to the correlation length of polymers, indicates the maximum length that an oil or water molecule can be separated from the surfactant membrane and still be influenced or have an effective interaction with the membrane. This average curvature equation is (1):

$$H_a = \frac{1}{2}\left(\left| \frac{1}{R_o} \right| + \left| \frac{1}{R_w} \right| \right) \geq \frac{1}{\xi^*} = \frac{n_s a_s}{6\phi_o \phi_w V_m} \qquad \text{Eq.5}$$

where H_a is the average curvature, n_s is the number of surfactant molecules in the system aggregated at the interface, a_s is the area per molecule of the surfactant at the interface, ϕ_o and ϕ_w are the volume fractions of oil and water in the bicontinuous system, and V_m is the volume of the middle phase bicontinuous system.

Equation 4 is used to calculate the oil or water radius in droplet type microemulsions (Type I or Type II microemulsion systems respectively) at different electrolyte concentration (S), using the optimum salinity of the system (S*), and the length constant (ξ°) which is proportional to the extended length of the surfactant tail (1).

For Type III bicontinuous systems Equations 4 and 5 are solved simultaneously (knowing the characteristic length of the system ξ^*).

There are several assumptions in Equations 4 and 5. One assumption is that the aggregates are spherical droplets. A second assumption is that the surfactant area per molecule (a_s) is a constant value independent of the curvature of the surfactant membrane, and a third assumption was that bicontinuous systems could be represented by coexistent oil and water droplets with an average curvature equal to the characteristic length of the system (1).

The net-average curvature model was initially developed and tested based on phase behavior data, which includes solubilization, phase transitions, phase volumes and interfacial tension data (1). "Droplet size" values were not directly measured but were rather estimated based on solubilization data and surfactant areas per molecule as obtained from the Gibbs equation and surface or interfacial tension data. The objective of this work is to obtain more direct measurements of droplet sizes and morphologies in an effort to further validate the net-average curvature model for describing the nanoscale environment of microemulsion systems.

In this work we use three spectroscopic techniques to investigate the nanoscale environment of toluene microemulsions (Types I, III and II): small angle neutron scattering (SANS), dynamic light scattering (DLS), both of which were measured in this work, and nuclear magnetic resonance (NMR) studies previously reported in the literature. We will compare the morphology of the microemulsion aggregates obtained by these techniques with that predicted by the net-average curvature model.

Small Angle Neutron Scattering (SANS) studies of microemulsions.

SANS techniques have been used in studying microemulsion morphology for the last 20 years (6,7,8,9,10,11). In SANS a neutron beam of wavelength λ is passed through the sample and the intensity of neutron scattering I(q) is obtained as a function of the magnitude of the scattering vector (q), where $q=[4\pi\sin(\theta/2)]/\lambda$ and θ is the scattering angle[†]. The relationship between I(q) versus q has two main contributions: scattering due to interference between aggregates, the structure factor (S(q)), and scattering due to the size and shape of the individual aggregates, the form factor (P(q)). The overall scattering pattern can be written as (6):

$$I(q)=P(q)*S(q) \qquad \text{Eq.6}$$

The appropriate expressions for a number of structures and form factors, as well as numerical solutions for these equations, can be found elsewhere (12). These models will be described later during the discussion associated with fitting the experimental scattering patterns. Porod's model has been widely used in interpreting neutron scattering data, which, for spherical droplets with sharp interfaces and at large enough q, can be written as (6):

$$I(q)=2\pi(n_w-n_o)^2 c_s a_s q^{-4} \qquad \text{Eq. 7}$$

where n_w and n_o are the scattering length densities (SLDs) of the water and oil, c_s is the concentration of the surfactant, a_s is the area per molecule of the surfactant, and I(q) and q are as defined before. Equation 7 presumes that the SLD of the surfactant has been

---

[†] In this work, scattering was isotropic. The discussion and analysis assumes this convention.

matched to the SLD of the continuous phase (water for Type I microemulsions and oil for Type II, we will refer to this as the droplet contrast) by using adequate mixtures of hydrogenated and deuterated species as will be described in the experimental section. In this model the surfactant film is "invisible" in terms of neutron scattering.

By matching the SLD of the oil and the water phases ($n_w = n_o$), rather than a droplet, a hollow shell structure consisting of the surfactant film will be "seen" by neutron scattering; in this case Porod's model becomes (6):

$$I(q)=2\pi(n_s-n_o)^2c_sa_sd^2q^{-2} \qquad \text{Eq. 8}$$

where n_s is the SLD of the surfactant and d is the thickness of the surfactant film.

Equations 7 and 8 only apply to high q values, and are commonly used to determine the area per molecule of the surfactant and the thickness of the surfactant film (6,11,13,14,15). We will use these equations to determine these parameters for the toluene-sodium dihexyl sulfosuccinate (SDHS) - water system investigated in this work.

Dynamic Light Scattering (DLS) studies of microemulsions.

We also use dynamic light scattering (DLS) to determine the hydrodynamic radius of the droplet type microemulsions (Type I and II microemulsions) (16,17,18). In this technique, the time-based variation of the scattering intensity at a given angle, (normally 90 degrees) is adjusted to a model where the time constant is used to determine the diffusion coefficient of the colloidal particle. The hydrodynamic radius is obtained from the diffusion coefficient using the Stokes-Einstein equation:

$$D_{\mathit{eff}} = \frac{k_B T}{6\pi\mu R_H} \qquad \text{Eq. 9}$$

where D_{iff} is the diffusion coefficient, μ is the viscosity of the continuous phase k_B is the Boltzman constant and R_H is the hydrodynamic radius of the colloid particles (droplets). We will compare the hydrodynamic radius of the droplet-type microemulsions with the radius predicted by the net-average curvature model.

NMR studies of Self-diffusion coefficients in microemulsions.

The final spectroscopic data used to benchmark the model is the self-diffusion measurements determined using pulse-gradient nuclear magnetic resonance. This technique monitors the relaxation of the magnetic moment of H^1 nuclide after a magnetic pulse. The initial pulse causes an orientation of the magnetic moments of the hydrogen-containing molecules, but after the pulse the molecular diffusion causes a disarrangement of this orientation which in turn produces a first order kinetic decay on the NMR signal. The time constant of this decay is then used to obtain the self-diffusion coefficient of the test molecule (19). This data demonstrates the mobility of molecules in confined colloidal space. For example in the case of oil contained in droplets their diffusion is regulated by the droplet size constriction and can be calculated using Equation 9. For the case of bicontinuous systems, this technique has revealed that oil and water molecules are relatively "free" within their phase and that the only restriction is that the volume fraction of such a phase in the bicontinuous system is less than one. For the case of bicontinuous systems the following equation has been proposed to predict the self-diffusion coefficients (19):

$$D_{iff}/D^0_{iff} = 0.66 + \beta(\phi - 1/2) \qquad \text{Eq. 10}$$

where D^0_{iff} is the diffusion coefficient of the pure phase (oil or water), β is the expansion coefficient which normally ranges between 0.6 and 0.8 (the higher values correspond to a more interconnected network of bicontinuous channels), and ϕ is the volume fraction of either oil or water in the bicontinuous phase.

For the NMR self-diffusion coefficient studies, we use literature data for the system sodium dodecyl sulfate (SDS) - butanol - toluene to fit the net-average curvature model. Using the model we will predict droplets sizes for Type I and Type II microemulsions and volume fractions of bicontinuous systems. With these values we will estimate the self-diffusion coefficients using Equations 9 and 10 and will compare these results with literature self-diffusion data for this system (20).

Experimental Section

Microemulsion phase behavior studies.

Microemulsion systems were formulated using sodium dihexyl sulfosuccinate (Fluka brand, 80% aqueous solution), toluene in either its hydrogenated form (Adrich brand, 99+%) or in its deuterated form (Aldrich brand, 99+%), nanopure water (18 MΩ/cm, Barnstead Nanopure® Infinity Base system) and/or deuterated water (Aldrich brand, 99+%). Sodium chloride (Fisher brand, 99.9+%) was added in increasing amounts to obtain the phase transition between microemulsion phases Type I-III-II. The oil to aqueous volume ratio was kept at 1/1 by adding 5 ml of aqueous solution containing the prescribed surfactant and electrolyte concentration to 5 ml of toluene in a 15-ml flat bottom test tube sealed with a Teflon-lined screwed cap. After mixing, the systems were

kept at room temperature (300K) and left to equilibrate for two weeks before analysis. The surfactant concentration in the microemulsion phase was measured using a Dionex 500 ionic chromatographic system, the toluene concentration was obtained using a UV-VIS Hewlett Packard model 8452 diode array spectrophotometer set at a wavelength of 260 nm. The phase volumes of the bicontinuous systems were obtained by measuring the heights of the separated phases. Additional experimental details can be found elsewhere (1,21). Table 3.1 summarizes the formulation and microemulsion types and composition for the systems containing hydrogenated toluene and hydrogenated water. Interfacial tension values between the excess phases was determined using a Texas 500 spinning drop tensiometer, following procedures described elsewhere (1,21).

Table 3.1. Microemulsion composition for the system hydrogenated water - sodium dihexyl sulfosuccinate (SDHS) - toluene and sodium chloride as electrolyte.

NaCl, g/100ml of aqueous solution	Phase Type	Surfactant SDHS % volume fraction in microemulsion phase	Water + NaCl % volume fraction in microemulsion phase	Toluene % volume fraction in microemulsion phase	Volume of microemulsion (ml)
1.2	I	3.9	94.7	1.4	5.07
1.7	I	3.8	91.9	4.3	5.21
2	I	3.8	90.5	5.7	5.29
2.3	I	3.7	87.7	8.6	5.43
2.5	III	9.7	60.0	30.3	2.36
3	III	13.2	42.5	44.3	2.25
3.5	III	9.2	21.4	69.4	2.57
3.8	II	3.7	6.5	89.8	5.36
4.1	II	3.8	5.1	91.1	5.28
4.5	II	3.8	4.7	91.5	5.21
6	II	3.9	3.8	92.3	5.15

Neutron scattering experiments.

Neutron scattering experiments were performed at the National Institute of Standards and Technology (NIST) Center for Neutron Research (NCNR, Gaithersburg, MD) NG7-30m SANS instrument using a neutron beam with λ = 6Å with the detector positioned at three different distances (1m, 4m and 15m) to give a combined q-range between 0.004 to 0.5 $Å^{-1}$. The two dimensional scattering data obtained at the three different distances were normalized, masked, and integrated to an I vs. q form for each distance, and later combined into a single I vs. q curve for each sample using the SANS data reduction software available through the NCNR website (22). The combined I vs. q data was later modified by subtracting the scattering background inherent to the amount of water and toluene present in each system. The measurements were made at room temperature with 1-mm cell path length titanium cells assembled using Teflon o-rings to prevent leakage of the toluene-containing samples.

Two sets of samples were prepared: one with the same formulation as the systems presented in Table 3.1 using a water-oil contrast and the second set using a film contrast. Table 3.2 summarizes the compositions on deuterated water and toluene used in the different sets for different microemulsion types and the absolute contrast obtained in each case. As an example, in Type I microemulsion systems prepared with an oil/water contrast the oil was deuterated toluene (C_7D_8) with a neutron scattering length density of 5.6E-6 $Å^{-2}$ and the aqueous phase was composed of 20% deuterated water (SLD= 6.3E-6 $Å^{-2}$) and 80 % hydrogenated water (SLD= -0.56E-6 $Å^{-2}$) to give an overall aqueous SLD of ~0.8 E-6 $Å^{-2}$ that matches the SLD estimated for the SDHS surfactant molecule using

on-line SLD calculators available from the NCNR website (23). The absolute contrast in this example is (5.6-0.8) E-6 $Å^{-2}$ = 4.8 E-6 $Å^{-2}$. The same kind of procedure was used in designing the composition of the rest of the systems presented in Table 3.2. One interesting note is that the systems formulated with 90% or more of deuterated water showed a slight decrease (~10%) in the amount of salt required compared to the hydrogenated water systems.

Table 3.2. Contrast match series used in SANS studies

Microemulsion Type	Contrast	% of D_2O in water	% C_7D_8 in oil	Contrast 1E-6 $Å^2$
I	Water-Oil (W/DO)	20	100	4.8
I	Film (DW/DO)	90	100	4.8
III	Water-Oil (DW/O)	100	0	5.4
III	Water-Oil (W/DO)	20	100	4.8
III	Film (DW/DO)	90	100	4.8
II	Water-Oil (DW/O)	100	0	5.4
II	Film (DW/DO)	90	100	4.8

Dynamic light scattering experiments.

The dynamic light scattering experiments were performed at room temperature using a BI-90 Brookhaven instrument. Samples of the Type I and Type II microemulsion systems were placed in standard 1-cm glass cells that were placed in the BI-90 sample holder at least 30 minutes before the measurement. Each sample was measured three times. The viscosity of the microemulsion phase was measured using a U-tube viscometer and this value was entered to the computer to calculate the average hydrodynamic radius. The refractive index of the continuous phase at 650 nm and 300K

(water 1.332 for Type I microemulsions and toluene 1.489 for Type II microemulsions, reference 24) was entered to the algorithm used to calculate the particle size.

NMR self-diffusion data

As indicated above, we used literature data of phase behavior studies for the system toluene - SDS - butanol - water to adjust the curvature model to predict self-diffusion values that are then compared with NMR self-diffusion measurements made on this system (20). Table 3.3 contains the formulation data for this system as reported by Guering and Lindman along with the calculated volume of the microemulsion phase for a 20 ml total volume system prepared at an oil/water volume ratio of 1:1.

Table 3.3 Microemulsion composition for water - sodium dodecyl sulfate - butanol - toluene systems with sodium chloride as electrolyte.

NaCl, g/100ml of aqueous solution	Phase Type	SDS wt. % in microemulsion phase (a)	Butanol wt. %. In microemulsion phase (a)	Brine wt. % in microemulsion phase (a)	Toluene wt. % in microemulsion phase (a)	Volume of microemulsion (ml)
3	I	3.6	3.5	84.7	8.2	11.1
4	I	3.6	3.4	83.4	9.6	11.1
4.5	I	3.4	3.4	80.9	12.3	11.8
5	I	3.4	3.4	78.9	14.3	11.8
5.7	III	4.5	4.1	64	27.4	8.9
6	III	4.9	4.3	57.2	33.6	8.2
6.3	III	5.2	4.6	51.4	38.8	7.7
6.7	III	5.3	4.9	43.7	46.1	7.5
7	III	5.1	5.0	38.2	51.7	7.8
8	II	3.1	5.3	16.8	74.8	12.9
8.5	II	3.2	5.4	15.3	76.1	12.5
9	II	3.3	5.5	13.9	77.3	12.1
9.5	II	3.3	5.6	12.6	78.5	12.1
10	II	3.3	5.7	11.8	79.2	12.1

a) Data extracted from Guering and Lindman, reference 20.

Results and discussions

Phase behavior studies and the net-average curvature model

Tables 3.1 and 3.3 present the compositions of the microemulsion phases prepared with SDHS and SDS + butanol respectively. In order to fit the net-average curvature model to these data, the solubilization of toluene and brine presented as volume fractions in these tables are transformed into equivalent spherical radius as follows:

$$R = \frac{3V}{\sum_i N_{av} n_i a_i} \qquad \text{Eq. 11}$$

where R is the radius of either oil (toluene) or water and "V" is the volume of oil or water in the microemulsion as obtained by multiplying the oil or water fraction by the volume of the microemulsion presented in each table. The denominator of Equation 11 is the total interfacial area provided by the adsorption of the surfactant at the oil/water interface, n_I is the number of moles of the surfactant present in the microemulsion, a_I is the area per molecule of the surfactants / cosurfactants present in the microemulsion and N_{av} is the Avogrado's number. The number of molecules of each surfactant are obtained from the mass of each surfactant in the microemulsion using their compositions in Tables 3.1 and 3.3, and the molecular weight of each surfactant (386 g/mol for SDHS, 272 g/mol for SDS and 74 g/mol for butanol). Regarding the area per molecule of the surfactants we use reported values for SDHS of 95$Å^2$/molecule (1,25,26), of 60 $Å^2$/molecule for SDS (13,26) and of 20 $Å^2$/molecule for butanol based on previous studies with similar alcohol and non-ionic surfactant molecules (1,26). The SDHS and SDS area per molecule values

were obtained after applying the Gibbs adsorption equation to surface and interfacial tension data.

Figure 3.1 shows the solubilization data of oil and water expressed as equivalent spherical droplet calculated using the procedure explained above. The net-average curvature model was used to fit both the solubilization data of the system SDHS-toluene (Figure 3.1a) and the system of SDS-butanol-toluene (Figure 3.1b). The model parameters are indicated in the respective figures. The optimum salinity (S*) data was determined as the salinity that leads to a microemulsion systems containing equal amounts of oil and water. The characteristic length (ξ^*) was taken as the radius of oil or water (they are the same at S*) at the optimum formulation conditions. Thus, the scaling length constant (ξ^o) is the only parameter that is adjusted in the model to fit the data.

The characteristic length of ξ^*=65 Å for the SDHS-toluene is consistent with a range of characteristic lengths found for SDHS systems with a variety of oils and will be discussed further in light of the SANS measurements (1). For the case of the SDS-butanol system the characteristic length of ξ^* = 95 Å is consistent with literature values (92 Å and 117 Å) determined using SANS.

Regarding the scaling length, the value of ξ^o = 10 Å for the SDHS-toluene system is the same value found for other SDHS systems previously studied (1). For the case of the SDS-butanol-toluene system the value of ξ^o = 15 Å is somewhat smaller than the value expected from the extended surfactant tail length (for 12 carbon tail, ξ^o ~20 Å) versus 10Å for 6 carbon tail SDHS. In this case the microemulsion is not formulated with

a single surfactant but with a mixture of surfactants, and considering that butanol has a shorter extended tail than SDS, a shorted effective tail length could be expected.

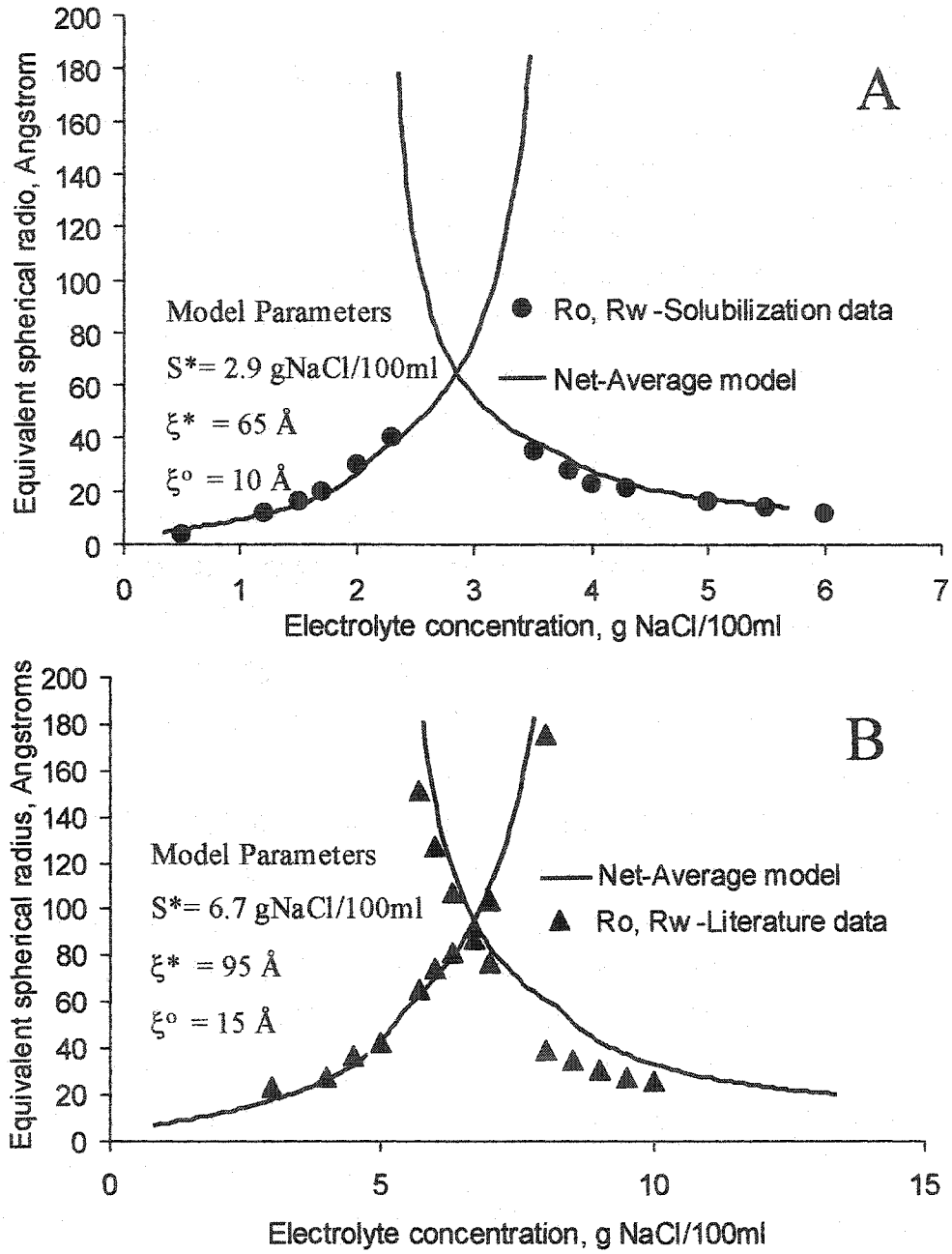

Figure 3.1. Equivalent spherical droplet radius based on solubilization data and the corresponding net-average curvature model fit. Part A corresponds to the sodium dihexyl sulfosuccinate (SDHS) - toluene system. Part B corresponds to SDS-butanol-toluene data from Guering and Lindman, reference (20)

Small Angle Neutron Scattering studies.

Table 3.4 summarizes the neutron scattering experiments performed on the system sodium dihexyl sulfosuccinate (SDHS) - toluene, including the type of contrast, models used to fit the scattering curves and the morphology parameters obtained after fitting the respective models. Figure 3.2 shows an example of scattering curves (dotted curves) for oil/water contrast as a function of the electrolyte concentration and microemulsion type. The model fit for each curve is also presented as a solid line, which is barely visible in some instances because of overlap with the data.

At low electrolyte concentration (1.2 g/100ml of NaCl) the best fit to the scattering curves was obtained assuming spherical oil droplets with no structure factor. The form factor (P) for spherical aggregates is (27):

$$P(q) = 3\phi V(n_o - n_w)^2 \left[\frac{\sin(qr) - qr\cos(qr)}{(qr)^3} \right]^2 \qquad \text{Eq. 12}$$

where ϕ is the volume fraction of the spheres, V is the volume of the individual sphere, q is the scattering vector and r is the radius of the spheres. The experimental data of selected systems (indicated in Table 3.4) were fitted to Equation 12 using software available through the NIST web site, which included the appropriate smearing procedures (12,22). Equation 12 is appropriate for a monodisperse system, but the SDHS-toluene system contains a distribution of micelle sizes typical of surfactant-based colloids (28). The level of polydispersity was qualitatively assessed using neutron beam wavelength dispersion. This procedure resulted in a $\Delta\lambda/\lambda \sim 0.5$, where the real wavelength dispersion is around $\Delta\lambda/\lambda \sim 0.1$. We then performed a numerical integration of the normal

distribution probability curve of the scattering models, good fit was obtained using a standard deviation of 40% the average radius size. These standard deviations are indicated in Table 3.4 as the ± interval indicated in the respective radii values.

Table 3.4. Small angle neutron scattering (SANS) morphology parameters for SDHS - toluene microemulsions.

NaCl, g/100ml	% SDHS in water	Phase Type	Contrast	Structure factor (S)	Form Factor (P)	Morphology parameters
1.2	4	I	W/DO	Flat = 1	Sphere	R= 35 ± 15 Å
1.7	4	I	W/DO	Flat = 1	Cylinder	R= 50 ± 20 Å ; L= 100 Å
2	4	I	W/DO	Flat = 1	Cylinder	R= 65 ± 20 Å ; L= 175 Å
2.3	4	I	W/DO	Flat = 1	Cylinder	R= 70 ± 25 Å ; L= 3500 Å
1.2	1	I	W/DO	N.D.	N.D.	N.D.
1.7	1	I	W/DO	Flat = 1	Cylinder	R= 40 ± 20 Å ; L= 80 Å
2	1	I	W/DO	Flat = 1	Cylinder	R= 55 ± 20 Å ; L= 90 Å
2.3	1	I	W/DO	Flat = 1	Cylinder	R= 70 ± 25 Å ; L= 240 Å
1.1	4	I	DW/DO	Flat = 1	Core-Shell sphere	R= 30 ± 10 Å ; d= 10 Å
1.5	4	I	DW/DO	Flat = 1	Core-Shell cylinder	R= 45 ± 15 Å ; L= 60 Å ; d= 10 Å
1.8	4	I	DW/DO	Flat = 1	Core-Shell cylinder	R= 55 ± 20 Å ; L= 150 Å ; d= 10 Å
2.1	4	I	DW/DO	N.D.	N.D.	N.D.
2.3	4	III	DW/O	Teubner - Strey		ξ = 72 Å , d'= 282 Å
2.8	4	III	DW/O	Teubner - Strey		ξ = 69 Å , d'= 236 Å
3.3	4	III	DW/O	N.D.		N.D.
2.5	4	III	W/DO	Teubner - Strey		ξ = 81 Å , d'= 268 Å
3	4	III	W/DO	Teubner - Strey		ξ = 68 Å , d'= 244 Å
3.5	4	III	W/DO	N.D.		N.D.
2.3	4	III	DW/DO	Strey - Winkler - Magid		d = 7.0 Å, a_s = 91 Å^2/mol
2.8	4	III	DW/DO	Strey - Winkler - Magid		d = 6.6 Å, a_s = 116 Å^2/mol
3.3	4	III	DW/DO	Strey - Winkler - Magid		d = 6.5 Å, a_s = 99 Å^2/mol
3.5	4	II	O/DW	Flat = 1	Cylinder	R= 50 ± 20 Å ; L= 1000 Å
3.8	4	II	O/DW	Flat = 1	Cylinder	R= 43 ± 20 Å ; L= 450 Å
4.3	4	II	O/DW	Flat = 1	Cylinder	R= 40 ± 20 Å ; L= 250 Å
5.5	4	II	O/DW	Flat = 1	Cylinder	R= 30 ± 15 Å ; L=100 Å
3.5	1	II	O/DW	Flat = 1	Cylinder	R= 50 ± 20 Å ; L= 500 Å
3.8	1	II	O/DW	N.D.		N.D.
4.3	1	II	O/DW	Flat = 1	Cylinder	R= 45 ± 20 Å ; L= 120 Å
5.5	1	II	O/DW	Flat = 1	Cylinder	R= 30 ± 15 Å ; L= 100 Å
3.5	4	II	DO/DW	Flat = 1	Core-Shell cylinder	R= 45 ± 20 Å ; L= 1500 Å ; d= 10 Å
3.8	4	II	DO/DW	Flat = 1	Core-Shell cylinder	R= 40 ± 15 Å ; L= 400 Å ; d= 10 Å
4.3	4	II	DO/DW	Flat = 1	Core-Shell cylinder	R= 40 ± 15 Å ; L= 150 Å ; d= 10 Å
5.5	4	II	DO/DW	Flat = 1	Core-Shell cylinder	R= 35 ± 15 Å ; L= 150 Å ; d= 10 Å

R: radius (either sphere or cylinder), L: cylinder length, d: surfactant film thickness, ξ correlation length of bicontinuous microemulsions, d': is the periodicity of the bicontinuos domain size, a_s: area per molecule of the surfactant. N.D.: morphology not determined due to experimental errors or otherwise explained in the text.

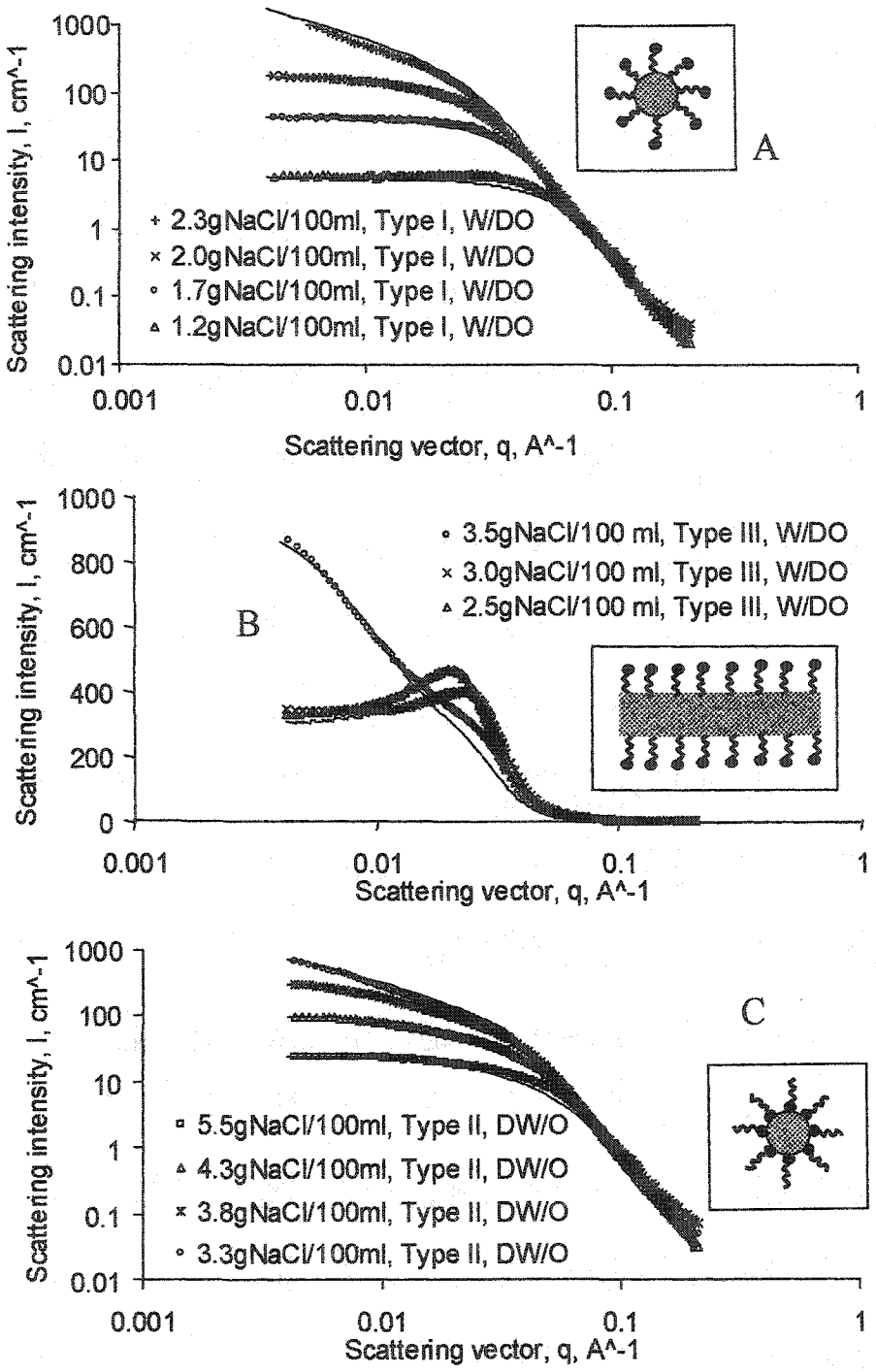

Figure 3.2. Scattering curves for the SDHS-toluene microemulsion systems with oil/water contrast. Part A corresponds to Type I systems, part B to bicontinuous Type III systems and part C to Type II microemulsion systems. The solid lines represent the scattering model fit described in Table 3.4. The shaded areas in the schematic represent the deutrated phase.

Another experimental factor that was evaluated was the possibility of multiple scattering. In the case of droplet-type microemulsions (Type I or II) with low surfactant concentration (normally less than 0.5 M) this phenomenon is not important (6). Even so, two sets of scattering data were obtained for droplet-type microemulsions: one at 4% (~0.1M) SDHS and one at 1% SDHS (~0.025M). Table 3.4 shows that there is good agreement between the morphology obtained at 4% and at 1% SDHS except for the system at 1.2 g NaCl/100 ml where at 4% SDHS the average radius of the sphere is 35 ± 15 Å and for the 1% SDHS no data is reported because the volume fraction of oil solubilized was small, yielding scattering too weak to analyze.

At higher electrolyte concentrations, the spherical aggregates grow into a cylindrical shape. The best way to observe this transition is by looking at the shape of the scattering curves in Figure 3.2a at low q values (<0.04 $Å^{-1}$). With increasing electrolyte concentrations the intensity at low q values increases characteristic of an increase in aggregate size due to the increase in oil solubilized. Given the size of spherical aggregates in this system, if the low q region is completely horizontal (as in 1.2% NaCl) it shows that the aggregate is spherical, but if the slope is non-zero (as in the 1.7% to 2.3% NaCl range), then one of the dimensions has increased, indicating cylindrical or ellipsoid aggregates. Both types of morphologies have been used to fit the scattering data (29,30). In this particular study the cylindrical models fit the data better. The form factor for the cylindrical model is given as (27):

$$P(q) = \frac{\phi}{V_{cyl}} \int_0^{\pi/2} \left[2(n_o - n_w) V_{cyl} j_0\left(\frac{qL\cos\alpha}{2}\right) \frac{J_1(qr\sin\alpha)}{(qr\sin\alpha)} \right]^2 \sin\alpha d\alpha \qquad \text{Eq. 13}$$

where V_{cyl} is the volume of the cylinder, and L is the length of the cylinder, r is the radius of the cylinder, $j_0(x)$ is the function $\sin(x)/x$ and J_1 is the Bessel function of first order, all the other variables and parameters were described previously.

The result of the model fit for Type I microemulsions with electrolyte concentration between 1.7 to 2.3 g NaCl/100ml for surfactant concentrations of 4% and 1% SDHS are presented in Table 3.4. The data shows that the "cylindrical" droplets grow both in radius and length as the electrolyte concentration approaches the transition point towards a bicontinuous system (~ 2.4 g NaCl/100 ml). The values of radius and length for 4% SDHS and 1% SDHS at 1.7 and 2.0 g NaCl/100 are identical within the experimental error. At 2.3 g NaCl/100 ml the measurements at 4% SDHS and 1% SDHS have identical cylindrical radii but different lengths. The radius corresponds to scattering at high q values while the cylinder length impacts the low q values; interparticle interference effects will be more important at low q. Neglecting the scattering due to interparticle interference is probably not appropriate for 2.3 g NaCl/100 ml at 4% SDHS since the volume fraction of droplets is relatively high (~ 9% of toluene for 4%SDHS, see Table 1). Here, our interpretation is that the length value of the 1% SDHS system is more correct and probably corresponds to the length at 4% SDHS.

Between electrolyte concentrations of 2.5 to 3.5 g NaCl/100 ml the system becomes bicontinuous. These systems have been modeled with the Treubner-Strey model (7,9):

$$I(q) = \frac{1}{a_2 + c_1 q^2 + c_2 q^4} \qquad \text{Eq. 14}$$

where a_2 , c_1 and c_2 are the fitting constants which are used to calculate the characteristic length (ξ) of the bicontinuous microemulsion:

$$\xi = \left[\frac{1}{2}\left(\frac{a_2}{c_2}\right)^{1/2} + \frac{1}{4}\frac{c_1}{c_2} \right]^{-1/2} \qquad \text{Eq.15}$$

The other parameter obtained from Equation 14 is the periodicity parameter d':

$$d' = 2\pi \left[\frac{1}{2}\left(\frac{a_2}{c_2}\right)^{1/2} - \frac{1}{4}\frac{c_1}{c_2} \right]^{-1/2} \qquad \text{Eq.16}$$

While this model has been widely used in bicontinuous microemulsions, some modifications have been made to improve the fit at high q values (31); in this work these additional modifications were not necessary as a satisfactory fit was achieved with the Teubner-Strey model as represented by Equation 14. Table 3.4 summarizes the correlation length and periodicity parameters obtained for the bicontinuous systems with different oil/water contrast (DW/O and W/DO). The correlation length (ξ)ranges between 68 to 81 Å and the periodicity between 236 to 282 Å. The bicontinous Type III microemulsion at high salinity (3.5 gNaCl/100 ml for W/DO and 3.3 gNaCl/100 ml for DW/O) did not fit the profile of the Teubner and Strey model or its modification because of the sloped profile at low q range (curve for 3.5 gNaCl/100 ml in Figure 3.2b) which suggested a extended cylindrical structure. The fit shown in Figure 3.2b was obtained using the cylinder model with radius of 80Å and 500 Å of length, although this fit was not reported in Table 3.4 because the assumption of no interparticle interference is questionable.

For the case of Type II microemulsions all the oil/water contrast experiments were fit using the cylindrical model (Equation 13) for the form factor. Examples of the scattering profile and model fit are presented in Figure 3.2c and the morphology parameters are summarized in Table 3.4. The values of radius and length presented in Table 3.4 shows the same trend as that shown by Type I microemulsions: as the electrolyte concentration becomes more distant from the transition point to Type III systems, the radius and length of the cylinders become smaller. The morphologies obtained using SDHS concentrations at 1% and at 4% are comparable, thus validating the assumptions of dilute non-interacting droplets and no multiple scattering.

The same systems described above were studied using film contrast. At low electrolyte concentration the scattering data was fitted using the flat model for the structure factor S(q)=1 and the core-shell sphere model as the form factor (27):

$$P(q) = \frac{\phi_s}{V_{shell}}\left[\frac{3V_{core}(n_{core} - n_{shell})j_1(qr_{core})}{qr_{core}} + \frac{3V_{shell}(n_{shell} - n_{solvent})j_1(q(r_{core}+d))}{q(r_{core}+d)}\right]^2 \quad \text{Eq. 17}$$

where ϕ_s is the volume fraction of surfactant, V_{shell} is the volume of the shell, V_{core} is the volume of the spherical core, n_{core}, n_{shell}, $n_{solvent}$ are the neutron scattering length densities of the core of the sphere, the shell and the solvent, in this case the core and solvent scattering length densities are the same, r_{core} is the radius of the core of the sphere and "d" is the thickness of the shell and the function $j_1(x) = [\sin(x) - x\cos(x)]/x^2$.

When the above model was applied to the low electrolyte concentration data (1.1gNaCl/100ml) the radius obtained was similar to that obtained with oil/water contrast

and the shell thickness (d) was determined to be 10 Å; however, the model was not too sensitive and alternative acceptable fits produced "d" values as low as 7Å.

The rest of the droplet-type (Type I and II) microemulsions were fitted using a core-shell cylinder model for the form factor:

$$P(q) = \frac{\phi_s}{V_{shell}} \int_0^{\pi/2} f^2(q,\alpha) \sin\alpha d\alpha \qquad \text{Eq. 18}$$

where f(q,α) is

$$f(q,\alpha) = 2\Delta n V_{core} j_0\left(\frac{qL\cos\alpha}{2}\right)\frac{J_1(qr\sin\alpha)}{qr\sin\alpha} + 2\Delta n V_{shell} j_0\left[q(L/2+d)\cos\alpha\right]\frac{J_1\left[q(r+d)\sin\alpha\right]}{q(r+d)\sin\alpha}$$

where Δn is the difference in neutron scattering length density between the shell and either the core or the solvent (is the same in film contrast) , V_{core} is the volume of the core of the cylinder, L is the length of the cylinder, r is the radius of the cylinder V_{shell} is the volume of the cylinder shell and "d" is the thickness of the shell. The functions j_0 and J_1 as described before.

A summary of the morphology parameters (R, L, d) obtained after fitting the model to Type I and Type II systems is presented in Table 3.4 and are also presented in Figure 3.3. The values of radius and length are quite similar to those found with the water/oil contrast and thus follow the same trends discussed in those cases. The shell or film thickness d was 10Å but the fit could have been obtained using a range between 7Å - 10Å. In addition, the polydispersity is noted only for the radius but in reality polydispersity also affects the length of the cylinder and the shell thickness.

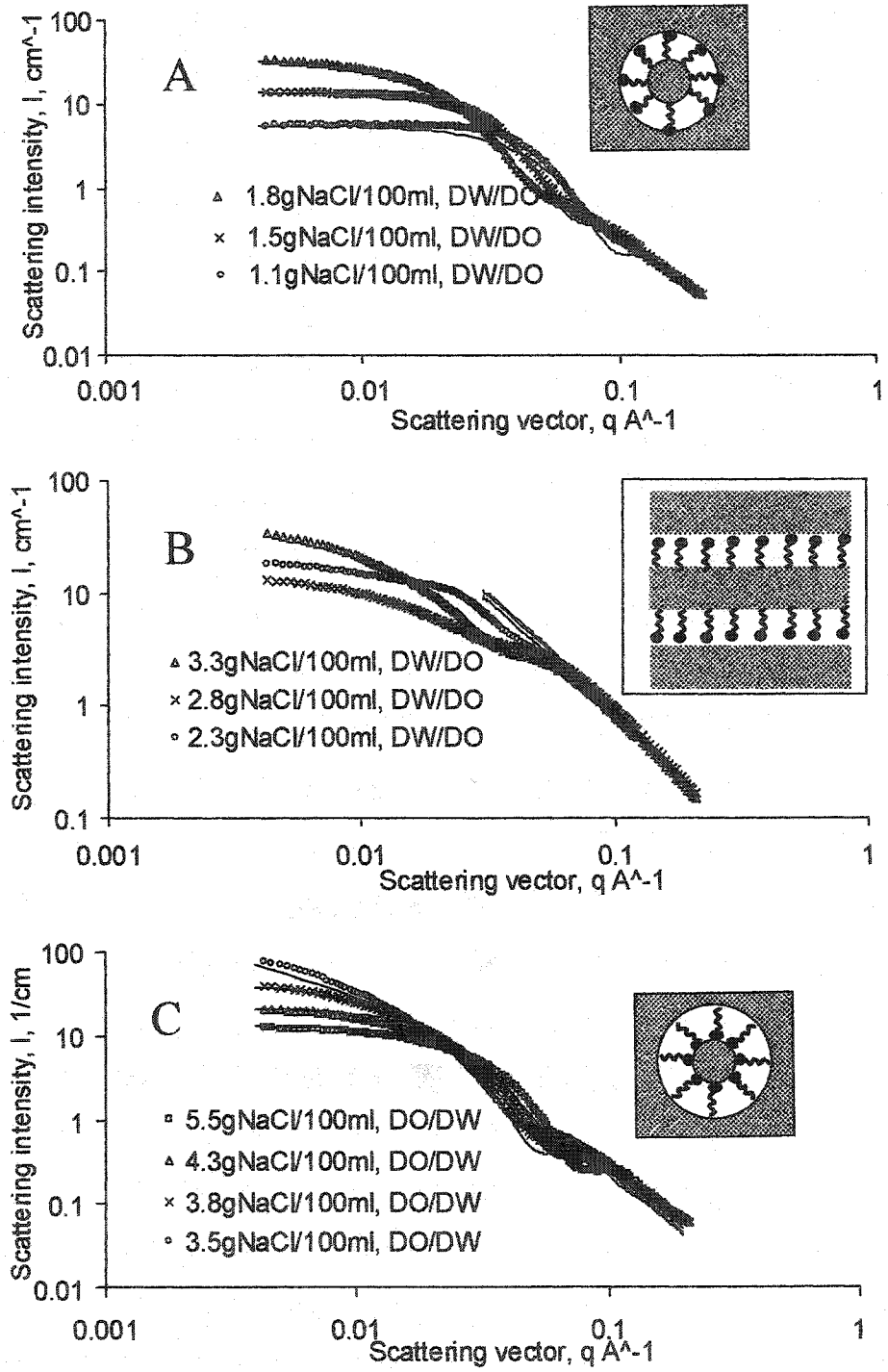

Figure 3.3. Scattering curves for the SDHS-toluene microemulsion systems with film contrast. Part A corresponds to Type I systems, part B to bicontinuous Type III systems and part C to Type II microemulsion systems. The solid lines represent the scattering model fit described in Table 3.4. The shaded areas in the schematic represent the deutrated phase.

In the case of middle phase bicontinuous microemulsions, the film contrast experiments render a morphology that resembles that of a sponge- L_3 phase. Different models have been used to characterize surfactant sponge phases and film contrasted bicontinuous microemulsions (8,32,33,34). The important morphological parameters are the correlation length of the sponge phase and the thickness of the surfactant membrane. In contrast to Type I or II systems (Figure 3a and 3c), the scattering profiles for Type III SDHS-toluene film contrast systems did not show a significant peak or breakpoint at low q (shown in Figure 3b) to make appropriate estimations of the correlation length (which was already determined using oil/water contrast). This lack of a breakpoint is not a rare phenomenon when studying L_3 phases (8). The profile at high q values did offer good information on the morphology of the surfactant film after fitting the high-q range scattering profile to the expression proposed by Strey et al. for monolayer sponge phases (8):

$$I(q) = 2\pi\phi_s \frac{v_s}{a_s} \frac{\Delta n^2}{q^2} e^{-q^2 t^2} \qquad \text{Eq. 19}$$

where ϕ_s is the volume fraction of the surfactant, v_s is the molecular volume of the surfactant (~650 $Å^3$/molecule for SDHS), a_s is the area per molecule of the surfactant, $t=d/(2\pi)^{0.5}$ where d is the thickness of the surfactant film. Table 3.4 shows the fitted parameters for the film contrast experiments in Type III systems, where the film thickness show to be slightly lower than those found for droplet type microemulsions. The area per molecule of the SDHS in this set of experiments result consistent with those

reported from Gibbs adsorption studies of interfacial and surface tension curves for this surfactant (25,26).

Net-average curvature model versus neutron scattering morphology

As indicated above, the main objective of this work was to test how well the net-average curvature model could reproduce the microemulsion morphology obtained through neutron scattering techniques.

The first simplification made by the net-average curvature model was to assume that the aggregates were of spherical shape. As indicated in Table 3.4, at low electrolyte concentration the assumption of spherical micelles is appropriate. However, as the system curvature approaches the zero net curvature, the micelles become elongated or "worm-like" micelles, i.e. this simplification is not appropriate at high electrolyte concentration. Worm-like micelle are, however, in agreement with results reported in the literature (35,36). The spherical droplet assumption was made to minimize the surface area exposed (which translates into surface excess energy) per unit of volume of the internal phase solubilized. The data suggest that when the droplet becomes large enough a change in shape occurs. The change in droplet shape with surfactant curvature was predicted by the net curvature equation (Equation 4), considering that if the real shape of the droplet is spherical, then the net curvature (H_N) should be equal to $1/R_O$ (or $1/R_W$) in Type I (or Type II) microemulsions. As the oil (or water) droplets grow to a comparable size to the virtual water - R_W (or oil- R_O) droplets in Type I (or II) microemulsions, the net curvature (H_N) is smaller than $1/R_O$ (or $1/R_W$). The latter suggests that the real shape of the droplets is not spherical, but some other less curved configuration (such as cylinders). The

explanation above helps explain the change in shape with electrolyte concentration, but also predicts changes in shape with surfactant concentration, which is somewhat supported by the values in Table 3.4 where for 4% SDHS the length of the cylinders is consistently longer than those for 1% SDHS. The prediction of the specific shape (radius and length of the cylinder) will be the topic of future modifications of the net-average curvature model.

Despite the difference in droplet shape, the best way to compare the size of the aggregates predicted by the net-average curvature model and that determined by SANS is to determine the equivalent spherical radius of the SANS morphology by determining the ratio of volume to surface area as: $R_{spherical}$ = 3*volume/surface area. Figure 4 presents a summary of all the equivalent spherical ratios for the Type I and II microemulsions systems described in Table 3.4 as a function of electrolyte concentration. The range bars shown in Figure 3.4 represent the dispersion of the size distribution (i.e. the range of droplet sizes found at one standard deviation around the average droplet size), not an error range. In the case of Type III systems, the correlation length is shown. The first important feature of Figure 3.4 is that the different SANS morphologies (obtained using oil/water contrast at different surfactant concentrations and film contrast) offer similar equivalent spherical radius. When values of the SANS equivalent spherical radius are compared to the spherical radius calculated by solubilization values and predicted by the net-average curvature model, the latter under-predict the size of the droplets by a margin such that the predicted radii are not even in the lower limit of the experimental size range distribution. On the other hand, the correlation length of the optimum formulation fits

quite well with the prediction made by the model, thereby helping to validate the assumption that in bicontinuous systems the characteristic length is constant and can be evaluated using Equation 5.

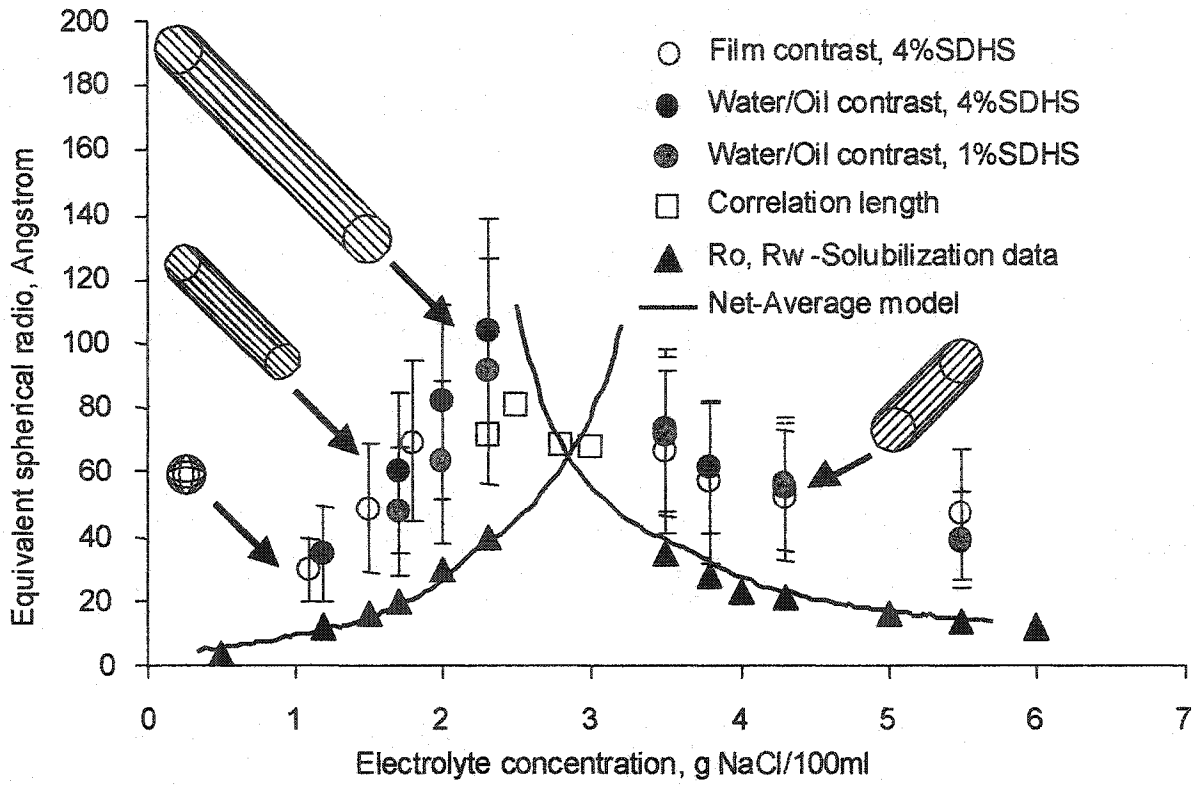

Figure 3.4. Equivalent spherical radius for SDHS-toluene microemulsion systems as calculated from the morphologies obtained from the SANS studies, the solubilization studies and the predicted from the net-average curvature model.

In summary, the spherical shape for droplet microemulsions was inadequate for systems with near zero curvature and the best way to compare these systems was using equivalent spherical radius. However assuming the characteristic length to be constant seems to be reasonable. These observations lead to the hypothesis that the surfactant area per molecule was not constant as the net-average curvature model assumed, and that this

variation is responsible for the disparity between the net-average radii prediction and the SANS equivalent spherical radii. The area per surfactant molecule was obtained from applying the Gibbs adsorption equation to surface and interfacial tension data (95$Å^2$/molecule), a value consistent with the values reported in Table 3.4 for film contrast experiments in Type III systems.

To investigate the area per molecule in Type I and II microemulsions we can apply the Porod equations to the oil/water contrast data and apply Equation 7 to determine the area per molecule of the surfactant a_s. Figure 5 shows the Porod plot ($I(q)q^4$ vs. q) for Type I microemulsions studied with oil/film contrast and 4% surfactant SDHS. At large q values (The Porod region) the value $I(q)q^4$ will provide an asymptotic value equivalent to $2\pi(n_w-n_o)^2c_sa_s$ (see Equation 7 for details). Thus the area per molecule of the surfactant can be calculated and this value is shown in Figure 3.5 for each of the curves presented. While the selection of the asymptotes was somewhat arbitrary due to the variability of the data, the asymptotes resulted in areas per molecule that are a factor of 2 - 3 lower than the 95 $Å^2$/molecule assumed.

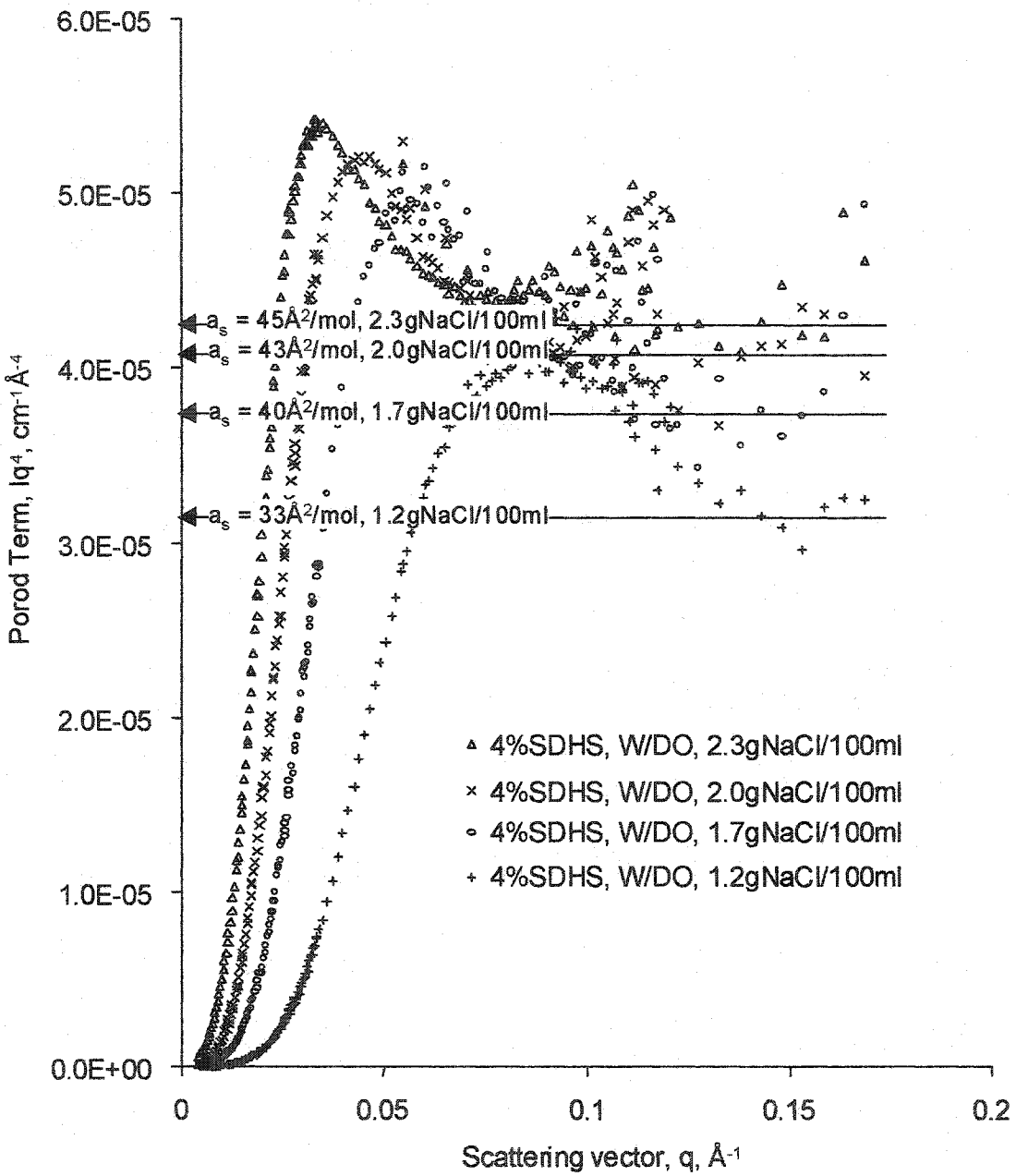

Figure 3.5. Porod plot for oil/water contrast experiments for Type I microemulsion formulated with 4% aqueous concentration of SDHS. The values of area per molecule of the surfactant (a_s) were obtained using Equation 7.

In order to corroborate this finding, the area per molecule was calculated for the surfactant in the rest of Type I and II systems with oil/water contrast. Figure 3.6a presents the values of surfactant area per molecule obtained from the Porod's plot as a function of electrolyte concentration. The area per molecule of the surfactant in Type I and II systems is consistent between the two surfactant concentrations (1% and 4% SDHS). Figure 3.6a also includes the area per molecule obtained after the film contrast experiments in Type III systems, only in this case the area per molecule resulted consistent with the value derived from surface and interfacial tension data (95 $Å^2$/molecule). The data in Figure 3.6a shows that the values of area per molecule in Type I and II system are lower than the value of area per molecule for Type III systems, the change in area per molecule is probably due to changes in curvature as explained later. These results also render inappropriate the assumption made in the net-average curvature model that the area per molecule is constant independent of microemulsion Type or curvature value. To our knowledge, there has not been a detailed study of the surfactant area per molecule as a function of a Winsor phase scan, as in this paper. To a certain degree the non-consistency in areas per molecules could be anticipated since the surfactant area per molecule would not be expected to be the same in a flat geometry versus a spherical shape. Figure 3.6b presents a schematic of the surfactant area per molecule "at the neck" (noted as "a_G", the area per molecule of the flat interface obtained applying the Gibbs absorption model to surface or interfacial tension data) and the surfactant area per molecule in contact with the internal microemulsion phase (noted as "a_S", or projected surfactant area per molecule) as a function of the surfactant membrane

curvature. According to Figure 3.6b it is expected that the projected area per molecule, "a_S", would be lower in Type I and II microemulsions (in comparison with bicontinuous Type III systems) after applying the proper geometrical considerations. In fact this was the building block of a model proposed by Hwan et al. where they established the projected surfactant area per molecule, a_S, applying geometrical projection rules assuming a droplet spherical shape, and were able to produce a curvature equation similar to the net curvature equation in the case of electrolyte scanned systems (1,37). Nave et al. (15,38) measured area per molecules of SDHS close to 60 $Å^2$/molecule in droplet and micelle systems using SANS and neutron reflectometry experiments which is in the range of area per molecules shown in Figure 3.6a for droplet microemulsion systems. In the case of SDS the area per molecule in droplets systems has been estimated near 20 $Å^2$/molecule (6) contrasting with the value of 60 $Å^2$/molecule reported after adjusting the Gibbs adsorption model to surface tension data (26).

In order to predict the equivalent spherical radius using the net-average curvature model an adjustment needs to be introduced to account for different surfactant areas per molecule as a function of location in the phase scan. Here we introduce a very simple modification to assess the effect of the area per molecule of the surfactant on the equivalent spherical ratio predicted by the net-average curvature model:

$$R_{spherical} = R_{net\text{-}average} * a_G / a_{s,\,SANS} \qquad \text{Eq. 20}$$

Where $R_{spherical}$ is the equivalent spherical radius, $R_{net\text{-}average}$ is the value originally calculated using the net-average model, a_G is the area per molecule of the surfactant obtained using the surface and interfacial tension data and the Gibbs adsorption model

(for SDHS 95Å^2/molecule) and $a_{s,SANS}$ is the area per molecule interpolated using the SANS data presented in Figure 3.6a.

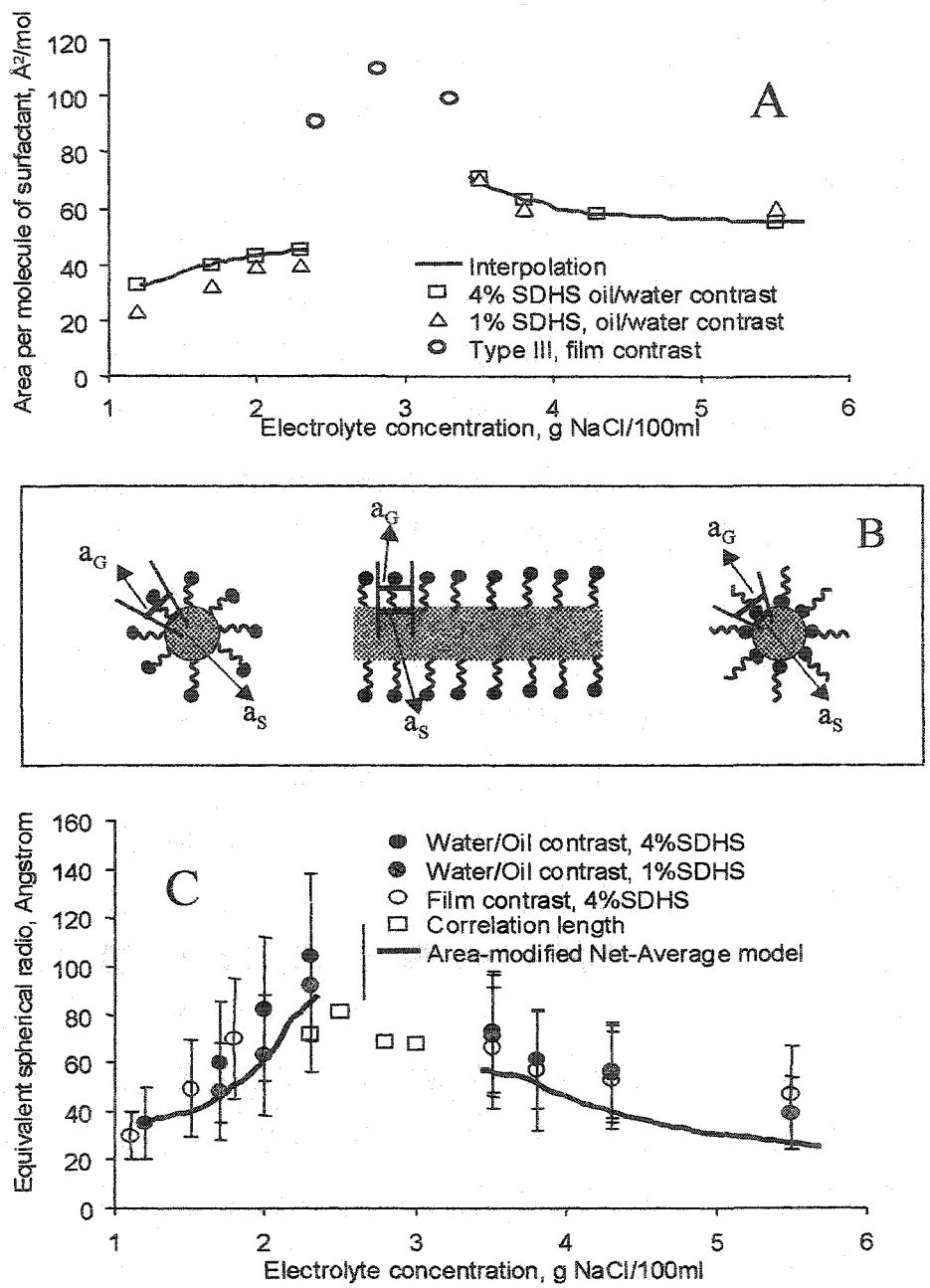

Figure 3.6. Modification of the net-average curvature model to account for changes in area per molecule of the surfactant. Part A indicates the area per molecule as a function of electrolyte concentration. Part B presents the projected area per molecule of the surfactant a_S for different curvatures. Part C presents the modified radii predicted by the net-average curvature model after modifying for surfactant area per molecule.

Figure 3.6c shows the modified net-average radius compared to the SANS equivalent radius. The data shows that after introducing this refinement to the net-average curvature model the experimental data and the prediction show good correlation. Instead of using SANS data, the surface area per molecule in droplet systems could be predicted using the approach proposed by Hwan et al. (37). However, the area projection model must assume a certain geometry, in the case of Hwan et al. a spherical shape was assumed, but as indicated above this assumption is not appropriate for systems near the phase transitions to Type III. In a future modification of the model, the projected area per molecule of the surfactant in the core of the micelle should include the prediction of the transition in shape from spherical to cylindrical micelles as indicated earlier.

Dynamic light scattering (DLS) studies.

The SANS data presented above is perhaps the most accurate way to asses the size and shape of the microemulsion aggregates. On the other hand, measurements of the hydrodynamic radius using dynamic light scattering (DLS) are more common. The objective of this section is to compare how the hydrodynamic radius compares to the equivalent spherical radius by SANS and the net-average curvature model. Figure 3.7 shows the radius of gyration (or hydrodynamic radius) for Type I and II microemulsions along with the SANS and net-average curvature model data. The DLS measurements agree quite well with SANS measurements when the shape of the aggregate is spherical. When the shape of the aggregate is cylindrical (as it approaches the transition points) the DLS hydrodynamic radius tends to over-estimate the size of the aggregates. The Brownian diffusion produces a tumbling effect on the cylindrical micelles such that the

effective radius of gyration appears greater than it really is. Figure 3.7 also presents the standard deviation of the DLS droplet size distribution (as a range bar) which is found to be close to the polydispersity observed in neutron scattering experiments.

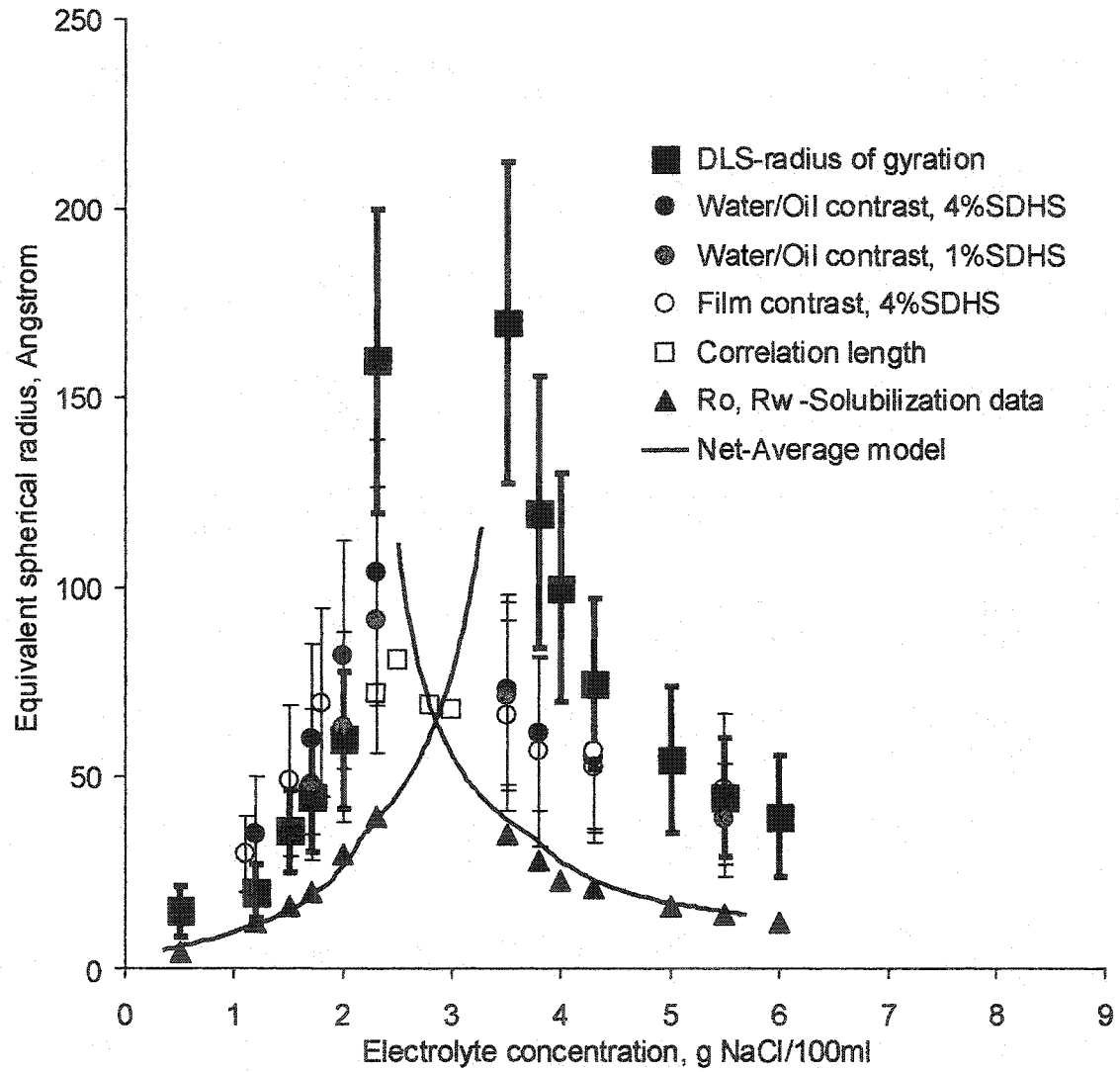

Figure 3.7. Comparison of the radius of gyration of Type I and II microemulsions determined by dynamic light scattering (DLS) with the equivalent spherical radius determined from SANS data and the net-average curvature model.

The correlation between the radius of gyration determined by DLS and the predicted net-average model is, as expected, very poor. If the model is corrected by the area per molecule as shown in Figure 6c a close correlation would be found as the system is farther away from the transition boundaries to Type III systems. The disparity between the hydrodynamic radius and the net-average curvature model predictions was previously reported (1). In that case the hydrodynamic radius was obtained from settling velocities obtained by centrifugation studies (37). In order to make better prediction of hydrodynamic coefficient and thus droplet diffusion data, the shape and size of microemulsion droplets should be estimated.

NMR self-diffusion coefficient studies

NMR self-diffusion coefficients measure the dynamic state of the molecules in the microemulsion system. In the case of droplet-type microemulsions, the dissolved phase is confined in the droplet and thus the diffusion is controlled by the diffusion of the microemulsion droplet which can be estimated using the hydrodynamic radius of the droplet and Equation 9. For bicontinuous systems, the mobility of the molecule in the bicontinuous channels determines the self-diffusion coefficient, which can be calculated using Equation 10. Figure 3.8 present the self-diffusion of toluene and water obtained from Lindman et al. (20) for the SDS-butanol-toluene system. The solid lines in Figure 3.8 were obtained using the net-average curvature model to obtain the radius of oil and water droplets for Type I and II systems and the volume fractions of oil and water for the Type III system. Equation 9 was used to estimate the diffusion coefficient of the droplets using literature values of viscosity (39). For Type III bicontinuous systems Equation 10

was used using a β expansion parameter of 1 which reveal the high level of interconection in the network of bicontinuous channels. According to Figure 3.8, and in the case of droplet-type microemulsions, very low self-diffusion coefficients are observed. In fact, data further away from the transition are even lower than estimates. This behavior likely reflects the fact that the actual hydrodynamic radius in this case is larger than the radius estimated using the net-average model, consistent with the previous discussion. The model fits well in the region of bicontinuous microemulsions. The transition region between droplet systems and bicontinuous phase shows an intermediate behavior, which is not reproduced by the net-average curvature model because there is no equation relating either droplet size or volume fraction to self diffusion data.

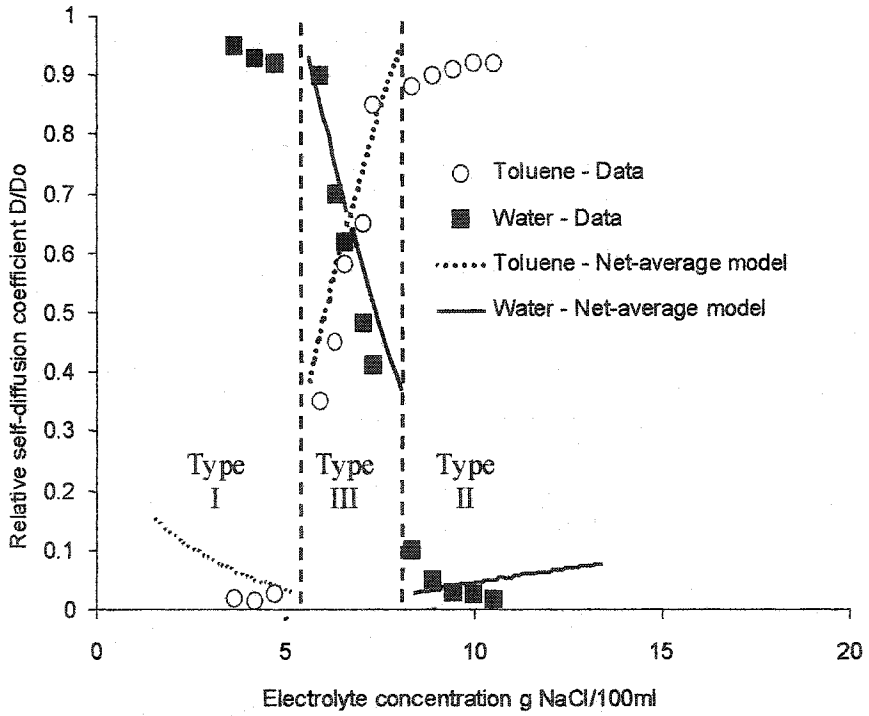

Figure 3.8. Relative self-diffusion coefficients (D/Do) for toluene and water for the toluene - SDS - butanol systems. Data points from Lindman et al. (20). Lines were estimated by combining the net-average curvature model and Equations 9 and 10.

Conclusions

The initial objective of this work was to evaluate how well the net-average curvature model could reproduce the nanoscale environment of microemulsion systems. We first confirmed that the model could reproduce the phase behavior of the microemulsion systems considered (SDHS-toluene and SDS-toluene) finding good agreement between data and predictions once the scaling length parameter was adjusted. When comparing the droplet size predictions with SANS-determined morphology, we determined that the assumption of spherical droplets for Type I and Type II microemulsions near the boundaries of Type III microemulsions was not adequate because the micelles become cylindrical in shape. The SANS studies show some evidence that in the transition points long cylindrical micelles are formed with radius close to the correlation length of the microemulsion. The prediction of the characteristic length by the net-average model was quite close to the values observed by SANS which supports the assumption of constant characteristic length in bicontinuous systems. Additional assessment of the surfactant area per molecule projected to the core of the droplets is shown to be the cause for the disparity between the equivalent spherical radius obtained from SANS morphology and the one predicted by the net-average model. Studies of the hydrodynamic radius using dynamic light scattering confirm the trends observed in SANS studies and to offer similar values of radius when the droplet has a spherical shape. In the case of the NMR self-diffusion studies, literature data was compared with predictions made using the net-average curvature model; the close agreement corroborates the appropriateness of the model in describing the bicontinuous

and droplet configuration of the system, although some disparity in certain values for the droplet systems suggest the actual hydrodynamic radius is larger than the one calculated using the net-average model consistent with the findings in the SDHS systems.

The net-average model can reproduce the microemulsion phase behavior observed at the macroscopic scale (i.e. solubilization, phase transitions, interfacial tensions) but to reproduce the actual morphology of the microemulsion droplets in Type I and II systems additional modifications must be introduced in terms of aggregate shape, and surface area per molecule of the surfactant projected into the core of the droplet systems. A simple correction introduced for the area per molecule using experimentally obtained values was able to quantitatively account for this deviation. In future models we will propose ways to estimate this projected surface areas without the need to determine experimental values of projected areas.

Acknowledgments

The authors thank Dr. Lionel Porcar of NIST for his assistance conducting the neutron scattering experiments at NIST. We acknowledge the support of the National Institute of Standards and Technology, U.S. Department of Commerce, in providing the neutron research facilities used in this work. Partial travel support for Mrs. Erika Szekeres was given by the University of Maryland neutron outreach program. This work was supported in part by an EPA grant no. 083090301

References

[1] Acosta, E.; E. Szekeres, D. A. Sabatini and J. H. Harwell, A Net-Average Curvature Model for Solubilization and Supersolubilization in Surfactant Microemulsions, *Langmuir* **2003**, 19(1), 186

[2] Bourrel, M. and Schecter R. *Microemulsions and Related Systems*. Marcell Dekker Inc. New York, 1988.

[3] Salager, J.L.; Antón R.E. *In Handbook of Microemulsion Science and Technology*. Kumar, P., Mittal, K.L. Marcel Dekker, New York, 1999. p 247-280

[4] Salager, J. L.; Marquez, N.; Graciaa, A.; Lachaise, J. Partitioning of Ethoxylated Octylphenol Surfactants in Microemulsion-Oil-Water Systems: Influence of Temperature and Relation between Partitioning Coefficient and Physicochemical Formulation. *Langmuir* **2000**, 16(13), 5534-5539.

[5] Marquez, N.; Anton, R.; Graciaa, A.; Lachaise, J.; Salager, J.L. Partitioning of ethoxylated alkylphenol surfactants in microemulsion-oil-water systems. *Colloids Surfaces, A.* **1995**, 100, 225-31.

[6] Auvray, L. The structure of microemulsions: experiments. In *Micelles, Membrane, Microemulsions and Monolayers*. William Gelbart, Avinoam Ben-Shaul and Didier Roux Editors. Springer-Verlag. New York, 1994., pp. 347-393.

[7] Teubner, M and Strey, R. Origin of the scattering peak in microemulsions. *J. Chem. Phys.* **1987**, 87(5), 3195-3199.

[8] Strey, R; Winkler, J. and Magid, L. Small Angle Neutron Scattering from Diffuse Interfaces 1. Mono- and Bilayers in the Water-Octane-$C_{12}E_5$ System. *J. Phys. Chem.* **1991**, 95, 7502-7507.

[9] Schubert, K.V. ; Strey R.; Kline, S. R. and Kaler E. W. Small angle neutron scattering near Lifshitz lines: Transition from weakly structured mixtures to microemulsions. *J. Chem. Phys.* **1994**, 101(6), 5343-5355.

[10] Gradzielski M., Langevin D. , Magid L. and Strey R. Small-Angle Neutron Scattering from Diffuse Interfaces 2. Polyshells in Water-Alkane-$C_{10}E_4$ Microemulsions. *J. Phys. Chem.* **1995**, 99, 13232-13238.

[11] Eastoe, J.; Hetherington K. J.; Sharpe D.; Dong J.; Heenan R. K.; Steyler D. Mixing Alkanes with Surfactant Monolayers in Microemulsions. *Langmuir.* **1996**, 12, 3876-3880.

[12] NIST center for neutron research web site at www.ncnr.nist.gov

[13] Auvray, L.; Cotton, J. P.; Ober, R.; Taupin, C. Evidence for zero mean curvature microemulsions. *J. Phys. Chem.* **1984**, 88(20), 4586-9.

[14] Auvray, L.; Cotton, J. P.; Ober, R.; Taupin, C. Concentrated Winsor microemulsions: a small angle x-ray scattering study. *J. de Physique.* **1984**, 45(5), 913-28.

[15] Nave, S.; Eastoe, J.; Heenan, R. K.; Steytler, D.; Grillo, I. What Is So Special about Aerosol-OT? 2. Microemulsion Systems. *Langmuir.* **2000**, 16(23), 8741-8748.

[16] Corti, M.; Degiorgio, V. Micellar properties and critical fluctuations in aqueous solutions of nonionic amphiphiles. *J. Phys. Chem.* **1981**, 85(10), 1442-5

[17] Robbins, M. L.; Bock, J.; Huang, J. S. Model for microemulsions. III. Interfacial tension and droplet size correlation with phase behavior of mixed surfactants. *J. Colloid Interface Sci.* **1988**, 126(1), 114-33.

[18] Kaler, E. W.; Prager, S. A model of dynamic scattering by microemulsions. *J. Colloid Interface Sci.* **1982**, 86(2), 359-69.

[19] Lindman, B.; Olsson, U. and Soederman, O. Characterization of microemulsions by NMR. *In Handbook of Microemulsion Science and Technology*. P. Kumar and K.L. Mittal Editors. Marcel Dekker, 1999, N.Y. pp. 309-356

[20] Lindman, B.; Guering, P. Droplet and Bicontinuous Structures in Microemulsions from multicomponent Self-Diffusion Measurements. *Langmuir* . **1985**, 1(4), 464-468.

[21] Acosta, E.; Tran, S.; Uchiyama, H.; Sabatini, D.A.; Harwell, J.H. Formulating Chlorinated Hydrocarbon Microemulsions Using Linker Molecules. *Environ. Sci. Technol.* **2002**, 36(21), 4618-4624

[22] http://www.ncnr.nist.gov/programs/sans/manuals/red_anal.html

[23] http://www.ncnr.nist.gov/resources/sldcalc.html

[24] Lide, D. R. Editor. *CRC handbook of chemistry and physics*. 75th. Edition, CRC Press (1994) pp. 10-300, 301

[25] Acosta, E.; Uchiyama, H.; Sabatini, D. A.; Harwell, J.H. The Role of Hydrophilic Linkers. *J. Surfactants Detergents.* **2002**, 5(2), 151

[26] Rosen, M. J. *Surfactants and Interfacial Phenomena*, Wiley, New York (1989) p. 431.

[27] Guinier, A. and G. Fournet, "Small-Angle Scattering of X-Rays", John Wiley and Sons, New York, (1955)

[28] Bumajdad, A; Eastoe, J.; Griffiths, P.; Steytler, D. C.; Heenan, R. K.; Lu, J. R.; Timmins, P. Interfacial Composition and Phase Structure in Mixed Surfactant Microemulsions. *Langmuir*. **1999**, 15, 5271-5278.

[29] Teixeira, C. V.; Itri, Ro.; Queiroz, L. Micellar Shape Transformation Induced by Decanol: A Study by Small-Angle x-ray Scattering (SAXS). *Langmuir*. **2000**, 16(15), 6102-6109.

[30] Hendrikx, Y.; Charvolin, J.; Rawiso, M. Segregation of two amphiphilic molecules within nonspherical micelles: a neutron scattering study. *J. Colloid Interface Sci.* **1984**, 100(2), 597-600.

[31] Chen , S. H., and Choi , S. M. Measurement and Interpretation of Curvatures of the Oil-Water Interface in Isomeric Bicontinuous Microemulsions. *J. Appl. Cryst.* **1997**, 30, 755-760.

[32] Berk, N.F. Scattering Properties of a Model Bicontinuous Structure with a Well Defined Length Scale. *Phys. Rev. Letters.* **1987**, 58(25), 2718-2721.

[33] Lei, N. ; Sarfinya, C. R.; Roux, D.; Liang K.S. Synchroton x-ray scattering studies on the sodium dodecyl sulfate-water-pentanol-dodecane L_3 sponge phase. *Phys. Rev. E.* **1997**, 56(1), 608-613.

[34] Porte, G. Micellar Polymorphism in Dilute Solutions. In *Micelles, Membrane, Microemulsions and Monolayers*. William Gelbart, Avinoam Ben-Shaul and Didier Roux Editors. Springer-Verlag. New York, 1994., pp. 106-151.

[35] Menge, U.; Lang, P.; Findenegg, G. H. From Oil-Swollen Wormlike Micelles to Microemulsion Droplets: A Static Light Scattering Study of the L1 Phase of the System Water + C12E5 + Decane. *J. Phys. Chem. B* . **1999**, 103(28), 5768-5774.

[36] Granek, R. Spontaneous Curvature-Induced Rayleigh-like Instability in Swollen Cylindrical Micelles. *Langmuir*. **1996**, 12(21), 5022-5027. CODEN: LANGD5 ISSN:0743-7463.

[37] Hwan, Rei-Nan; Miller C.A.; Fort, T. Determination of microemulsion phase continuity and drop size by ultracentrifugation. *J. Colloid Interface Sci.* **1979**, 68(2), 221-234.

[38] Nave, S; Stoe, J; Penfold, J. What Is So Special About Aerosol-OT? 1. Aqueous systems. *Langmuir*. **2000**, 16, 8733-8740

[39] Gradzielski, M and Hoffman, H. Rheological Properties of Microemulsions. *In Handbook of Microemulsion Science and Technology*. P. Kumar and K.L. Mittal Editors. Marcel Dekker, 1999, N.Y. pp. 357-386.

CHAPTER 4

Coalescence and Solubilization Kinetics in Linker-Modified Microemulsions and Related Systems[†]

Abstract

Previously, we reported on formulating microemulsions with combined linker molecules. These linker molecules enhance the interaction of the dynamic surfactant membrane with water, in the case of hydrophilic linkers, or oil, in the case of lipophilic linkers, thereby yielding microemulsions with desirable properties. In this paper we evaluate the coalescence and solubilization kinetics of trichloroethylene emulsions and microemulsions using sodium dihexyl sulfosuccinate and different linker formulations. Sodium mono and dimethyl naphthalene sulfonate (SMDNS) was used as the hydrophilic linker and dodecanol was used as the lipophilic linker. The interfacial properties (interfacial thickness / tension / rigidity) of these linker-based microemulsions were also studied. The turbidity curves of optimum middle phase microemulsions are fitted with a second order kinetic equation, with the coalescence activation energy being a function of the interfacial rigidity of the systems. It was found that the addition of lipophilic linkers tends to increase the interfacial thickness and the interfacial rigidity, and tends to decrease the coalescence rate. In contrast, hydrophilic linkers showed the opposite effect

---

[†] This chapter or portions thereof have been published previously in Langmuir under the title " Coalescence Kinetics in Linker-Modified Microemulsions and Related Systems" Langmuir 2003, 19(3), 566-574. The current version has been formatted for this dissertation.

to lipophilic linkers. A combination of both linkers shows an intermediate effect. Finally, the solubilization of TCE in surfactant solution and in surfactant and hydrophilic linker is tracked by turbidity, with the SMDNS-based formulation showing a faster solubilization rate than the surfactant alone formulation.

Key words: microemulsion, solubilization, coalescence, kinetics, linkers, hydrophilic, lipophilic.

Introduction

Previously we introduced the use of both hydrophilic and lipophilic linker molecules to enhance the solubilization capacity of chlorinated hydrocarbon microemulsions (1-3).

Graciaa, et al. first proposed the use of long chain alcohols or non-ionic surfactants with low degree of ethoxylation as lipophilic linkers, proposing that these linkers segregate in the palisade layer near but not adsorbed at the interface, serving as an extension of the surfactant tail (4-6). In contrast, medium chain alcohols (propanol to octanol) have traditionally been used as cosurfactants in the formulation of microemulsions to decrease the rigidity of interfacial membranes and prevent the formation of liquid crystal phases and metastable gel or macroemulsion phases (7). We will later show that long chain alcohols (dodecanol in particular) have a completely different effect on the formulation of microemulsions.

Hydrophilic linkers were first introduced by Uchiyama, et al (1). Hydrophilic linkers were found to coadsorb with the surfactant at the oil/water interface but have poor

or no interaction with the oil phase (2). Upon co-addition of both hydrophilic and lipophilic linkers a synergistic interaction has been observed which increases the solubilization capacity of the corresponding microemulsions as each linker incorporates into the interface (3). In this work we will use variations in linker concentrations to systematically control the properties of the dynamic surfactant membrane (thereafter referred to as surfactant membrane). This will allow us to use linkers to test the dependence of the coalescence and solubilization rates on the interfacial rigidity of the surfactant membrane.

While our previous work has elucidated the equilibrium behavior of linker-modified microemulsions, the current work concentrates on how linker addition modifies the interfacial and dynamic properties of emulsions and microemulsions. These studies will evaluate trichloroethylene (TCE) middle phase microemulsions (Type III) and excess oil and water using sodium dihexyl sulfosuccinate (SDHS) as the surfactant.

Solubilization in microemulsions and macroemulsion coalescence are generally treated as independent processes. Solubilization refers to the process by which a micelle (or reverse micelle) is filled with oil (or water) to form a Type I (or Type II) microemulsion. Coalescence, on the other hand, is the process by which two macroemulsion droplets collide to form a bigger droplet (8). The two processes are closely related, as discussed in Bourrel and Schecter (9), because both are controlled by the properties of the surfactant membrane.

Solubilization dynamics in microemulsion systems is less well understood than coalescence in the corresponding macroemulsion systems since fewer studies have

investigated the former phenomenon. Karaboni, et al. used molecular dynamics to study the solubilization kinetics of nonionic molecules and identified three solubilization mechanisms (10), as shown in Figure 4.1. Figure 4.1a shows the mechanism by which a micelle collides with an oil emulsion droplet, thereby deforming the surface of the droplet. The micelle eventually departs from the droplet surface as an oil-laden micelle. Figure 4.1b shows the solubilization mechanism by which a surfactant rich phase (liquid crystal) forms on the surface of oil droplets, which subsequently becomes filled with oil, and eventually departs from the surface as micelles filled with oil. The third mechanism (Figure 4.1c) requires the oil to be dissolved in the aqueous solution and, once it is dissolved in water, then diffuse into the micelles.

Several different authors have identified at least one of these three mechanisms (11-23). The lack of convergence to a single mechanism is why there is no complete agreement on a dynamic model for microemulsion solubilization. As an example, Evilevitch, et al. (11), studied the solubilization kinetics of decane by pentaethyleneoxide dodecyl ether (C12E5) surfactant solutions by measuring turbidity versus time once the system was subjected to temperature jumps. They found that oil diffusion in the aqueous phase and then into micelles was initially the dominant solubilization mechanism (Figure 4.1c). However, after a few temperature cycles they found a much faster solubilization rate due to the presence of both big and small droplets (Figure 4.1a). Evilevitch, et al. (12) later interpreted the above results using a molecular diffusion model where oil droplets larger than equilibrium swollen micelles provide oil to droplets smaller than the equilibrium size.

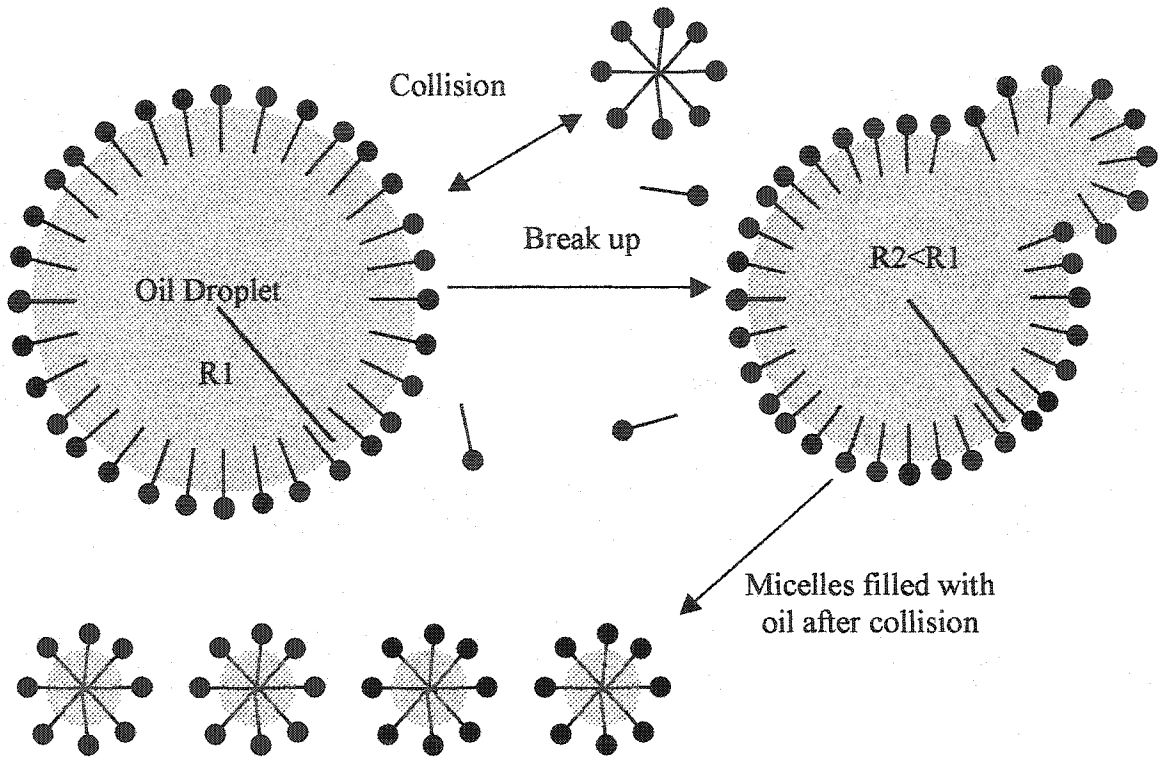

Figure 4.1a. Solubilization mechanism based on oil exchange between droplets and micelles after a soft collision. Adapted from Karaboni et al (10).

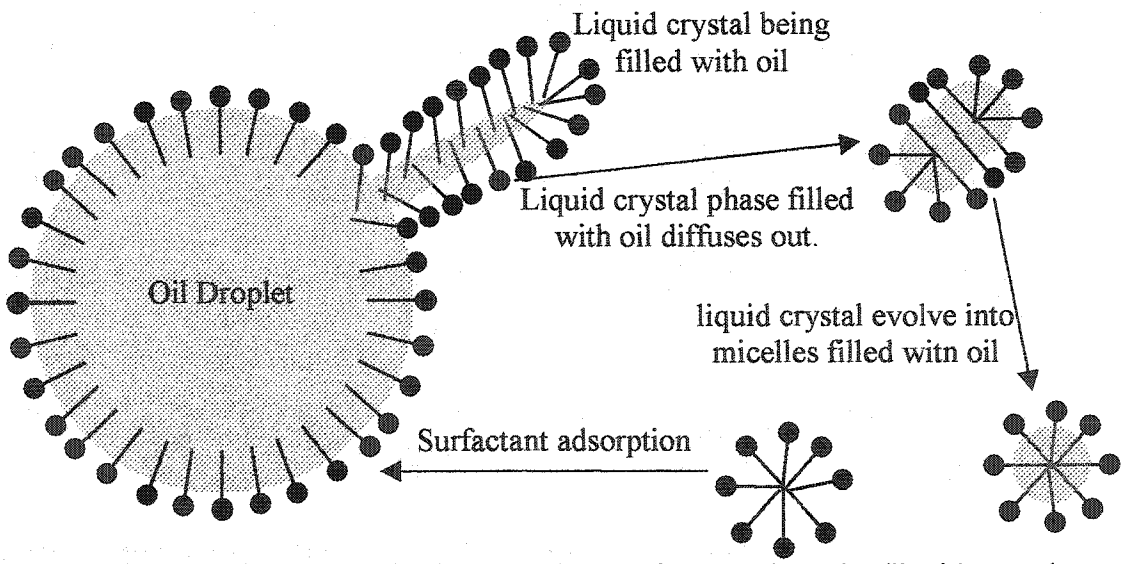

Figure 4.1b. Solubilization mechanism based on surfactant adsorption/liquid crystal formation followed by oil uptake and collective desorption of surfactant and oil. Adapted from Karaboni et al (10).

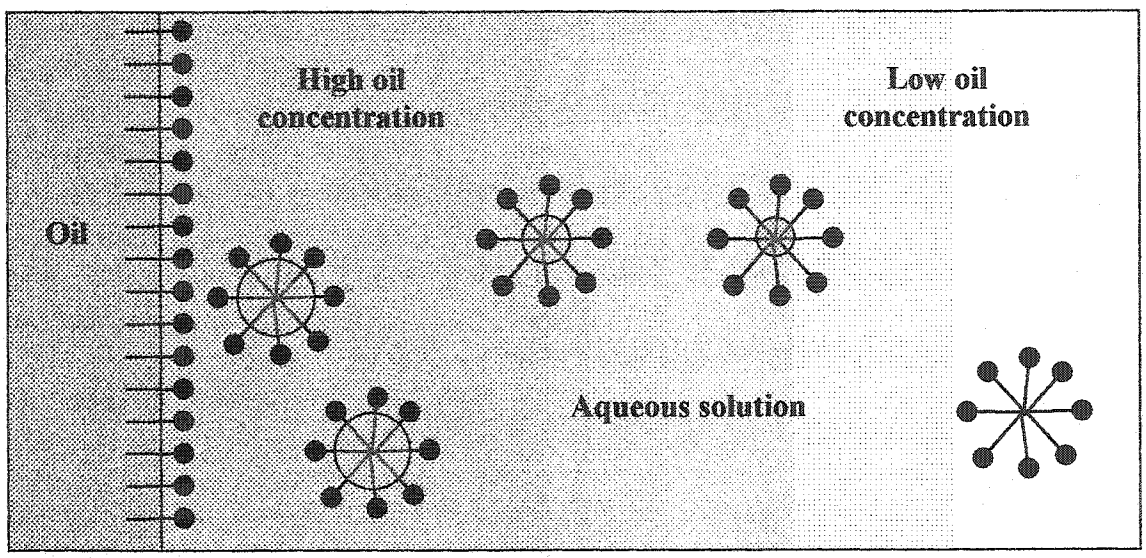

Figure 4.1c. Solubilization mechanism based on molecules of oil dissolved in water before being dissolved in micelles. Adapted from Karaboni et al (10).

The mechanism illustrated in Figure 4.1b has been extensively reported by Miller, et al. (13-18). Using video microscopy, they have consistently observed that "spontaneous" emulsification occurs when a lamellar liquid crystal forms on the surface of an oil droplet, thereby extracting oil from the droplet. They have argued that this mechanism (Figure 4.1b) results in a much faster solubilization than molecular solubilization (Figure 4.1c). Recently, they compared a molecular diffusion model to a mass transfer model using a mass transfer constant based on dissolution rates of individual oil droplets undergoing spontaneous emulsification and found better agreement with experimental data (18).

Despite the above observation, Friberg, et al. (19) have indicated that the presence of surfactant liquid crystals at the oil/water interface significantly reduces the rate of solubilization. While appearing contradictory, the observations of Miller and Friberg may

be compatible, considering that liquid crystals phases can be of different types and viscosities. For example, a high viscosity, rigid liquid crystal (cubic phases) would be expected to slow the solubilization process.

Carroll and O'Rourke conducted a series of solubilization kinetics studies of non-polar oils in non-ionic surfactant micelles (20-23). Their data followed the model depicted in Figure 4.1a, and confirmed that the temperature dependence can be reproduced assuming an Arrhenius kinetics (when the reaction rate decreases exponentially to the inverse of temperature), where the activation energy corresponds to the step where the micelles collide with the oil/water interface and modify the interface structure.

The activation energy identified by Carroll and O'Rourke (20-23), and the solubilization behavior observed by Miller and Friberg, can be explained in terms of the "rigidity" of the surfactant membrane. A rigid membrane (such as cubic liquid crystals) requires more energy to deform and therefore produces solubilization more slowly than a less rigid membrane. This illustrates the important observation that surfactant membranes can have widely varying levels of rigidity.

The role of the surfactant membrane is more obvious in emulsion coalescence. Helfrich (24) developed a mathematical model to account for the rigidity of amphiphile membranes:

$$\frac{dG}{dA} = \frac{K}{2}(c_1 + c_2 - 2c_0)^2 + \underline{K}c_1c_2 \qquad \text{Eq. 1}$$

Where dG/dA is the free energy cost of extending the interfacial area of the surfactant dynamic membrane, K is the membrane's elastic modulus (energy units), $\underline{K}$ is the

Gaussian modulus, c_1 and c_2 are the orthogonal curvatures of the amphiphile membrane and c_0 is the natural curvature of the amphiphile (an equilibrium property). This expression has been widely used in studying microemulsion systems, and their correspondent macroemulsions (8, 25,26).

Kalbanov (25) developed an expression for droplet coalescence rates as a function of the elastic modulus of the surfactant membrane. In general, the model uses an approximation where the kinetics is first order in the number of droplets and second order with respect to their size. He proposes that the activation energy required to deform the membrane is a power function of the membrane's elastic modulus.

The studies in this brief review suggest that the dynamic properties of microemulsions, both in the coalescence rates of their corresponding macroemulsions and the rate of solubilization by the microemulsion, are dictated by the toughness (rigidity) of the surfactant membrane. A rigid membrane requires more energy to deform and thus leads to slower macroemulsion coalescence and lower microemulsion solubilization rates.

Based on our understanding of the role of linker molecules in equilibrium systems, we herein hypothesize that as linker molecules modify the equilibrium interfacial properties of trichloroethylene microemulsions, they will also modify the interfacial rigidity. These changes will thereby impact the dynamic behaviors of coalescence in the corresponding macroemulsions as well as oil solubilization by the aqueous microemulsion solution.

To test this hypothesis, the interfacial tension, characteristic length and interfacial rigidity of optimum bicontinuous microemulsions (volume of oil = volume of water) of

trichloroethylene (TCE) – sodium dihexyl sulfosuccinate (SDHS) and water are evaluated as a function of different linker concentrations and combinations. These results are compared to coalescence of the corresponding macroemulsions and solubilization kinetics of oil uptake by the corresponding aqueous surfactant solutions.

Experimental procedures.

Materials

The following chemicals were obtained from Aldrich (Milwaukee, WI) at the concentrations shown in parenthesis, and used without further purification: trichloroethylene (TCE, 99%+), n-dodecanol (98+%), sodium chloride (99%+), and sodium dihexyl sulfosuccinate (80% wt. solution in water, Fluka brand). Sodium mono and dimethyl naphthalene sulfonate (SMDNS, 95+%) was supplied by CKWitco (Houston, TX). The main impurity in SMDNS (~less than 5%) is reported to be sodium sulfate; our own ion chromatography analysis reflects that the proportion of additional salt is less than 1%, and the proportion of mono to dimethyl isomers is approximately 65/35.

Methods.

Phase behavior studies were performed using equal volumes of aqueous solution and oil (5 mL each) in 15 mL flat bottom test tubes (15 cm height) sealed with silicon-lined screw caps. Electrolyte scans were performed by varying the sodium chloride concentration at constant temperature, initial aqueous concentration of sodium dihexyl sulfosuccinate, dodecanol, and SMDNS; and pressure (1 atm). Phase studies were

conducted in a water bath at 27°C, shaken once a day for three days, and left to equilibrate for two weeks. The volumes of excess oil, water and microemulsion phases at equilibrium were determined by measuring the levels of each phase in the test tube with a graduated ruler (precision of ± 0.15 ml). The concentrations of the surfactant, sodium dihexyl sulfosuccinate, and the hydrophilic linker, SMDNS, in the middle phase microemulsion and excess aqueous phase were measured using a Dionex ion chromatograph (equipped with a NS1 reverse phase column and a ionic suppressor ASRS 4mm and conductivity detector CD25). The mobile phase was a mixture of acetonitrile and water. Concentrations of dodecanol in the middle phase microemulsion and in the excess oil phase were measured using a Varian 3300 gas chromatograph equipped with a SPB-25 capillary column. Mass balance was used to determine the concentration of dodecanol in the excess water phase and the surfactant and SMDNS in the excess oil phase. Electrical conductivity of middle phase microemulsions was measured using a Fisher Scientific electric conductivity meter model 09-326-2.

Interfacial tension was measured using a model 500 University of Texas spinning drop interfacial tensiometer by injecting one to five microliters of the middle phase microemulsion into a 300 μl tube filled with the excess heavy phase (TCE). Turbidity during coalescence or solubilization was measured using a device shown schematically in Figure 4.2. The light source was a white light (72mW). The detector was a phototransistor with proportional voltage signal. The voltage signal was registered by a digital voltmeter (METEX M3850D) with computer interface. The signal was converted into turbidity using the following expression (27):

$$\tau = \frac{1}{L}\ln\left(\frac{I_0}{I}\right) = \frac{1}{L}\ln\left(\frac{V_o}{V}\right) \qquad \text{Eq. 2}$$

Where τ is the turbidity, with units of inverse length, L is the light path length, "I" is the intensity of light, and "I_0" is the intensity of light detected with the "clear" sample. The light intensity (I) was measured by the voltage (V) of the phototransistor as registered by the voltmeter.

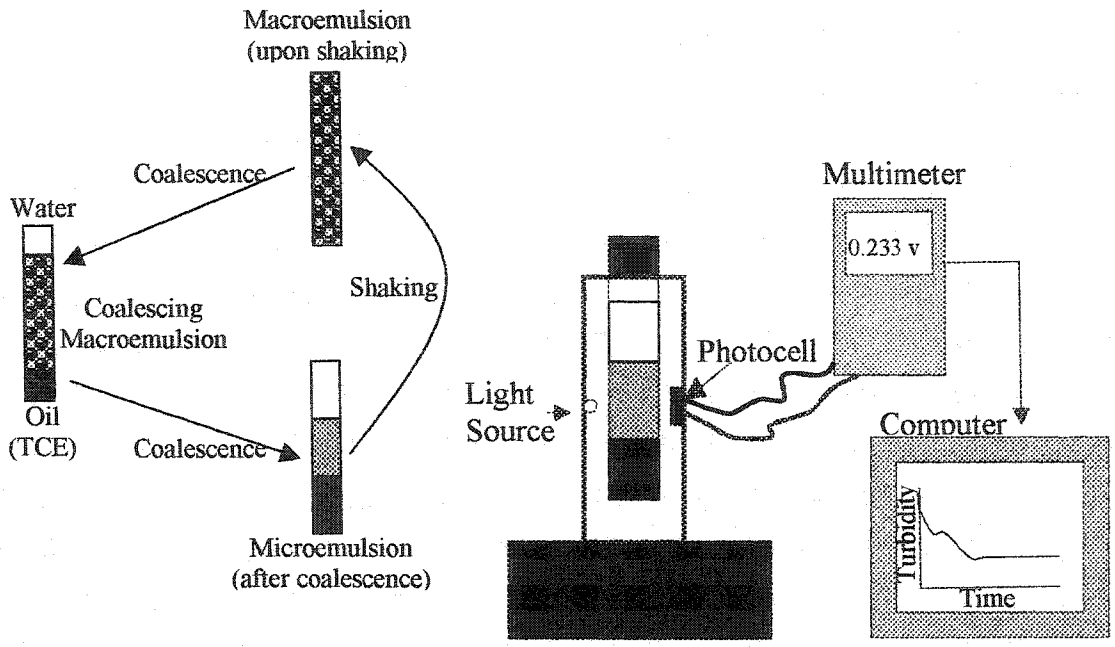

Figure 4.2. Schematic of the turbidity meter designed to study the kinetics of coalescence of macroemulsion and solubilization of microemulsions. Test tubes illustrate the relationship between the equilibrium middle phase microemulsion, the corresponding macroemulsion produced upon shaking and the intermediate states that occur in between.

The coalescence curves were obtained by shaking optimum middle phase microemulsions, followed by measuring the turbidity versus time as the macroemulsion droplets coalesce and the system approaches the equilibrium microemulsion condition. The light source and detector were aligned at the center of the test tube, where the middle

phase microemulsion forms after coalescence of the macroemulsion, as depicted in Figure 4.2. The test tubes in Figure 4.2 illustrate the relationship between the equilibrium microemulsion and the corresponding macroemulsion that forms upon shaking. Solubilization curves were obtained by injecting 250 μL of TCE into a 5ml-surfactant solution. The initial aqueous surfactant and linker concentrations are reported in the figures and tables. The turbidity was measured at the middle of the surfactant solution. To verify the validity of the tests, all experiments were conducted in triplicate.

Results and discussions

To study linker effects on coalescence kinetics for trichloroethylene (TCE)/ sodium dihexyl sulfosuccinate (SDHS) / water microemulsions, optimum bicontinuous microemulsions (volume of oil = volume of water) were obtained by electrolyte scans with different concentrations of hydrophilic linker (SMDNS) and lipophilic linker (dodecanol). At optimum formulation, the bicontinuous microemulsion is composed of equal volumes of oil and water and the interfacial tension between the middle phase and both excess oil and water phases is ultralow and at its minimum for a given scan. The optimum formulations for all systems are summarized in Table 4.1, with concentrations referring to the initial aqueous concentration before mixing with the oil.

Bourrel and Schecter (9) describe optimum bicontinuous microemulsions using the following criteria: (A) measuring the volume of oil and water (which are equal at optimum formulation) that participate in the microemulsion, (B) verifying that the interfacial tension between the middle phase and the excess water was the same as the

interfacial tension between excess oil and middle phase and ultralow (less than 0.1 mN/m) and (C) corroborating that the electrical conductivity of the bicontinuos middle phase is intermediate between the conductivity of the excess oil and water phases. The conductivity of all excess oil phases was less than 0.1 μS. The conductivity of middle phases and excess aqueous phases are presented in Table 4.1 for all the systems considered in this work. While other researches have used NMR techniques to determine the bicontinuity of microemulsion systems (28), we relied on the three techniques discussed above to provide sufficient evidence of bicontinuity.

Table 4.1. Optimum formulation of Type III formulations and electrical conductivity of corresponding bicontinuous middle phase microemulsion and excess aqueous phase.

[SDHS] mol/Lt	[SMDNS] mol/Lt	[$C_{12}H_{26}O$] mol/Lt	S*, % Wt. NaCl	Bicontinuos μS	Aqueous μS
0.103	0	0	1.25	1800	20000
0.103	0	0.045	1.15	1500	18000
0.103	0	0.09	0.85	1000	15000
0.103	0.045	0	1.9	3800	24000
0.103	0.09	0	3	9400	38000
0.103	0.135	0	5	17000	55000
0.103	0.045	0.045	1.4	3400	22000
0.103	0.09	0.09	1.6	3600	25000
0.103	0.135	0.135	2.3	9000	33000

S*: Electrolyte (NaCl) concentration necessary to reach optimum formulation.
Note: Conductivity of all excess oil phases is less than 0.1 μS.

Figure 4.3 shows the middle phase microemulsion scans for selected systems. These phase diagrams present the phase boundaries as a function of the surfactant SDHS (y-axis) and electrolyte NaCl concentration (x-axis). For a given surfactant concentration, as we increase the electrolyte concentration we cross from a Winsor Type I to Type III microemulsion, which is the first line crossed. The middle line, which occurs within the Winsor Type III region, indicates the optimum electrolyte concentration (i.e., the middle

phase microemulsion containing equal volumes of oil and water), and the last line indicates the transition from Type III to Type II microemulsion. The point where the three lines merge at high surfactant concentration is when the bicontinuous phase occupies the entire volume of the vial (no excess oil or water phases), and corresponds to a Type IV microemulsion. Bourrel and Schecter present a series of these type of phase diagrams for ionic surfactant systems (9). Others have presented phase diagrams for nonionic surfactants with temperature as the scanning variable (instead of electrolyte concentration), and with temperature on the y-axis and the surfactant concentration in the x-axis (reversed from above). Since this orientation can result in a phase diagram that has the appearance of a fish, it is sometimes referred to as a "fish diagram" (29-31).

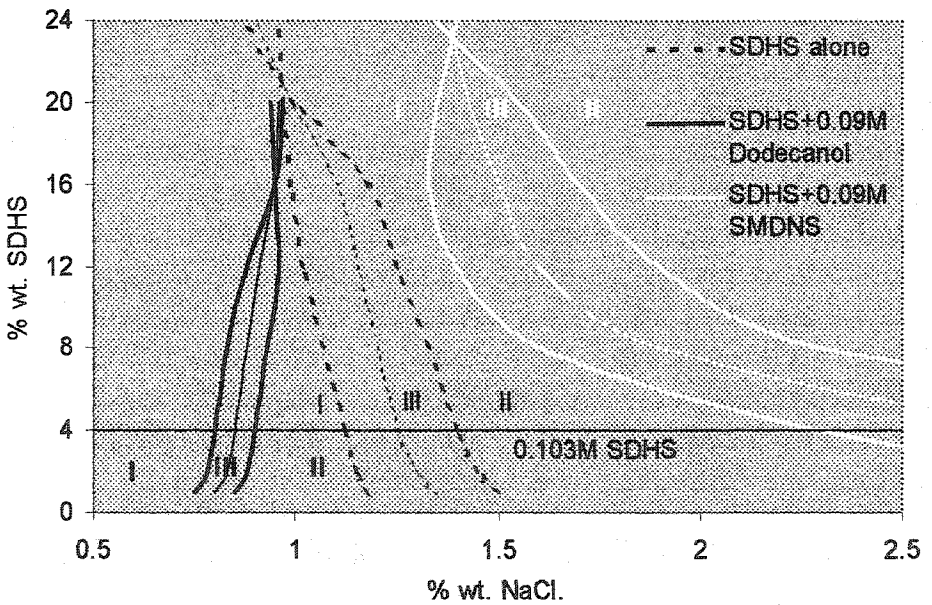

Figure 4.3. Phase diagram of TCE-SDHS microemulsions with and without lipophilic linker (0.09M dodecanol) or hydrophilic linker (0.09M SMDNS). The centerline of each system corresponds to the optimum middle phase microemulsion (equal volumes of oil and water in the middle phase) for a given scan @ 27°C.

The orientation (slope) of the phase diagrams varies as a function of other additives present along with the surfactant. From Figure 4.3 we note that for the surfactant alone the phase diagram is more or less vertical, while addition of the more hydrophobic dodecanol causes it to shift towards the left, and addition of the more hydrophilic SMDNS, causes it to shift towards the right. This trend has been observed previously for short chain and long chain alcohols (3,4-6, 9).

Once the equilibrium microemulsion phase was attained, each test tube was shaken to form a macroemulsion and introduced into the turbidity cell (Figure 4.2). Discrete turbidity values were then determined using voltage readings taken from the light detector and equation 4.2. Figure 4.4a shows selected examples of coalescence curves for different linker combinations. The coalescence curves register the decrease of turbidity (y-axis) versus time (x-axis). In all cases, the surfactant (SDHS) concentration was 0.103M.

Figure 4.4a shows that for the SDHS-TCE system without linkers, coalescence was complete (turbidity values begin to level off) in approximately 4 minutes (~240 seconds). When the hydrophilic linker, SMDNS, was added, the coalescence time reduced to 2 minutes (120 seconds). However, when the lipophilic linker (dodecanol) was added to the SDHS/ TCE/ water system, the coalescence time was extended to over fifteen minutes (900 seconds). When 0.09 M of SMDNS and 0.09 M of dodecanol were combined, the coalescence time was close to 5 minutes (300 seconds), similar to the time when surfactant SDHS alone was present.

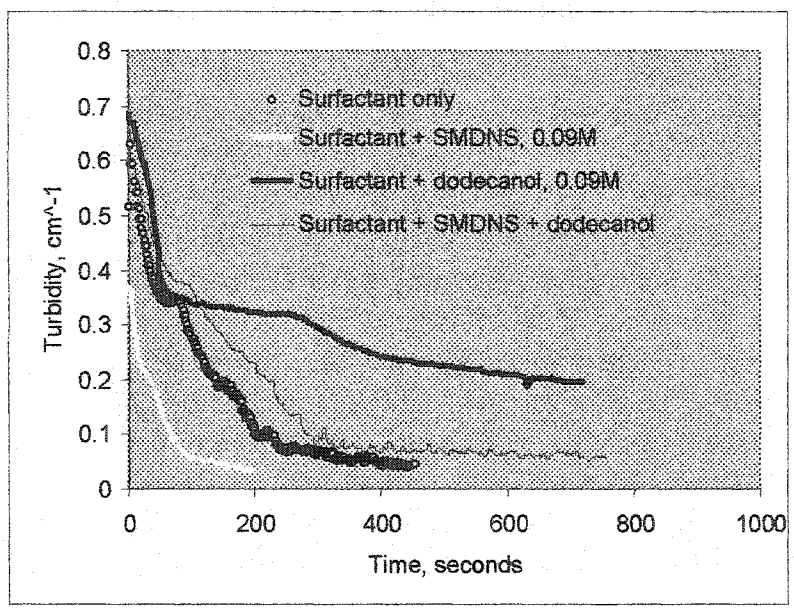

Figure 4.4a. Turbidity curves during coalescence of macroemulsions made from optimum middle phase TCE microemulsions, and excess TCE and aqueous phase with different linker combinations @ 27 °C, [SDHS] = 0.103 M.

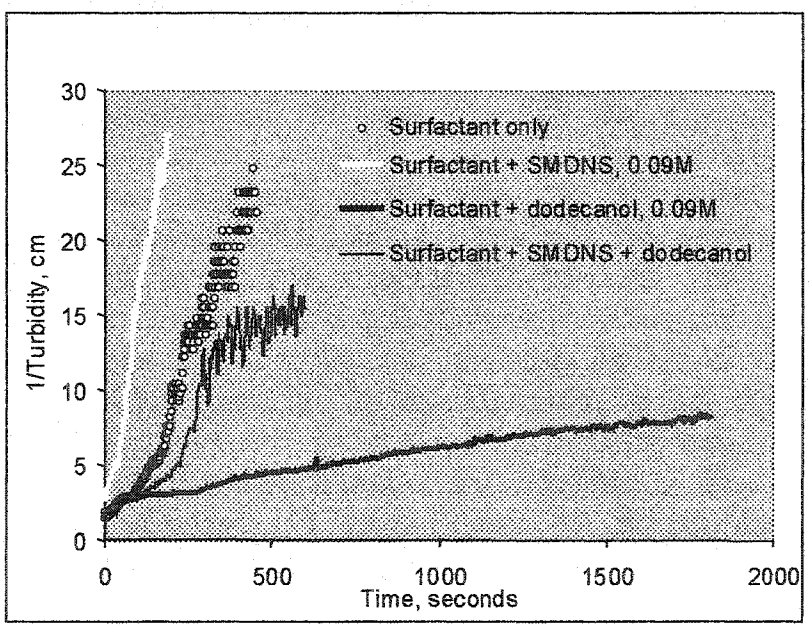

Figure 4.4b. Inverse turbidity curves during coalescence of macroemulsions made from optimum middle phase TCE microemulsions and excess TCE and aqueous phases at different linker combinations @ 27 °C, [SDHS] = 0.103 M.

This experiment confirms our initial hypothesis: as linker molecules alter the nature of the surfactant membrane they also impact the coalescence rates of the corresponding macroemulsions (which results upon shaking). Having established this effect, we next desire to identify the reason behind this effect, and, more importantly, to investigate how to exploit this effect to achieve desired dynamic properties, either faster or slower coalescence or solubilization rates.

Using turbidity to quantify coalescence curves is complicated since turbidity (τ) results from the light scattered by the colloidal system (Tyndall Effect). While turbidity can be measured easily by reduction in light intensity (Eq. 2), its correlation to the size and number of droplets is a more complicated function. Fletcher and Morris used the following expression to study the droplet size in microemulsions (27):

$$\tau = \frac{24\pi^3}{\lambda^4} P^2 * N * V_p^2 \qquad \text{Eq.3}$$

where λ is the light wavelength, P is a function of the refractive index of oil and water, N is the number of droplets per unit volume and V_p is the volume of each individual drop (assuming mono-disperse drop size distribution of the corresponding macroemulsion).

Using equation 3 to interpret coalescence curves requires certain assumptions regarding the correlation between the size and number of droplets. We assumed that upon shaking of Type III equilibrium microemulsions a macroemulsion is formed where excess oil and water phases form droplets that are suspended and undergoing coalescence into a bicontinous middle phase microemulsion phase. This assumption was confirmed by measuring the electrical conductivity of the corresponding macroemulsions during

coalescence. While the conductivity fluctuated throughout the coalescence, it remained close to the equilibrium middle phase microemulsion conductivity presented in Table 1. In addition, the "apparent" volume of the middle phase shrinks as the excess oil and water leave the coalescence region (i.e., as separate oil and water phases result from coalescence). We will subsequently assume that the volume of individual oil and water drops (V_p) remains constant throughout the coalescence process but the number of drops per unit volume (N) decreases. This assumes that as soon as two droplets (either oil or water droplets) coalesce into a larger droplet, the larger droplet rapidly departs from the macroemulsion to enter the corresponding excess phase (oil or water phase) (see Figure 2). Another way to understand this assumption is that the initial collision of the smaller droplets is the rate-limiting step of the coalescence. Under this assumption, the turbidity is proportional to the number of droplets per unit of volume ($\tau \propto N$), since any larger droplets resulting from coalescence immediately exit the macroemulsion.

The emulsion coalescence rate is normally expressed as the rate of decrease in the number of droplets per unit volume (-dN/dt). Rosen derives the coalescence rate of a mono-dispersed emulsion assuming that the diffusion and effective collision of droplets is the rate limiting step (32). This model is based on second order kinetics relative to the number of droplets per unit of volume ($-dN/dt = K*N^2$); the assumptions used by Rosen are consistent with our constant droplet volume assumption above for interpreting turbidity data. The explicit expression of this model is (32):

$$\frac{1}{N} = \frac{4K_BT}{3\eta} * t * e^{-\frac{E}{K_BT}} + C \qquad \text{Eq.4}$$

where N is the number of droplets per unit volume of the macroemulsion, K_B is the Boltzman constant, T is the absolute temperature, η is the viscosity of the bicontinous microemulsion medium, t is the time, E is the activation energy of droplet collision, and C is the integration constant and corresponds to the initial inverse droplet concentration. Writing a similar expression in terms of turbidity, results in:

$$\frac{1}{\tau} = k_c * t + \frac{1}{\tau_0} \qquad \text{Eq.5}$$

where the coalescence kinetic constant (k_c) is :

$$k_c = \frac{1}{A}\frac{4K_B T}{3\eta} e^{-\frac{E}{K_B T}} \qquad \text{Eq.6}$$

and where A is the proportionality constant between the turbidity and the droplet concentration ($\tau = A*N$) after lumping the constants in Eq. 3.

Figure 4.4b shows the inverse turbidity curves for the same systems plotted in Figure 4.4a. The nearly linear shape of the "inverse" turbidity curves confirms that the constant drop volume assumption is, in general, a good first approximation for these particular systems. Likewise, the same types of curves were generated and the same linear trend was observed for the rest of the formulations indicated in Table 4.1.

From equation 5, we see that the slope of the linear trend of the inverse turbidity curves versus time corresponds to the coalescence kinetic constant. Figure 4.5 summarizes the coalescence kinetic constants (k_c) as a function of linker concentration for the various linker combinations. To simplify the display of the results, the concentration of linker molecules shown in the x-axis is the initial aqueous linker

concentration (also in Figures 4.7 through 4.9). The actual linker concentration in the middle phase microemulsion is presented in Table 4.2 (noted as interfacial concentration), and is observed to increase proportionally to the initial aqueous concentration; thus the trends in Figure 4.5 and Figures 7 to 9 would be the same if plotted against interfacial concentrations. In a recent paper we have discussed the details of linker partitioning in middle phase microemulsion (3).

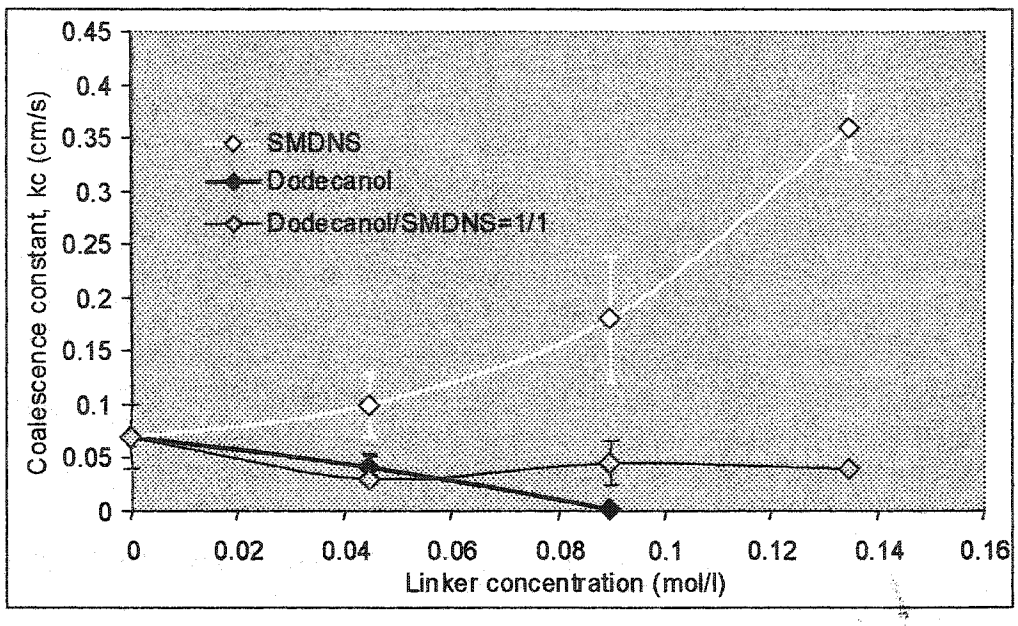

Figure 4.5. Coalescence kinetic constant (k_c) for macroemulsions made from optimum middle phase microemulsions and excess TCE and aqueous phases at different linker concentrations @ 27 °C, [SDHS] = 0.103 M.

Table 4.2. Optimum middle phase (Type III) viscosity, concentrations of SMDNS and dodecanol, and percentage of SMDNS in the middle phase microemulsion.

[SDHS] mol/Lt	[SMDNS] mol/Lt	[$C_{12}H_{26}O$] mol/Lt	$(\eta/\rho)^*$ Cst	[SMDNS] interface mol/Lt	[$C_{12}H_{26}O$] interface mol/Lt	φ_{SMDNS} (%)
0.103	0	0	4.3 ± 0.2			
0.103	0	0.045	4.3 ± 0.4		0.03	
0.103	0	0.09	4.1 ± 0.2		0.05	
0.103	0.045	0	4.1 ± 0.3	0.03		30
0.103	0.09	0	4.5 ± 0.2	0.11		55
0.103	0.135	0	5.3 ± 0.2	0.2		65
0.103	0.045	0.045	4.1 ± 0.4	0.05	0.023	60
0.103	0.09	0.09	4.0 ± 0.2	0.09	0.05	60
0.103	0.135	0.135	5.1 ± 0.3	0.15	0.083	75

η: Viscosity of the middle phase microemulsion
ρ: Density of the middle phase microemulsion
φ_{SMDNS}: percentage of the SMDNS present in middle phase microemulsion

The data in Figure 4.5 show that when the hydrophilic linker (SMDNS) is added to the surfactant formulation, the coalescence rate constant increases with increasing linker concentration (initial or interfacial). When the lipophilic linker (dodecanol) is added to the surfactant formulation, the coalescence rate constant decreases (slower coalescence rate). Upon simultaneous addition of both linkers, the coalescence rate constant is intermediate between the two single linker effects. The data presented in Figure 4.5, along with the initial observation made in Figure 4.4a, thus confirm our hypothesis that linker molecules modify the interfacial properties of the microemulsion system, as reflected by their impact on the coalescence rate of the corresponding macroemulsion systems.

Recall that Eq. 6 gives an expression for the coalescence constant (k_c) as a function of only two basic microemulsion properties: the viscosity (η) and the activation energy of collision (E) (all the others parameters are constant for these systems). Table 2

summarizes the kinematic viscosity (η/ρ) of the different linker combinations, which are observed to be quite similar for the different linker combinations. In addition, the density (ρ) of all the middle phase microemulsions were quite similar, ranging between 1.22 g/ml to 1.26 g/ml. From this analysis we conclude that the viscosity (η) must not be the factor impacting the coalescence constant, and we must conclude that the linkers directly affect the collision activation energy (E). But how does the presence of linker molecules affect the activation energy?

Kalbanov (25) provides a partial response to this question. He found that the activation energy for coalescence (E) of middle phase microemulsion systems is a power function of the surfactant dynamic membrane bending rigidity modulus (K). He also observed that the activation energy increases as the rigidity increases.

Helfrich and Kozlov (33) derived an expression showing that when short chain cosurfactants (which are similar to our hydrophilic linkers) are added to a surfactant system, the bending rigidity (K) is reduced. From this result, a hydrophilic linker would also be expected to decrease the bending rigidity (K), and, according to Kalbanov (25), this should be evidenced by lower activation energy of coalescence (E), and therefore, faster coalescence, as observed in our experiments.

Corroborating this line of reasoning, Nazario, et al. (34) used a laser induced temperature jump to study the dynamic behavior of reverse AOT micelles in isooctane. They found that addition of a long chain alcohol, such as decanol, increased the bending rigidity (K), thereby retarding the relaxation time of the surfactant membrane. On the other hand, the addition of non-ionic cosurfactant (e.g. $C_{10}E_8$) was observed to reduce the

bending rigidity (K) and shorten the relaxation time after the laser pulse. The observation of Nazario et al. (34) that decanol increases the rigidity of the surfactant membrane contrasts with the expected behavior for medium chain alcohols, which reduce this rigidity (7). Zana reviewed the role of alcohols in microemulsions, commenting on the distinctive behavior of decanol by explaining that neutron scattering data shows that the decanol molecules tend to be segregated towards the central core of the micelle (7). This observation is consistent with the lipophilic linker concept of Graciaa and Salager, which formed the basis for this work (4-6).

From the results of Kozlov and Nazario, it is logical to hypothesize that the presence of linker molecules modifies the interfacial rigidity, the activation energy for coalescence and thereby the coalescence constant (k_c) in the macroemulsion. To test this hypothesis, the interfacial rigidity of these linker-modified microemulsions must be evaluated. This is not a trivial task, especially because there is not a standard technique to do so.

Recently, we have proposed a technique to estimate this interfacial rigidity, based on interfacial tension and solubilization data (35):

$$\gamma^* = \frac{E_r}{4\pi\xi^{*2}} \qquad \text{Eq. 7}$$

where γ^* is the interfacial tension (either middle phase/ excess water or middle phase/ excess oil) at optimum formulation, E_r is the interfacial rigidity (expressed in K_BT units at 300 Kelvin), and ξ^* (Å) is the characteristic length of the surfactant membrane in the middle phase microemulsion at optimum formulation. Figure 4.6 shows a schematic of

the characteristic length of the surfactant dynamic membrane (ξ) based on a microscopic lattice model of the bicontinuous microemulsion.

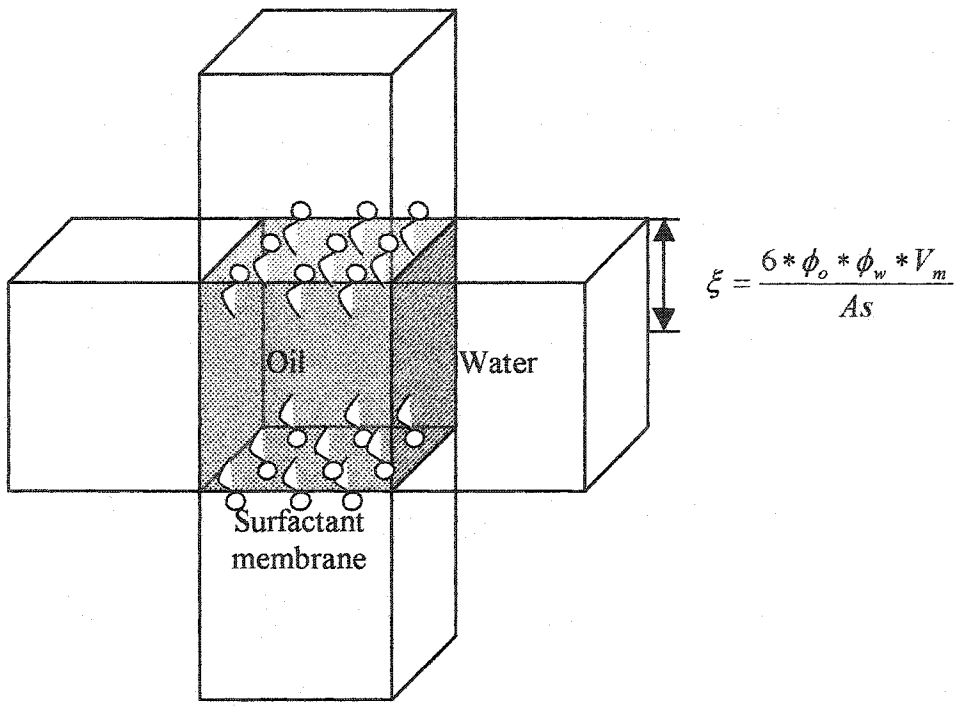

Figure 4.6. Microscopic lattice model of an optimum bicontinuos microemulsion showing the surfactant dynamic membrane and the characteristic length (ξ)

The surfactant membrane characteristic length (ξ), in general, can be calculated as:

$$\xi = \frac{6 * \phi_o * \phi_w * V_m}{As} \qquad \text{Eq.8}$$

where ϕ_o , ϕ_w are the volume fractions of oil and water in the middle phase microemulsion, respectively, V_m is the total volume of the middle phase microemulsion (in $Å^3$), and As is the interfacial area making up the surfactant membrane by the surfactant, cosurfactant and hydrophilic linkers (in $Å^2$). The interfacial area can be calculated as:

$$As = \sum_i Cs_i * V_w * \varphi_i * 6.023 * 10^{23} * a_i \qquad \text{Eq.9}$$

where Cs_i is the initial concentration of the surfactant "i" in the aqueous solution, V_w is the initial volume of the aqueous solution in the system, φ_I is the fraction of surfactant, cosurfactant or hydrophilic linker in the middle phase microemulsion (with respect to the total surfactant concentration) and a_i is the area per molecule of the surfactant "i".

A similar set of equations has been proposed by Ruckenstein and Nagarajan (36), but in their case, the interfacial tension used is that between the excess oil and excess water phases ($\gamma_{o/w} \sim 2\gamma^*$). According to their equation, the interfacial rigidity (E_r) is approximately $1K_BT$. It has been found, however, that the bending elasticity (K), a similar concept to the interfacial rigidity (E_r), can have different values for different formulations (37). De Gennes and Taupin also have proposed an expression similar to equation 7 for micelles (38). Our equation is unique because it is a general expression that can be applied to both micelles and bicontinuous microemulsions.

Using equation 7 to evaluate the interfacial rigidity requires knowledge of the characteristic length of the different linker series, which were evaluated using equations 8 and 9, with the area per molecule taken to be 100Å^2 /molecule for SDHS and 90 Å^2 /molecule for SMDNS (2). Lipophilic linkers are not included in the calculation of the area because, based on the lipophilic linker effect, they don't adsorb at the interface (4-6). For medium chain alcohols, that behave as cosurfactants (as discussed above), the interfacial area occupied by the alcohol should be included (7). While SDHS was measured to be 99+% in the middle phase, SMDNS was only partially present in the

middle phase, as shown in Table 4.2 (φ_{SMDNS}, expressed in percent of initial SMDNS added).

Figure 4.7 presents the middle phase microemulsion characteristic length at optimum formulation (ξ^*,Å) as a function of the initial linker concentration (hydrophilic, lipophilic or each when combined linkers) in the aqueous surfactant solution. As can be seen from Figure 4.7, increasing concentrations of hydrophilic linker decrease the characteristic length of the interface by spreading the surfactant molecules and probably reducing the ordering of the oil that interacts directly with the surfactant tails. Conversely, increasing concentrations of lipophilic linker (dodecanol) increase the characteristic length likely due to an increase in the ordering of the oil next to the surfactant tails (4). The use of combined linkers, which integrate these effects, has an intermediate impact.

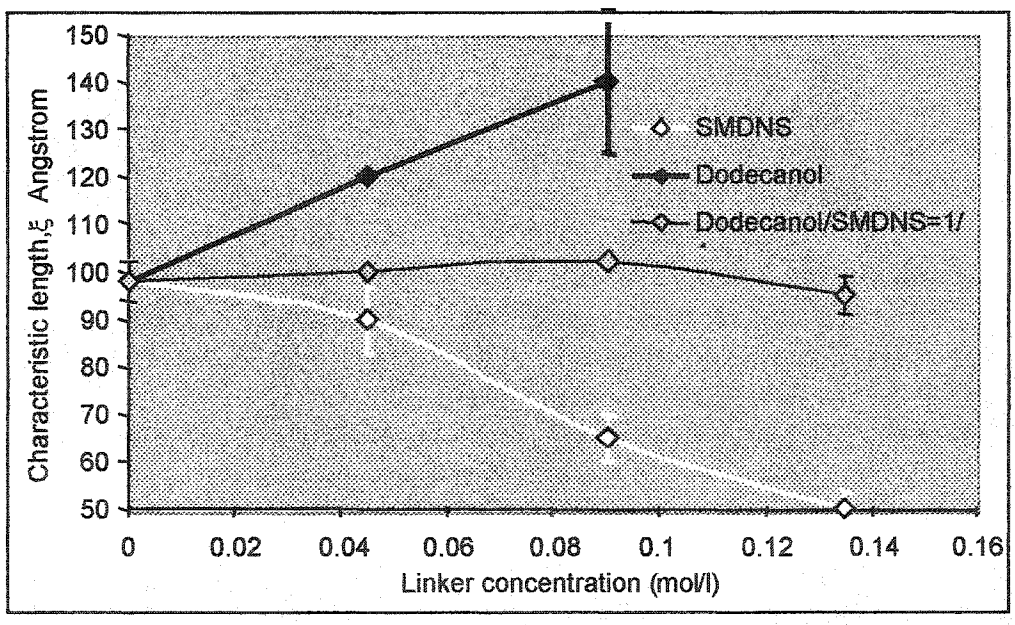

Figure 4.7. Characteristic length (ξ) of optimum middle phase TCE microemulsions at different linker concentrations @ 27 °C, [SDHS] = 0.103 M.

Figure 4.8 shows the measured interfacial tension at optimum formulation (γ^*) for the various linker systems. Under optimum formulation conditions, the interfacial tension is the same between the middle and excess water phases as between the middle and the excess oil phases. Here the trend is that lipophilic linkers tend to decrease the interfacial tension, hydrophilic linkers to increase it and a combination of linkers tends to decrease the interfacial tension as well.

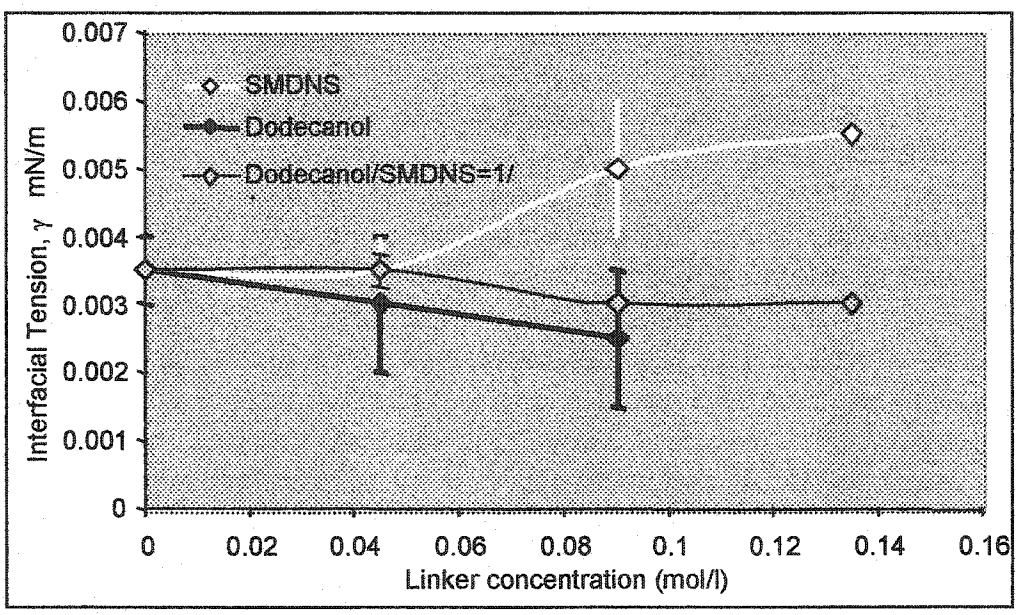

Figure 4.8. Interfacial tension of optimum middle phase TCE microemulsions at different linker concentrations @ 27 °C, [SDHS] = 0.103 M.

With the data of Figures 4.7 and 4.8 and the aid of equation 7, the interfacial rigidity (E_r) can be estimated. In Figure 4.9 this interfacial rigidity is plotted versus the initial linker concentration in the aqueous phase for the various linker systems previously considered. Figure 4.9 shows that the interfacial rigidity increases with increasing concentrations of the lipophilic linker (dodecanol), but decreases with increasing

concentrations of the hydrophilic linker (SMDNS). The combined linkers have an intermediate effect. These results agree with the results of Nazario and Kozlov (33,34).

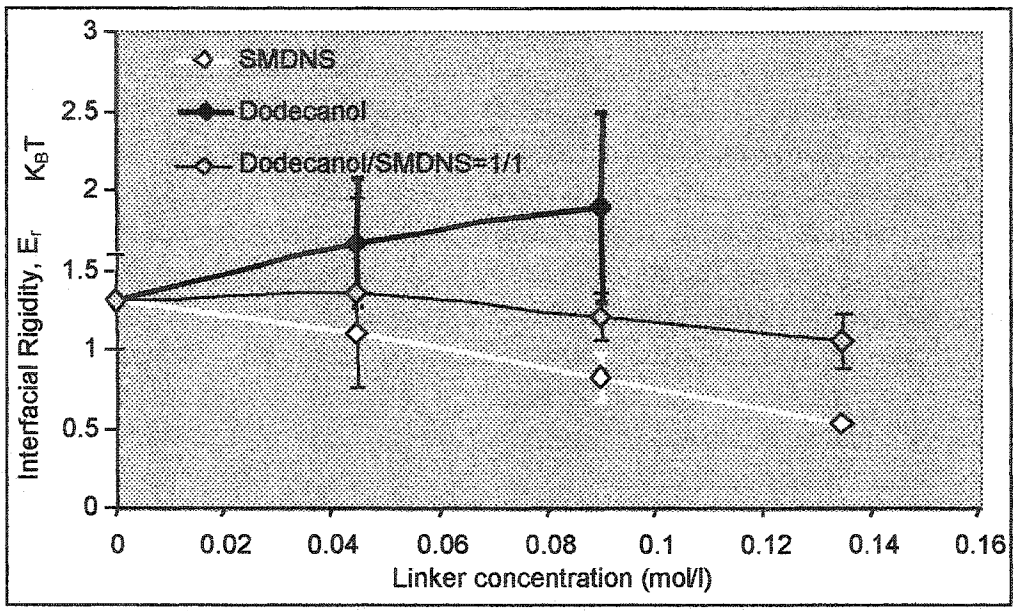

Figure 4.9. Interfacial rigidity (E_r) of optimum middle phase TCE microemulsions at different linker concentrations @ 27 °C, [SDHS] = 0.103 M.

Throughout the description of these results we have seen that the addition of both linkers shows an intermediate effect between hydrophilic and lipophilic linkers. While this result seems natural, a parallel study on the partition of each linker showed that an equimolar combination of SMDNS and dodecanol increased the partition of each linker into the middle phase to form what appears to be a "self-assembled surfactant at the interface" between these linker molecules (3). Moreover these combined linkers can, to an extent, replace the main surfactant at the interface, such that middle phase microemulsions can be as much as ten times more concentrated in linker molecules than the concentration of the surfactant (3). The intermediate behavior of combined linkers is consistent with the hypothesis of a self-assembly between lipophilic and hydrophilic

linkers to form a surfactant-like structure at the interface. This intermediate behavior could also be due to the solubilization site of the lipophilic linker being closer to the interface due to the presence of the hydrophilic linker, but we don't yet have spectral data (NMR, SANS) to fully answer these questions; such will be the focus of future research.

De Gennes and Taupin (38) predicted that the characteristic length (ξ) and the surfactant dynamic membrane elasticity modulus (K) are related through the following equation:

$$\xi = \alpha * e^{\frac{2\pi K}{K_B T}} \qquad \text{Eq. 10}$$

where α is a length constant specific to the oil-surfactant system, and all the other variables are as previously defined. We have compared equation 7 to the expression of De Gennes and Taupin (38) for interfacial tension and concluded that $E_r \sim 2\pi K$ (35). Replacing this equivalence in equation 10:

$$\xi = \alpha * e^{\frac{E_r}{K_B T}} \qquad \text{Eq. 11}$$

The data of characteristic length (Figure 4.7) and its corresponding interfacial rigidity (Figure 4.9) are plotted in Figure 4.10. Along with the data, we plot values from equation 11 using an α value of 35 Å (fitted). The agreement in trend between the experimental data and the curve plotted using equation 11 shows that the fundamental equation of De Gennes (Eq. 10) holds true for this data, which confirms the validity of the surfactant dynamic membrane interfacial rigidity (E_r) concept previously introduced (35).

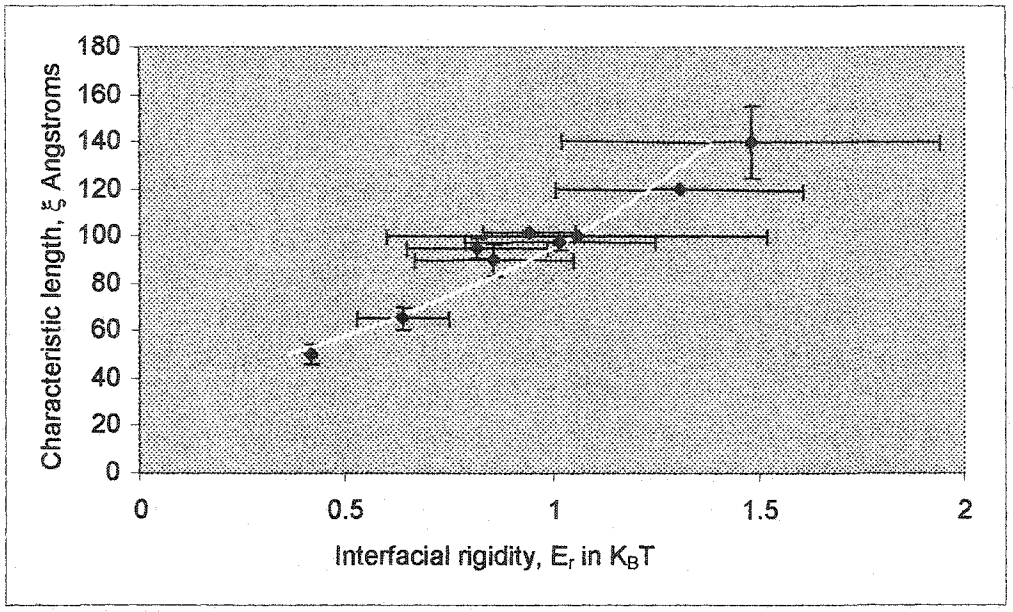

Figure 4.10. Correlation between characteristic length (ξ) and interfacial rigidity (E_r). White line represents the DeGennes correlation using α=35Å.

The data in Figure 4.9 serve to further confirm the first part of our hypothesis, that linker molecules do modify the interfacial rigidity. Next we want to consider whether the surfactant dynamic membrane interfacial rigidity affects the macroemulsion coalescence rate. We thus plot the coalescence constant (k_c) versus the interfacial rigidity (Er) in Figure 4.11. An exponential relationship was found to best fit the data (note that Figure 4.11 is a semi-log plot). While the error range in the coalescence constant (k_c) and the interfacial rigidity (E_r) are not minor, the data does confirm the hypothesis that interfacial rigidity is a component of the activation energy of coalescence. If we compare the empirical correlation obtained in Figure 4.11 with equation 6, the activation energy of coalescence is observed to be over three times the interfacial rigidity (E~3.8*E_r). Kalbanov (25) showed the activation energy of coalescence to be a function of the elasticity modulus (E~ 7K), which is similar to our results, but we can not directly

compare these results since the assumptions in his kinetic model are different from the assumptions in our study.

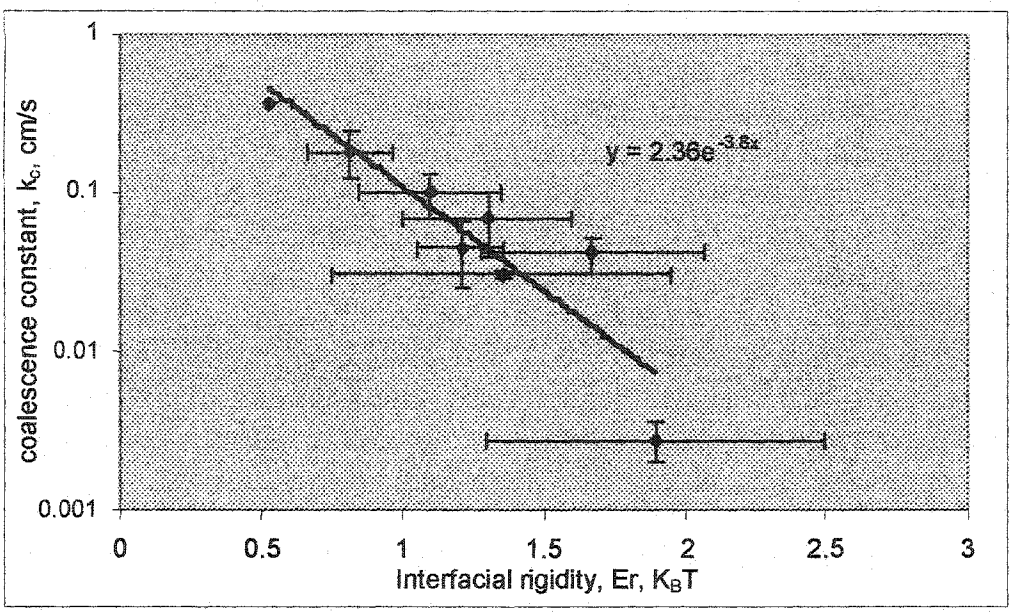

Figure 4.11. Correlation between coalescence constant (k_c) and interfacial rigidity (E_r).

Up to this point, the effect of linkers on interfacial properties (characteristic length, interfacial tension, and interfacial rigidity) and on kinetics of coalescence have been studied. We conclude this paper by reporting an initial solubilization study in an attempt to verify the proposed effect of linkers on the solubilization kinetics of TCE in SDHS microemulsions, based on the central role of the surfactant dynamic membrane in both macroemulsion coalescence and microemulsion solubilization rates.

As indicated in the method section, this solubilization rate study was performed by injecting 250 μL of TCE into 5 mL of the surfactant solution. Figure 4.12 shows the turbidity evolution for the solubilization of trichloroethylene in the surfactant solution alone (SDHS) and in a solution of SDHS + 0.135 M SMDNS. The addition of lipophilic

linkers or combined linkers could not be considered because the introduction of TCE into solution containing dodecanol produced a surfactant-rich separate phase containing the surfactant, the oil and the linker(s).

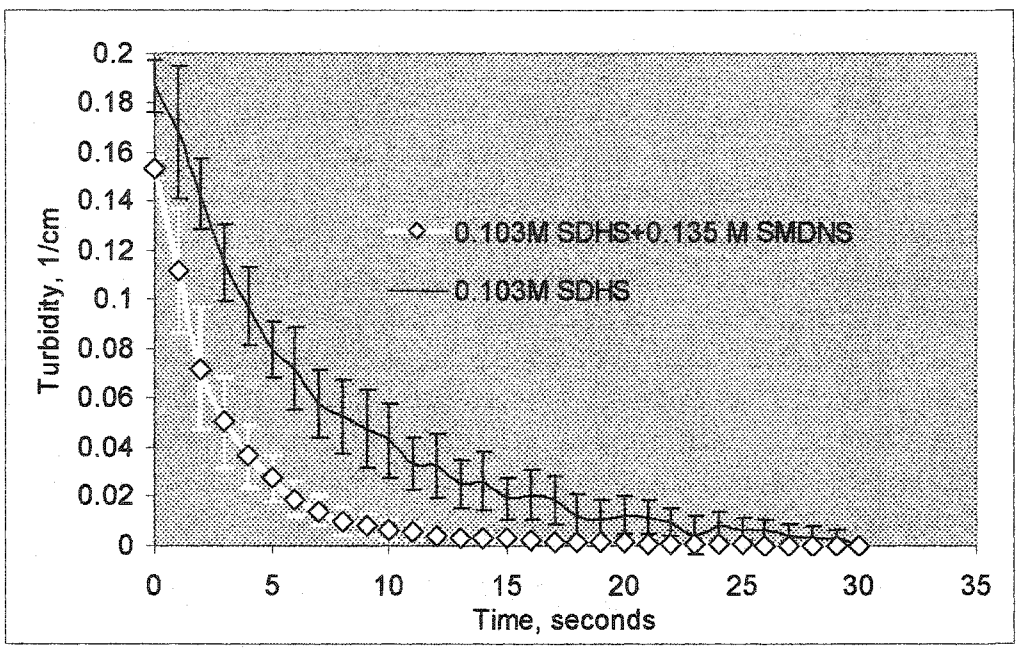

Figure 4.12. Turbidity curves during solubilization of 250 µl of TCE injected into 5ml of SDHS solution to form a type I microemulsion @ 27 °C, [SDHS] = 0.103 M.

From the data that could be obtained, however, it is seen that the presence of the hydrophilic linker, SMDNS increases the rate of solubilization, just as it increased the rate of coalescence. Nonetheless, the interpretation of these curves is even more complex than the coalescence curves. According to Carroll and O'Rourke (20-23) the solubilization rate is a function of the surfactant concentration, which in this case held constant (0.103 M SDHS). The solubilization rate is also a function of the proximity to the cloud point for non-ionic surfactants (20,21). In our case this is analogous to the

proximity to the optimum formulation; for both series, the electrolyte concentration was 70% of the optimum salinity. While the method is not amenable to numerical evaluation of the activation energy of solubilization; it does give an appreciation of the effect of hydrophilic linkers on solubilization kinetics. When lipophilic linkers are added, the equilibration time for the formation of the surfactant-rich separate phase is on the order of several hours.

Conclusions

Through turbidity curves, we have evaluated the ability of linker molecules to affect the dynamic behavior and the interfacial properties of middle phase microemulsions and their related macroemulsions. In our study, hydrophilic linkers reduced the interfacial thickness (characteristic length) of TCE microemulsions. This result agrees with the picture of hydrophilic linkers adsorbing at the oil/water interface, thereby opening "holes in the interface" and "loosening" the packing of the surfactant at the interface, which thus explains the reduced rigidity (E_r) in hydrophilic linker microemulsions. This reduced rigidity makes it easier for the interface to modify its shape, which seems to help reduce the activation energy of coalescence and solubilization processes.

Lipophilic linkers had an opposite effect to their hydrophilic counterpart. Since lipophilic linkers segregate in the palisade layer of the interface, they extend the thickness of the interface, increasing the characteristic length of the microemulsion dynamic membrane. They also increase the "tightness" of the surfactant dynamic membrane, leading to increased rigidity, higher activation energy, slower coalescence, and we

hypothesize, a slower solubilization. Combined linkers had an intermediate effect between hydrophilic and lipophilic linkers. Combined linkers can be interpreted as an assembled surfactant system. More important they lead to increased solubilization capacity without sacrificing kinetic performance.

Acknowledgement

We would like to acknowledge the industrial sponsors of the Institute for Applied Surfactant Research of the University of Oklahoma for helping to support this research.

References

1. Uchiyama, H.; Acosta, E.; Tran, S.; Sabatini, D. A. and Harwell, J. H. Supersolubilization in Chlorinated Hydrocarbon Microemulsions: Solubilization Enhancement by Lipophilic and Hydrophilic Linkers. *Ind. Eng. Chem. Res.* **2000**, 39(8), 2704
2. Acosta, E.; Uchiyama, H.; Sabatini, D. A. and Harwell, J. H. The role of hydrophilic linkers. *J. Surfact. Deterg.* **2002**, 5(2), 151
3. Acosta, E.; Uchiyama, H.; Tran, S; Sabatini, D.A. and Harwell, J.H. Formulating Chlorinated Hydrocarbon Microemulsions Using Linker Molecules. *Environ. Sci. Technol.* **2002,** 36(21), 4618

4. Graciaa A.; Lachaise J.; Cucuphat C., Bourrel M. and Salager J.L. Improving solubilization in microemulsions with additives. 1. The lipophilic linker role. *Langmuir.* **1993**, 9(3), 669
5. Graciaa A.; Lachaise J.; Cucuphat C., Bourrel M. and Salager J.L. Improving solubilization in microemulsions with additives. 2. Long chain alcohols as lipophilic linkers. *Langmuir.* **1993**, 9(12), 3371
6. Salager, J. L.; Graciaa, A. and Lachaise J. Improving solubilization in microemulsions with additives. Part III: lipophilic linker optimization. *J. Surfactant Detergents.* **1998**, 1(3), 403.
7. Zana, R. Aqueous surfactant-alcohol systems: a review. *Adv. Colloid Interface. Sci.* **1995**, 57, 1
8. Binks, Bernard P. In *Modern Aspects of Emulsion Science*. Binks, Bernard P. Ed. Royal Society of Chemistry, Cambridge, UK, 1998, p. 1
9. Bourrel, M. and Schecter R. *Microemulsions and Related Systems*. Marcell Dekker Inc. New York, 1988
10. Karaborni, S; Van Os, N. M.; Esselink, K. and Hilbers, P.A. Molecular dynamics simulations of oil solubilization in surfactant solutions. *Langmuir* **1993**, 9(5), 1175
11. Evilevitch, A.; Olsson, U.; Jönsson, B. and Wennerström, H. Kinetics of oil solubilization in microemulsion droplets. Mechanism of oil transport. *Langmuir* **2000**, 16(23), 8755
12. Evilevitch, A.; Olsson, U.; Jönsson, B. and Wennerström, H. Molecular Transport in a Nonequilibrium Droplet Microemulsion System. *Langmuir* **2001**, 17(22), 6893

13. Nishimi, T.; Miller, C. A. Spontaneous Emulsification of Oil in Aerosol-OT/Water/Hydrocarbon Systems. *Langmuir* **2000**, 16(24), 9233

14. Rang, M. J.; Miller, C. A. Spontaneous emulsification of oils containing hydrocarbon, nonionic surfactant, and oleyl alcohol. *J. Colloid Interface Sci.* **1999**, 209(1), 179

15. Miller, C. A. Solubilization and intermediate phase formation in oil-water-surfactant systems. *Tenside Deterg.* **1996**, 33(3), 191

16. Lim, J. C.; Miller, C. A. Dynamic behavior and detergency in systems containing nonionic surfactants and mixtures of polar and nonpolar oils. *Langmuir.* **1991**, 7(10), 2021

17. Miller, C. A. Spontaneous emulsification produced by diffusion. *Colloids Surf.* **1988**, 29(1), 89

18. Pena, A. A.; Miller, C. A. Kinetics of Compositional Ripening in Emulsions Stabilized with Nonionic Surfactants. *J. Colloid Interface Sci.* **2001**, 244(1), 154

19. Friberg, S. E.; Neogi, P. In *Surfactant-Based Separation processes.* Scamehorn J. F. & Harwell, J.H Eds. Surfactant Science Series vol. 33. Marcel Dekker, N.Y.,**1989**, p. 119

20. Carroll, B. J. The kinetics of solubilization of nonpolar oils by nonionic surfactant solutions. *J. Colloid Interface Sci.* **1981**, 79(1), 126

21. Carroll, B. J.; O'Rourke, B. G. C. and Ward, A. J. I. The kinetics of solubilization of single component nonpolar oils by a nonionic surfactant. *J. Pharm. Pharmacol.* **1982**, 34, 287

22. O'Rourke, B. G. C.; Carroll, B. J. and Ward, A. J. I. Investigations of the solubilization kinetics of binary mixtures of nonpolar oils by nonionic surfactants. *J. Pharm. Pharmacol.* **1987**, 39, 865

23. Carroll, B. J.; Doyle, P. J. Solubilization kinetics of a triglyceride/n-alkane mixture in a nonionic surfactant solution. *J. Pharm. Pharmacol.* **1988**, 40, 229

24. Helfrich, W. Elastic properties of lipid bilayers. *Z. Natureforsch.* **1973**, 28c, 693

25. Kabalnov, A. S. In *Modern Aspects of Emulsion Science*. Binks, Bernard P. Ed. Royal Society of Chemistry, Cambridge, UK, **1998**, p. 205

26. Gelbart, W. M., Ben-Shaul, A. and Roux, D. Editors. *Micelles, Membranes, Microemulsions and Monolayers*, Springer-Verlag, New York, 1994

27. Fletcher P. D. I.; Morris, J. S. Turbidity of oil-in-water microemulsion droplets stabilized by nonionic surfactants. *Colloids Surf. A.* **1995**, 98, 147

28. Guering, P.; Lindman, B. Droplet and bicontinuous structures in microemulsions from multicomponent self-diffusion measurements. *Langmuir* **1985**, 1, 464

29. Schubert, K.-V.; Kaler, E. W. Nonionic microemulsions. *Ber. Bunsen-Gesell.* **1996**, 100(3), 190

30. Cates, M. E.; Andelman, D.; Safran, S. A. and Roux, D. Theory of microemulsions: comparison with experimental behavior. *Langmuir* **1988**, 4(4), 802

31. Kahlweit, M.; Strey, R.; Haase, D.; Kunieda, H.; Schmeling, T.; Faulhaber, B.; Borkovec, M.; Eicke, H. F.; Busse, G.; et al. How to study microemulsions. *J. Colloid Interface Sci.* **1987**, 118(2), 436

32. Rosen, Milton J. *Surfactants and Interfacial Phenomena*. 2nd Ed. John Wiley & Sons, New York, 1989

33. Kozlov, M. M.; Helfrich, W. Effects of a cosurfactant on the stretching and bending elasticities of a surfactant monolayer. *Langmuir*. **1992**, 8(11), 2792

34. Nazario, L. M. M.; Crespo, J. P. S. G.; Holzwarth, J. F. and Hatton, T. A. Dynamics of AOT and AOT/Nonionic Cosurfactant Microemulsions. An Iodine-Laser Temperature Jump Study. *Langmuir* **2000**, 16(14), 5892

35. Acosta, E. J.; Szekeres, E.; Sabatini, D. A. and Harwell, J. H. Net-Average Curvature Model for Solubilization and Supersolubilization in Surfactant Microemulsions. *Langmuir* **2003**, 19(1), 186-195.

36. Nagarajan, R.; Ruckenstein, E. Molecular theory of microemulsions. *Langmuir* **2000**, 16(16), 6400

37. Langevin, D.; Guest, D. and Meunier, J. Correlation between interfacial tension and microemulsion structure in Winsor equilibria. Role of the surfactant film curvature properties. *Colloids Surf.* **1986**, 19(2), 159

38. De Gennes, P.G.; Taupin C. Microemulsions and the flexibility of oil/water interfaces. *J. Chem Phys.* **1982**, 86, 2284

CHAPTER 5

Linker-Modified Microemulsions for a Variety of Oils and Surfactants[†]

Abstract

Previously we reported on the use of hydrophilic and lipophilic linker molecules to enhance the solubilization capacity of chlorinated hydrocarbons using sodium dihexyl sulfosuccinate. In this work we extend the use of linker molecules to a wider range of oils and surfactants. The data show that the linker effect not only works for all the systems studied, but also demonstrate that linker-based systems are even more economical than surfactant-only systems for more hydrophobic oils. Using a more hydrophobic surfactant, such as sodium dioctyl sulfosuccinate (Aerosol-OT), requires a formulation enriched with hydrophilic linker, where as the formulation for the more hydrophilic sodium dihexyl sulfosuccinate (Aerosol-MA) required the use of more lipophilic linker. By considering the properties and appearance of the formulation before contacting with the oil, and by evaluating the coalescence dynamics, it was found that hydrophilic-linker-rich formulations are preferred. These formulations are tested as fabric pretreatment for removing motor oil and hexadecane from cotton, and as a flushing solution for glass bead columns contaminated with these oils. The cleaning performance of these linker-based systems was superior to common surfactant and pretreatment formulations in the

---

[†] This chapter or portions thereof have been published previously in Journal of surfactant and detergents under the title " Linker-Modified Microemulsions for a Variety of Oils and Surfactants " J. Surfactant Detergents 2003, 6(4), 353-363. (J. Surfactant Detergents best paper of 2003) The current version has been formatted for this dissertation.

detergency tests, and it could achieve more than 80% removal of motor oil and hexadecane trapped in the packed column flushing tests.

Keywords: microemulsion, linkers, hexadecane, motor oil, detergency, column, formulation.

Introduction

Microemulsions are single-phase systems that contain oil and water domains separated by surfactant films. The oil and/or water domains in microemulsions are of nanometer size (1-100 nm) (1,2). While microemulsions were initially identified by Schulman in 1943, it was not until the 1970s that they became of widespread interest, resulting from their potential use in enhanced oil recovery (EOR) (2).

Microemulsions have the distinction of producing ultralow interfacial tension (less than 0.1 mN/m) between the microemulsion phase and the excess oil and/or water phases, thereby overcoming the capillary forces that "trap" oil in a porous medium. This property of a microemulsion, along with its capacity to cosolubilize oil and water, is what promoted their use in tertiary oil recovery, and later its use in cleaning oil-contaminated aquifers in an approach called surfactant enhanced aquifer remediation (SEAR)(3).

Microemulsions can be of three types: Type I microemulsions correspond to oil solubilized in swollen micelles with water as the continuous medium. Type II microemulsions correspond to water solubilized in swollen reverse micelles having oil as the continuous medium. Type III microemulsions are bicontinuous in oil and water (1) where oil and water are present in channels of net zero curvature. Figure 5.1 shows a schematic of a microemulsion phase behavior study of a system containing the surfactant

sodium dihexyl sulfosuccinate (SDHS) and tetrachloroethyene as the oil phase. With increasing concentrations of sodium chloride the double layer thickness reduces, allowing the curvature of micelles (Type I microemulsion) to reduce and thus form surfactant films of coexisting concave and convex curvature producing a net zero curvature (4) (Type III microemulsions), and eventually forming reverse micelles (Type II microemulsions).

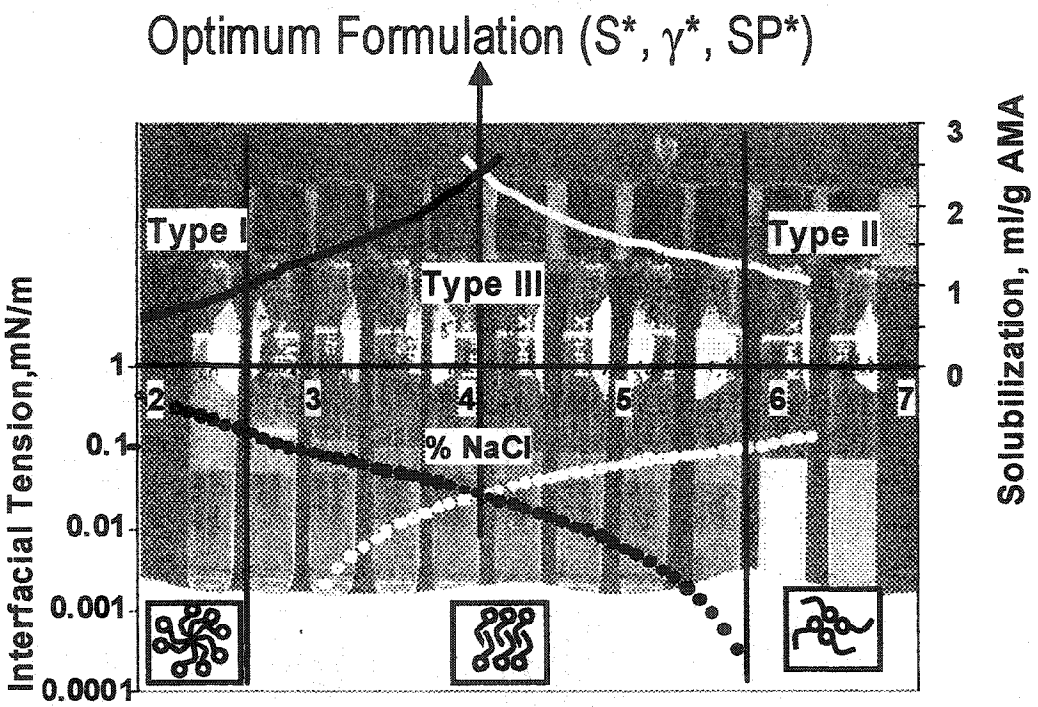

Figure 5.1. Phase behavior of microemulsions with SDHS and tetrachloroethylene showing Winsor phases (Type I-III-II) and corresponding interfacial tension and solubilization

The solubilization data presented in Figure 5.1 is presented as the solubilization parameter (SP), which is the amount of oil (SPo) or water (SPw) solubilized per mass of surfactant. Figure 5.1 shows that while the solubilization of oil (SPo, black line) increases as the concentration of electrolyte increases, the solubilization of water (SPw, white line) decreases with increasing electrolyte concentration. The point at which the interfacial

tension between the middle phase (Type III) microemulsion and the excess water ($\gamma_{m/w}$*, white dots in Figure 5.1) is the same as the interfacial tension between the middle phase and the excess oil phase ($\gamma_{m/o}$*, black dots in Figure 5.1) is called the optimum formulation (noted with an asterisk); at this location the interfacial tension is simply reported as the optimum interfacial tension ($\gamma^* = \gamma_{m/w}^* = \gamma_{m/o}^*$). At optimum formulation, the oil and water reaches the same solubilization level (Spo = SPw = SP*) and the magnitude of this solubilization is simply called the optimum solubilization parameter.

The optimum solubilization parameter (SP*) is an indication of the solubilization potential of a microemulsion system. The larger this value, the more economically attractive the system becomes for cleaning formulations. While in EOR surfactant formulations routinely had solubilization parameters of 20-30 ml/g, and even up to 50 ml/g, for most SEAR formulations, SP* is less than 5 ml/g (5). This is due in part to the desire to avoid vertical migration concerns associated with dense oils which may be released by low interfacial tensions. One way to increase the solubilization capacity of microemulsions is the use of linker molecules, as explained below.

Linker molecules are chemical additives used in surfactant systems that enhance the surfactant-oil (lipophilic linkers) or surfactant-water (hydrophilic linkers) interactions. Graciaa et al. (6,7,8) initially introduced long chain alcohols and ethoxylated fatty alcohols having a low degree of ethoxylation as lipophilic linkers. These lipophilic linkers would segregate near the oil side of the interface close to the tails of the surfactants, as depicted in the schematic in Figure 5.2 for oleyl alcohol. The

presence of the lipophilic linker extends the surfactant impact deeper into the oil phase, and probably promotes additional orientation of the oil molecules (6,7).

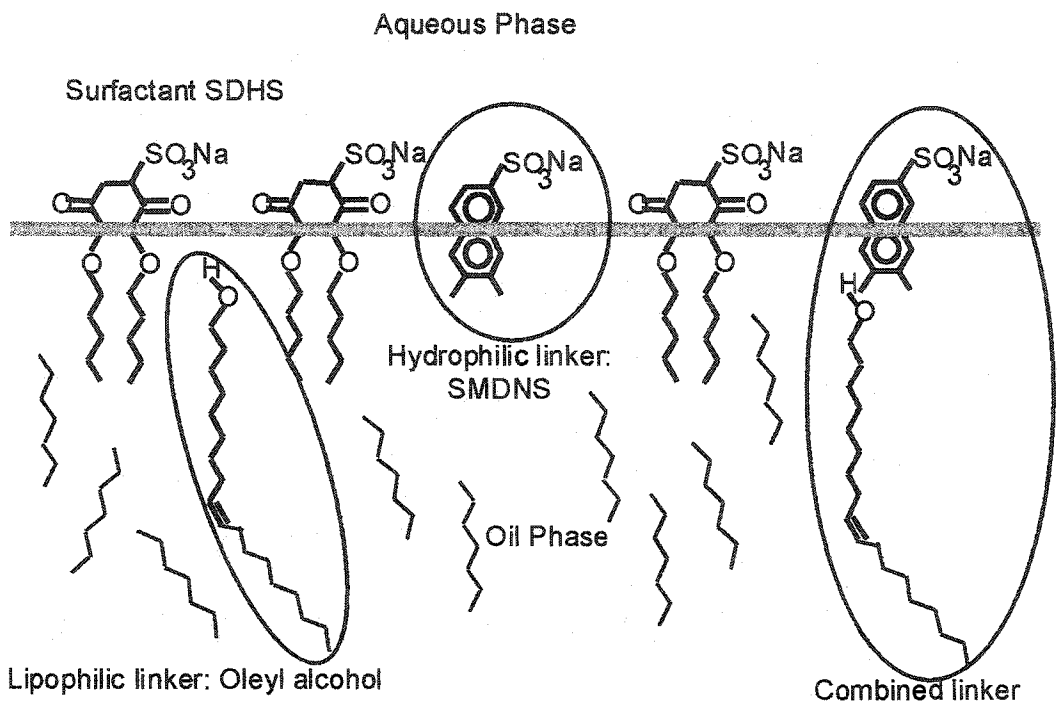

Figure 5.2. Schematic of the linker effect, showing the surfactant, lipophilic, and hydrophilic linker at the oil/water interface.

Earlier we found that adding lipophilic linkers alone to SDHS-trichloroethylene microemulsion only marginally enhanced the solubilization capacity of this system (9). We therefore introduced the hydrophilic linker concept whereby an amphiphilic molecule coadsorbs with the surfactant at the oil water interface so that its interaction with oil molecules would be very weak (9,10).

We proposed the use of sodium mono- and di-methyl naphthalene sulfonate (SMDNS) as a hydrophilic linker, as depicted in Figure 5.2 (9). The adsorption of the hydrophilic linker at the oil/water interface increases the total interfacial area, thereby

allowing more room for the lipophilic to segregate and further enhancing the solubilization capacity of the system. While hydrophilic linkers alone did not increase the solubilization capacity of the microemulsion, the combination of lipophilic and hydrophilic linkers behaved just like a self-assembled surfactant at the oil/water interface, and the resulting solubilization enhancement was proportional to the combined linker concentration (9,10).

We investigated this novel "self-assembly" by measuring the partition coefficient of each of linker and found that the lipophilic linker became inefficient because, above a certain concentration, it partitions more into the excess oil phase, especially if the oil is polar (11). While hydrophilic linkers also have a partial participation at the interface, adding both hydrophilic and lipophilic linkers increased the partition of each at the interface (11).

More recently, we found that linker molecules also modify the mechanical properties of the surfactant membrane, and thereby the kinetics of coalescence and solubilization (12). Specifically, lipophilic linkers, due to their tendency to pack near the surfactant tails, increase the rigidity of the interface. Hydrophilic linkers, on the other hand, adsorb at the interface, but because of their short tails they create a loose packing that decreases the rigidity of the interface. We have found that the more rigid the interface, the slower the rate of coalescence and solubilization (12).

Thus far we have concentrated on linker-based systems for oils representative of SEAR applications (e.g. trichloroethylene, tetrachloroethylene and hexane). This approach can also be used in other applications such as hard surface cleaners (e.g. orange

oil cleaners), nanolatex synthesis and drug delivery systems among others. Our objective in this work is to extend the combined linker approach to different oils and surfactants, while learning how to combine the linker molecules in different systems. Specifically, we are interested in more hydrophobic oils such as hexadecane and motor oil, which are not only important to detergency and hard surface cleaning but are also common in environmental spills.

Our hypothesis is that our previous observations on the role of linker molecules in chlorinated hydrocarbon microemulsions will hold true for systems containing different oils and surfactants. The confirmation of this hypothesis will show that the linker effect is indeed an interfacial self-assembly phenomena that can occur with different oils and surfactant systems.

To test this hypothesis, we will start by targeting a range of oils (from trichloroethylene to motor oil), with SDHS as the surfactant, oleyl alcohol as lipophilic linker and SMDNS as the hydrophilic linker (schematic depicted in Figure 5.2). For successful microemulsion phases we will present the optimum salinity (S*), and the characteristic length at optimum formulation (ξ*), which is analogous to the solubilization parameter (SP*). The characteristic length (ξ*) is the average radius of the oil and water channels present in the middle phase microemulsion, and can be calculated using the following expression (13):

$$\xi = \frac{6 * \phi_o * \phi_w * V_m}{As} \qquad \text{Eq. 1}$$

where ϕ_o and ϕ_w are the volume fractions of oil and water in middle phase microemulsion, V_m is the volume of the middle phase, and A_s is the interfacial area, provided by the surfactant adsorption (13):

$$As = \sum_i V_{w,o} Cs_i \times \phi_i \times 6.023 \times 10^{23} \times a_i \qquad \text{Eq. 2}$$

where $V_{w,o}$ is the initial volume of the aqueous solution containing the surfactant and linkers, Cs_I is the initial aqueous molar concentration of the surfactant, cosurfactant and hydrophilic linker added to the formulation, ϕ_i is the fraction of the surfactant/cosurfactant that is present in the middle phase microemulsion and a_I is the area per molecule of the species considered (in $Å^2$/molecule). Lipophilic linkers are not considered in this calculation because they do not adsorb at the oil/water interface (7,12,13).

We will also report the interfacial tension at optimum conditions (γ^*). The equation used to correlate the solubilization parameter (SP*) and the interfacial tension has traditionally been the Chun Huh relationship ($\gamma^* = C/SP^{*2}$) (14). Recently, we have proposed an alternative expression (13):

$$\gamma^* = \frac{E_r}{4\pi(\xi^*)^2} \qquad \text{Eq. 3}$$

where E_r is the interfacial rigidity with energy units. Normally, the interfacial rigidity has values close to $1K_BT$ (K_B, Boltzman constant) (12,13). Since values of E_r higher than $1K_BT$ will produce slow solubilization and coalescence, it is a thermodynamic parameter that has profound implications on the dynamic behavior of the system.

In the second part of this paper we will switch surfactants by using sodium bis(2-ethyl) dihexyl sulfosuccinate (Aerosol-OT, AOT) instead of SDHS. This will allow us to assess the role of the surfactant molecular structure on the performance and formulation of linker microemulsions. Finally we will use the best formulation, as determined above, to remove hexadecane and SAE 10W-30 motor oil from glass beads packed columns and from cotton fabric.

Experimental Procedures

Materials

The following chemicals were supplied by Aldrich (Milwaukee, WI) at the concentrations shown in parenthesis and used without further purification: trichloroethylene (TCE, 99%+), tetrachloroethylene (PCE, 99%+), hexane (99%+), decane (99%+), hexadecane (99%+), 1-octadecene (99%+), oleyl alcohol (85+%), sodium chloride (99%+), sodium dihexyl sulfosuccinate (Fluka brand, 80% solution in water), sodium bis-(2-ethyl) dihexyl sulfosuccinate (AOT, ~100%). Sodium mono and dimethyl naphthalene sulfonate (SMDNS, Morwet M ®) was supplied by CKWitco (Houston, TX). Unused motor oil, SAE 10W-30 grade (Castrol brand) was purchased from a local gas station. A bleached white 100% cotton fabric was purchased from local store. Tables 5.1a and 5.1b show the relevant properties of the oils and amphiphilic molecules used in this work, respectively.

Table 5.1a. Properties of the oils formulated in microemulsions

Oil	Equivalent Alkane Number (EACN)	Density (g/ml)[d]	Viscosity (mPa*s)[d]	Molecular Structure
Trichloroethylene (TCE)	-3.8[a]	1.60	0.84	$Cl_2C=CHCl$
Tetrachloroethylene (PCE)	2.9[a]	1.42	1.11	$Cl_2C=CHCl_2$
Hexane (C6)	6[b]	0.67	0.30	C_6H_{14}
Decane (C10)	10[b]	0.72	0.84	$C_{10}H_{22}$
Tetradecane (C14)	14[b]	0.75	2.12	$C_{14}H_{30}$
Hexadecane (C16)	16[b]	0.77	3.03	$C_{16}H_{34}$
SAE 10W-30 oil (Mot)	19[c]	0.82	100	Mixture
Squalene (Sqln)	24[d]	0.80	80	$CH_3(CH_3C=C(CH_2)_2)_5CH_3$

(a): From reference (16)
(b): From the definition of alcane carbon number, ACN reference (17,18)
(c): From reference (19)
(d): This work

Table 5.1b. Properties of the amphiphilic molecules used in this work

Amphiphilic Molecule	Area per molecule Å^2/molecule	Molecular weight g/mol	Molecular Structure
Sodium dihexyl sulfosuccinate (SDHS)	100[a]	376	$C_6H_{13}O_2CH_2CH(SO_3Na)CO_2C_6H_{13}$
Sodium mono- and di-methyl naphthalene sulfonate (SMDNS)	90[a]	250	$CH_3(C_{10}H_6)SO_3Na$ (65%) $(CH_3)_2(C_{10}H_5)SO_3Na$ (35%)
Oleyl alcohol	N.A[a].	266	$C_8H_{17}C=CC_8H_{16}OH$
Sodium bis (2-ethyl) dihexyl sulfosuccinate (AOT)	110[b]	432	$C_4H_9CH(C_2H_5)CH_2O_2CH_2CH(SO_3Na)CO_2CH_2(C_2H_5)$ CH C_4H_9

(a): These amphiphilic molecules were characterized in references (9,10,11). In the case of oleyl alcohol, the are per molecule does not apply .
(b): From reference (21)

Methods.

Phase behavior studies were performed using equal volumes of aqueous solution and oil (5 mL each). Electrolyte scans were performed by varying the sodium chloride concentration while holding constant the temperature, additive content, and pressure (1 atm). Test tubes were placed in a water bath at 27°C (300K), shaken once a day for three days, and left to equilibrate for two weeks. The phase volumes were determined by measuring the levels of each phase in each test tube. The middle phase volume and the surfactant concentration of the optimum middle phase were used to calculate the solubilization parameter (SP*), and the characteristic length (ξ^*) at this condition. The electrolyte concentration (in weight percent) necessary to form the middle phase microemulsion is also reported (S*).

The interfacial tension of the optimum middle phase microemulsion (γ^*) was measured using a tensiometer model 500. For excess oil/water interfacial tension ($\gamma^*_{o/w}$) measurements, the tube is filled with the heavier phase and a 1 to 5 µl drop of the less dense phase is injected. At optimum middle phase $\gamma_{o/w}$ reaches a minimum value and the interfacial tension we report can be approximated as $2\gamma^* = \gamma^*_{o/w}$ (15). While it is physically possible to measure the interfacial tension between excess water-middle phase and excess oil-middle phase, using the middle phase as the continuum phase or droplet introduces more error than using the method described above due to partial phase separation of the oil or water which is initially solubilized in the middle phase. All these measurements were performed at 27°C (300K).

The concentration of SMDNS, SDHS and AOT were measured using a Dionex ion chromatograph (Sunnyvale, CA) in reverse phase mode using a NS1 column with a water-acetonitrile mixture as a mobile phase containing 10 mN of tetrabutyl ammonium hydroxide as a coupling agent. The coupling agent forms neutral complexes with the anionic surfactants mentioned above which are then separated in the NS1 column. The effluent of the column is contacted with an anionic suppressor (ASRS-4mm) where the complexes de-couple and the anionic surfactants are detected by their conductivity signal using a CD-25 conductivity detector. All the oils (except for motor oil; see below) and the oleyl alcohol concentrations were measured using a Varian 3300 gas chromatograph equipped with a FID detector and SPB-25 column.

The column studies were performed by flushing several pore volumes of the surfactant solution through a 15cm (length) × 2.5cm (diameter) glass column packed with 0.5 mm glass beads that were precontaminated with the oil (hexadecane or motor oil). The glass column was wet-packed, and the pore volume was the volume of water added to pack the column (fill the void spaces between glass beads). The precontamination was done by injecting one pore volume of the oil and then flushing with water at 10 ml/min (ten times the flow rate of the surfactant formulation) to remove the oil that was not trapped by capillary forces. Samples of the column effluent were collected and analyze to obtain the recovery of the surfactant, linkers and oil.

Detergency studies were performed using "in house" stained fabrics. The staining was performed by immersing a piece of fabric in a methylene chloride solution containing 20% by volume of the oil (hexadecane or motor oil) died with 200 ppm of red

sudan III. The fabric was dried under a ventilated hood and then cut in pieces of 3"×4". The detergency studies were performed using a terg-o-meter USA Testing model 7243 using the standard ASTM D3050-98 "Standard guide for measuring soil removal from artificially contaminated soils". For comparison purposes, we used a commercial detergent in its powder form as the model detergent and a commercial pretreater as reference pretreatment system. The linker formulations generated in this study were used as pretreatment for the oily stains. For this purpose, four stained fabric swatches (3"×4" pieces) were contacted with 30 ml of the surfactant solution for 30 minutes, and then washed with the detergent in a 0.2% weight dosage in 1L of water with 10 minutes washing – 5 minutes rinsing cycle. The initial and final concentrations of hexadecane were measured by extraction with methylene chloride followed by gas chromatography. For the case of motor oil, the concentration of motor oil was indirectly measured through the intensity of the red color (measured with an UV-VIS Hewlett Packard model 8452 diode array spectrophotometer, at 600 nm) after extraction.

Results and Discussions

Formulating microemulsions with sodium dihexyl sulfosuccinate (SDHS):

As indicated above, our first task was formulating middle phase microemulsions with the oils shown in Table 5.1a. The surfactant sodium dihexyl sulfosuccinate (SDHS) was selected as a baseline surfactant because it has been studied alone and in combination with linker molecules, making it a good benchmark to evaluate the performance of linker microemulsions for different oils (9,10,11,12,13,16).

Formulating microemulsions with ionic surfactants requires finding the right combination of variables that will produce an optimum middle phase microemulsion. Salager et.al proposed a semiempirical equation that relates the different formulation variables (17,18):

$$\ln(S^*) = K(ACN) + f(A) - \sigma + aT\Delta T \qquad \text{Eq. 4}$$

where S* is the optimum salinity, or electrolyte concentration; K is a constant, normally between 0.1 to 0.17; and ACN is the alkane carbon number. For non-linear hydrocarbons, the ACN becomes the equivalent alkane carbon number (EACN). The values for non-linear hydrocarbons in Table 5.1a have been obtained from the literature (16,19). In the case of motor oil (SAE 10W-30), the EACN value is estimated based on the optimum salinity obtained in our microemulsion studies. The effect of alcohol or additives is noted by f(A), σ is a function of the type of the surfactant, α is a constant, and T is the temperature of the system, held constant in this study at 27°C.

We selected the initial concentration of SDHS to be 4% (mass/volume, gr/100ml) or 0.103 M. The initial aqueous concentration of oleyl alcohol and the SMDNS concentration was set at 0.18 M since, based on a previous study, we found that equimolar concentration of lipophilic and hydrophilic linkers shows the most efficient solubilization enhancement (11).

Table 5.2 shows the optimum salinity (S*) for the different microemulsion systems considered in this work. For SDHS microemulsions we are only able to report results with trichloroethylene (TCE), tetrachloroethylene (PCE), hexane (C6), decane (C10), tetradecane (C14) and hexadecane (C16). As predicted by Equation 4, for more

hydrophobic oils (higher EACN) the optimum salinity (S*) increased, as shown by the data in Table 5.2.

Table 5.2. Properties of optimum middle phase microemulsions - formulation.

System	S*, %NaCl	Vm* ml	$\gamma^*_{o/w}$ mN/m	ϕ-% Surf	ϕ-% SMDNS	[oleyl] middle phase
SDHS-TCE	1.9	4.8	3.8E-03	100	52	0.09
		±0.2	±4E-4	±9	±4	±0.01
SDHS-PCE	4.7	4.4	6.3E-03	100	57	0.10
		±0.2	±7E-4	±7	±4	±0.01
SDHS-C6	6.3	4.6	4.6E-03	100	57	0.14
		±0.2	±6E-4	±4	±3	±0.01
SDHS-C10	11.0	3.5	9.3E-03	96	60	0.17
		±0.2	±8E-4	±4	±3	±0.02
SDHS-C14	14.0	3.0	1.8E-02	92	60	0.21
		±0.2	±3E-3	±4	±4	±0.02
SDHS-C16	16.3	2.7	2.3E-02	89	57	0.25
		±0.2	±3E-3	±5	±5	±0.02
AOT-C14	0.5	4.8	5.7E-03	100	48	0.07
		±0.2	±7E-4	±7	±5	±0.01
AOT-C16	2.0	3.5	9.5E-03	96	43	0.09
		±0.2	±8E-4	±5	±4	±0.01
AOT-Mot	5.0	3.0	1.1E-02	81	59	0.11
		±0.2	±2E-3	±7	±4	±0.01
AOT-Sqln	10.0	1.4	8.1E-02	75	49	0.23
		±0.2	±9E-3	±8	±4	±0.02

Using high electrolyte concentrations (S*) is inconvenient for most applications such as environmental remediation and detergency where the ultimate fate of the electrolyte may affect the ecosystem of subsurface aquifers or surface rivers and fresh water reservoirs. Adding high concentrations of electrolyte (more than 10% NaCl, in this case) promotes the precipitation of surfactant solutions, but with linkers, it promotes the formation of a separate phase containing the surfactant and linkers that show similar behavior to a coacervate phase. This separate phase disappears with the addition of the oil

(to form its respective microemulsion phase). While the formation of a separate phase may not prevent the use of these formulations in cleaning applications (two phase cleaners), it is inconvenient for environmental subsurface remediation where it is desired to inject a single phase isotropic surfactant solution.

In addition to electrolyte concentration (S*), there are other aspects to consider when formulating a microemulsion. One of these is the solubilization capacity, and as indicated before, we prefer to express this parameter as the size of the oil (or water) channels at optimum middle phase (ξ^*), as expressed in equation 1. We use this thickness value instead of the traditional solubilization parameter (volume of oil/volume of surfactant or volume of oil/mass of surfactant) because it can be more readily compared with non-linker formulations. Figure 5.3a shows the values of optimum characteristic length (ξ^*) for the different microemulsion formulations with SDHS. The data in Figure 3a shows that with increasing oil hydrophobicity (EACN), the solubilization (ξ^*) decreases (although initially constant for the less hydrophobic oils TCE, PCE and hexane). We have previously investigated these oils with SDHS alone, finding that (applying equation 1) the optimum characteristic length (ξ^*) is 108Å, 46Å and 42 Å for TCE, PCE and hexane respectively. In the case of PCE and hexane, the use of linkers increase their solubilization capacity by almost three fold (9). The same trends of decreasing solubilization (ξ^*) has also been observed by Sotmann et al who have actually measured the values of the characteristic length by small angle neutron scattering (20). This trend has also been predicted by Huh based on analysis of the Hamaker constant of alternative layers of oil and water (14).

Figure5.3a

Figure5.3b

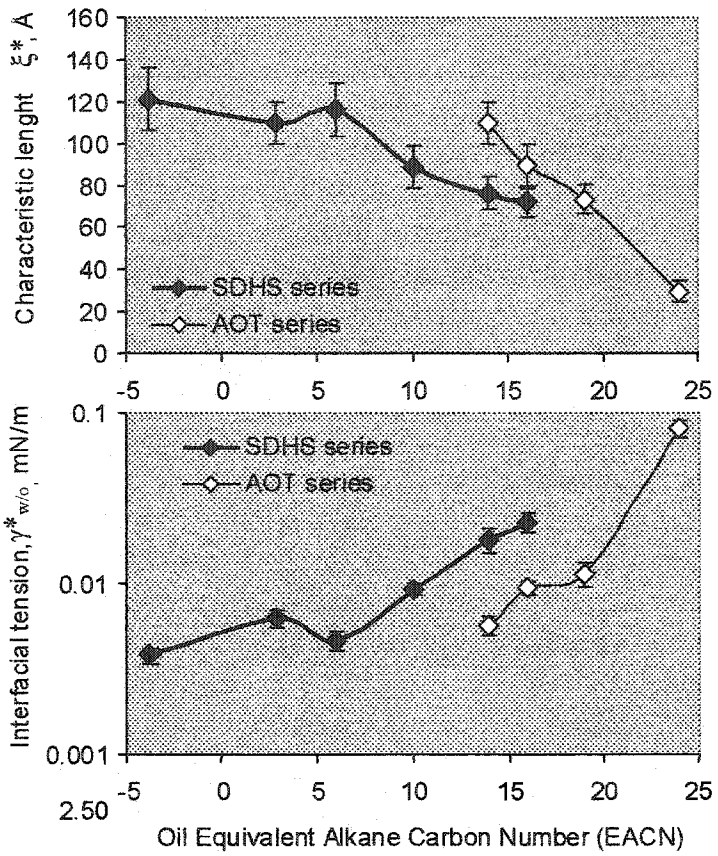

Figure 5.3. Interfacial tension and characteristic length of the microemulsions as a function of EACN and surfactant series.

Based on these solubilization capacities we have estimated that for PCE and hexane microemulsions, this increased solubilization can produce cost savings of up to 60%. For SDHS alone, the most hydrophobic microemulsion that can be formulated is with octane; for more hydrophobic oils SDHS alone forms either liquid crystals or precipitates.

We also measured the interfacial tension between the excess oil and water phases as a function of oil EACN (Table 5.2 and plotted in Figure 5.3b). According to equation 3, the interfacial tension is inversely proportional to the square of the optimum

characteristic length, and therefore the decrease in solubilization capacity (ξ^*) corresponds to an increase in the interfacial tension ($\gamma^*_{o/w}$). This trend is confirmed when comparing Figures 5.3a and 5.3b where the lower solubilization for more hydrophobic oils corresponds to a higher interfacial tension. The low interfacial tension is desired when formulating a surfactant flood to displace oil from porous media, where the capillary forces are proportional to the interfacial tension between the oil trapped and the surfactant solution. Low interfacial tensions are also desired in detergency since both the adhesion coefficient ($\gamma_{o/w}(\cos\theta+1)$, where θ is the contact angle) and the cohesion coefficient ($2\gamma_{o/w}$) of the oil droplet are proportional to the interfacial tension. A reduction of both the adhesion and cohesion coefficients of the oily stain promote the detergency performance by means of roll-up and snap-off mechanisms (21,22). In certain instances, such as the remediation of chlorinated hydrocarbons, the solubilization mechanism is preferred over the displacement of bulk oil (to prevent the potential for further downward migration of the contaminant) and therefore formulations with higher interfacial tensions that still maintain substantial solubilization are desired (11,23).

The relationship established by equation 3 between the interfacial tension (γ^*, in this case $\gamma^*_{o/w}$) and the optimum characteristic length (ξ^*) has a proportionality constant which indicates the interfacial rigidity (E_r), which is normally expressed in Boltzman energy units (KbT). Figure 5.4 shows the interfacial rigidity values of the studied microemulsions as a function of the oil hydrophobocity (EACN). As was indicated before, the most common value of interfacial rigidity for flexible, liquid-like surfactant membranes is 1KbT, which is valid for the SDHS formulations from EACN –3.8 (TCE)

to 10 (decane). For the SDHS microemulsions with tetradecane and hexadecane, the interfacial rigidity tends to increase. In the bottom of Figure 5.4 is plotted the ratio of molar concentration of hydrophilic linker SMDNS in the middle phase to the molar concentration of oleyl alchol at the same conditions (noted as the H/L ratio) as a function of oil hydrophobicity (EACN). In general, as the middle phase becomes enriched with oleyl alcohol (H/L decreases) the interfacial rigidity (Er) increases. This observation is in agreement with a previous study on the effect of linkers in interfacial rigidity, where it was shown that hydrophilic linkers tend to decrease the interfacial rigidity by promoting a loose packing of the surfactant molecules at the interface, and the lipophilic linkers tend to increase this rigidity by adsorbing between the tails of the surfactants, thereby creating a tighter packing at the interface (12).

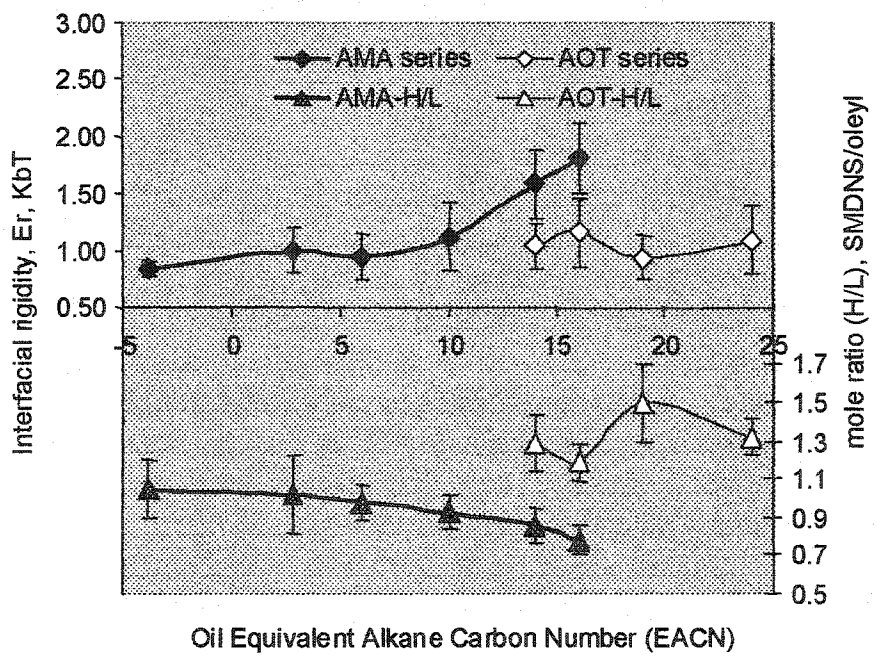

Figure 5.4. Interfacial rigidity (Er) and SMDNS/oleyl mole ratio in middle phase as a function of oil EACN and surfactant series.

The increased interfacial rigidity in microemulsions brings about, according to this same study referenced above, a slower kinetics of solubilization and coalescence of the system, which can be a detriment to the performance of certain formulations, specially those designed with cleaning purposes (12). We tested whether this observation holds true when formulating linker microemulsions for different oils by following the coalescence of middle phase microemulsions, measured as the turbidity of the middle phase as a function of time, according to the procedure described elsewhere (12). Figure 5.5 shows these coalescence curves for the SDHS microemulsions formulated with hydrocarbon oils. For the SDHS hexane (SDHS-C6) system, the system coalesced (approached turbidity = 0 cm^{-1}) faster than the rest of the oil phases considered. The trend of slower coalescence for hydrophobic oils is consistent with the increased rigidity of these systems (Figure 5.4). Since the correlation between the interfacial rigidity and the kinetics coalescence is affected by the viscosity of the middle phase (Table 5.3) and the oil (Table 5.1a), the slower coalescence of the SDHS- C16 and SDHS-C14 systems is also explained by this effect.

One last performance parameter that is worth noting is the partition of each linker into the interfacial layer, in this case the middle phase microemulsion. Table 5.3 and Figure 5.6 show the partition coefficient of SMDNS between the middle phase and the excess water phase (K_{SMDNS}) and the partition coefficient of oleyl alcohol between the middle phase and the excess oil phase (K_{Oleyl}):

$$K_{SMDNS} = \frac{[SMDNS]_{middle-phsse}}{[SMDNS]_{excess-water}} \qquad \text{Eq.5}$$

$$K_{Oleyl} = \frac{[Oleyl - alcohol]_{middle-phsse}}{[Oleyl - alcohol]_{excess-oleyl}} \qquad \text{Eq.6}$$

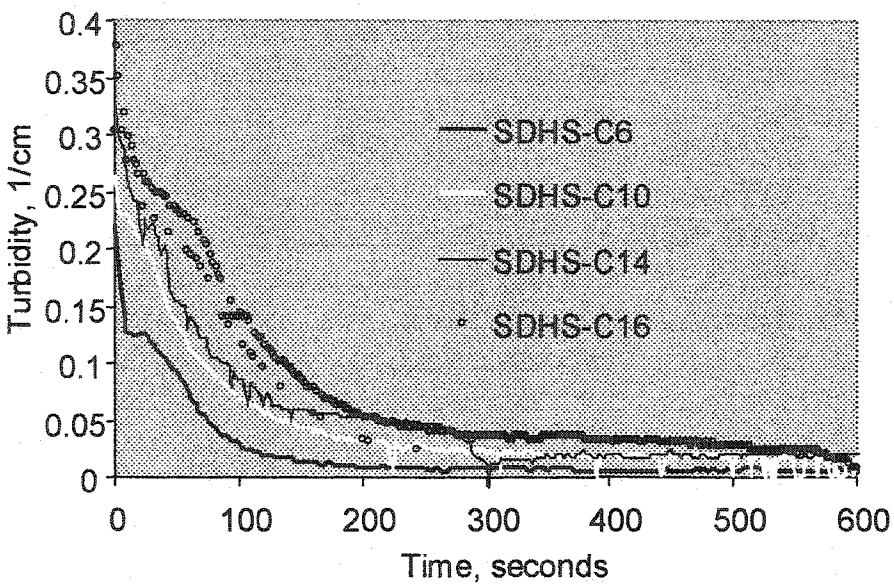

Figure 5.5. Turbidity versus time for coalescence of middle phase for SDHS microemulsion with different oils.

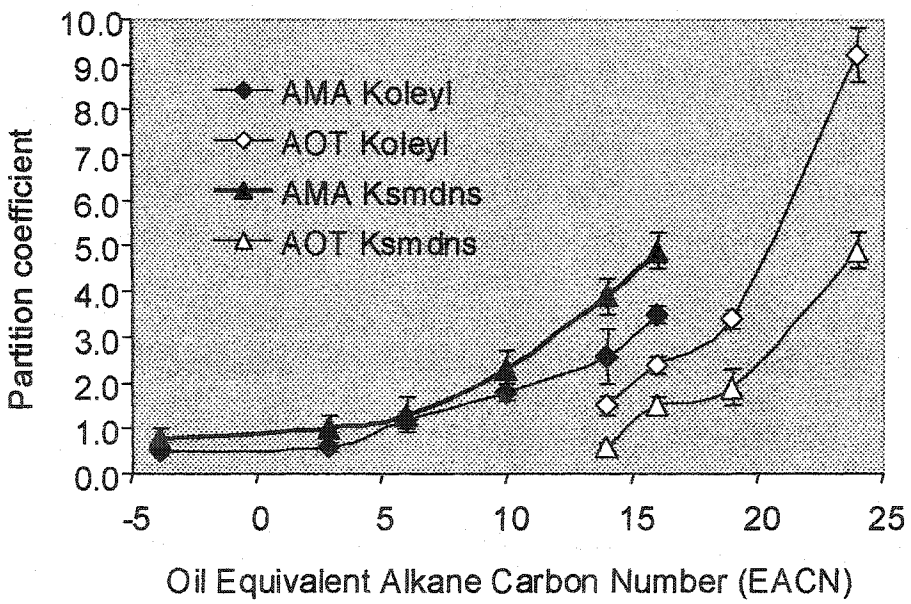

Figure 5.6. Partition of linkers into the middle phase as a function of oil EACN (see equations 5 & 6 for definitions).

Table 5.3. Properties of optimum middle phase microemulsions - characteristic length, interfacial rigidity, viscosity and partition of linkers.

System	ξ^* Å	Er KbT	μ^* mPa-s	K_{SMDNS} Middle/water	K_{oleyl} Middle/oil
SDHS-TCE	120 ±15	0.84 ±0.07	6.0 ±0.5	0.8 ±0.2	0.5 ±0.1
SDHS-PCE	108 ±10	1.0 ±0.2	7.8 ±0.6	1.0 ±0.3	0.6 ±0.1
SDHS-C6	116 ±13	0.9 ±0.2	5.0 ±0.4	1.3 ±0.4	1.2 ±0.2
SDHS-C10	89 ±10	1.1 ±0.3	5.5 ±0.5	2.3 ±0.4	1.8 ±0.2
SDHS-C14	76 ±8	1.6 ±0.3	16 ±2	3.9 ±0.4	2.6 ±0.6
SDHS-C16	72 ±7	1.8 ±0.3	17 ±3	4.9 ±0.4	3.5 ±0.2
AOT-C14	110 ±10	1.0 ±0.2	6.3 ±0.8	0.6 ±0.1	1.5 ±0.1
AOT-C16	90 ±10	1.2 ±0.3	11 ±2	1.5 ±0.2	2.4 ±0.2
AOT-Mot	73 ±7	0.9 ±0.2	90 ±5	1.9 ±0.4	3.2 ±0.2
AOT-Sqln	30 ±5	1.1 ±0.3	51 ±3	4.9 ±0.4	8.9 ±0.6

While other partition coefficients can be calculated, these are the most important since the SMDNS tends to be mostly present in the middle phase and the excess aqueous phase, and the oleyl alcohol is mostly present in the middle phase and the excess oil phase. It is important that most of the linker partition into the middle phase so that the solubilization enhancement is maximized. According to Figure 5.6, for more hydrophobic oils (higher EACN) the partition of both, hydrophilic and lipophilic linkers improved.

This result is consistent with previous studies on the partition coefficient of linker molecules (11).

It is important to clarify that the partition coefficients defined by Eq. 5 and 6 and presented in Figure 5.6 are a simple way to represent how much of the linker participates in the middle phase microemulsion, which includes the linker that is segregated near the interface and linker solubilized in the oil and water regions of the bicontinuous structure. Further studies are being pursued to characterize and model the segregation behavior of linker molecules.

In summary, formulating microemulsions with SDHS is appropriate for polar oils such as chlorinated hydrocarbons, and even for hexane and decane. For more hydrophobic oils, the high electrolyte concentration required will promote the formation of coacervate phases before adding the oil, and will produce less solubilization (ξ^*), higher interfacial tension, higher interfacial rigidity (E_r), and slower coalescence kinetics. Despite this set of undesirable performance parameters for hydrophobic oils, the partition of linkers into the middle phase improves for more hydrophobic oils, which is the most efficient use of the linker molecules.

Formulating microemulsions with Aerosol-OT (AOT):

Based on the results discussed above, we selected a more hydrophobic surfactant sodium bis(2-ethyl)dihexyl sulfosuccinate (Aerosol-OT, AOT), to formulate microemulsions for more hydrophobic oils. Our initial idea was to formulate these set of microemulsions under the same conditions used for formulation with SDHS (i.e. 0.18M SMDNS and 0.18M oleyl alcohol). However, we found that the formulation was too

hydrophobic even for hexadecane (i.e. S* less than 0.25% NaCl), therefore we proceeded to formulate this microemulsions with 0.18M SMDNS and reduce the oleyl alcohol concentration to 0.09M. Table 5.2 shows the optimum salinity (S*) for these formulations. For the case of tetradecane (C14), the optimum salinity reduces from 14% NaCl (SDHS-C14) to 0.5% NaCl (AOT-C14), whereas for hexadecane it reduces from 16.2% (SDHS-C16) to 2% (AOT-C16). This significant decrease in electrolyte concentration makes this systems better suited for cleaning applications, and also prevented the formation of a separate surfactant phase, which is desirable for subsurface injection in oil wells or for aquifer remediation. We could not obtain the microemulsion Type I-III-II transition for more hydrophilic oils (lower EACN) because even with no added electrolyte, we obtained Type II microemulsions.

In Figure 5.3a we observe that for tetradecane (EACN=14) and hexadecane (EACN=16) the optimum characteristic length (ξ^*) is significantly higher for the formulation with AOT. As discussed before, the larger the value of ξ^*, the more efficient is the solubilization and the less the cost of solubilization. For these hydrophobic oils the formulation with AOT is more economic than with SDHS. This result is consistent with systems formulated with or without linker molecules because of the larger hydrophobic group of AOT (2*C8 for AOT versus 2*C6 for SDHS) shows a greater interaction with the oil than that of the SDHS (1,6,13)

Similarly to the SDHS case, for AOT formulations, more hydrophobic oils (higher EACN), such as motor oil and squalene, show lower solubilization (ξ^*).

While the solubilization of squalene is quite low (ξ^*~30Å) it is worth noting that we have not found previous references for microemulsions produced with this highly hydrophobic oil. In fact we questioned whether this was a real microemulsion and we tested for liquid crystaline phases with a cross-polarized lenses, but found no signs of such phases. We also tested the interfacial tension between the excess oil and water (γ^*), which is plotted in Figure 5.3b, as a function of EACN, and the result was just below the borderline value where we consider a microemulsion (γ<0.1 mN/m). In some cases the middle phase microemulsion can be confused with a coacervate phase (not a liquid crystal) that locates itself between the excess oil and water phases, and is sometimes designed a D' phase, with interfacial tensions between 0.1 to 1 mN/m (24). In addition a D' phase is continuous in aqueous phase and therefore it has very little if any oil solubilized, while we found that this microemulsion had the same proportions of oil and water solubilized.

Figure 5.3b also shows that for AOT-C14 and AOT-C16 formulations the interfacial tension was significantly lower than for their homologous SDHS formulations. This is consistent with the higher solubilization (measured as the optimum characteristic length, ξ^*) of the AOT systems.

Based on the optimum characteristic length (ξ^*) and the interfacial tension ($\gamma^*_{o/w}$) we calculated the interfacial rigidity (Er) for these systems. Figure 5.4 present this interfacial rigidity value as a function of oil EACN, along with the molar ratio of hydrophilic linker (SMDNS) to lipophilic linker (oleyl alcohol) present in the middle phase microemulsion and noted as H/L. For these systems formulated with AOT the

interfacial rigidity remains close to 1KbT, which corresponds to very fluid and flexible surfactant membranes. For the case of tetradecane and hexadecane, the formulations with AOT have a significantly lower interfacial rigidity than its equivalent SDHS formulations. The reason for the low interfacial rigidity of these systems can be linked to the fact that the AOT formulations are enriched with the hydrophilic linker (SMDNS), as demonstrated by the significantly higher H/L ratios observed in Figure 5.4.

We next proceeded to test whether this lower interfacial rigidity granted a faster coalescence kinetics. Figure 5.7 shows the colaescence curves (turbidity vs. time) for the AOT systems. For tetradecane (C14) the coalescence was actually slower for the AOT formulations than for the SDHS formulation (Figure 5.7), this result was unexpected not only because the interfacial rigidity of the AOT system is lower but because the viscosity of the AOT-C14 middle phase (Table 5.3) is lower than the viscosity of the SDHS-C14 system. One possible explanation for this effect is that for the AOT-C14 system the salinity window is very small (this is the span electrolyte concentration that grants the presence of a middle phase), approximately 0.6%NaCl, and therefore the system is very sensitive to temperature changes. The experimental setup to measure coalescence does allow heating of the vial of up to 2°C.. This change in temperature could have been enough to change the position of the optimum middle phase microemulsion towards the borderline with Type I microemulsion where the coalescence kinetics is much slower than for optimum Type III microemulsions. For the AOT-C16 system, this effect is less severe because the salinity window is more extended (~ 5%NaCl) and therefore is less sensitive to temperature changes, and comparing Figures 5.7 and 5.5 we can observe a

faster coalescence of the AOT-C16 systems as predicted by its lower rigidity and viscosity of the middle phase (Table 5.3). For the case of the motor oil, Figure 5.7 shows a fast coalescence (decrease in turbidity) during the initial three minutes (180 seconds) but after that the process becomes very slow, probably due to the high viscosity of both the oil (Table 5.1a) and the middle phase (Table 5.3). Another unexpected feature of Figure 5.7 is that the AOT-squalene system showed similar coalescence kinetics to that of AOT-C14 and AOT-C16 systems; this is surprising because the viscosities of oil and middle phase where higher than the AOT-C14 and AOT-C16 systems.

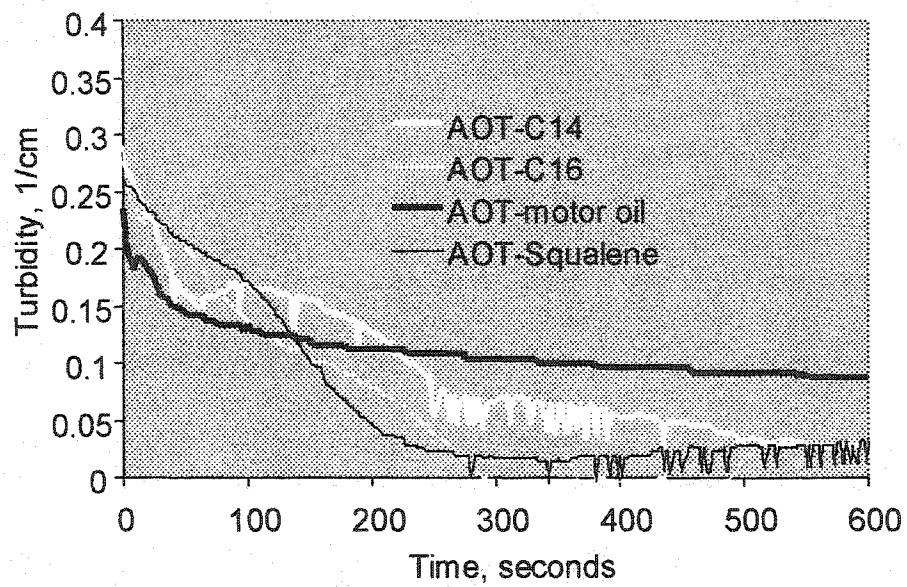

Figure 5.7. Turbidity versus time for coalescence of middle phase for AOT microemulsion with different oils.

We also studied the partition of linkers for this AOT series. Figure 5.6 show these partition values for SMDNS and oleyl alcohol as a function of oil EACN. For the C14 and C16 microemulsion systems the partition of both oleyl alcohol and SMDNS into the middle phase is significantly lower for the systems formulated with AOT. This lower

partition could be due to the fact that in AOT microemulsions we did not use an equimolar ratio of SMDNS to oleyl alcohol. As mentioned before, the equimolar addition of linkers is the best scenario because the presence of one type of linker at the interface improves the partition of the other one (10,11). Considering that we added more SMDNS than oleyl alcohol, this explanation will also help understand why the partition of SMDNS in the AOT systems is consistently lower than the partition of oleyl alcohol. For the case of motor oil and squalene they follow the same trend as the SDHS systems: the more hydrophobic the oil, the better the partition of linkers into the middle phase.

In both SDHS and AOT formulations, the partition of linkers is a phenomenon that seems to involve both the surfactant-linker-water interaction and surfactant-linker-oil interaction. This observation is consistent with the segregation phenomenon observed by our group as well as Graciaa et al. (6,7,8,11,25)

Based on the observations made for both formulations (SDHS and AOT) we can summarize that the surfactant hydrophobicity is important when selecting how to formulate a particular system. In the case of SDHS we extended the range of oils where we could formulate microemulsions from octane to hexadecane, but its best performance was between trichloroethylene (EACN –3.8) and decane (EACN 10). For the AOT system we could formulate microemulsions for more hydrophobic oils, from tetradecane to squalene (not reported before). In formulations, the proper technique to design a microemulsion or even an emulsion is select a surfactant with a hydrophilic/lipophilic balance (HLB) close to that of the oil to be formulated. The linker technique can be used

as a tuning technique that can enhance not only the solubilization capacity of the formulation but also its dynamic behavior.

Cleaning Performance of Linker Microemulsions

In the previous sections we have discussed how to formulate microemulsions using the linker technique and the physical properties of these microemulsions. We also wanted to observe the performance of these microemulsions in two different cleaning setups: removal of oil from packed columns and removal of oil from textile. To do so we selected the AOT formulations with hexadecane and motor oil, which were selected because they are commonly used in detergency tests and they represent common hydrophobic spills found in industrial sites.

The first set of tests was the removal of oil from glass bead - packed columns. We measured the concentration of oil, surfactant and linkers eluting from the column. Figure 5.8a shows the conditions at which this study was run and the removal of oil and recovery of surfactant and linkers. A front of mobilized "bulk" hexadecane oil showed up within the second pore volume, while during the third and fourth pore volume the formulation solubilized virtually all the oil that remained in the column. We recovered all the surfactant and linkers with no chromatographic separation between these phases. This shows an excellent performance of the formulation because we did not lose any of the linkers to the other phases, which was somewhat predicted by the equilibrium partition coefficients.

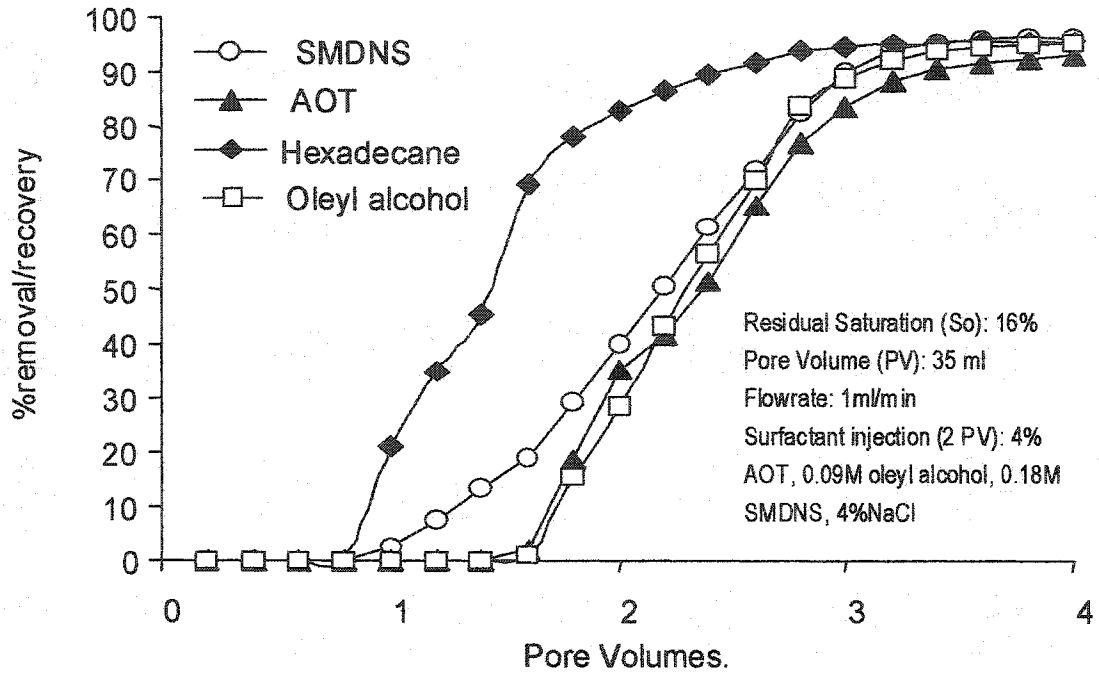

Figure 5.8a. Hexadecane column study with AOT + linker formulation.

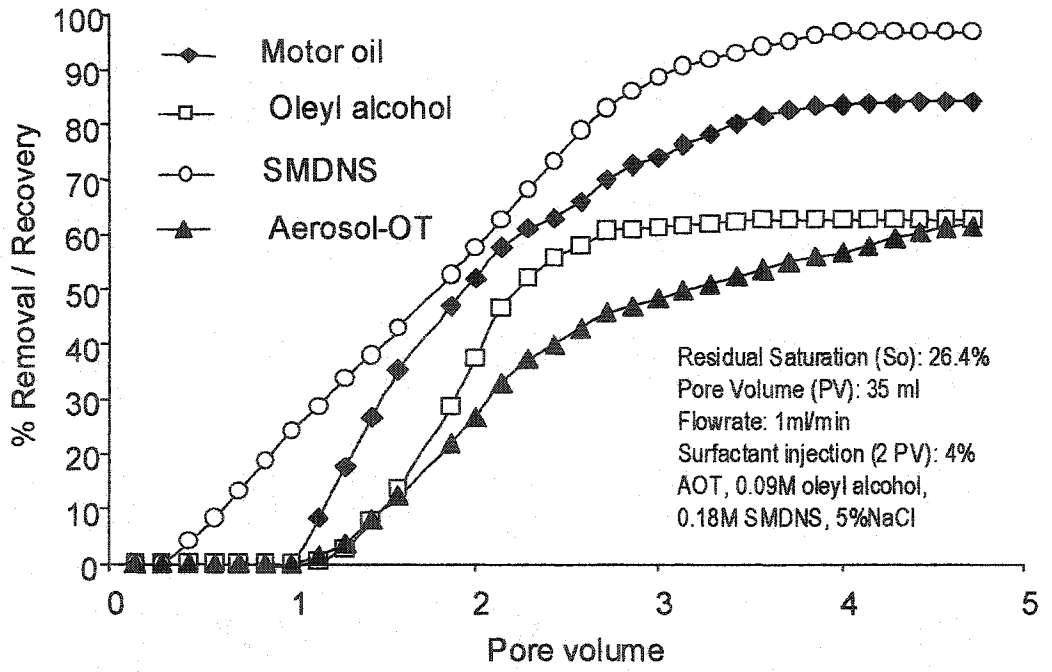

Figure 5.8b. Motor oil column study with AOT + linker formulation.

We repeated the same test for motor oil, and the results and the operating conditions are presented in Figure 5.8b. This test was not as successful as the hexadecane test because, while we could remove a good portion of the motor oil (~84%), around one third of the surfactant and lipophilic linker remained in the column. We also observed some chromatographic separation of the hydrophilic linker that eluted from the column before the surfactant and the lipophilic linker. While doing this experiment we observed that behind the first front of mobilized oil there was a front that appeared to have similar composition to the middle phase, nonetheless a good portion of this phase got trapped in the column. One potential interpretation is that once we injected the surfactant solution, it formed a middle phase system with the motor oil which had a high viscosity (~90 mPa-s) and was able to "push" the oil that also has a high viscosity (~100 mPa-s). However, once the oil was displaced and we switched to water-only flush (viscosity ~ 1mPa-s) the viscosity of the aqueous solution was not enough to push the remaining middle phase in the column, and therefore created preferential flow paths along the bed. We hypothesize that we can use polymers to control the viscosity changes and thus reduce this effect and achieve similar performance to that of the hexadecane system.

In the next set of tests we investigated the detergency performance of these linker microemulsions used as pretreatment for the removal of hexadecane and motor oil from 3"×4" cotton swatches (see the experimental procedure described in the method section). To simulate the pretreatment conditions we contacted 30 ml of the surfactant formulation with 4 swatches for 30 minutes. Figure 5.9a shows the results in removing hexadecane from cotton swatches, where it shows that hexadecane removal is significantly higher

when using the linker formulation than when using the commercial pretreatment. Most commercial pretreatments have as much as 20% surfactant and alcohols. The linker formulation has no volatile components, and the concentration of the surfactant is as low as 4%. Figure 5.9b shows the removal of motor oil from the cotton swatches under the same conditions as Figure 5.9a, except for a higher concentration of sodium chloride in the formulation. In the case of motor oil the performance of the linker formulation is significantly superior to that of the commercial pretreatment. While the total removal for the case of motor oil –linker formulation (~85%) is less than the hexadecane-linker formulation (~98%) this result was expected due to the higher viscosity of motor oil. Each of these removal levels are very similar to the removal levels of the corresponding formulations used in column studies. This last comment suggests a similar removal mechanism in both cleaning settings.

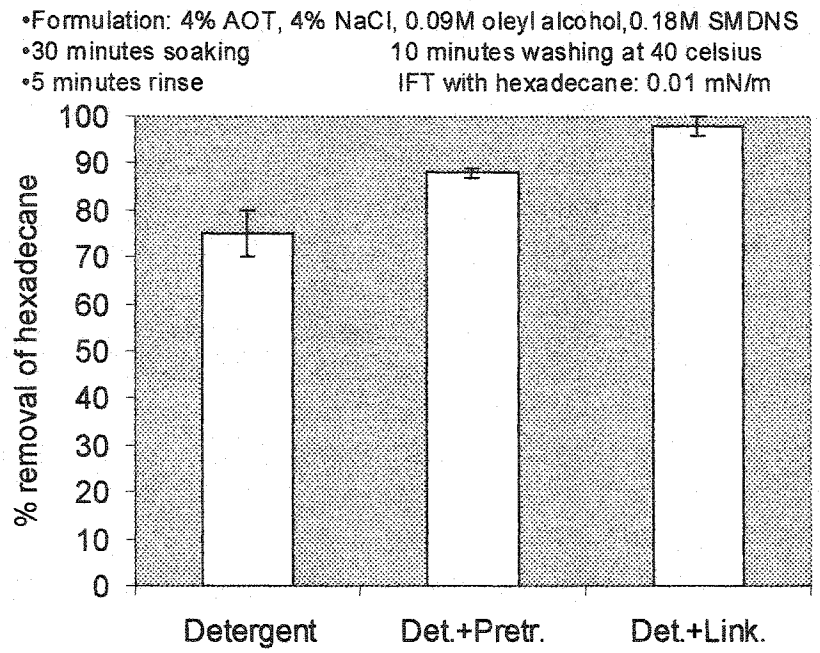

Figure 5.9a. Detergency performance of linker formulation for hexadecane on cotton: detergent alone, detergent plus commercial pretreatment, detergent plus linker formulation.

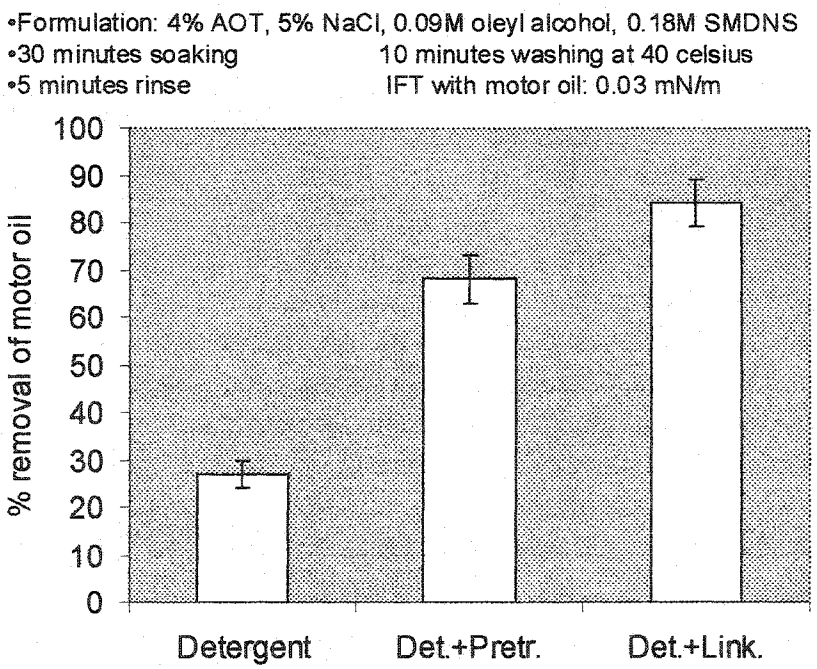

Figure 5.9b. Detergency performance of linker formulation for motor oil on cotton: detergent alone, detergent plus commercial pretreatment, detergent plus linker formulation.

Literature

[1] Bourrel, M. and Schecter R. *Microemulsions and related systems*. Marcell Dekker Inc. New York, 1988.

[2] Promod Kumar and K.L. Mittal, Editors. *Handbook of Microemulsion Science and Technology*. Marcel Dekker, Inc., New York, 1999.

[3] Sabatini, D. A., R.C. Knox and J.H. Harwell. Editors, *Surfactant-Enhanced Subsurface Remediation*. ACS Symp. Ser. 594, Washington, DC, 1995, pp.300.

[4] Scriven, L. E. Equilibrium bicontinuous structure. *Nature*. **1976,** 263(5573), 123

[5] Pope, G. A.; Wade W. H., Lessons From Enhanced Oil Recovery Research for Surfactant-Enhanced Aquifer Remediation, *In Surfactant-Enhanced Subsurface Remediation*. Harwell, J.H. and Sabatini, D.A. Eds. ACS Symposium Series 594, Washington, DC, 1995, p. 142-160.

[6] Graciaa A.; Lachaise J.; Cucuphat C., Bourrel M. and Salager J.L. Improving Solubilization in Microemulsions With Additives.1. The Lipophilic Linker Role. *Langmuir*. **1993**, 9(3), 669

[7] Graciaa A.; Lachaise J.; Cucuphat C., Bourrel M. and Salager J.L. Improving Solubilization in Microemulsions With Additives.2. Long chain alcohol as lipophilic linkers. *Langmuir*. **1993,** 9(12), 3371.

[8] Salager, J. L.; Graciaa, A. and Lachaise J. Improving Solubilization in Microemulsion with Additives. Part III: Lipophilic Linker Optimization. *J. Surfactant Detergents.* **1998,** 1(3), 403.

[9] Uchiyama, H; Acosta, E.; Sabatini, D.A. and Harwell, J.H. Supersolubilization in Chlorinated Hydrocarbon Microemulsions: Solubilization Enhancement by Lipophilic and Hydrophilic Linkers. *Ind. Eng. Chem. Res.* **2000,** 39(8), 2704.

[10] Acosta, E.; Uchiyama, Hirotaka; Sabatini, David A.; Harwell, Jeffrey H. The Role of Hydrophilic Linkers. *J. Surfactants Detergents.* **2002,** 5(2), 151.

[11] Acosta, E., H. Uchiyama, S. Tran, D. A. Sabatini and J. H. Harwell, Formulating Chlorinated Hydrocarbon Microemulsions Using Linker Molecules. *Environ. Sci. Technol.* **2002,** 36(21), 4618 .

[12] Acosta, E.; M. A. Le, J. H. Harwell and D. A. Sabatini, Coalescence and Solubilization Kinetics in Linker-Modified Microemulsions and Related Systems. Langmuir **2003,** 19(3), 566-574..

[13] Acosta, E.; E. Szekeres, D. A. Sabatini and J. H. Harwell, A Net-Average Curvature Model for Solubilization and Supersolubilization in Surfactant Microemulsions, *Langmuir.* **2003,** 19(1), 186.

[14] Huh, Chun. Interfacial Tensions and Solubilizing Ability of a Microemulsion Phase that Coexists with Oil and Brine. *J. Colloid Interface Sci.* **1979,** 71(2), 408.

[15] Nagarajan, R.; Ruckenstein, E. Molecular theory of microemulsions. *Langmuir*. **2000,**16(16): 6400.

[16] Baran, J. R.; G. A. Pope; W. H. Wade; V. Weerasooriya; A. Yapa. Microemulsion Formation With Mixed Chlorinated Hydrocarbon Liquids. *J. Colloid Interface Sci*. **1994,** 168(1), 67

[17] Salager, J.L.; Morgan ,J.; Schechter, R.S.; Wade ,W.H. and Vasquez E. Optimum Formulation of Surfactant/Water/Oil Systems for Minimum Interfacial Tension or Phase Behavior, *Soc. Petrol. Eng. J.* **1979,** 19, 107.

[18] Salager, J.L.; Morgan ,J.; Schechter, R.S.; Wade ,W.H. Mixing Rules for Optimum Phase Behavior Formulations of Surfactants/Water/Oil Systems, *Soc. Petrol. Eng. J.* **1979,** 19, 271 .

[19] Wu, Bin; D. A. Sabatini. Using Partitioning Alcohol Tracers To Estimate Hydrophobicity of High Molecular Weight LNAPLs. *Environ. Sci. and Technol.* **2000,** 34(22), 4701 .

[20] Sottmann, T.; Strey, R. Ultralow Interfacial Tensions in Water-n-Alkane-Surfactant Systems. *J. Chem. Phys.* **1997,** 106(20), 8606 .

[21] Rosen, M. J.: *Surfactants and Interfacial Phenomena,* Wiley, New York (1989).

[22] Childs J., Acosta E., Scamehorn J. F and Sabatini D. A, Surfactant-Enhanced Treatment of Oil-Based Drill Cuttings. Submitted to JERT journal, April 2003.

[23] Pennell, Kurt D.; Pope, Gary A.; Abriola, Linda M. Influence of Viscous and Bouyancy Forces on the Mobilization of Residual Tetrachloroethylene During Surfactant Flushing. *Environ. Sci. Technol.* **1996,** 30(4), 1328 .

[24] Raney, Kirk H.; Miller, Clarence A.. Optimum Detergency Conditions with Nonionic Surfactants. *J. Colloid Interface Sci.* **1987,** 119(2), 539 .

[25] Graciaa A.; Lachaise J.; Cucuphat C., Bourrel M. and Salager J.L. Interfacial segregation of an ethyl oleate/hexadecane oil mixtures in microemulsion systems. *Langmuir*. **1993,** 9(6), 1473 .

CHAPTER 6

Self-Assembly in Linker-Modified Microemulsions[†]

Abstract

Linker molecules are added to microemulsion systems to enhance the interaction between the surfactant and oil (lipophilic linkers) or water (hydrophilic linkers) phases. Previous results suggest that when lipophilic and hydrophilic linkers are combined they behave as a self-assembled surfactant at the oil/water interface. In this work we investigate this self-assembly phenomenon as a function of surfactant, linker and electrolyte concentration. We find that middle phase microemulsion appears at a specific concentration higher than the critical micelle concentration (CMC), which we denote as the critical middle phase microemulsion concentration (CμC). When the lipophilic linker dodecanol is added in equimolar ratio to the hydrophilic linker sodium mono- and di-methyl naphthalene sulfonate (SMDNS), the middle phase microemulsion did not appear until the surfactant sodium dihexyl sulfosuccinate (SDHS) concentration was larger than the CμC of the SDHS-alone system. Dodecanol is shown to segregate near the surfactant tails following a Langmuir-type adsorption process. This segregation is not affected by the electrolyte concentration but is significantly reduced when the

[†] This chapter or portions thereof have been submitted to Journal of Colloid and Interface Science under the title " Self-Assembly in Linker-Modified Microemulsions ". The current version has been formatted for this dissertation.

surfactant (SDHS) concentration approaches the CμC. The data suggest that the self-assembly between hydrophilic and lipophilic linkers to form middle phase microemulsions is only possible if a minimum amount of surfactant is present.

Keywords: microemulsion, trichloroethylene, tetrachloroethylene, lipophilic, hydrophilic, linkers, partition, interfacial, tension.

Introduction

Surfactant systems can self-assemble into many structures, the simplest of which is the micelle (1). The thermodynamic basis of micelle formation has been well documented and modeled (2). Despite being widely studied, higher order structures, such as microemulsion and liquid crystal phases, are more complicated to understand and thus to model. In this work we deal with yet another self-assembly phenomenon: the self-assembly of linker molecules in microemulsion systems (3,4,5,6,7,8,9). The purpose of this research is not to provide a thermodynamic model of this novel self-assembly but rather to describe its properties. The concept of linker molecules in surfactant systems is relatively new (3,8). The novelty of this phenomenon, and the implication it has on commercial surfactant formulations, makes it an emerging area of research.

Graciaa and coworkers pioneered the field of linker molecules by first introducing lipohilic linkers (3,4,5,6). These lipophilic linkers are amphiphilic molecules such as fatty alcohols, acids or amines that segregate near the surfactant tails. Figure 6.1 shows a schematic of the linker effect. In this case, the lipophilic linker is dodecanol, which tends to segregate near the tails of the surfactant (sodium dihexyl sulfosuccinate (SDHS)), or at

the palisade layer of the interface. Graciaa and coworkers found that lipophilic linkers significantly increased the oil solubilization in middle phase microemulsions (3,5).

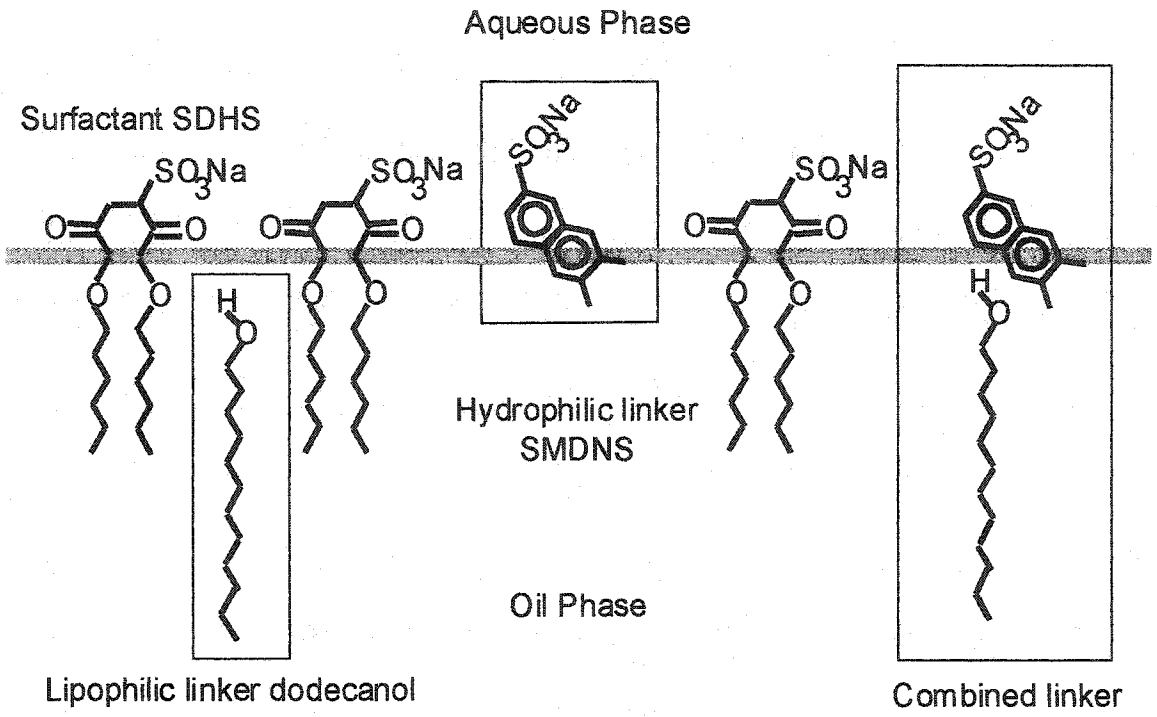

Figure 6.1. Schematic of the linker effect. The lipophilic linker and the hydrophilic linker self-assemble to act as a surfactant at the interface.

The segregation of a long chain alcohol is part of the self-assembly phenomenon of linker molecules (4,5). Medium chain alcohols (propanol to octanol) are considered cosurfactants that adsorb at the oil/water interface (10). Alcohols with longer hydrocarbon chain length (decanol and higher) have been shown to segregate deeper into the oil side of the interface (11). It is worth mentioning that segregation of long chain alcohols has also been observed in micellar system devoid of a non-polar oil (12). In some instances long chain alcohols are considered oil-cosolvents, which implies the lack

of surface activity of these molecules (13). We have studied the partition of dodecanol in SDHS microemulsions, finding that some but not all of this lipophilic linker segregates near the surfactant tails (7).

Hydrophilic linkers were first proposed in an effort to compensate for certain effects of lipophilic linkers. The hydrophilic linker molecule was selected to have a short hydrophobe and a strong hydrophile such that while being able to adsorb and/or segregate at the oil/water interface (see Figure 6.1), it weakly interacts with the oil phase, thereby increasing the interfacial area and the number of sites available for the lipophilic linker to segregate near the interface. We proposed the use of sodium mono- and di-methyl naphthalene sulfonate (SMDNS, as depicted in Figure 6.1) as the hydrophilic linker and found that by combining with dodecanol (lipophilic linker) and SMDNS we could increase the solubilization of chlorinated hydrocarbons beyond that possible with the lipophilic linker alone (8). Further investigation on the role of hydrophilic linkers revealed that these molecules partially coadsorb with the surfactant and certainly expand the interfacial area but do not interact substantially with the oil phase (9). The exact orientation of SMDNS at the oil/water interface is unknown and is depicted as a shallow penetration into the oil phase in Figure 6.1. These properties of hydrophilic linkers differentiate them from common hydrotropes (that don't coadsorb at the oil/water interface) and from cosurfactants (that coadsorb at the oil/water interface and strongly interact with the oil molecules) (9). It was also found that the combination of lipophilic and hydrophilic linkers in equimolar ratio increased the partitioning into the middle phase of each linker in middle phase microemulsions (7,9). It is worth noting that the

combination of hydrophilic and lipophilic linkers can replace the main surfactant to a certain degree and still retain the same solubilization of oil, which again supports the idea that hydrophilic and lipophilic linkers self-assemble at the interface, as suggested in Figure 6.1 (7). If the schematic proposed in Figure 6.1 is accurate, the self-assembly of hydrophilic and lipophilic linkers is driven by the presence of the surfactant that would allow the segregation of both linkers near the interface. To obtain a middle phase microemulsion with combined linkers, a minimum amount of surfactant is required, and this aspect of the self-assembly will be further investigated here.

In this work we will investigate the properties of this self-assembly phenomenon and how it relates to the self-assembly of single surfactant microemulsions. Our hypothesis is that when hydrophilic and lipophilic linkers are combined they form a self-assembled structure which has surfactant-like properties. According to this depiction, the dodecanol (lipophilic linkers) comes from the oil phase and the SMDNS (hydrophilic linkers) is adsorbed from the aqueous phase. As these molecules individually partition into the different phases, the only way for them to self-assemble is at an interface.

To test this hypothesis we obtained the phase diagrams of microemulsions with trichloroethylene (TCE), and tetrachloroethylene (PCE) as oil phases, and with the surfactant sodium dihexyl sulfosuccinate (SDHS) either alone or in combination with dodecanol and SMDNS as the linkers. In particular we will define the phase map (the area of surfactant and electrolyte concentration where a microemulsion exists) and characterize the microemulsion systems for their interfacial tension and solubilization of oil and water. If the hypothesis is true, in the absence of surfactant or at low surfactant

concentration, we would not be able to observe the formation of a middle phase bicontinuous microemulsion system because of the inability of these linker molecules to cross the interface and setup a net-zero curvature system. We will also study the segregation of each linker at different surfactant and linker concentrations, electrolyte concentrations and oil polarity.

Materials and Methods

Materials

The following chemicals were purchased from Aldrich at the concentrations shown in parenthesis and were used without further purification: trichloroethylene (TCE, 99%+), tetrachloroethylene (PCE, 99%+), n-dodecanol (98+%), sodium chloride (99%+), sodium dihexyl sulfosuccinate (SDHS, Fluka brand 80% solution in water). Sodium mono and dimethyl naphthalene sulfonate (SMDNS, 95%+) was purchased from CKWitco (Houston, TX). Table 6.1a presents selected properties of the oils used in this work (TCE and PCE) and Table 6.1b presents selected properties of the amphiphilic species (SDHS, SMDNS and dodecanol).

Table 6.1a. Properties of the oils formulated in microemulsions

Oil	Equivalent Alkane Number (EACN)	Dipolar moment (D)	Molecular Structure
Trichloroethylene (TCE)	-3.8[a]	0.77	$Cl_2C=CHCl$
Tetrachloroethylene (PCE)	2.9[a]	0.00	$Cl_2C=CHCl_2$

(a): From reference (8)

Table 6.1b. Properties of the amphiphilic molecules used in this work

Amphiphilic Molecule	Area per molecule $Å^2$/molecule	Molecular weight g/mol	Molecular Structure
Sodium dihexyl sulfosuccinate (SDHS)	100[a]	376	$C_6H_{13}O_2CH_2CH(SO_3Na)CO_2C_6H_{13}$
Sodium mono- and di-methyl naphthalene sulfonate (SMDNS)	90[a]	250	$CH_3(C_{10}H_6)SO_3Na$ (65%) $(CH_3)_2(C_{10}H_5)SO_3Na$ (35%)
Dodecanol	N.A[a].	186	$C_{12}H_{25}OH$

(a): These amphiphilic molecules were characterized in references (9). In the case of oleyl alcohol, the area per molecule does not apply since lipophilic linkers don't adsorb at the oil/water interface.

Methods.

Phase behavior studies were performed using equal volumes of aqueous solution and oil (5 ml each). For a given surfactant concentration and linker concentration, the sodium chloride concentration was systematically increased to obtain the transition from Type I microemulsions (micelles) to Type III (bicontinuous microemulsions) to Type II (reverse micelles). To obtain the equilibrium conditions, flat bottom test tubes (15 ml, 10 mm diameter) were placed in a water bath at 27°C then shaken once a day for three days, and left to equilibrate for two weeks. The phase volumes were determined by measuring the height of each phase in the test tube (precision of ± 0.07 ml). One important parameter in studying microemulsion is the solubilization parameter at "optimum" formulations where oil and water are solubilized in the same magnitude, and are normally expressed as volume solubilized per mass or volume of surfactant (11). One alternative way to express the solubilization capacity is to use the characteristic length of the microemulsion (ξ) which expresses the volume of oil (or water) solubilized at optimum

formulation per interfacial area of the adsorbed surfactant, and thus the larger this length, the larger the solubilization capacity of the system (14,15). The characteristic length (ξ) for microemulsions can be calculated using the following expression (14,15):

$$\xi = \frac{6 * \phi_o * \phi_w * V_m}{A_s} \qquad \text{Eq.1}$$

where ϕ_o , ϕ_w are the volume fractions of oil and water in the middle phase microemulsion, respectively, V_m is the total volume of the middle phase microemulsion (in $Å^3$), and A_s is the interfacial area of the surfactant membrane consisting of the surfactant, cosurfactant and hydrophilic linkers (in $Å^2$). The interfacial area can be calculated as:

$$A_s = \sum_i Cs_i * V_w * \varphi_i * 6.023 * 10^{23} * a_i \qquad \text{Eq.2}$$

where Cs_i is the initial concentration of the surfactant "i" in the aqueous solution, V_w is the initial volume of the aqueous solution in the system, φ_I is the fraction of surfactant, cosurfactant or hydrophilic linker in the middle phase microemulsion (with respect to the total surfactant concentration) and a_i is the area per molecule of the surfactant "i" (Table 6.1b).

Only SMDNS and SDHS were considered in the calculation of the interfacial area because the dodecanol is envisioned to either fit in between SDHS tails or to self-assamble with SMDNS. The concentration of both of these molecules was obtained by ion-coupled chromatography performed with a Dionex 500 chromatograph equipped with a reverse phase column (NS1-4mm). The concentration of dodecanol was measured by

gas chromatography using a Varian 3300 with FID detector and a SPB20 capillary column with programmed temperature ramping from 50°C to 250°C at 15°C/min.

Within the Type III middle phase microemulsion, the optimum formulation was observed as the point where equal volumes of oil and water were solubilized (11). At optimum formulation, the maximum cosolubilization of both oil and water are achieved. For optimum middle phase microemulsions, the interfacial tension between the excess oil and water ($\gamma^*_{o/w}$) was measured using a University of Texas spinning drop interfacial tensiometer model 500, injecting 1 to 5 μl of the less dense phase in a 300 μl tube filled with the heavier phase. While it is most common to report the interfacial tension between the middle phase and each of the excess phases, at low surfactant concentrations it is very difficult to sample the middle phase microemulsion. In this work we use the approximation that in optimum middle phase microemulsion the interfacial tension between the middle phase and each of the excess phases is one half of the interfacial tension between the excess phases ($\gamma^*_{o/w} \cong 2\gamma^*_{m/w} \cong 2\gamma^*_{o/m}$) (16).

Results and Discussions

SDHS microemulsions phase maps.

In this first section we describe the SDHS-alone microemulsion systems (no linkers) to provide a baseline for comparing with linker-based systems. Figure 6.2 shows the phase map of SDHS microemulsion systems for TCE (Figure 6.2a) and PCE (Figure 6.2b). These phase maps, sometimes referred to as fish diagrams due to their shape (11,13), show the regions of surfactant and electrolyte concentrations that produce a

given type of microemulsion phase (17). The region labeled as "I" corresponds to a two phase system (excess oil phase and Type I microemulsion), the region "III" enclosed by the phase boundaries has three phases in equilibrium (excess oil, water and Type III microemulsion), the region "II" has two phases (excess water and Type II microemulsion) and region "IV" is a single phase system containing oil, water and SDHS. The amount of surfactant that corresponds to the cross point where Types I, II, III and IV meet is the minimum amount of surfactant required to achieve a single phase microemulsion (11). The dotted line in the middle of the Type III region indicates the optimum formulation (equal volumes of oil and water solubilized).

To understand the shape of the phase maps, we need to understand the properties of the different oils. Table 6.1a presents the equivalent alkane carbon number (EACN) of TCE and PCE. The EACN parameter was introduced by Salager et al. and indicates the hydrophobicity of a given oil phase (18). The larger and more positive the value of the EACN, the more hydrophobic the oil. For the case of PCE, an EACN of 2.9 means it is almost as hydrophobic as propane. The lower EACN of TCE is due to its polarity (Table 6.1a, third column). Negative EACN values indicate that the oil is more hydrophilic than methane.

Figure 6.2 reveals three major characteristics of SDHS phase diagrams. The first characteristic is that more polar oil molecules tend to form middle phase microemulsions at lower electrolyte concentrations, which is predicted by the lower EACN of the oil (8,15,18). Second, the middle phase region tends to shrink for more polar oils. Third, the minimum surfactant concentration to achieve the formation of a middle phase (Type III)

microemulsion is higher for the more polar TCE. For TCE the lower boundary of the type III region is about 0.4% SDHS and for PCE it is close to 0.1% SDHS.

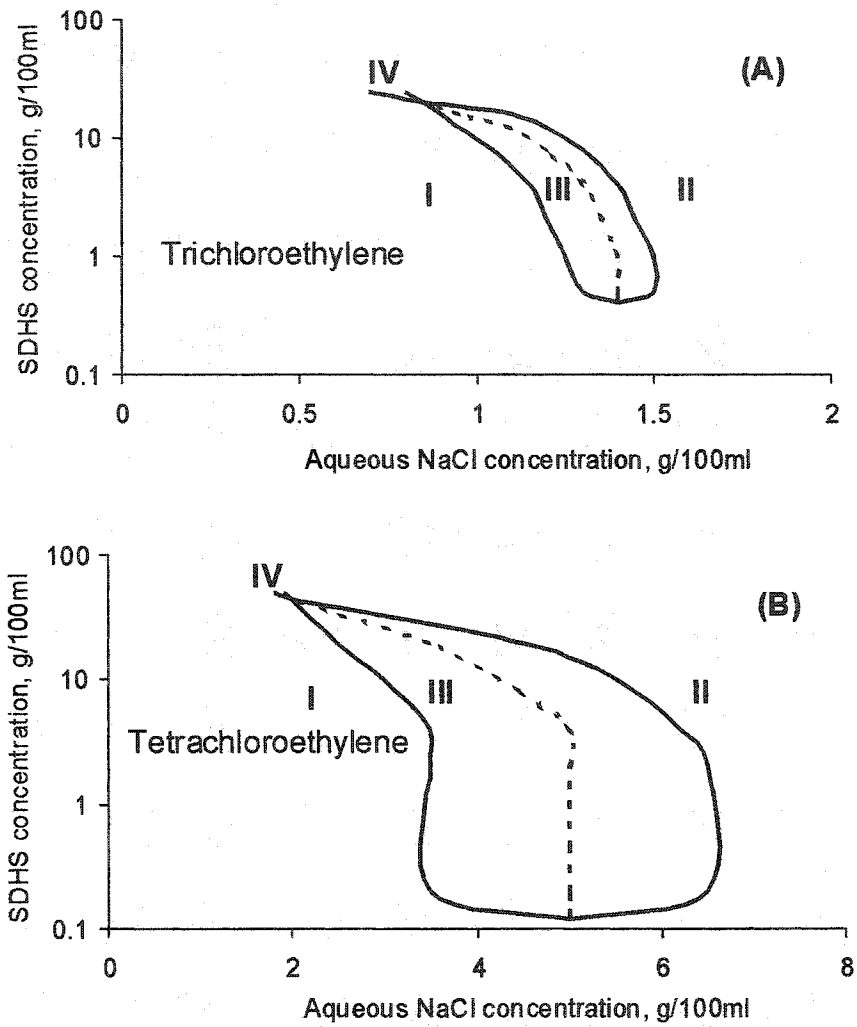

Figure 6.2. "Fish" phase diagrams for (A) SDHS-TCE microemulsion, (B) SDHS-PCE microemulsions. The roman numerals indicate the different types of microemulsion systems. The solid lines represent the phase transitions and the dotted lines indicate the optimum middle phase microemulsion.

The results in Figure 6.2 can be interpreted based on the polarity of the oil. The more polar the oil the greater the affinity between the surfactant and oil, reducing the

amount of electrolyte needed to obtain the middle phase microemulsion (notice that the x-axis varies between the three plots). The width of the Type III region is also reduced for polar oils. The optimum salinity and salinity windows of these systems have been modeled using the surfactant affinity difference concept and the net-average curvature model (15,18). In the extreme case, if the oil is polar enough, the middle phase region disappears (19).

Finally, it is worth commenting on the curved rather than vertical shape of the phase maps. For anionic systems, an increase in surfactant concentration not only increases the concentration of the amphiphile, but also the concentration of the counterion. It is known that in micelles only 60 to 70 percent of the counterion is bound to the surfactant (20). If we extrapolate this result to microemulsion membranes we can propose the following expression:

$$[NaCl]_{ad} + ub*[SDHS]=[Na]_t \qquad \text{Eq.3}$$

where $[NaCl]_{ad}$ is the molar concentration of sodium chloride added to the aqueous solution (that we note as optimum salinity, S*), *ub* is the molar fraction of unbound sodium added with the anionic surfactant, in this case SDHS, *[SDHS]* is the molar concentration of SDHS and $[Na]_t$ is the total molar concentration of sodium in the aqueous solution (not bound to the surfactant membrane). Figure 6.3 presents the data of molar aqueous surfactant concentration versus the molar optimum salinity for all the systems considered in Figure 6.2, where the curves are equivalent to the dotted lines in Figure 6.2 but expressed on a molar basis in Figure 6.3. The model (equation 3) is presented along with the data. The unbound fraction for TCE and PCE was 0.19 and 0.45

(all dimensionless), respectively, and the total sodium concentration was 0.24 M, and 0.88 M for the same systems. A discussion of the difference in unbound fraction and total sodium concentration for the different systems is warranted but is beyond the scope of this particular article. Nonetheless it is important to highlight that the good fit between the data and the model reflects the validity of the sodium balance proposed in equation 3, as will become evident in the next section.

The critical microemulsion concentration (CμC).

As previously discussed, one of the objectives of this work is to determine the role of the surfactant concentration in the self-assembly between hydrophilic and lipophilic linkers. In previous studies we have reported that a minimum surfactant concentration is needed to promote the linker self-assembly (7). In this section we investigate the minimum amount of surfactant needed to form a middle phase microemulsion. We do this by holding constant the optimum electrolyte concentration (S*) experienced at low surfactant concentration, which is 1.4% NaCl and 5% for PCE. We then varied the surfactant concentration and measured the interfacial tension across each point of the scan.

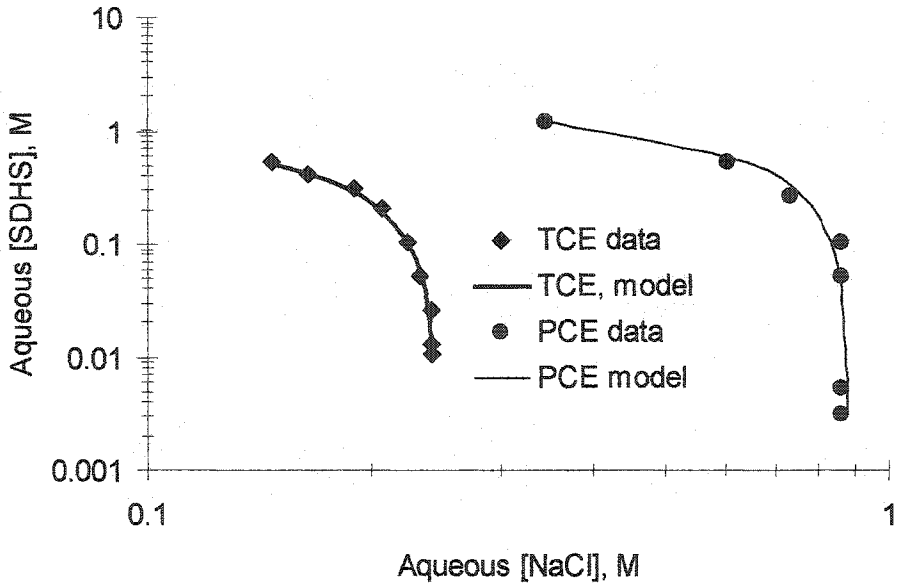

Figure 6.3. Optimum electrolyte concentration for SDHS-alone microemulsions with TCE and PCE.

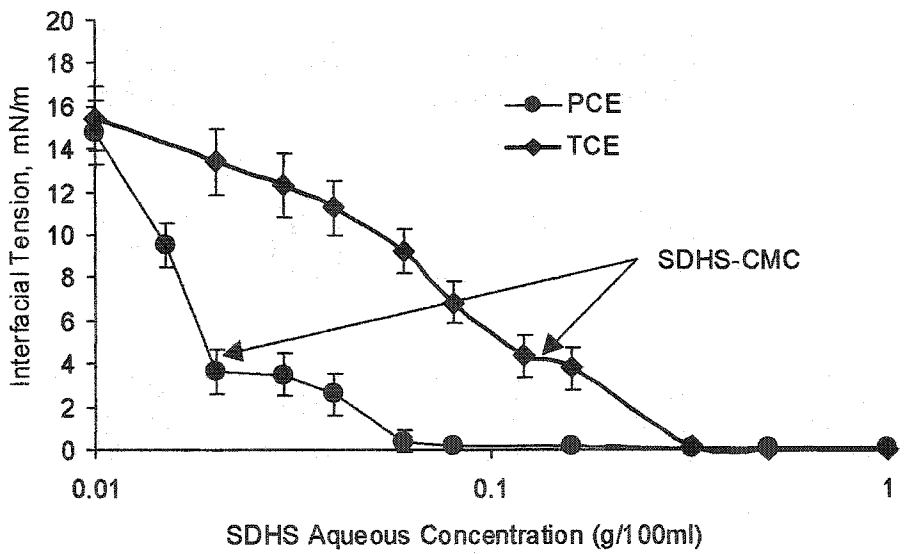

Figure 6.4. Interfacial tension versus SDHS concentration at constant NaCl concentration (TCE-1.35%NaCl and PCE-5.0%NaCl). Black circles correspond to the interfacial tension of the SDHS solution and PCE. Black diamonds correspond to the SDHS-TCE system.

Figure 6.4 presents the interfacial tension versus the initial surfactant concentration for phase diagrams with the these oils. At low surfactant concentration we observe a typical IFT decrease due to monomer adsorption at the oil/water interface. Above the CMC there is a range of surfactant concentrations where the IFT remains constant, until at still larger surfactant concentrations the IFT further decreases to ultra-low levels which are typical of middle phase microemulsions. The point at which the IFT finally levels off (at an ultralow IFT value) is the point at which the first droplets of middle phase microemulsion (non-wetting droplets) appear. Aveyard et al. (21) coined the term "critical microemulsion concentration" to indicate the minimum surfactant concentration needed to attain the microemulsion phase. Here we use this same definition and denote this concentration as the CμC. The initial definition of Aveyard et al (21) was based on the change of slope of the solubilization curve of swollen micelles (Type I microemulsions), whereas here we extend this concept to middle phase systems based on the IFT studies presented in Figure 6.4.

One question generated by the data in Figure 6.4 is what type of transition occurs between the CMC and the CμC. Because of the relative novelty of the CμC concept, to our knowledge there has not been previous research on this topic. While our work does not directly address this issue we can offer one plausible explanation. In 1972 Kodama et al first proposed the concept of a second CMC (22). According to this concept, the first micelles formed at the CMC are spherical but beyond a certain surfactant concentration rod-like micelles start forming; this surfactant concentration is known by some as the second CMC and also as the sphere to rod micelle transition. Here we will refer to this

point as the micellar transition concentration (MTC). This phenomenon has been experimentally studied and modeled using molecular thermodynamic methods (23,24). Both experimental data and models agree that the sphere to rod transition corresponds to a change in curvature of the micellar phase due to conditions such as temperature, electrolyte, packing factor of the surfactant, etc. If this concept can be translated to the microemulsion systems the transition between the CMC and the CμC can be due to the formation of the first swollen micelles of near zero curvature that eventually yield to the formation of a separate middle phase microemulsion system. Thus the MTC and the CμC seem to be a similar concept except that in the latter case the micelle is swollen with dissolved oil. To further support to this hypothesis, Guo et al (24) observed that for SDS micelles the MTC is approximately three times the CMC. In Figure 6.4 we observe that the CμC is also approximately three times the CMC. While this ratio may vary from one system to another, the close agreement between our result and that of Guo et al. (24) supports the equivalence of the MTC and CμC concepts. We should clarify that there could be alternative explanations to the origin of the CμC, such as micelle-micelle interactions, which merits future research in this area.

Phase maps of SDHS microemulsions with linker molecules.

In this section we discuss the phase maps for SDHS microemulsions for TCE and PCE with mixed linker molecules (0.09M SMDNS as hydrophilic linker and 0.09M dodecanol as lipophilic linker in aqueous solution). Figure 6.5 shows these phase maps (similar to Figure 6.2). The best way to interpret the phase maps in Figure 6.5 is to compare them to their SDHS-alone counterparts presented in Figure 6.2. The first

noticeable feature of the mixed linker phase maps in Figure 6.5 is that the optimum electrolyte concentration (dotted line) varies by close to one order of magnitude between the high SDHS concentration (10 to 20 g/100ml SDHS) and the one at low SDHS concentration (0.1 g/100 ml). In contrast, the phase maps in Figure 6.2 have a salinity variance of only two to three fold difference in optimum electrolyte (S*). Additionally at low surfactant concentration, the optimum electrolyte concentration for SDHS alone microemulsions varies significantly, 1.4% NaCl for TCE (Figure 6.2a), and 5% for PCE (Figure 6.2b), whereas for the mixed linker systems the optimum electrolyte concentration is much more similar for the three oils (9% NaCl for TCE, and 11% for PCE). For the linker-based systems, the shape of the phase map at low surfactant concentration is strongly asymmetric and extended towards higher electrolyte concentration. This "slanting" of the phase diagrams in linear systems is likely due to the different partitioning of the linkers. Graciaa et al. have found that in nonionic surfactant microemulsion systems the optimum ethoxy group number (similar to S*) changes with surfactant concentration due to partition effects (25). Ryan and Kaler have observed similar asymmetry in nonionic microemulsions (in their case the asymmetry extends towards higher temperatures) when highly hydrophilic decyl glucoside was added (26). In our system, the hydrophilic linker seems to have the same effect as the decyl glucoside. Another important observation is that the lower phase boundary of the middle phase region (CμC) is relatively high for the SDHS system alone (0.15 g/100ml to 0.8 g/100ml) but less than 0.1 g/100ml SDHS for the systems with linker molecules. In fact the value of 0.1 g/100 ml concentration was reported based on the presence of a visible middle

phase microemulsion but, as will be discussed latter, interfacial tension values reflect a much lower value.

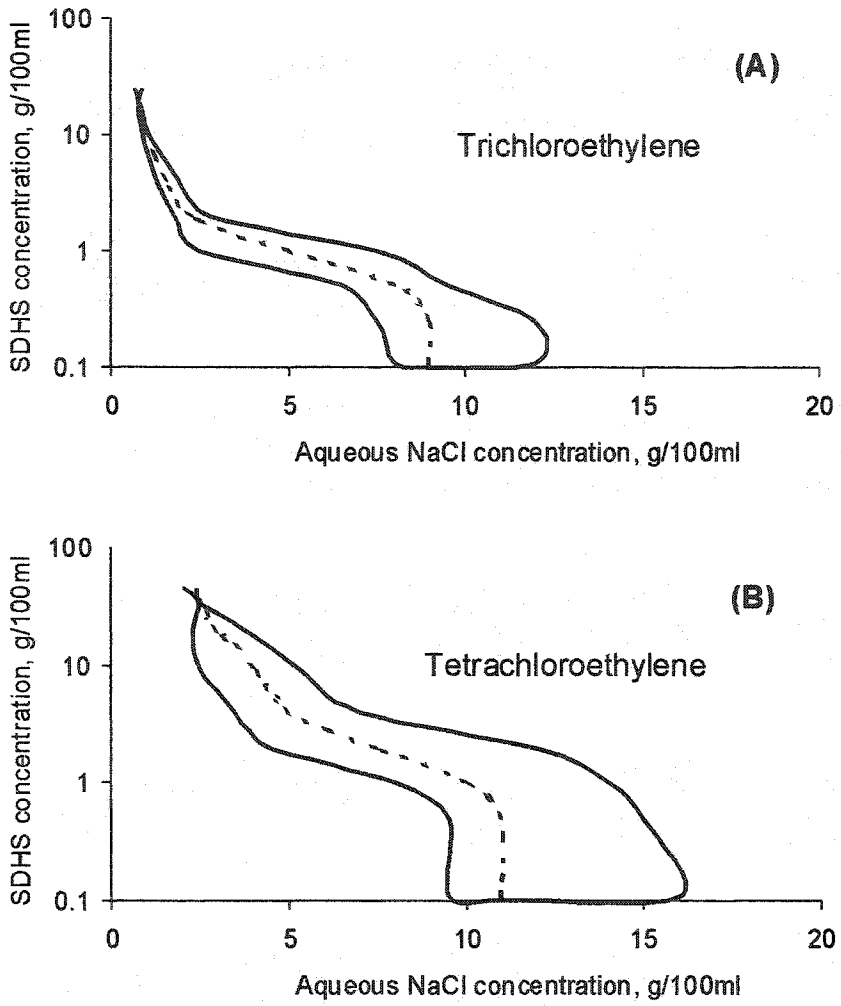

Figure 6.5. "Fish" phase diagrams for (A) SDHS-TCE microemulsion, and (B) SDHS-PCE microemulsions. All systems contained 0.09M of SMDNS and 0.09M of dodecanol. The solid lines represent the phase transitions and the dotted line indicate the optimum middle phase microemulsion.

These results raise a new set of questions regarding the behavior of linker molecules in microemulsions. The reason for the requirement of a higher electrolyte concentration in the mixed linker microemulsion can be partially answered by a previous

study (7). In particular, we found that for different linker combinations and at a constant surfactant concentration, the optimum salinity of the system can be estimated as (7):

$$\ln\left(\frac{S^*}{S_0^*}\right) = X_{SMDNS} * A * [SMDNS] - X_{dodecanol} * B * [dodecanol] \qquad \text{Eq.4}$$

where S* and S_o* are the optimum electrolyte concentration in the presence and absence of linkers respectively, A and B are constants that depend on the type of linker, X_{linker} is the molar fraction of the linker (e.g. $X_{SMDNS} = [SMDNS] / \{[SMDNS]+[dodecanol]\}$), and *[SMDNS]* and *[dodecanol]* are the initial aqueous molar concentrations of SMDNS and dodecanol. For the case of different linker concentrations we have found the following empirical equation to be valid for a wide range of compositions:

$$\ln\left(\frac{S^*}{S_0^*}\right) = X_{SMDNS} * A' * \frac{[SMDNS]}{[SDHS]} - X_{dodecanol} * B' * \frac{[dodecanol]}{[SDHS]} \qquad \text{Eq.5}$$

where S_o* is calculated based on equation 3, A' and B' are dimensionless constants that depend on the type of linker; [SDHS] is the initial aqueous molar concentration of SDHS. Figure 6.6 presents the data and model predictions (equation 5) for the optimum formulation systems (dotted line) presented in Figure 6.5. The model predictions in Figure 6.6 uses an A' of 1 and a B' of 0.5. While the model works well for medium to high SDHS concentrations, below an SDHS concentration of 0.01M the system behaves quite different from the original SDHS microemulsion system. Indeed, in this case close to 90% of the middle phase system is composed of SMDNS and very little SDHS is present. In the next section we will further discuss the low SDHS concentration zone of the phase map.

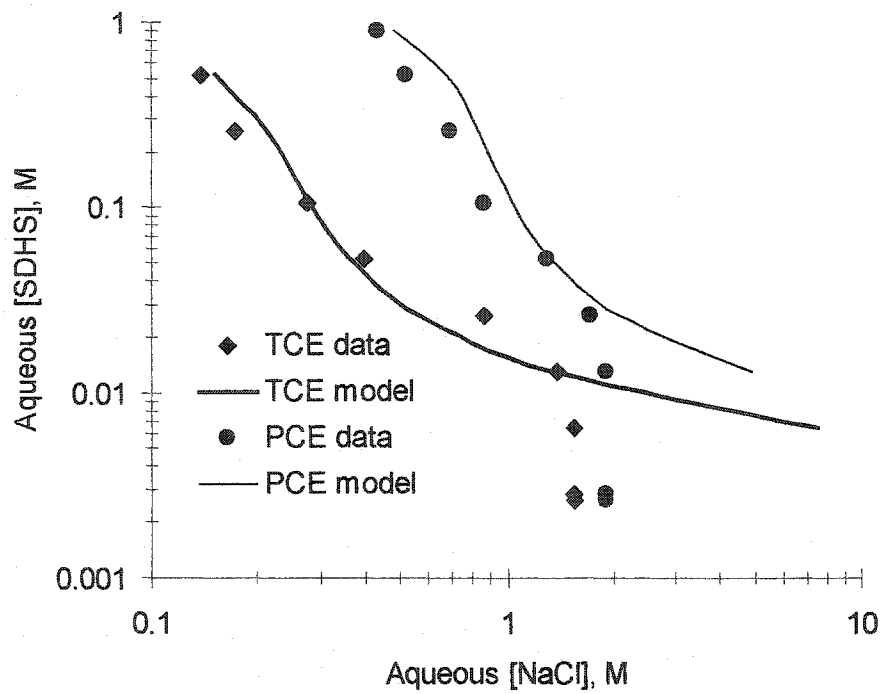

Figure 6.6 Optimum electrolyte concentration for SDHS microemulsions formulated with 0.09M SMDNS and 0.09M dodecanol; and with TCE and PCE as oil phases.

Linker self-assembly as a function of surfactant concentration.

In this section we will study how the surfactant concentration influences the segregation of linker molecules in the middle phase microemulsion. As indicated above, the SDHS-linker microemulsion systems does not evidence a discrete SDHS critical microemulsion concentration (CμC) in Figure 6.5, which is in contrast with SDHS-alone systems presented in Figure 6.2. Figure 6.7 illustrates this point in more detail. Figure 6.7a presents the interfacial tension between the excess oil and water phases as a function of the SDHS initial aqueous concentration for the TCE and PCE optimum systems indicated by the dotted line in SDHS-alone microemulsions (Figures 6.2a and 6.2b) and in the SDHS-linker systems (Figures 6.5a and 6.5b). For the systems without linkers, the

log scale for IFT in Figure 6.7a shows that ultralow IFT (i.e. 0.1 mN/m or less) is achieved by the TCE-SDHS and PCE-SDHS systems at the CμC and it does not change significantly with increasing surfactant concentrations. Kurlat et al. (27) measured the interfacial tension of optimum systems within the type III region at different surfactant concentration (similar to Figure 6.7a, but above the CμC only) and found that the interfacial tension tends to increase slightly but remains ultralow with increasing surfactant concentration, which is consistent with the no-linker data presented in Figure 6.7a. On the other hand the data for the TCE-SDHS-linkers and PCE-SDHS-linkers systems is not as clear as their single surfactant counterparts. In the case of linker systems there is no obvious breakpoint in the IFT curve but rather a smooth lowering of the IFT (i.e. a clear CμC is not apparent). Also, with linkers it is observed that even at low SDHS concentrations (0.01g/100ml) the IFT is below 1mN/m.

It is important to note the visual appearance of these systems with low SDHS concentration. There was no visible middle phase system in these cases but rather a fuzzy layer concentrated in SMDNS. For this reason the optimum formulation was pinpointed based on the minimum IFT found between the excess oil and water phases of the vials scanned at a given SDHS concentration.

This SMDNS fuzzy layer, formed at low SDHS concentration, has the characteristics of a surfactant sponge L_3 phase since it was clear and did not show the birefringent and viscous behavior expected of liquid crystals or oil solubilization typical of bicontinuous microemulsion systems. Additional research is necessary to characterize

these systems and investigate the role of these sponge phases in the partition of the linkers and the unusual behavior at low surfactant concentration.

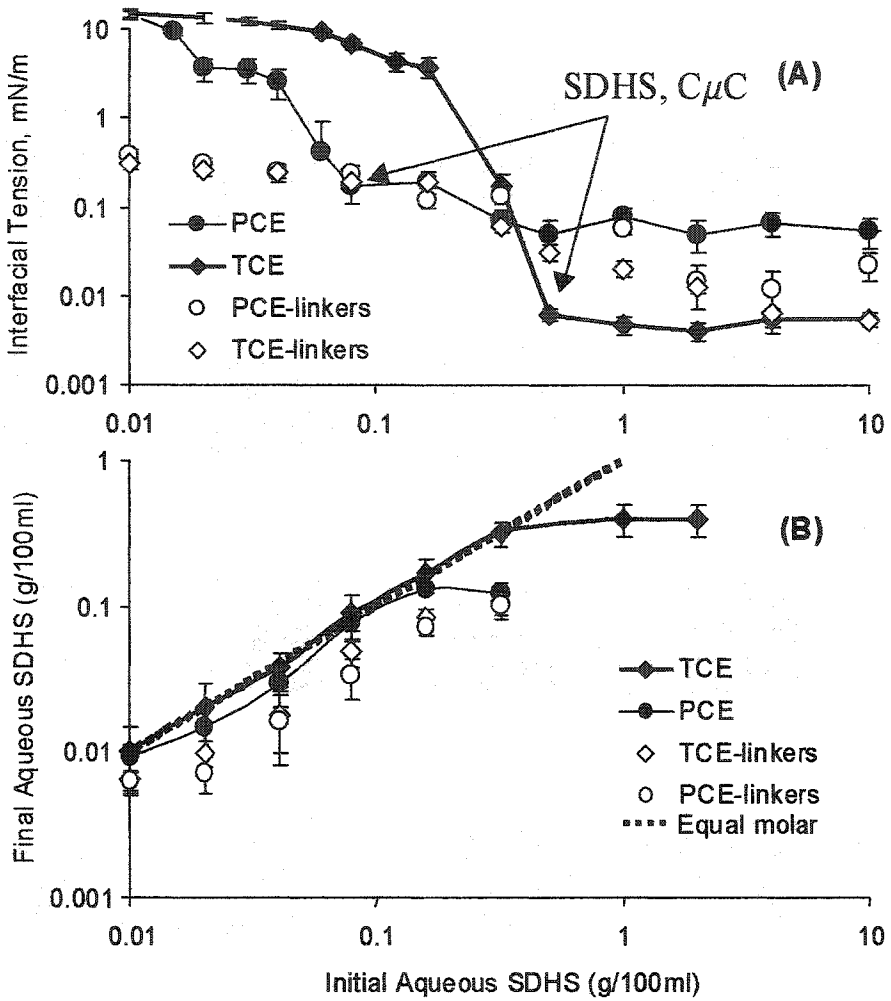

Figure 6.7. Interfacial tension and composition of SDHS microemulsions of PCE and TCE at 0.09M of SMDNS and 0.09M of dodecanol. Part (A) Interfacial tension between the excess oil and water phases as a function of SDHS concentration at optimum formulation. Part (B) SDHS aqueous concentration at optimum formulation, the dotted line indicates the initial aqueous concentration of SDHS.

While the IFT curves reveal the thermodynamic state of the interface, the question remains as to where the SDHS is located before and after reaching the CμC, both with

and without linkers. Figure 6.7b presents the SDHS concentration in the excess aqueous phase for the same systems considered in Figure 6.7a. For the case of the TCE and PCE we observe that, before reaching the CμC, the aqueous concentration of SDHS in equilibrium with the excess oil phase is the same as the initial aqueous concentration (dotted line of Figure 6.7b). Beyond the CμC the concentration of SDHS in the excess aqueous phase is somewhat constant at a level close to that of the CμC. This observation is important because it suggests that the transition between the CMC and the CμC occurs in the bulk aqueous phase and is not due to additional adsorption at the oil/water interface. In the case of the linker formulations, Figure 6.7b shows that the equilibrium SDHS aqueous concentration was slightly lower than the initial concentration, suggesting that there was some degree of participation of the SDHS in the fuzzy layer that was concentrated in SMDNS. This observation corroborates the observation made with the interfacial tension curves that there is not a clear CμC level in the linker formulations. The linker systems with low SDHS (less than CμC) seem to be able to form a "local" microemulsion membrane at macroscopic oil/water interfaces (such as the droplet in IFT measurements or the interface between the oil and water phases in the sample tube); but can not form a separate middle phase microemulsion until the concentration of the SDHS approaches the CμC of the SDHS alone systems. It should be mentioned that the concentration of the surfactant in the oil phase was negligible (less than 0.1mM or 0.004 g/100ml, the detection limit). This observation supports our working hypothesis: the hydrophilic and lipophilic linker molecules cannot self-assemble to form middle phase microemulsion systems unless there is a certain minimum amount of surfactant present.

In addition, we also have some evidence that in the absence or very low concentration of surfactant, there is some degree of segregation of the linkers at macroscopic oil water interfaces (such as droplet surfaces in emulsion systems), as observed by the lower IFT values below the CμC in Figure 6.7a.

The discussion provided above suggests that the "self-assembly" of hydrophilic linker (SMDNS) and lipophilic linker (dodecanol) depicted in Figure 6.1 is affected by the concentration of the surfactant, especially at low surfactant concentration. Figure 6.8 presents the magnitude of the self-assembly of each linker as a function of the SDHS concentration for the TCE and PCE optimum microemulsions. Here the magnitude of the SMDNS self-assembly is expressed as the percentage of SMDNS adsorbed:

$$\%SMDNS_{adsorbed} = \frac{([SMDNS]_m / [SDHS]_m)}{([SMDNS]/[SDHS])} * 100\% \qquad \text{Eq.6}$$

where [SMDNS] and [SDHS] are the initial aqueous concentration of SMDNS and SDHS added to the system and $[SMDNS]_m$ and $[SDHS]_m$ are the concentration of SMDNS and SDHS in the middle phase microemulsion.

The data presented in Figure 6.8 shows that at low SDHS concentration (4 g/100ml or lower) the fraction of SMDNS adsorbed is only 30 to 40% and is slightly higher for PCE than for TCE. At larger SDHS concentrations (10g/100ml or larger) the percentage adsorbed increases to 50% - 60%. The reason for this increased adsorption of SMDNS with higher SDHS concentration is not clear at this moment but could be due to the reduction in the volume of the excess water as the system approached a type IV

system (no excess oil or water phase). The SMDNS not present in the middle phase tends to be present in the excess water phase.

To understand the phenomena of lipophilic linker segregation, here we propose the use of the surface excess concentration (Γ) of the lipophilic linker, dodecanol, as the number of molecules adsorbed per unit interfacial area:

$$\Gamma = \frac{([C12OH]_{m-o} - [C12OH]_{b-o})V_{o,m} * Nav}{A_s} \qquad \text{Eq. 7}$$

where $[C12OH]_{m-o}$ is the dodecanol concentration in the oil present in the middle phase microemulsion, $[C12OH]_{b-o}$ is the dodecanol concentration in the excess "bulk" oil phase, $V_{o,m}$ is the volume of the oil solubilized in the middle phase., Nav is the Avogadro's number, and A_s is the interfacial area provided by the surfactant and calculated based on Eq. 2.

For the case of the dodecanol, Figure 6.8 shows that the segregation of dodecanol (measured as the surface excess concentration) achieves a maximum value at intermediate SDHS concentration (2 to 4 g/100ml). At lower SDHS concentrations, and especially for TCE, we observe a significant decrease in the segregation of dodecanol as it approaches the SDHS concentration that produces a well defined middle phase microemulsion (which is close to the CμC of the SDHS-alone system). This diminished segregation of dodecanol at lower surfactant concentration is consistent with higher effect

of partitioning in nonionic surfactant systems when the total surfactant concentration is reduced (25). This result also reinforces the idea that the self-assembly of SMDNS and dodecanol is mediated through the surfactant (SDHS). At high concentrations of SDHS, the area (A_s) increases significantly, which increases the number of sites for the dodecanol to segregate but due to the limited amount of dodecanol (constant 0.09 M added), the surface excess concentration decreases. In the next section we will evaluate the segregation of dodecanol in more detail by interpreting the segregation as an adsorption phenomenon

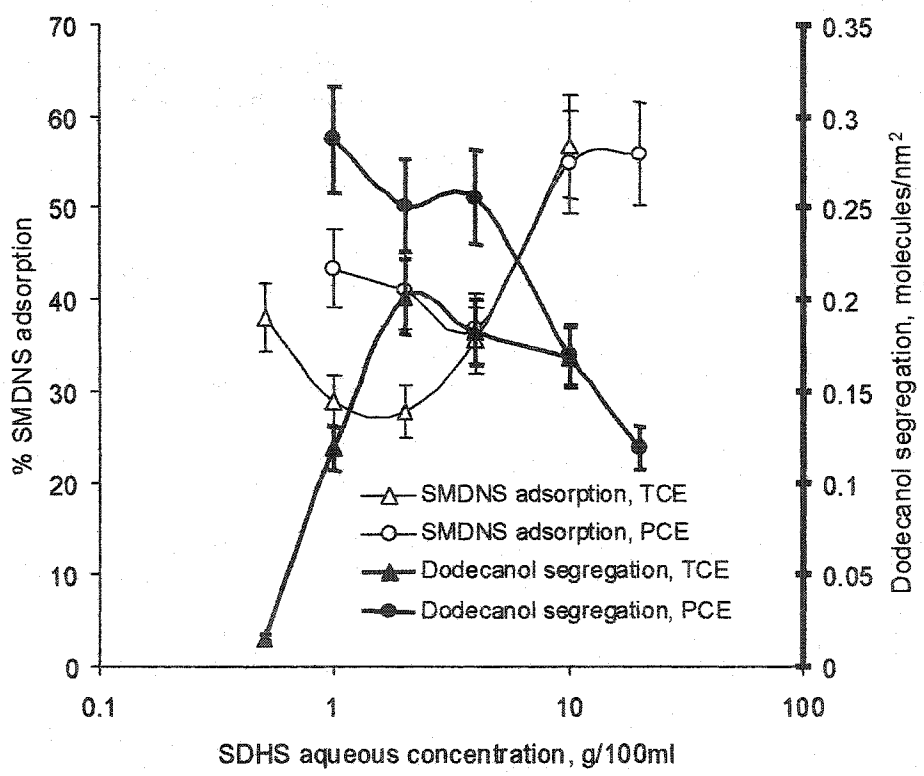

Figure 6.8. Percentage of SMDNS adsorption and dodecanol segregation expressed as thickness of dodecanol-rich palisade layer for the SDHS-linker optimum formulation (dotted line) systems presented in Figures 6.5a (TCE) and 6.5b (PCE).

A final observation regarding linker microemulsions formulated at different SDHS concentration regards the solubilization efficiency. The solubilization efficiency is presented in Figure 6.9 using the characteristic length concept ξ^* (equation 1). The characteristic length of the linker microemulsion systems is very close to that of the SDHS alone system and has a very weak dependence on SDHS concentration. Previous research evaluated the characteristic length for different linker combinations (28) and found that equimolar mixtures of hydrophilic linker (SMDNS) and lipophilic linker (dodecanol) yielded systems with similar characteristic length to the surfactant alone. In the next section we will investigate the role of each linker in the magnitude of the self-assembly.

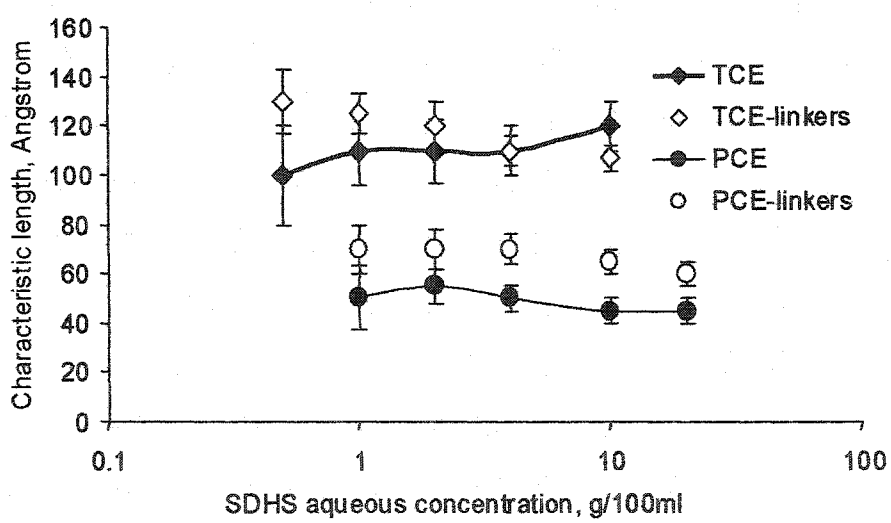

Figure 6.9. Characteristic length of SDHS optimum middle phase microemulsions for TCE and PCE with and without linkers (0.09 M SMDNS and 0.09 M dodecanol).

Linker self-assembly as a function of linker concentration

In the previous sections we have studied the self-assembly of surfactant-alone microemulsion systems and systems containing a fixed amount of hydrophilic linker

(SMDNS, 0.09 M) and lipophilic linker (dodecanol, 0.09 M). In this section we will concentrate on systems of constant surfactant concentration (SDHS, 0.103 M) and different concentrations of hydrophilic and lipophilic linkers. In previous studies we have evaluated some of the combinations presented in this work (7,8,28) but without using the concept of segregation length for the lipophilic linker. As explained above, herein we assume that the self-assembly of these linkers can be modeled as an adsorption process.

Table 6.2 presents a list of formulations for different linker concentrations used in this section.

Figure 6.10 presents the segregation length of dodecanol (calculated using equation 7) for TCE (Figure 6.10a) and PCE (Figure 6.10b) as a function of the equilibrium bulk dodecanol concentration (concentration in the excess oil phase) at different initial aqueous concentrations of SMDNS. For the case of TCE and no SMDNS, the segregation behavior approaches a Langmuir-type adsorption with a saturation value close to 0.13 molecules/nm^2. When SMDNS is added, the concentration of dodecanol to reach saturation increases from close to 0.05 M with no added SMDNS to 0.1M of dodecanol with 0.09M of SMDNS added and close to 0.15 M - 0.20 M dodecanol with 0.18 M dodecanol added. This increase in adsorption (which is higher than dodecanol saturation levels) is due to the additional adsorption or segregation sites provided by the adsorption of the SMDNS at the interface. It is important to note that the saturation level of segregation itself is not modified by the presence of the hydrophilic linker, thus the saturation level (~0.13 molecules/nm^2 for TCE) should be more a function of the oil-linker type of interaction.

Table 6.2. Interfacial concentrations of surfactant and linkers for selected systems in Figures 6.10 through 6.13

System	Vm* ml	[SDHS] middle phase	[SMDNS] middle phase	[oleyl] middle phase	[oleyl] excess phase
TCE 0.045 C12OH 0.000 SMDNS	3.3±0.2	0.16±0.02		0.054±0.004	0.041±0.003
TCE 0.090 C12OH 0.000 SMDNS	3.5±0.2	0.15±0.02		0.100±0.008	0.085±0.007
TCE 0.180 C12OH 0.000 SMDNS	3.6±0.2	0.14±0.02		0.193±0.01	0.173±0.01
TCE 0.045 C12OH 0.045 SMDNS	3.0±0.2	0.17±0.02	0.044±0.005	0.052±0.004	0.042±0.004
TCE 0.090 C12OH 0.090 SMDNS	3.5±0.2	0.15±0.02	0.077±0.008	0.115±0.01	0.077±0.007
TCE 0.180 C12OH 0.180 SMDNS	4.3±0.3	0.12±0.01	0.126±0.01	0.229±0.02	0.143±0.02
PCE 0.045 C12OH 0.000 SMDNS	1.4±0.1	0.37±0.03		0.080±0.002	0.039±0.003
PCE 0.090 C12OH 0.000 SMDNS	1.8±0.2	0.29±0.03		0.131±0.01	0.081±0.007
PCE 0.180 C12OH 0.000 SMDNS	2.5±0.2	0.21±0.03		0.226±0.02	0.165±0.02
PCE 0.045 C12OH 0.045 SMDNS	1.7±0.2	0.30±0.03	0.065±0.007	0.081±0.007	0.038±0.004
PCE 0.090 C12OH 0.090 SMDNS	2.6±0.2	0.20±0.02	0.087±0.006	0.172±0.01	0.061±0.005
PCE 0.180 C12OH 0.180 SMDNS	4.2±0.3	0.12±0.01	0.107±0.01	0.279±0.02	0.107±0.01

The results in Figure 6.10b give a little more insight into the role of the linker-oil interaction. Specifically, Figure 6.10b shows the segregation of dodecanol in PCE-SDHS microemulsions. The first observation from Figure 6.10b is that the adsorption does not approach saturation in any of the formulations. Nonetheless, it seems that for the no added SMDNS case the adsorption curve starts leveling off at a value of 1 molecule/nm^2. The plateau value of the dodecanol segregation in the PCE case is significantly higher than the TCE case. We suspect that this is due to the polar nature of TCE (see Table 6.1) and because of its polarity TCE might compete with dodecanol for segregation sites near the surfactant tails (which we refer to as the palisade layer)

In addition to the segregation of dodecanol, it is necessary to analyze the adsorption of SMDNS for the same systems considered in Figure 6.10. Figure 6.11 shows the percentage of SMDNS adsorption (calculated using equation 6) as a function of the equilibrium dodecanol concentration in the excess oil phase (noted as bulk [C12OH], as in Figure 6.10). Figure 6.11a shows these results for the case of TCE microemulsions. For the case of 0.09 M added SMDNS, the adsorption of SMDNS increases over its adsorption in the absence of dodecanol (bulk [C12OH]=0) as the concentration of dodecanol increases. The same kind of trend was observed for the addition of 0.18 M of SMDNS, and in both cases the maximum adsorption appears to occur at [C12OH]/[SMDNS] of between 0.5 and 1.0. In the case of the PCE we observe the same trend for the case of 0.09M of SMDNS.

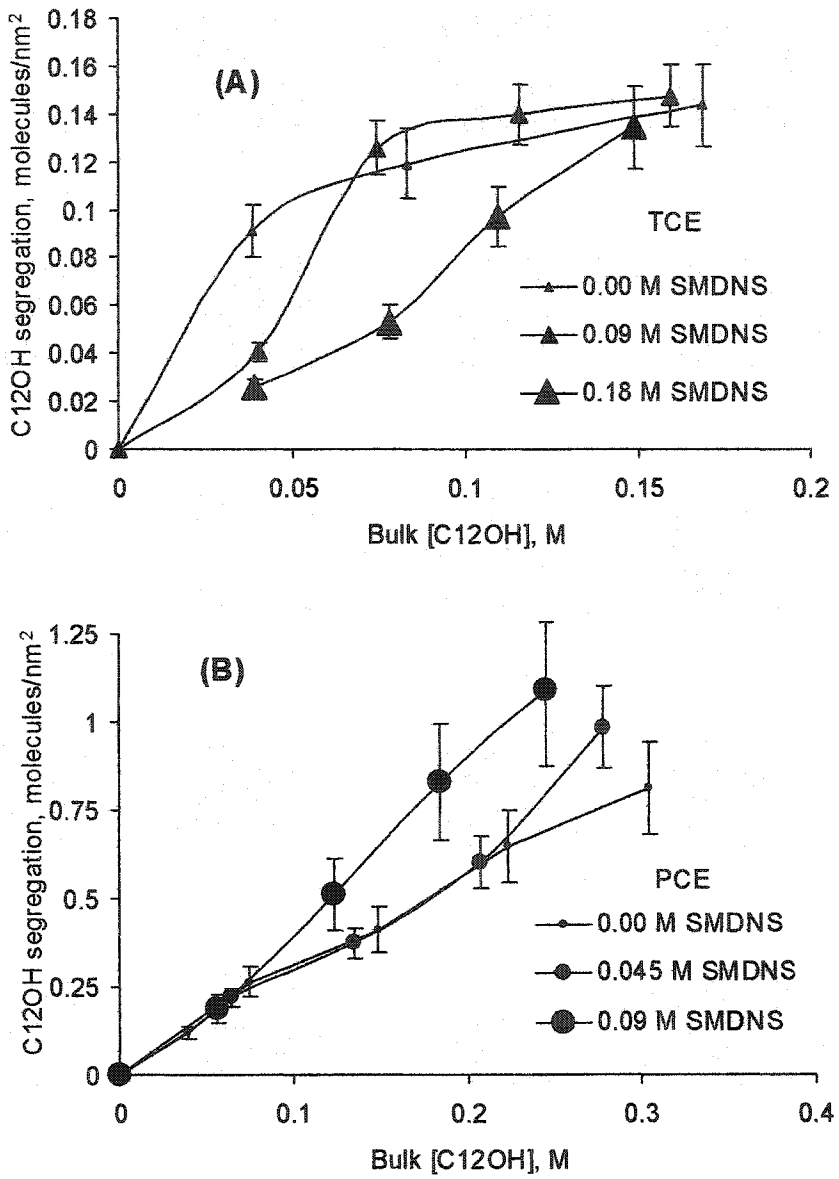

Figure 6.10. Dodecanol segregation expressed as molecules segregates per nm^2 of interfacial area as a function of the concentration of dodecanol in the bulk excess oil phase for TCE (part A) and PCE (part B) at different initial concentration of SMDNS and 0.103 M (4 g/100ml) of SDHS.

In previous papers we have reported that the addition of lipophilic linkers in combination with the hydrophilic linkers increases the participation of SMDNS at the interface (9), which is consistent with the results in Figure 6.11 when the concentration of

dodecanol is less than or approaching the equimolar ratio to SMDNS. This also might help explain an earlier observation that the optimum solubilization enhancement occurs near equimolar addition of linker molecules (7). It is interesting to note that when dodecanol is added in higher proportion than the SMDNS, the synergism between dodecanol and SMDNS seems to be diminished. While we can't fully explain this phenomenon now, two possible explanations are as follow: (1) excess dodecanol (in relation to SMDNS) could increase the rigidity of the surfactant membrane (28) hindering the SMDNS adsorption at the interface; and (2) excess dodecanol (in relation to SMDNS) promote the lipophilic linker behavior (i.e. the SDHS-dodecanol interaction) over the self-assembly between the SMDNS and dodecanol. Future research should further explore this phenomenon.

One final detail that needs to be addressed in this section concerns the characteristic length (ξ, equation 1) of the different formulations. In previous papers we noted that adding lipophilic linker alone for the case of TCE, produced a "saturation" effect on solubilization enhancement at high dodecanol concentration (8). Comparing this observation with the type of behavior of the segregation curve for TCE (a Langmuir type adsorption, Figure 6.10a) suggests that the increased solubilization capacity achieved with lipophilic linkers might be proportional to the amount of linker segregated near the surfactant tails, which is expressed as the surface excess concentration (equation 7).

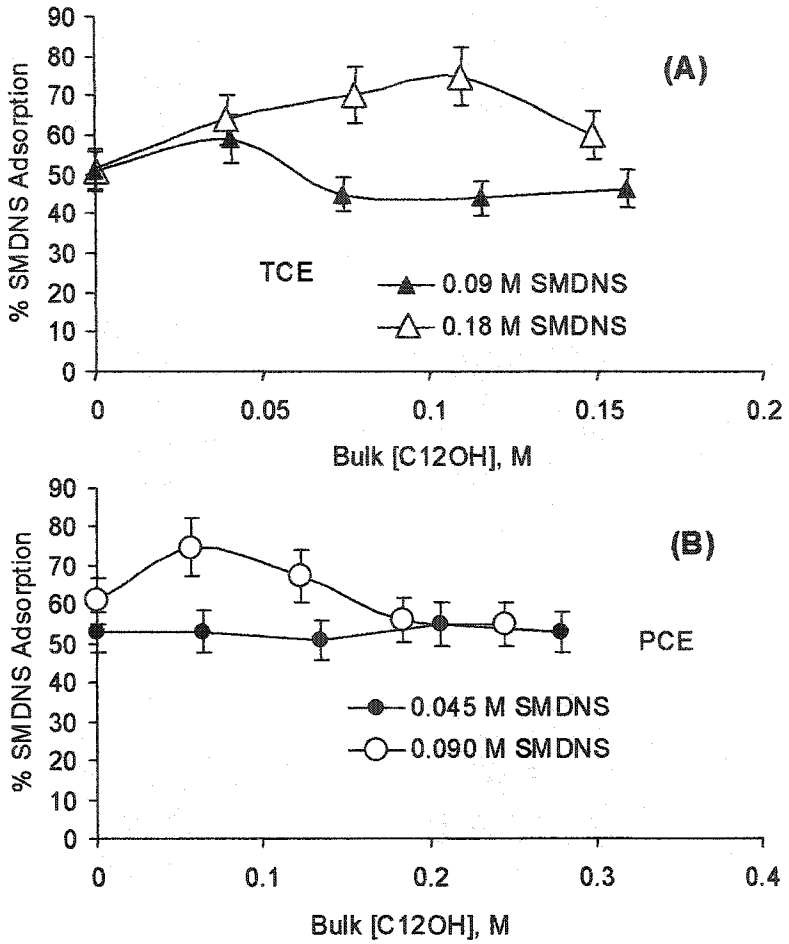

Figure 6.11. SMDNS percentage middle phase adsorption as a function of the concentration of dodecanol in the bulk excess oil phase for TCE (part A) and PCE (part B) at different initial concentration of SMDNS and 0.103 M (4 g/100ml) of SDHS.

In Figure 6.12 we have combined the increase in characteristic length of the system ($\Delta\xi=\xi-\xi_0$) relative to the solubilization capacity of the system without dodecanol (ξ_0) of the different systems considered above (TCE - triangles and PCE - circles) as a function of the dodecanol segregation expressed as surface excess concentration. The combined data in Figure 6.12 show a linear relationship between the increase

solubilization and the magnitude of dodecanol segregation, corroborating our suspicion based on the described earlier solubilization enhancement studies.

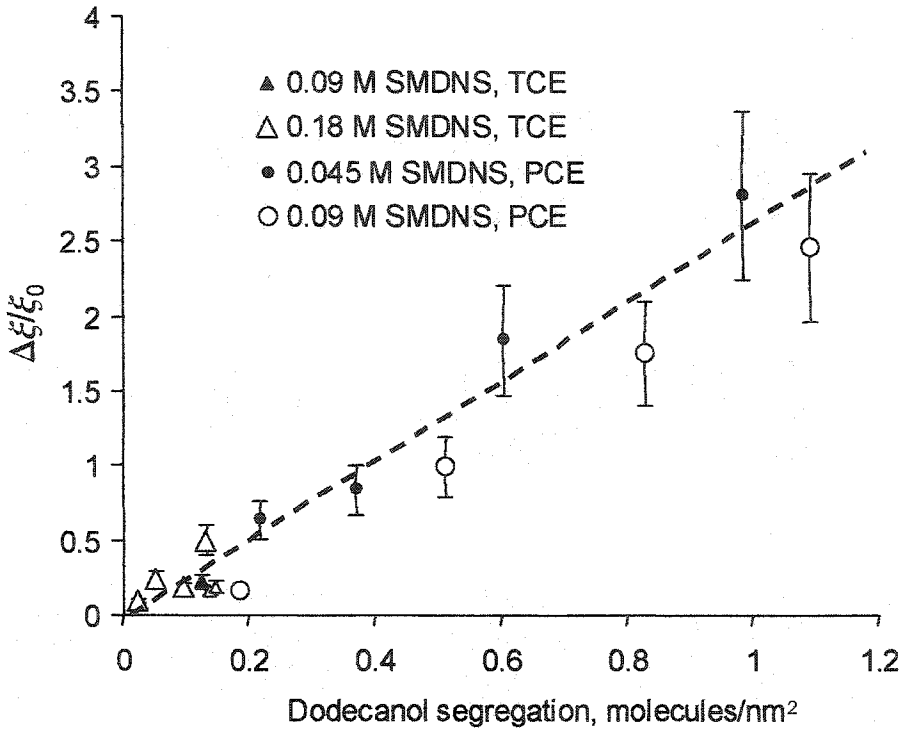

Figure 6.12. Relative increase in characteristic length of microemulsion systems (ξ) with the segregation of dodecanol for TCE (triangles) and PCE (circles).

Linker self-assembly as a function of electrolyte concentration

All the self-assembly studies with linker molecules reported thus far have been based on optimum middle phase microemulsion. One research question that needs to be addressed is the validity of these results at conditions deviating from optimum conditions. The results in Figure 6.12 suggest that the major contribution to the solubilization efficiency, measured by the characteristic length, is provided by the segregation of dodecanol. We thus proceeded to determine this segregation at electrolyte concentrations lower than the optimum salinity ($S/S^*<1$). Figure 6.13 presents these results for TCE

(triangles) and PCE (circles) microemulsions formulated with 0.103 M SDHS and 0.09 M of dodecanol and SMDNS, respectively. For both oils the segregation is independent of the electrolyte concentration. All the points at S/S*<1 correspond to Type I microemulsions. The independence of the segregation phenomenon from the electrolyte concentration supports an earlier interpretation of the segregation curves in Figure 6.10 where it was proposed that the segregation was mainly a product of the oil-lipophilic linker interaction. In this case the increase in electrolyte concentration only affects the interactions on the aqueous side of the interface.

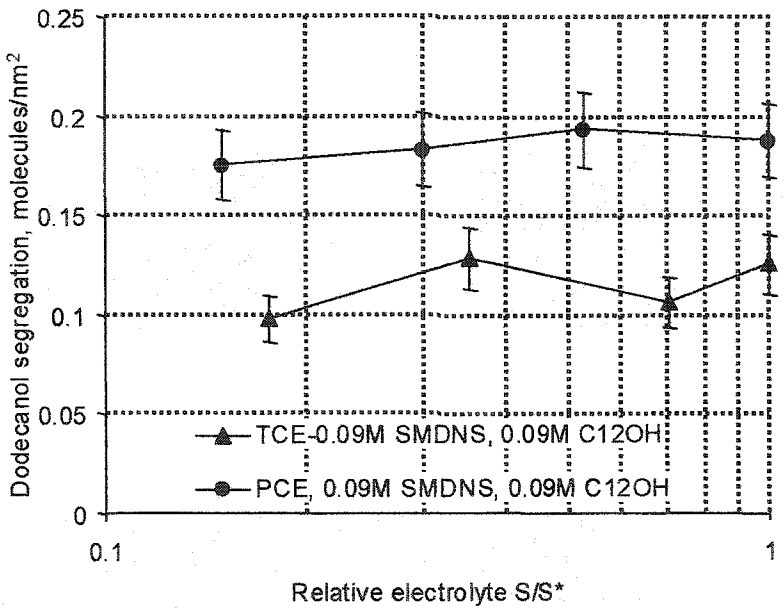

Figure 6.13. Dodecanol segregation for TCE (triangles) and PCE (circles) with 0.104M SDHS and 0.09M of each SMDNS and dodecanol as a function of relative electrolyte concentration.

Linker self-assembly at constant surfactant - linkers molar ratio.

In the previous sections we have investigated the effect of the surfactant and each linker concentration on the self-assembly properties of the combined linker systems. While this information helps to picture a molecular arrangement at the interface similar to

that depicted in Figure 6.1, there is something more important from the practical point of view concerning the response of the self-assembly of these linkers at constant linker to surfactant ratio upon dilution. In particular when a linker system is formulated for application purposes, chances are the formulation is likely to be diluted, wherein the relative ratio of linker and surfactants is maintained but the total concentration changes.

Figure 6.14 shows the phase map for a mixture of 10 molar parts of SDHS to 9 molar parts of hydrophilic linker SMDNS to 9 molar parts of lipophilic linker dodecanol (C12OH) with TCE. For ease of comparison Figure 6.14 also shows the surfactant-alone phase map presented in Figure 6.2. For TCE we observe that the addition of combined linker reduces by roughly half the concentration of SDHS necessary to achieve a Type IV single phase microemulsion and also reduced the lower boundary of the phase map (critical microemulsion concentration CμC) by the same magnitude. At medium to low concentrations of SDHS the optimum electrolyte concentration is also increased by the addition of linkers (can be reproduced by using equation 5). The addition of a constant ratio of linkers also widens the middle phase Type III region but it does not alter the phase maps as in the case of Figure 6.5. The same trends were observed for the case of the PCE system.

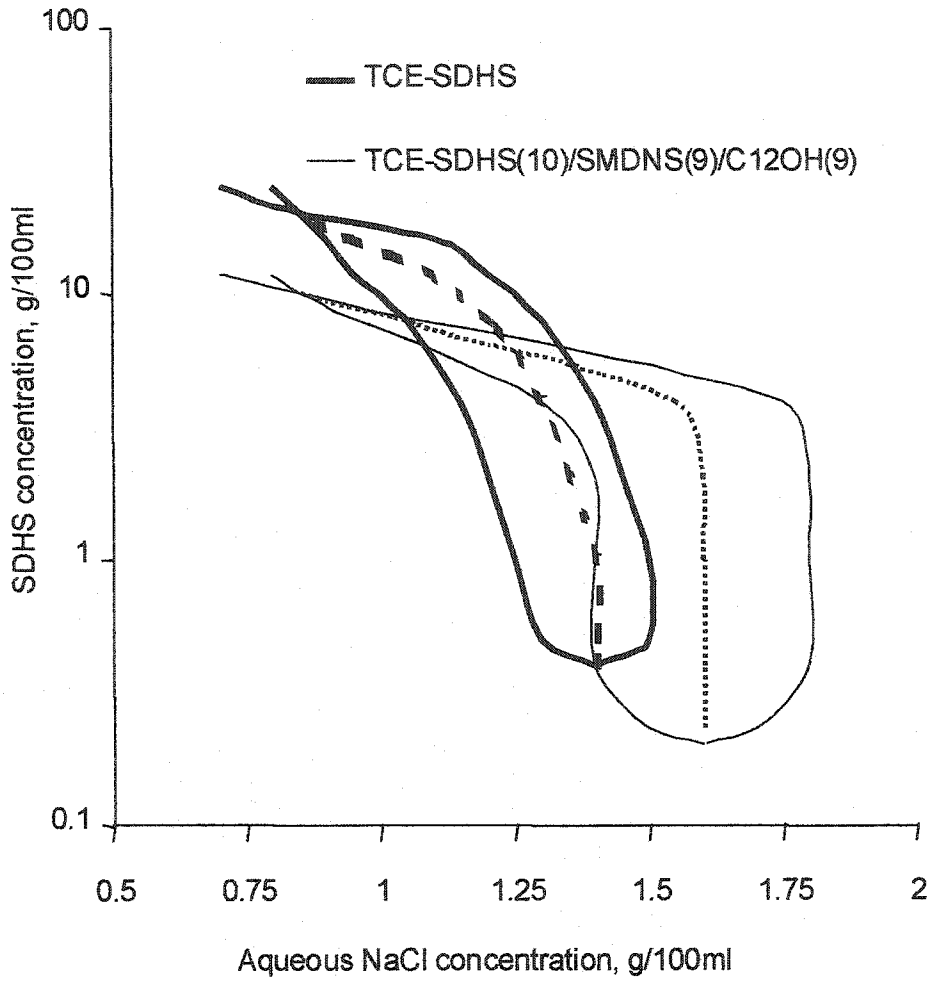

Figure 6.14. "Fish" phase diagrams for SDHS-alone TCE microemulsion (thick lines), and a mixture of constant ratio of 10 molar parts of SDHS to 9 SMDNS to 9 dodecanol (C12OH) (thin lines).

It is important to highlight that when adding incremental amounts of medium chain alcohols to microemulsion systems, the amount of the surfactant required to achieve a single phase microemulsion (Type IV) tends to increase, while in the case of the combined linkers, this amount tends to decrease (10). The difference between the role of the combined linkers and medium chain alcohols could be explained by the data-supported hypothesis that combined linker behave more like a surfactant itself (7,8,9),

helping to increase the thickness of the interface that in turns represent a higher characteristic length of the microemulsion. In the case of medium chain alcohols, these are mostly used to reduce the rigidity of the surfactant membrane thus making the interface more dilute and reducing the interfacial thickness, they can also behave as cosolvents that increase the partition of the surfactant in the excess oil and water phases which reduces the surface activity of the surfactant itself (10).

In the case of SDHS-alone systems and constant linker concentration systems, we supplemented the phase maps studies with interfacial tension studies to localize the CμC. We performed the same type of studies in this case, and in Figure 6.15 we present the interfacial tension between the excess oil and water as a function of initial aqueous SDHS concentration. Figure 6.15 shows the IFT curves for the SDHS-alone microemulsion systems for TCE (close diamonds) and for the SDHS-linker constant ratio (open dots). For the case of TCE it is observed that the IFT curves is shifted to approximately half the concentration of SDHS, which means that the surfactant becomes more surface active when it is mixed with the linker molecules. These data suggest that upon dilution the mixed linker system remains self-assembled at the interface until the surfactant concentration is lower than its CμC.

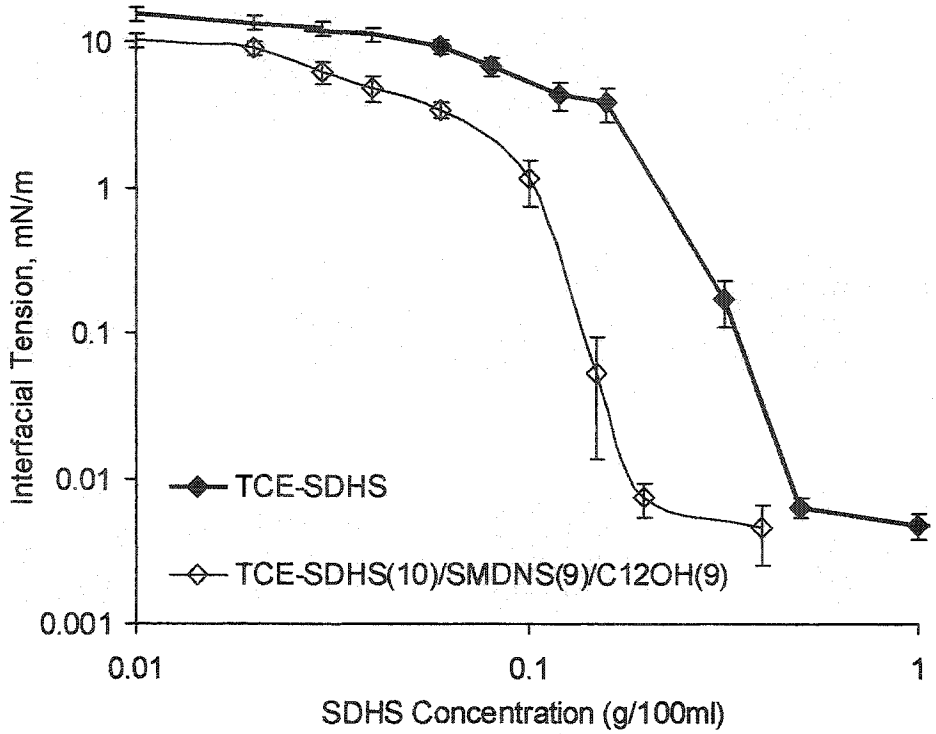

Figure 15. Interfacial tension SDHS microemulsions of TCE without linkers (solid dots) and with linkers at constant molar ratio SDHS(10)/SMDNS(9)/C12OH(9) (open dots) as a function of SDHS concentration.

Summary

In this work we investigated the self-assembly properties of the hydrophilic linker SMDNS and the lipophilic linker dodecanol when combined with SDHS to make microemulsions of TCE, and PCE. We first identified the critical microemulsion concentration (CμC) of the SDHS-alone microemulsions and found that at the CμC, the first non-wetting middle phase microemulsion is formed which corresponds to the point where the IFT reaches an ultralow value. When mixing SDHS at different concentrations with constant amounts of SMDNS (0.09M) and dodecanol (0.09M) it was found that no middle phase microemulsion was observed until SDHS reached the CμC level of the

surfactant-only formulation which confirmed our hypothesis that some level of surfactant was necessary to produce the self-assembly in microemulsion systems. Nonetheless, for linker-based systems no obvious CμC was obtained based on IFT curves, suggesting that the hydrophilic and lipophilic linkers could, in the absence of the surfactant, segregate near the surface of droplets in emulsion systems. We also learned that the segregation of the lipophilic linker occurs in a Langmuir-type fashion and that at dodecanol/SMDNS molar ratios less than unity, the dodecanol seems to preferentially segregate near the SMDNS hydrophobe. Finally we also observed that the addition of combined linker not only promotes a synergism between the linkers but also improves the surface activity of the surfactant.

It is necessary to clarify that while the data presented in this work supports the hypothesis of linker self-assembly as depicted in Figure 6.1, it does not represent final proof of this hypothesis. In future studies we will present scattering and spectroscopic techniques that will study this self-assembly.

Aknowledgements

This research was financed through the Institute for Applied Surfactant Research of the University of Oklahoma. The authors would like to thank Dr. Allan Mackie for helpful discussions on the second CMC concept.

Literature

[1] Tanford, C. "The Hydrophobic Effect: Formation of Micelles and Biological Membranes", 2nd ed., Wiley, New York, 1980.

[2] Israelachvili J. N." Intermolecular and Surface Forces". 2nd ed., Academic Press, New York, 1992

[3] Graciaa A.; Lachaise J.; Cucuphat C., Bourrel M. and Salager J.L. Improving solubilization in microemulsions with additives 1. The lipophilic linker role. *Langmuir.* **1993,** 9, 669.

[4] Graciaa A.; Lachaise J.; Cucuphat C., Bourrel M. and Salager J.L. Interfacial segregation of an ethyl oleate/hexadecane oil mixture in microemulsion systems. *Langmuir.* **1993,** 9, 1473.

[5] Graciaa A.; Lachaise J.; Cucuphat C., Bourrel M. and Salager J.L. Improving solubilization in microemulsions with additives 2. Long chain alcohols as lipophilic linkers. *Langmuir.* **1993,** 9, 3371.

[6] Salager, J. L.; Graciaa, A. and Lachaise J. Improving solubilization in microemulsions with additives. Part III: lipophilic linker optimization. *J. Surfactant Detergents.* **1998,** 1, 403.

[7] Acosta, E.; Uchiyama, H; Tran, S.; Sabatini, D. A. and Harwell, J. H. Formulating Chlorinated Hydrocarbon Microemulsions Using Linker Molecules. *Environ. Sci. Technol.* **2002,** 36, 4618.

[8] Uchiyama, H; Acosta, E.; Sabatini, D.A. and Harwell, J.H. Supersolubilization in Chlorinated Hydrocarbon Microemulsions: Solubilization Enhancement by Lipophilic and Hydrophilic Linkers. *Ind. Eng. Chem. Res.* **2000,** 39, 2704.

[9] Acosta, E.; Uchiyama, Hirotaka; Sabatini, David A.; Harwell, Jeffrey H. The role of hydrophilic linkers. *J. Surfactants Detergents.* **2002,** 5, 151.

[10] Zana, R. Aqueous surfactant-alcohol systems: a review. *Adv. Colloid Interface. Sci.* **1995**, 57, 1

[11] Bourrel, M. and Schecter R. "Microemulsions and related systems". Marcell Dekker Inc. New York, 1988

[12] Hendrikx, Y.; Charvolin, J.; Rawiso, M. Segregation of two amphiphilic molecules within nonspherical micelles: a neutron scattering study. *J. Colloid and Interface Sci.* **1984**, 100(2), 597-600.

[13] Kahlweit, M. ; Strey, R. and Busse, G. Effect of alcohols on the phase behavior of microemulsions. *J Phys. Chem.* **1991,** 95, 5344 .

[14] Auvray, L. in "Micelles, Membranes, Microemulsions and Monolayers". Gelbart, W. M., Ben-Shaul, A. and Roux, D. Eds. p 347. Springer-Verlag, New York, 1994.

[15] Acosta, E.; Szekeres, E.; Sabatini, D. A.; Harwell, J. H. Net-Average Curvature Model for Solubilization and Supersolubilization in Surfactant Microemulsions. *Langmuir* **2003,** 19, 186.

[16] Nagarajan, R.; Ruckenstein, E. Molecular theory of microemulsions. *Langmuir* **2000**, 16(16), 6400.

[17] Bourrel, M. and Schecter R. *Microemulsions and related systems*. Marcell Dekker Inc. New York, 1988

[18] Salager, J. L.; Bourrel, M.; Schechter, R. S.; Wade, W. H. Mixing Rules for Optimum Phase Behavior Formulations of Surfactants/Water/Oil Systems. *Soc. Pet. Eng. J.* **1979,** 19, 271

[19] Kahlweit, M.; Strey, R.; Firman, P. Search for tricritical points in ternary systems: water-oil-nonionic amphiphile. *J. Phys. Chem.* **1986,** 90, 671.

[20] Rosen, M.J. *Surfactants and interfacial phenomena*. 2nd. Ed. John Wiley & Sons, New York, 1989, pp 431

[21] Aveyard, R.; Binks, B. P.; Fletcher, P. D. I. Interfacial tensions and aggregate structure in pentaethylene glycol monododecyl ether/oil/water microemulsion systems. *Langmuir* **1989,** 5,1210.

[22] Kodama, M.; Miura, M. Second CMC [critical micelle concentration] of the aqueous solution of sodium dodecyl sulfate. II. Viscosity and density *Bulletin of the Chemical Society of Japan.* **1972,** 45, 2265.

[23] Al-Anber, Z. ; Bonet-A., J.; Floriano, M.; Mackie, A. phere-to-rod transitions of micelles in model nonionic surfactant solutions. *J. Chem. Phys.* **2003,** 118, 3816.

[24] Guo, R.; Ding, Y.; Liu, T. J. Diffusion coefficients and structure properties of Triton X-100/n-C6H13OH/H2O system. *Dispers. Sci. Technol.* **2000,** 21, 935.

[25] Graciaa, A.; Lachaise, J.; Sayous, J. G.; Grenier, P.; Yiv, S.; Schechter, R. S.; Wade, W. H. The partitioning of complex surfactant mixtures between oil/water/microemulsion phases at high surfactant concentrations. *J. Colloid and Interface Sci.* **1983,** 93, 474.

[26] Ryan, L. D. and Kaler E. W. Alkyl polyglucoside microemulsion phase behavior. *Colloids Surf. A.* **2001,** 176, 69.

[27] Kurlat, D. H.; Ginzberg, B.; Condori, B. Interfacial tension in microemulsions along a path in the middle phase region up to the tricritical point. *Phys. Chem. Liq.* **1990,** 21, 195.

[28] Acosta, E. J.; Le, M. A.; Harwell, J. H.; Sabatini, D. A. Coalescence and Solubilization Kinetics in Linker-Modified Microemulsions and Related Systems. *Langmuir* **2003,** 19, 566.

CHAPTER 7

Linker-based Non-toxic Microemulsions

Abstract:

Lecithin-based microemulsions have been of great interest over the past decade because of their potential application in drug delivery systems and in cosmetic and food additive formulations. While the literature presents examples of lecithin-based microemulsion for drug delivery systems, most of these formulations contain alcohols and/or polyglycols to prevent liquid crystalline phases. Alcohol addition increases the toxicity of the formulation, and polyglycols increases the viscosity of the formulation, thereby making the delivery system less desirable. In this work we use linker-based formulations to mitigate the toxicity concerns and achieve substantial solubilization capacity. We studied lecithin-based microemulsions using sorbitol monooleate as the lipophilic linker and hexyl polyglucoside as the hydrophilic linker. The phase behavior of linker-based lecithin microemulsion with isopropyl myristate (IPM) was studied as a function of hexyl polyglucoside to lecithin ratio and at different temperature, electrolyte and pH conditions. From these studies it was found that the zwiterionic characteristic of lecithin rules its response to these different formulation conditions. Compared to other lecihtin IPM microemulsions, the linker-based lecithin system required the least amount of lecithin to achieve a single-phase microemulsion. By studying the ratio of the lipophilic linker Span 80 to lecithin, it was found that a certain portion of the lectihin could be replaced by a

combination of Span 80 and hexyl polyglucoside. These linker-based formulations were able to produce microemulsions for a wide variety of oils, from polar oils like chlorinated hydrocarbons to hydrophobic oils such as hexane, hexadecane and squalene. These formulations were obtained using a constant electrolyte concentration (isotonic solutions containing 0.9% NaCl), at room temperature, at constant lecithin and sorbitol monoleate (Span 80) concentration, and by varying the concentration of the hydrophilic linker hexyl glucoside. In addition to formulating with low electrolyte concentration, the solubilization capacity of these lecithin systems was higher than linker-based microemulsions formulated with alkyl sulfosuccinate anionic surfactants.

Keywords: lecithin, linkers, polar, non-polar, oils, microemulsions, toxicity, solubilization.

Introduction

By enhancing the solubilization of otherwise immiscible water and oily components, microemulsions have been utilized in a wide range of fields (1). In tertiary oil recovery research the ultralow oil-water interfacial tension produced by these systems decreases the capillary forces which trap residual crude oil in reservoirs (2). More recently microemulsions are being used in surfactant enhanced remediation of oil-impacted aquifers, production of nanoparticles, drug delivery, and cosmetic formulations (1,3,4,5,6). Biodegradable and non-toxic surfactant formulations are necessary for applications such as drug delivery and food additives, cosmetic formulations, personal care and cleaning products and in some surfactant enhanced remediation applications.

Surfactant toxicity varies with surfactant type and molecular structure. In general, cationic surfactants are highly toxic and are normally used as antiseptics or preservatives (7,8,9). While anionic surfactants are generally milder than cationic surfactants, their tendency to disrupt cell membranes causes them to irritate the skin. Nonetheless, their relative toxicity depends on the molecular structure of the surfactant itself (10,11,12,13). In contrast, nonionic surfactants are generally slightly toxic or non-toxic, although their toxicity also depends on the molecular structure. For example, nonionic surfactants of medium molecular weight and containing aromatic groups or branched hydrophobes generally demonstrate some level of toxicity (11,14,15). "Sugar-derived" surfactants, such as the sorbitol esters, are amongst the most biocompatible surfactants. For example, even at dosage levels as high as 20 g/Kg sorbitol monoleate showed no adverse effect on rats (16). More hydrophilic versions of sorbitol monoleate, with either ethoxylated groups or shorter hydrophobes, demonstrate some level of toxicity or tendency to produce skin irritation (16). Depending on the molecular structure and pH of the system, zwitterionic surfactants, surfactants having both positive and negative charges in the molecule, can be relatively biocompatible, showing low or no skin irritation effects and low toxicity (17,18).

Phospholipids are naturally-produced surfactant molecules that self-assemble in vesicles to form cell walls. In terms of consumer product formulation lecithin or phosphatidyl cholines are the most relevant phospholipids as they can be easily extracted from egg yolks, soy beans and other natural sources (19,20).

Non-toxic microemulsions

Formulation of non-toxic microemulsion has been studied for over a decade, as summarized in recent review articles (21,22,23,24,25). For pharmaceutical applications, Malmsten concludes that anionic microemulsion systems are typically undesirable because of their inherent toxicity, and because medium chain alcohols are frequently used as cosurfactants and these alcohols also have adverse toxicity (21). Malmsten also points out that nonionic surfactant formulations, especially those including sorbitol or glucoside-derived surfactants, have a better toxicity profile than anionic surfactant formulations. Finally, Malmsten states that lecithin-based formulations are especially desirable because they tend to mimic the phospholipid nature of cell walls, thus proving to be more biocompatible. At the same time, since medium chain alcohols are often needed to produce lecithin-based microemulsions, the toxicity concerns associated with these alcohols again limits this approach (21).

Lecithin-based formulations in the literature include a triglyceride microemulsion with butanol for transdermal delivery of ketoprofen (26). Hexadecane microemulsions were formulated by mixing the lecithin with a series of small and medium chain alcohols, which produced large solubilization enhancement and ultrlow interfacial tensions (~10^{-4} mN/m) (27). Isopropyl myristate microemulsions have been formulated with lecithin and medium chain alcohols for drug delivery purposes (28,29,30,31,32).

The goal of this research is to formulate lecithin-based microemulsions for a wide range of oils whitout the use of medium chain alcohols, thus producing non-toxic microemulsion systems that could be used in a range of applications (e.g. drug and food

additives delivery, cosmetics, cleaners and environmental remediation formulations). The hypothesis for this study is that we can formulate alcohol-free microemulsion systems using lecithin as the main surfactant by using biocompatible linkers molecules, thus reducing the overall toxicity of this formulation.

Linker-based microemulsions.

Linker-based microemulsions use a lipophilic and/or a hydrophilic linker additive to modify the interfacial properties of the microemulsion system to achieve larger and/or faster solubilization (33,34,35,36,37,38). Graciaa et al. (33,34,35) first introduced lipophilic linkers as polar oil molecules (e.g. long chain alcohols, fatty acids, amines, low HLB ethoxylated alcohols) that segregate near the surfactant tails, thereby serving to "extend" the surfactant tail into the oil and increasing the solubilization capacity of these systems. Later, Uchiyama et al. (36) found that the solubilization enhancement was limited above certain concentrations of the lipophilic linker. Uchiyama introduced the concept of hydrophilic linker as surfactant-like molecules that would adsorb at the oil/water interface, but due to their short tail would offer little interaction with the oil phase (36). Combinations of hydrophilic and lipophilic linkers can produce a surfactant-like self-assembled system that offers solubilization enhancements proportional to the combined linker concentration, and then can up to a certain point replace the main surfactant (36,38,39). Using this approach we have been able to formulate microemulsions for a wide range of oils, and a variety of surfactants with applications ranging from environmental remediation to detergent formulations (40,41).

The linkers studied in this research were selected in this study based on their biocompatibility: sorbitan monoleate was used as the lipophilic linker (41) and alkyl polyglucoside was used as the hydrophilic linker. Figure 7.1 shows a schematic of a linker-based microemulsion using these non-toxic surfactants and linkers. In Figure 7.1 lecithin is represented by phosphatidyl choline dialkyl, hexyl polyglucoside is represented by hexyl glucoside and used as the hydrophilic linker (42) and sorbitol monoleate is used as the lipophilic linker. In Figure 7.1 we have depicted sorbitol monoleate as residing closer to the water interface than other lipophilic linker molecules (34,36) because this molecule is slightly more polar than other long chain alcohols commonly used as lipophilic linkers, and because sorbitol monoleate has shown behavior intermediate between a lipophilic linker and a cosurfactant (41).

Selected properties of lecithin, sorbitol monoleate and hexyl polyglucoside are summarized in Table 7.1. Since it is a mixture, the molecular weight reported for lecithin is an average (43). For this same reason, lecithin's critical micelle concentration is given as an order of magnitude value (43,44). Lecithin area per molecule is pH and concentration dependent, and the area per molecule value in Table 7.1 corresponds to a neutral pH in diluted aqueous solutions (i.e. lecithin less than 75%) (45). In the case of hexyl polyglucoside, the molecular weight is an average value because the product (AG™ 6206) is a mixture of isomers with one and two glucoside groups (46). The hexyl polyglucoside CMC and area per molecule values were determined in this study using methods discussed below. Sorbitan monoleate data was readily available in the literature (47).

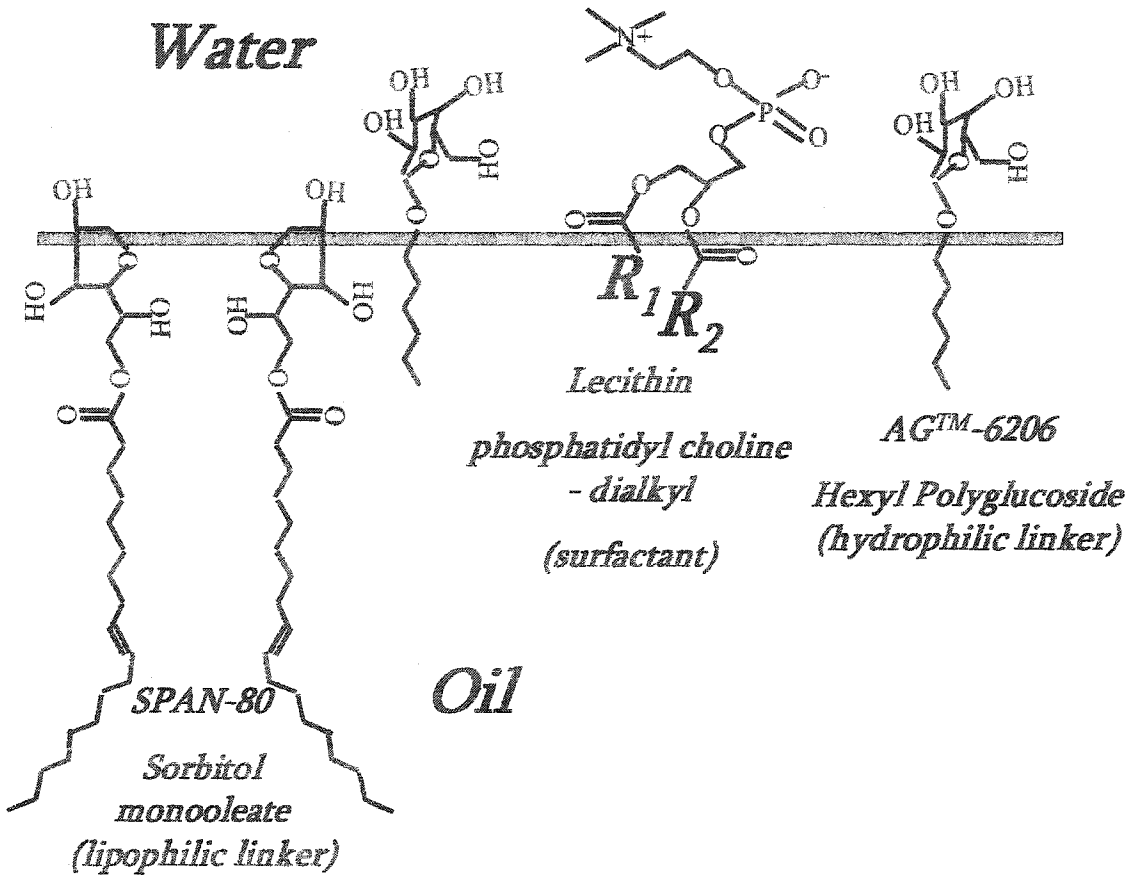

Figure 7.1. Schematic of the linker effect using non-toxic surfactant lecithin, exemplified by phosphatiyl choline dialkyl (R1 an R2 are alkyl groups ranging from C14 to C18, see reference 29). Hexyl polyglucoside (exemplified by hexyl glucoside) is shown as hydrophilic linker and sorbitol monoleate as lipophilic linker.

Table 7.1. Selected properties for lecithin (surfactant), sorbitan monoleate (lipophilic linker) and hexyl polyglucoside (hydrophilic linker).

Surface active molecule	Molecular weight, g/mol	Critical Micelle concentration, M	Area per molecule $Å^2$/molecule
Lecithin[a]	~ 770	~ 10^{-10}	~ 90
Sorbitol Monoleate[b]	428	$1.8x10^{-5}$	35
Hexyl polyglucoside[c]	~550	$1.8x10^{-2}$ [d]	65[d]

(a) From references 43 and 44
(b) From reference 47
(c) From reference 46
(d) Current work

Table 7.2. Selected properties of the oils used in this study.

Oil	EACN	Molecular weight, g/mol	Molecular Formula
Tetrachloroethylene	2.9[a]	166	$Cl_2C=CCl_2$
Hexane	6[b]	86	C_6H_{14}
Decane	10[b]	142	$C_{10}H_{22}$
Methyl oleate	<13[c]	296	$C_8H_{17}CH=CH\ C_7H_{14}COOCH_3$
Isopropyl Myristate	13[c]	270	$C_{13}H_{27}COOCH(CH_3)_2$
Hexadecane	16[b]	226	$C_{16}H_{34}$
Squalene	24[d]	423	$[(CH_3)_2CH(CH_2)_3(CH_3)CH(CH_2)_3(CH_3)CH(CH_2)_2-]_2$

(a) From reference 36
(b) From references 48,49
(c) From this work
(d) From reference 40

The primary objective of this work is to formulate and characterize microemulsion systems using the biocompatible surfactants and linkers discussed above and oils of relevance to consumer products. We selected isopropyl myristate as the primary oil of interest because lecithin - isopropyl myristate microemulsions have been previously studies for drug and cosmetic delivery applications (28,29,30,31,32). A secondary objective of this work is to study the effect of temperature, electrolyte and pH on the phase behavior of linker-based isopropyl myristate microemulsions. The third objective of this work is to demonstrate the ability of these linker-based biocompatible systems to produce microemulsion systems with a wide range of oils, from polar oils like tetrachloroethylene to more hydrophobic oils like hexadecane and squalene. Table 7.2 summarizes characteristics of the oils studied in this work, including the oil EACN or equivalent alkane number (48,49). The oil EACN, which indicates the hydrophobicity of the oil, has been correlated to the surfactant affinity difference (SAD). The SAD is a semi-empirical equation that indicates the difference between the chemical potential of the surfactant in water and oil phases as follows:

$$\frac{SAD}{RT} = -\ln S + K * ACN + f(A) - \sigma + a_t(T - T_{ref}) \qquad \text{Eq.1}$$

where S is the electrolyte concentration, K is a constant for a given surfactant (ranging from 0.1 to 0.2), and ACN is the alkane carbon number of the oil (for non-hydrocarbon it becomes EACN equivalent-ACN). The parameter f(A) is a function of the alcohol/cosurfactant concentration, σ is a parameter that is a function of surfactant, a_t is a constant (~ 0.01 when temperature is in Celsius), and T_{ref} is a reference temperature.

The SAD equation can be considered a "formulation equation" because it relates the formulation variables into a simple equation. The SAD equation will be used in this work to both interpret and model the non-toxic linker formulations.

In a recent study, we formulated middle phase microemulsion systems for similar oils as studied here using alkyl sulfosuccinated surfactants, oleyl alcohol as lipophilic linker and sodium mono and dimethyl naphthalene sulfonate SMDNS as hydrophilic linker (40); we will compare the performance of these systems with the lecithin-based microemulsion systems studied in the current work.

Experimental procedures.

Materials

The following chemicals were obtained from Aldrich (Milwaukee, WI) at the concentrations shown and were used without further purification: trichloroethylene (TCE, 99%+), tetrachloroethylene (PCE, 99%+), hexane (99%+), decane (99%+), hexadecane (99%+), isopropyl myristate (99%), methyl oleate (60%, technical grade), squalene (99%+), sorbitan monoleate (99%+) and sodium chloride (99%+), sodium dihexyl sulfosuccinate (SDHS, 80% aqueous solution, Fluka brand). Laboratory grade soybean lecithin (99%) was purchased from Fisher Scientific; the composition of soybean lecithin has been reported elsewhere (29,30). Hexyl polyglucoside AG 6206™ was donated by Akzo Nobel (Chicago, IL), the product was received as a 75% wt. aqueous solution, with no alcohols or unreacted materials in the reremaining 25% and was used without further purification.

Methods.

Phase behavior studies were performed using equal volumes of aqueous solution and oil (5 mL of each). Hexyl polyglucoside scans were performed by varying the hexyl polyglucoside concentration at constant temperature (300K unless otherwise stated), electrolyte concentration, lecithin and sorbitol monoleate concentration, and pressure (1 atm). Test tubes were placed in a water bath at 300K (unless otherwise noted), shaken once a day for three days, and left to equilibrate for two weeks. The phase volumes were determined by measuring the heights of each phase in the test tube.

It is important to mention that these microemulsion systems were very sensitive to the ratio of sorbitan monoleate and lecithin added to the system, and the best way to prepare these solutions was to prepare a 20% lecithin solution in water with the prescribed amount of sorbitol monoleate. Another important observation is that Type I and III microemulsion systems also showed signs of algae/bacterial growth after one month of being prepared when left at room temperature (a potential sign for biocompatibility) and thus the characterization of these systems had to be done within two weeks timeframe.

Interfacial tensions were measured using a Model 500 University of Texas spinning drop interfacial tensiometer, injecting 1-5 μl of the equilibrated middle phase in a 300 μl tube filled with the excess denser phase from the 10-ml microemulsion sample tube. The concentration of hexyl polyglucoside was determined using a UV-VIS Hewlett Packard model 8452 diode array spectrophotometer set at a wavelength of 280 nm.

Dynamic light scattering experiments were performed at room temperature using a BI-90 Brookhaven instrument. Samples of the Type I and Type II microemulsion systems were placed in standard 1-cm glass cells that were placed in the BI-90 sample holder at least 30 minutes before the measurement. Each sample was measured three times. The viscosity of the microemulsion phase was measured using a U-tube viscometer and this value was entered to the computer to calculate the average hydrodynamic radius. The viscosity of selected samples were measured at different shear rates using a Brookhaven LV-DVIII rheometer. The refractive index of the continuous phase at 650 nm and 300K (water 1.332 for Type I microemulsions and isopropyl myristate 1.433 for Type II microemulsions, reference 50) was entered into the algorithm used to calculate the particle size. Additional details of the experimental procedures can be found elsewhere (36,37,39,40,42).

Results and discussions

Characterization of hexyl polyglucoside.

The first step of this work was to identify a non-toxic hydrophilic linker. In a previous study we found that each surfactant "family" is likely to have at least one hydrophilic linker molecule, and that the hydrophilic linker typically exists inbetween a common hydrotrope and a surfactant, with 6 to 9 carbons in the tail per hydrophilic ionic head group (42). We selected the alkyl polyglucoside family because of their low toxicity, because they are among the most hydrophilic of the non-toxic surfactant; and because there is a precedent for the success of alkyl polyglucoside formulations in non-

toxic formulations (29,51,52). Initially hexyl and octyl polyglucosides were tested as hydrophilic linkers (42), but we soon realized that alcohol was necessary to form middle phase microemulsions with octyl or longer polyglucosides. Since hydrophilic linkers have been shown to prevent the formation of liquid crystal and metastable phases and to help increase the solubilization and coalescence kinetics (37), the fact that formulations with octyl and longer polyglucoside requires the use of medium chain alcohols suggests that they do not behave as hydrophilic linkers.

We began by studying the behavior of trichloroethylene (TCE) microemulsions using an aqueous solution of 0.1M SDHS with varying amounts of electrolyte and in combination with 0.09M of the hydrophilic linker (concentration based on aqueous solution) and also in combination with both 0.18M of dodecanol as lipophilic linker and 0.18M of the hydrophilic linker. Table 7.3 summarizes the results from using hexyl polyglucoside as a hydrophilic linker. From previous results we observed that a hydrophilic linker shows the following characteristics: (1) the addition of the hydrophilic linker should not significantly impact the solubilization capacity of the microemulsion expressed as volume of oil (or water) solubilized at optimum formulation (i.e. equal amounts of oil and water are solubilized in the middle phase microemulsion) per unit mass of surfactant; (2) the co-addition of hydrophilic and lipophilic linkers should produce a significant increase in the solubilization capacity of the system; (3) the addition of the hydrophilic linker should significantly increase the optimum salinity (the electrolyte concentration needed to obtain an optimum formulation); and (4) the co-addition of hydrophilic and lipophilic linker should increase the fraction of hydrophilic

linker present in the middle phase (42). Not only do the results in Table 7.3 demonstrate that hexyl polyglucoside fulfills these characteristics, hexyl glucoside has a very similar performance to sodium mono and dimethyl naphthalene sulfonate (SMDNS), as previously reported (42).

Table 7.3. Characterization of hexyl polyglucoside as a hydrophilic linker using SDHS (0.10M) as surfactant.

Hydrophilic linker	Concentration hydrophilic linker	Dodecanol concentration	Solubilization parameter (ml/g SDHS)	Fraction of hydrophilic linker in Type III (%)	Optimum salinity S* (gNaCl/100ml)
Blank[a]	0.00 M	0.00 M	5.7±0.7		1.4±0.05
SMDNS[a]	0.09M	0.00 M	5.4±0.7	50±4	3.1±0.1
SMDNS[a]	0.18 M	0.18 M	10.7±0.7	75±6	2.8±0.1
Hexyl[b] polyglucoside	0.09 M	0.00 M	6.1±0.7	52±4	3.5±0.1
Hexyl[b] polyglucoside	0.18 M	0.18 M	10.4±0.7	76±4	2.5±0.1

(a) From reference 42
(b) This work

In addition to testing the hydrophilic linker performance for hexyl polyglucoside, Figure 7.2 shows the interfacial tension of hexyl polyglucoside solutions with isopropyl myristate in the presence of 0.9 g/100ml of NaCl (isotonic solution). The breakpoint on the curve corresponds to the critical micelle concentration (CMC ~ $1.8*10^{-2}$ M). The surface area per molecule of the surfactant can be calculated using the Gibbs adsorption equation for nonionic surfactants using the slope of the dotted line in Figure 2 (17):

$$\Gamma = \frac{-1}{RT}\left(\frac{d\gamma}{d\ln C}\right) \qquad \text{Eq. 2}$$

where Γ is the surface excess concentration of the amphiphile, γ is the interfacial tension, C is the concentration of the amphiphile, R is the gas constant and T is the absolute temperature of the system.

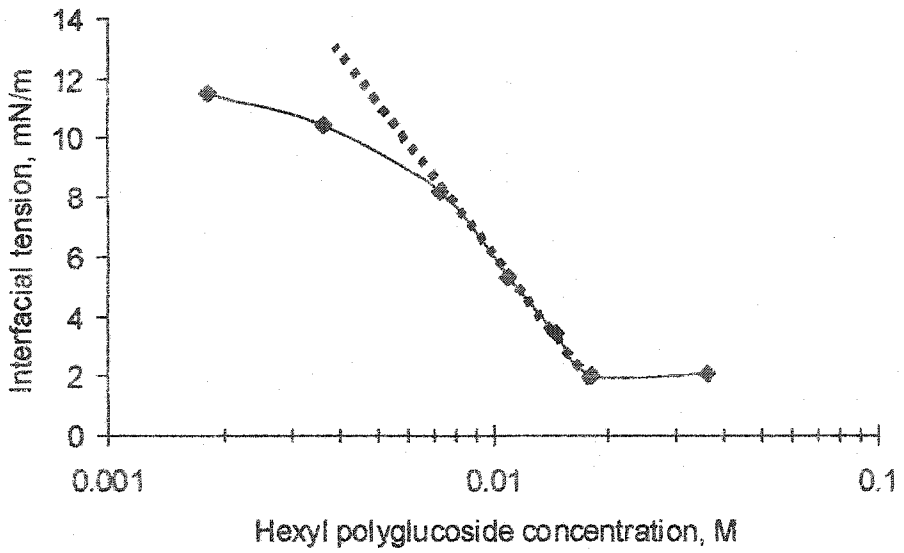

Figure 7.2. Interfacial tension of isopropyl myristate/ hexyl polyglucoside solutions as a function of hexyl polyglucoside concentration at 300K and 0.9 g NaCl/100 ml. The slope of the dotted line was used to calculate the surface area per molecule of the surfactant.

From the surface excess concentration (Γ, mol/m^2) it is possible to calculate the area per molecule (a, Å^2):

$$a = \frac{10^{20}}{N_A \Gamma} \qquad \text{Eq. 3}$$

where N_A is the Avogadro's number and 10^{20} is a conversion factor. Applying this method, the area per molecule for hexyl polyglucoside is 65 Å^2/mol. Later, this value will be used to estimate the characteristic length of the microemulsion systems.

Phase behavior of linker-based isopropyl myristate (IPM) microemulsions.

The phase behavior of linker-based IPM microemulsions was obtained by scanning the concentration of the hydrophilic component of the surfactant mixture, in this case hexyl polyglucoside. In this manner, the following transition occurred: Type II (water-swollen reverse micelles) - Type III (bicontinuous) - Type I (oil-swollen micelles) (29,53).

Figure 7.3 shows the relative phase volumes of the different microemulsion phases resulting from mixing an aqueous lecithin solution (4 % w/v or g/100ml), sorbitol monoleate (4% w/v), electrolyte (0.9% w/v NaCl) and varying amounts of hexyl polyglucoside with isopropyl myristate (IPM). The oil to aqueous solution ratio was kept at 1/1 (v/v). As expected, the addition of incremental amounts of hexyl polyglucoside produced a phase transition of II-III-I as a result of the increasing hydrophilicity of the surfactant mixture. Figure 7.3 also presents a solid line representing the phase volumes calculated using the net-average curvature model of microemulsions, as discussed later (54).

The findings in Figure 7.3 help confirm our hypothesis that it is possible to form middle phase microemulsion systems using lecithin as surfactant and a combination of non-toxic linkers while avoiding the use of alcohols. The question now remains as to how does this formulation compare to those previously reported in the literature that use lecithin as a surfactant in combination with alcohols. Perhaps the best comparison can be made with the systems formulated by Corswant et al. (29) where they were able to form a single phase microemulsion with IPM using 7% lecithin (or 3.5% based on total volume

oil+water), 3% octyl glucoside (1.5% based on total volume) and 8% isopropanol. While our results in Figure 7.3 show the formation of a middle phase microemulsion, this was not yet a single-phase microemulsion, and thus needed additional surfactant to form a single-phase.

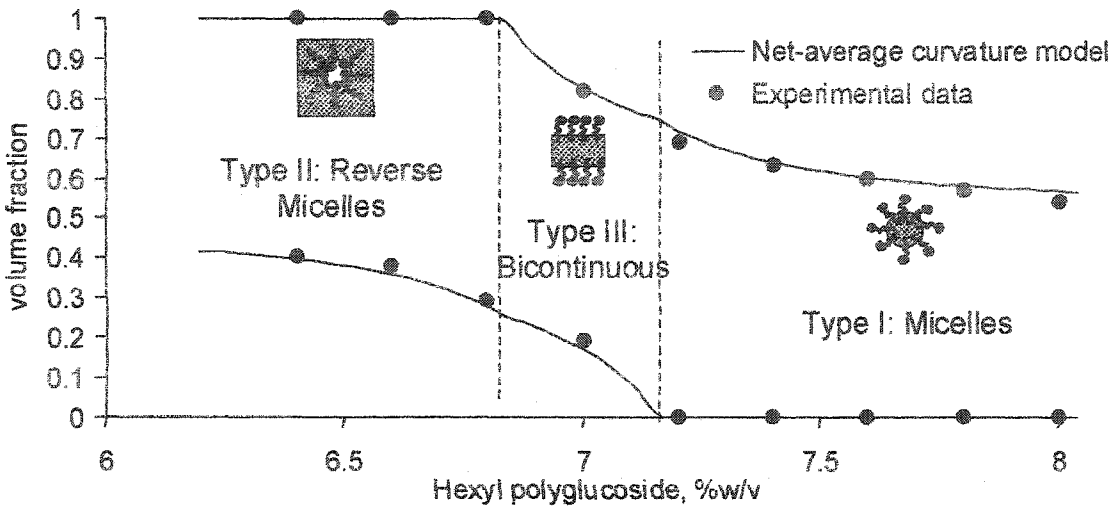

Figure 7.3. Phase behavior study of linker-based isopropyl myristate microemulsion formulated with 4% w/v Lecithin, 4% w/v sorbitol monoleate, 0.9%w/v NaCl (all concentrations based in aqueous solution). Oil to aqueous solution volume ratio =1/1. Adding incremental amounts of hexyl glucoside yielded a microemulsion phase transition Type II-Type III-Type I. Solid lines correspond to the net-average curvature model fitted with a length parameter ξ° = 24Å and characteristic length of ξ^{*}=217 Å.

Figure 7.4 shows the "phase map" of IPM microemulsions where the boundaries between the different types of microemulsion phases are plotted in terms of the lecithin concentration (y-axis) and the hexyl polyglucoside to lecithin ratio (x-axis), while holding a constant weight ratio of sorbitol monoleate to lecithin of 1/1, a temperature of 300K and a sodium chloride concentration of 0.9% w/v. According to this phase map, formation a single phase (Type IV) microemulsion containing equal volumes of oil and water required the following minimum concentrations: lecithin of 6%, sorbitol

monoleate of 6% and hexyl polyglucoside of 9% (ratio ~1.5). When this formulation is compared with that of Corswant et al. (29), our combined linker formulation required less lecithin and avoided the need for alcohol in the system.

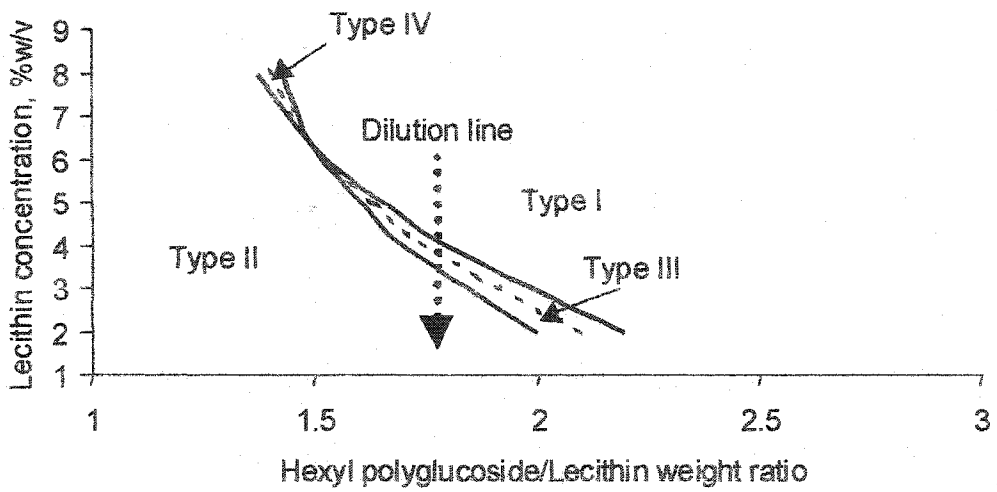

Figure 7.4. Phase map for IPM microemulsions prepared with sorbitol monoleate to lectihin weight ratio = 1/1 at 300K and 0.9 % w/v NaCl. The dotted line indicates the optimum formulation (equal volumes of oil and water solubilized in middle phase). The dilution line represents the potential changes in phase behavior as the total surfactant concentration is diluted.

We should clarify that the formulation of Corswant et al. (29) is very efficient in terms of solubilization. Another similar formulation was obtained by Moreno et al. (55) where they formulated Type I microemulsions with close to 30% lecithin+polysorbate 80 (an ethoxylated version of sorbitan monoleate) that could only solubilize 10 to 15% of oil and did not report any system that could form a middle phase microemulsion.

Since linker molecules are not cosurfactants, they can show significant partition into the bulk oil and/or water phases (38). This phenomenon makes the linkers less

efficient than a typical cosurfactant (e.g. octyl glucoside) in terms of solubilization capacity, as discussed above in reference to the formulation of Corswant et al (29).

The partition of the linkers, and especially hexyl polyglucoside, is an important factor in the appearance of the phase diagram. Accounting only for the CMC of hexyl polyglucoside (~ 1%, see Table 7.1 and Figure 7.2) we can produce a simple calculation to illustrate this effect: at 2% lecithin, 4.4 % hexyl polyglucoside was needed to obtain an optimum middle phase (See Figure 4), but considering that 1% of hexyl polyglucoside can be present as monomer, only 3.4% of hexyl polyglucoside is associated with the lecithin. If this concentration was used to calculate the hexyl polyglucoside to lecithin ratio, this value would be close to 1.7, which is close to the value needed to form a single phase microemulsion (~ 1.5, see Figure 7.4). It is thus necessary to clarify that the CMC is not the only source of deviation because partitioning effects are involved, including the partition of the lipophilic sorbitan monoleate that needs to be further evaluated but is beyond the scope of this work.

Another important feature of Figure 7.4 is that it can be used as a dilution test of a given formulation. The dotted dilution line indicates that a microemulsion phase which is initially Type I will upon dilution with a mixture of water and oil with a ratio close to 1/1, undergo a phase transition Type I- Type III-Type II. Thus, a vertical phase map for this surfactant system would be desirable so as to not transition out of the optimal phase. At the same time, if the dilution is made with an aqueous solution Figure 7.4 does not apply since the oil to water ratio will vary as the dilution occurs and this would further alter the shape of the phase map.

Characterization of linker-based IPM microemulsions

Recalling that the goal of this research was not only to formulate microemulsion systems with non-toxic surfactant and linkers but also to characterize these systems. Figure 7.5 shows the radius of droplet-type microemulsions (Type I and II) obtained from dynamic light scattering (DLS) measurements and values predicted by the net-average curvature model, as will be explained later. Both DLS measurements and model predictions showed an increase in droplet size as the formulation approaches the Type III bicontinuous system. The disparity between the model radius and hydrodynamic radius obtained from DLS diffusion measurements has been reported before and discussed in terms of the nature of the hydrodynamic radius being dependent on the shape of the droplet (54). The droplet sizes measured using dynamic light scattering are within the range of lecithin - IPM microemulsion formulations reported in the literature (55,32). In addition to droplet sizes, Figure 7.5 also presents the viscosity of the different microemulsions. For Type I microemulsions viscosity values are two to three times the viscosity of water, while in the case of Type II systems viscosity values are close to twice the viscosity of pure IPM (~ 5 cp). For the case of Type III systems, viscosity values are in between the Type I and II system. Relative viscosities of 2 to 3 times those observed here are typical of microemulsion systems (56). It is worth mentioning that some of the data points where evaluated at different spinning speeds of the rehometer and the viscosity remained constant at all speeds which suggests a newtonian-like behavior for these systems. The observed viscosity values (between 2 and 10 cp) are appropriate for

applications except for some transdermal applications where a higher viscosity may be desired.

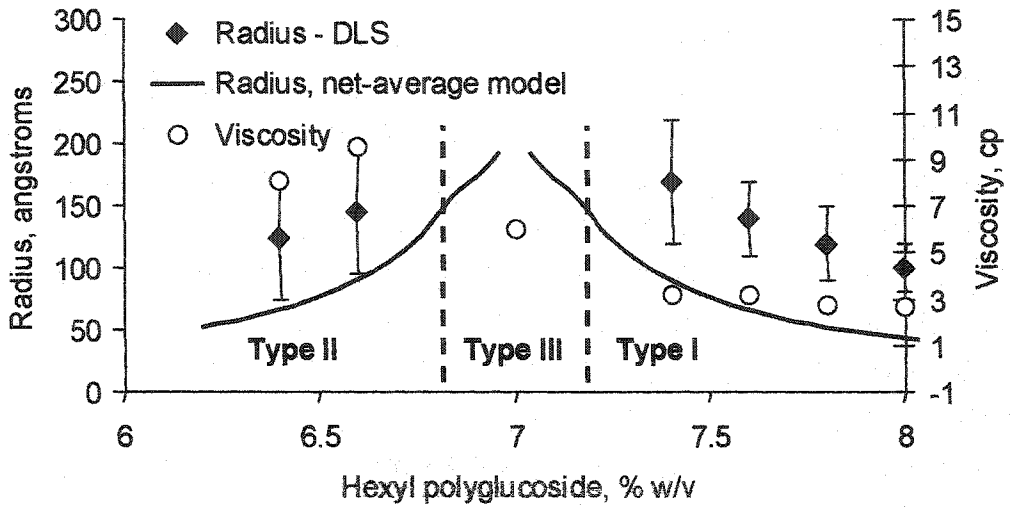

Figure 7.5. Characterization of isopropyl myristate microemulsion prepared with 4% lecithin, 4% sorbitol monoleate, 0.9% w/v NaCl and varying amounts of hexyl glucoside.

One important characteristic of microemulsion systems is their ability to reduce the interfacial tension between oil and water. Figure 7.6 presents the interfacial tension between the different microemulsion phases and the excess phase (oil for Type I systems and water for Type II). The solid line represents the net-average curvature model fitted with an interfacial rigidity of E_r=2.5 K_BT. The values of interfacial tension presented in Figure 7.6 are typical of microemulsion systems, and these values are consistent with the large solubilization produced by these lecithin microemulsion systems, and also the low interfacial tension reported for lecithin microemulsion systems with alkanes (27). These low interfacial tension values are especially desirable in formulation of detergents and other cleaners.

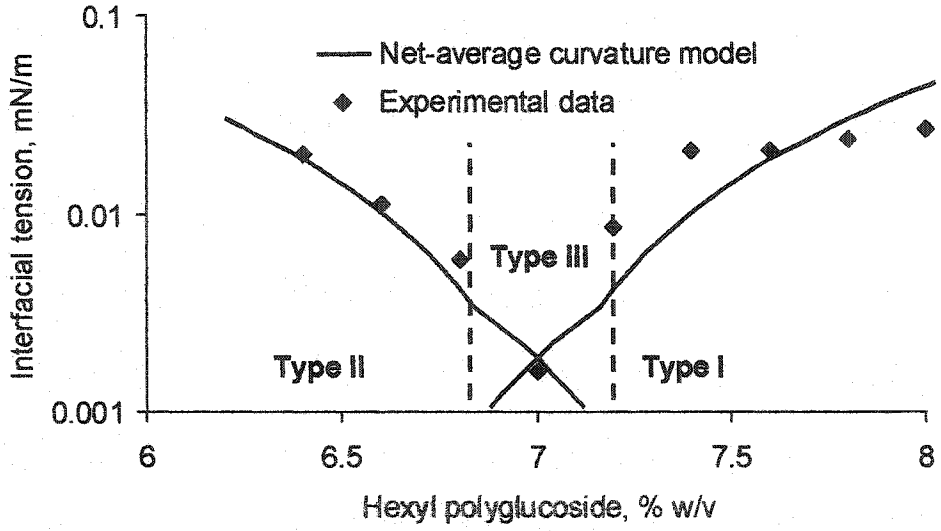

Figure 7.6. Interfacial tension of IPM microemulsion formulated with 4% lectihin, 4% sorbitol monoleate and varying concentration of hexyl polyglucoside. Solid lines obtained using the net-average curvature model and a value of interfacial rigidity of E_R=2.5 K_BT

Effect of formulation conditions on linker-based IPM microemulsions.

During the application of microemulsion in drug and cosmetic delivery or in general cleaning applications they can be exposed to a series of changes in environmental conditions such as temperature, electrolyte concentration, and pH. For this reason we studied how the phase maps of linker-based lecithin - IPM microemulsions change under these different conditions.

Figure 7.7 shows the phase maps for linker-based lecithin microemulsions with IPM using a sorbitan monoleate to lecithin weight ratio of 1/1, a concentration of 0.9% w/v NaCl, and three different temperatures (10°C, 27°C, 40°C). The Figure 7.7 data show that increasing the temperature of the systems promotes a shift in the phase map towards lower hexyl glucoside to lecithin ratios (AG-6/le), increases the minimum concentration of lecithin required to achieve a Type IV concentration (which suggests a

less efficient formulation in terms of solubilization), and widens the region of Type III microemulsions. The shift towards lower AG-6/le ratios with increasing temperature indicates that the system becomes more hydrophilic. In other words, for a given formulation, increasing the temperature will produce a transition between microemulsions types Type II - Type III - Type I. The response of the system is typical of ionic microemulsion systems (2). Thus, although there is no pure ionic surfactant in this formulation, it seems that the zwiterionic nature of lecithin shows the same response as single ionic surfactants. In the case of hexyl glucosides, it has been observed that glucoside-based microemulsions are insensitive to temperature, which is a unique property of these surfactants compared to other non-ionic surfactant microemulsion systems (51,52). In practical terms, the results in Figure 7.7 indicate that if a microemulsion is prepared as a Type IV single microemulsion systems at room temperature (e.g. using 7% lecithin aqueous concentration, and AG-6/le = 1.5/1) but once is applied at a body at 37°C it may transition to a Type I system and release excess IPM. The previous comment does not mean that these formulations are not appropriate for delivery applications but that the formulator needs to be aware of possible phase transitions, and should make the proper adjustments to asses potentially undesirable phases (e.g reduce the amount of solubilized oil below the solubilization capacity).

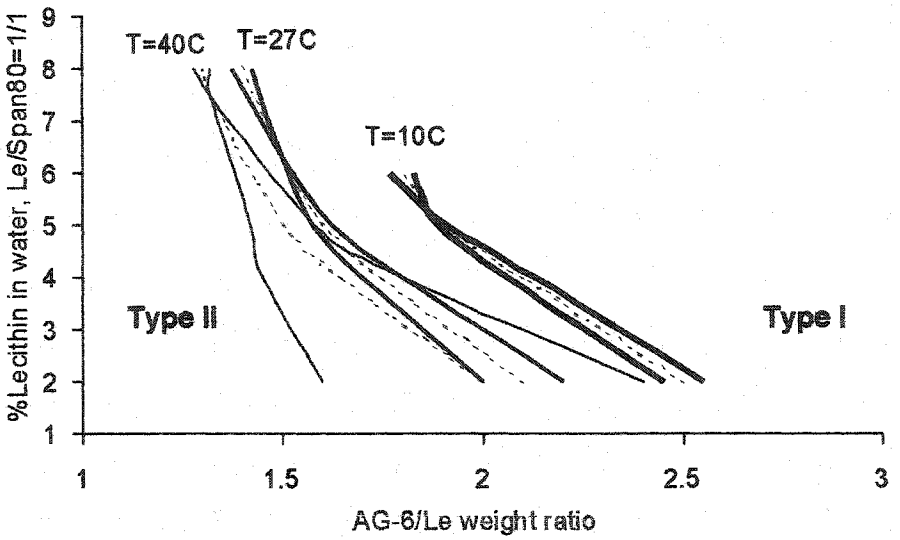

Figure 7.7. Phase maps for IPM microemulsions prepared with sorbitol monoleate to lectihin weight ratio = 1/1 at different temperatures (10°C, 27°C, 40°C) and 0.9 % w/v NaCl. The dotted line indicates the optimum formulation (equal volumes of oil and water solubilized in middle phase).

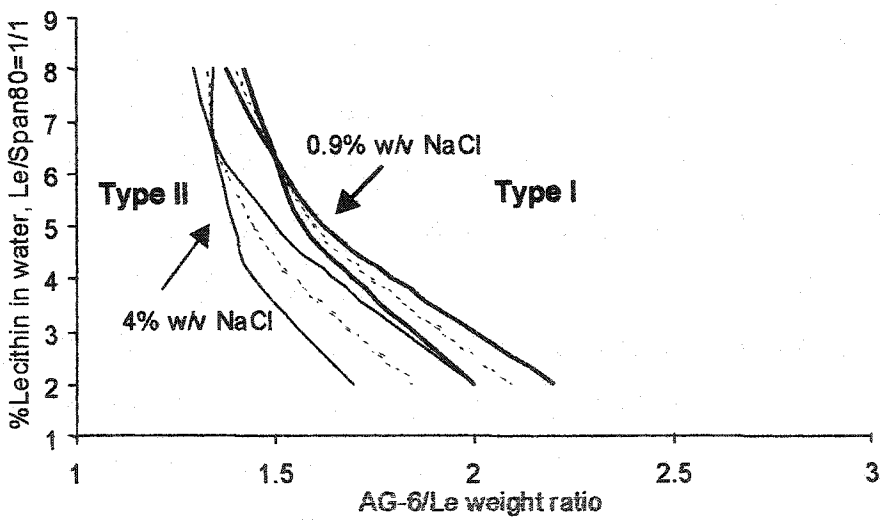

Figure 7.8. Phase maps for IPM microemulsions prepared with sorbitol monoleate to lectihin weight ratio = 1/1 at 300K and at two levels of electrolyte: 0.9 % and 4% w/v NaCl. The dotted line indicates the optimum formulation (equal volumes of oil and water solubilized in middle phase).

Figure 7.8 presents the phase maps for IPM microemulsion with two levels of electrolyte concentration (0.9% and 4.0% NaCl). The data shows that with increasing electrolyte concentration the phase map shifts to lower ratios of hexyl polyglucoside to lecithin (AG-6/le). In other words, with increasing electrolyte concentration, the system transitions from II - III- I similar to the case of increasing temperature as discussed earlier. This result is unusual since even in non-ionic surfactant microemulsion, addition of electrolyte tends to produce a transition of Type I-III-II. The explanation for this phenomenon is not clear, but it could result from the fact that at neutral pH lecithin has positive and negative charges that could have a net attractive interaction between head groups (which is the opposite to ionic surfactants where the interactions is repulsive), and that since adding electrolyte can help to screen these ionic interactions, it can weaken this attraction and promote the respective changes in curvature. Further studies are needed to test this possibility.

Figure 7.9 shows the effect of pH on linker-based lecithin IPM microemulsions. The curves show that increasing pH has the same effect as increasing temperatrure or electrolyte, i.e. promotes the transition II-III-I (the system becomes more hydrophilic). The trend previously explained is significant between pH 6.5 and 10.8 but is subtle between pH 3.5 and 6.5. The explanation for this behavior could be related to the fact that the lecithin compound shows positive charge below pH 3 (considered the lecithin isoelectric point) and start showing an anionic form at pHs larger than 5.2 (pKb for lecithin) (57,58). According to this, at pH 3.5 lecithin has somewhat balanced number of negative and positive charges which produces a strong hydrophile-hydrophile interaction

between the lecithin groups (same as in the low electrolyte case) that leads to a hydrophobic formulations. At pH 6.5 the system has started to develop a net anionic charge which improves its interaction with water molecules (makes the system more hydrophilic) but is close enough to the range of net electroneutrality (pH ~ 3 to 5.2) that it produces only a subtle change in the phase behavior. At pH 10.8 lecithin molecules have already become fully anionic which is reflected in a significant change in the phase map. The above explanation is preliminary and further studies are required to investigate this behavior in more detail. The pH effect study is most relevant for oral applications where the formulation will be exposed to the acidic media in the digestive system or in formulations for surface cleaners where the pH of typical formulation is in the basic range (e.g. pHs between 10 and 12).

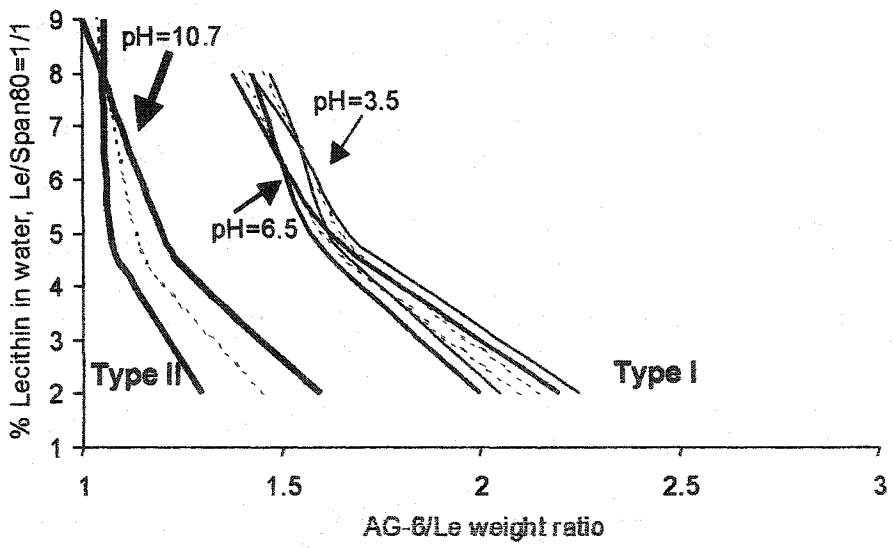

Figure 7.9. Phase maps for IPM microemulsions prepared with sorbitol monoleate to lectihin weight ratio = 1/1 at 300K, at 0.9 % w/v NaCl and at three different levels of pH (3.5, 6.5 and 10.7). The dotted line indicates the optimum formulation (equal volumes of oil and water solubilized in middle phase).

Figure 7.10 shows the effect of using different sorbitol monoleate (Span 80) to lecithin ratios. The data in Figure 7.10 indicates that increasing the proportion of sorbitol monoleate makes the mixture lecithin + sorbitol monoleate more hydrophobic, thus requiring a larger amount of hexyl polyglucoside (AG-6) to compensate and achieve a Type III system. Perhaps more important in terms of cost of the formulation is that increasing the concentration of sorbitol monoleate reduces the minimum concentration of lecithin required to achieve a Type IV microemulsion, although at the same time it increases the amount of sorbitol monoleate and hexyl polyglucoside required. The main message of Figure 7.10 is that lecithin can be replaced in certain proportion by a combination of hydrophilic and lipophilic linkers, as has been previously demonstrated in other linker-based microemulsions (39).

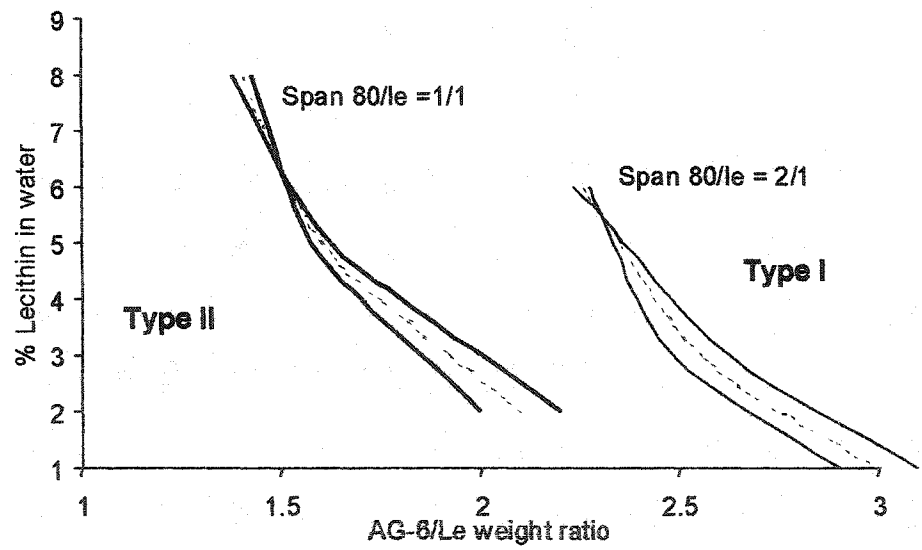

Figure 7.10. Phase maps for IPM microemulsions prepared with two different ratios of sorbitol monoleate (Span 80) to lectihin weight ratio (1/1 and 2/1) at 300K, at 0.9 % w/v NaCl. The dotted line indicates the optimum formulation (equal volumes of oil and water solubilized in middle phase).

Thus far we have learned about how to formulate linker-based lecithin microemulsions with isopropyl myristate (IPM), we have characterized these microemulsions, and we have learned how different formulation conditions affect the phase map of this system. The final objective of this work is to use this formulation approach to develop microemulsions for a wide range of oils and compare the performance of these formulations to other linker-based microemulsion systems.

Linker-based lecithin microemulsion with a variety of oils.

The same basic approach used to produce linker-based lectihin microemulsion with ispropyl myristate was used to produce microemulsions with the other oils listed in Table 7.2. The basic conditions for these microemulsions were a sorbitol monoleate to lecithin ratio of 1/1, a temperature of 27°C (300K), and a neutral pH. Figure 7.11 shows the minimum aqueous concentration of lecithin required to achieve a Type IV microemulsion and the hexyl polyglucoside to lecithin ratio (AG-6/le) required to achive such a point as a function of the oil equivalent alkane number of each oil (see Table 7.2). In terms of the minimum amount of lecithin concentration rquired to achieve a Type IV microemulsion, the data in Figure 7.11 shows that as the oil becomes more hydrophobic (higher EACN), more lecithin is required, which indicates that it is more difficult to solubilize such oils, which is classical for microemulsion systems (2). In regard to the hexyl polyglucoside to lecithin ratio, Figure 7.11 shows a linear relation between the EACN and the AG-6/le ratio. For more hydrophobic oils (higher EACN values), the overall formulation must be more hydrophobic in order to match the hydrophobicity of the oil, and thus less hexyl polyglucoside is required to achieve the optimum formulation.

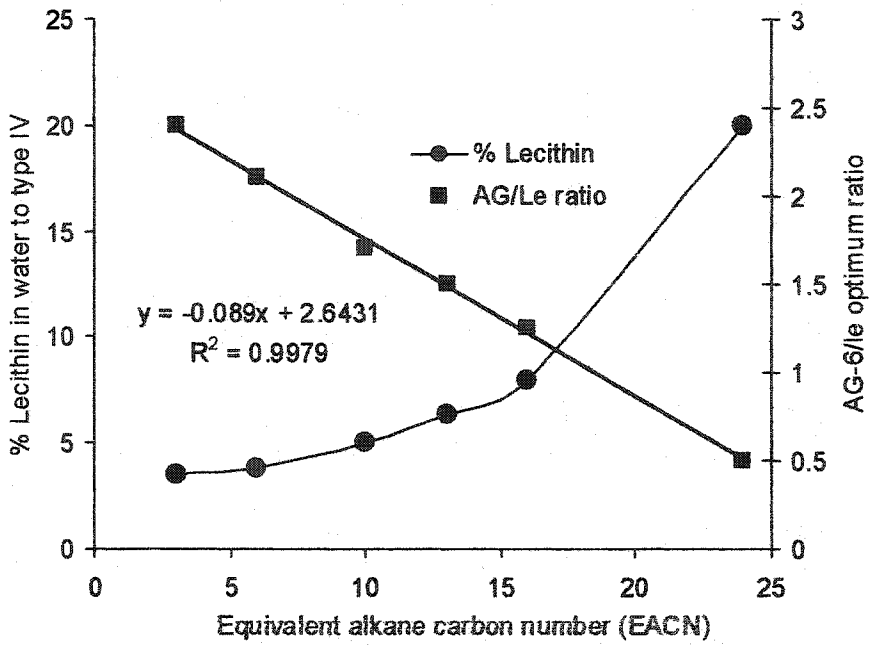

Figure 7.11. Formulation of linker lecithin microemulsion with a wide variety of oils, indicating the hexyl polyglucoside (AG-6) to lectihin ratio to achieve a single phase microemulsion and the minimum amount of lecithin required to form a single phase microemulsion. Other conditions: sorbitol monoleate to lecithin ratio 1/1, T= 300K, 0.9 % w/v NaCl. EACN values for each oil presented in Table 7.2.

In previous linker systems we have learned that the ratio of hydrophilic linker to surfactant (in this case AG-6/le) is a linear relationship with the surfactant affinity difference equation (Equation 1) (39), which in this case is:

$$\frac{SAD}{RT} = -\ln S + K * EACN + f(A) - \sigma + a_t(T - T_{ref}) + b(AG_6/le) \qquad \text{Eq. 4}$$

where b is a constant, AG-6/le is the hexyl polyglucoside to lecithin ratio, and other variables and constants as described before.

Equation 4 predicts a linear relationship between EACN and AG-6/le. If Equation 4 is expressed in a differential (Δ) form with constant electrolyte and temperature, for no alcohol and for the same type of surfactants, then:

$$\frac{\Delta SAD}{RT} = K * \Delta EACN + b\Delta(AG_6/le) \qquad \text{Eq. 5}$$

In Figure 7.11 all of the AG-6/le ratios are optimum formulations (i.e. same volume of oil and water solubilized in the microemulsion phase) for the range of oils considered, and thus, in all these cases SAD/ RT = 0 (48,49). Using this condition in Equation 5, the slope of Figure 7.11 is -K/b = -0.089. Values of K typically range between 0.1 and 0.2, with an average value of 0.17 (36,48,49). Thus the value of "b" is estimated to be 1.9. This value is used later in the net-average curvature model curves presented in Figures 3, 5 and 6 for IPM microemulsions.

In addition to describing the formulation of linker-based lecithin microemulsions, Figure 7.12 presents two important parameters for these formulations: the characteristic length and the optimum interfacial tension (between the optimum middle phase microemulsion phase and the excess phases). The characteristic length is a parameter that indicates the half thickness of the average bicontinuous channels of optimum middle phase microemulsion and can be calculated as (54,59):

$$\xi = \frac{6 * \phi_o * \phi_w * V_m}{As} \qquad \text{Eq. 6}$$

where ϕo and ϕw are the volume fractions of oil and water in middle phase microemulsion, V_m is the volume of the middle phase, and As is the interfacial area, provided by the surfactant adsorption that can be calculated as (54):

$$As = \sum_i V_{w,o} Cs_i \times \phi_i \times 6.023 \times 10^{23} \times a_i \qquad \text{Eq. 7}$$

where $V_{w,o}$ is the initial volume of the aqueous solution containing the surfactant and linkers, Cs_i is the initial aqueous molar concentration of the surfactant, cosurfactant and hydrophilic linker added to the formulation, ϕ_i is the fraction of the surfactant/cosurfactant that is present in the middle phase microemulsion and a_i is the area per molecule of the species considered (in $Å^2$/molecule). Because the systems presented in Figures 7.11 and 7.12 correspond to single phase microemulsions all values of ϕ_i are equal to 1 (no excess phases to partition into). Also, in contrast to common lipophilic linkers, sorbitol monoleate is more surface active than its alcohol counterparts, and thus the area per molecule of this group (see Table 1) is also considered in As. The values of the characteristic length for the different oils, as represented by their respective EACN values in Table 7.2, are presented in Figure 7.12. As was discussed previously, for more hydrophobic oils (i.e. higher EACN values) the solubilization capacity of the system decreases as denoted by smaller values of characteristic length.

The great advantage of expressing the solubilization capacity of microemulsions as a characteristic length value instead of a solubilization parameter is that it allows a direct comparison with microemulsion systems formulated with a completely different set of surfactant and additives. This advantage permits the comparison between the linker-based lecithin microemulsions and linker-based alkyl sulfosuccinated microemulsion recently reported by our group (40). Figure 7.12 shows the characteristic length of microemulsions formulated with sodium dihexyl sulfosuccinate (SDHS) and sodium bis(2-hexyl) dihexylsulfosuccinate (AOT) as surfactants, SMDNS as a hydrophilic linker

and oleyl alcohol as lipophilic linker. For most cases the characteristic length of linker-based lecithin microemulsions is twice or more the characteristic length of the alkyl sulfosuccinate microemulsions. The greater solubilization in lecithin microemulsions is attributed to the longer extended tail of lecithin (between 14 to 18 carbons) compared to that of SDHS and AOT (six carbons). There is some evidence that suggests that the characteristic length is proportional to the extended length of the surfactant (59), which is supported by the findings of this work. In addition, for lectihin-based microemulsions the electrolyte concentration was kept constant at a value of 0.9% NaCl (isotonic solution) even for formulations with hydrophobic oils, but in the case of the alkyl sulfosuccinated surfactants, for more hydrophobic oils it was necessary to increase the electrolyte as high as 16% NaCl to achieve this transition, which is inappropriate for many applications.

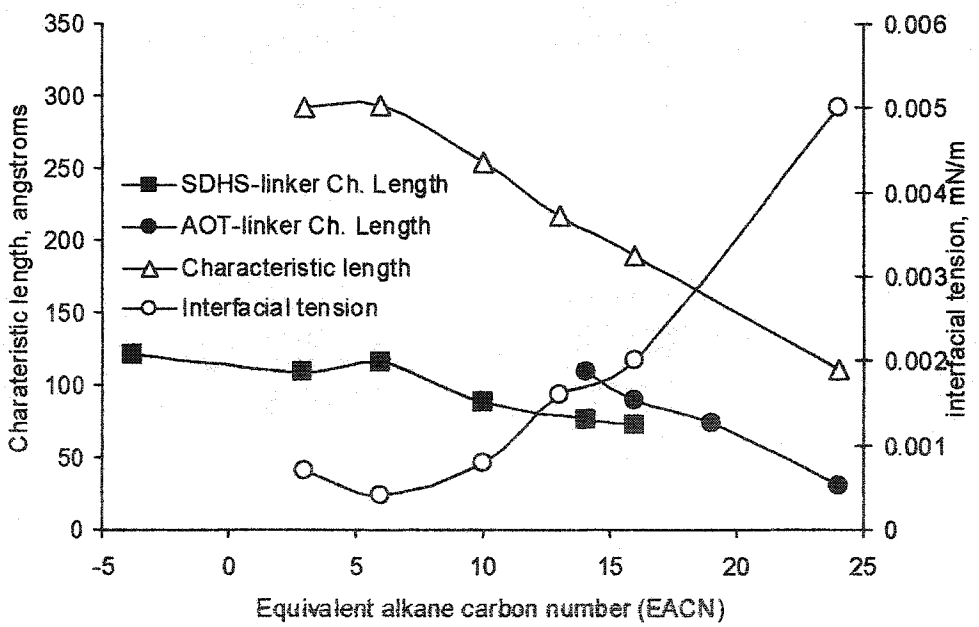

Figure 7.12. Properties of linker lecithin microemulsion with a wide variety of oils, indicating the characteristic length and interfacial tension of the microemulsions whose formulation is described in Figure 7.11. The characteristic length for AOT and SDHS linker microemulsions obtained from reference (40)

The interfacial tension values presented in Figure 7.12 are well below values reported for microemulsion systems produced with alkyl sulfosuccinated surfactants (40); this is consistent with the higher solubilization values of lecithin-based microemulsions. These interfacial tension values are similar to those produced by others with medium chain alcohols as cosurfactants and alkanes as oil phase (27); thus our alcohol-free systems perform competitively with systems reported by others.

One important observation in regard to the formulation of linker-based lecithin microemulsion with methyl oleate, is that the formation of middle phase microemulsion was only possible at temperatures 60°C or larger, since at lower temperatures atypical two phase systems were obtained. At this large temperature the methyl oleate system presented an unusual high solubilization capacity such that it could form a single-phase microemulsion with close to 6% Lecithin and AG-6/Le ratio of close to 1.4. The IPM systems at the same conditions formed single-phase microemulsion systems at lower AG-6/Le ratios, which according to Figure 7.11 suggests that methyl oleate has a lower EACN than IPM. Graciaa et al. have reported that ethyl oleate (a similar molecule to methyl oleate) show polar behavior and segregation near the surfactant tails, just as a lipophilic linker, and that the EACN for ethyl oleate approaches a value of 6 (60). Further research is necessary to explore the role of the ester group on the formulation of linker-based lecithin microemulsion.

Modeling linker-based lecithin microemulsions of isopropyl myristate (IPM).

Recently our research group has introduced a microemulsion critical scaling model called the net-average curvature model. In this model the net curvature (H_N) is

scaled to the non-dimmensional surfactant affinity difference ($SAD^{\#}$ = SAD/RT) as follows (54):

$$H_N = \frac{1}{R_O} - \frac{1}{R_W} = \frac{SAD^{\#}}{\xi_0} = \frac{b[(AG_6/le) - (AG_6/le)^*]}{\xi_0} \qquad \text{Eq. 8}$$

where R_O and R_W are coexistent oil and water droplets (R_O is virtual if the systems is Type III or Type II and R_W is virtual if the system is Type I or III), ξ_0 is the length parameter or scaling constant, which is proportional to the extended length of the surfactant, $SAD^{\#}$ is the dimmensionless SAD, and the right hand expression results from expressing $SAD^{\#}$ in terms of the hexyl polyglucoside to lecithin ratio as indicated by Equation 5: this is accomplished by using the ratio of hexyl glucoside to lecithin that produces the optimum formulation (equal volumes of oil and water solubilized in the middle phase), where AG-6/le* is the critical point since it is at this point where the net curvature of the surfactant membrane (H_N) becomes zero.

The second important term of the model is the average curvature (H_A) which indicates the average size of the aggregates in bicontinuous (Type III) microemulsions (54):

$$H_A = \frac{1}{2}\left(\left|\frac{1}{R_o}\right| + \left|\frac{1}{R_w}\right|\right) \geq \frac{1}{\xi^*} \qquad \text{Eq. 9}$$

where ξ^* is the characteristic length (calculated using Equation 6) of the optimum microemulsion system. Equation 9 indicates that the average aggregate size in bicontinuous systems can not be larger than the characteristic length of the system. The details of how to solve these equations are described elsewhere (54). The expression for

the net curvature was produced using the data in Figure 7.11 and the SAD equation, while the characteristic length ξ^* for the IPM system is also obtained from Figure 7.12 (ξ^*~217 Å). The only fitting parameter of the net-average model is the length parameter or scaling constant. The relative phase volumes data presented in Figure 7.3 were used to fit the model resulting in a length parameter of $\xi_0 \sim 24$ Å. For comparison, the length parameter of SDHS (2*C6 tail) was found to be 10Å and for SDS (C12 tail) found to approach 20 Å (54). Thus the value of $\xi_0 \sim 24$ Å for lecithin is reasonable considering that lecithin is a mixture of components with a range of 14 to 18 carbons in saturated and unsaturated tails (29). The net-average curvature model was used to produce radii values for Figure 7.5, where, as discussed above, the disparity between DLS values and the net-average curvature model has been observed and discussed elsewhere (54).

One final equation that relates to the net-average curvature model is the interfacial rigidity equation (37,54):

$$\gamma = \frac{E_R}{4\pi R^2} \qquad \text{Eq. 10}$$

where E_R is the interfacial rigidity express in energy units, γ is the interfacial tension and R is the oil or water droplet radius as calculated by the net-average model. In this equation the only fitting parameter is the interfacial rigidity. The interfacial rigidity is a similar concept to the bending modulus of surfactant membranes, but in this case it reflects the energy provided by the self-assembly of the surfactant molecules to protect the dynamic equilibrium of the microemulsion. Values of E_R are typically around 1 K_BT; values larger than this reflect a more rigid membrane which normally leads to a slower

kinetics of coalescence and solubilization (37). The values of interfacial tension in Figure 7.6 were used to fit the model and obtain a value for interfacial rigidity, finding that $E_R \sim 2.5\ K_BT$.

While not shown here, the interfacial tension values presented in Figure 12 also follow Equation 10 and, with the exception of hexane ($E_R \sim 1\ K_BT$), all the other oils show interfacial rigidities between 1.8 and 2.5 K_BT. These somewhat higher values are common in long chain surfactants which have a tendency to form lamellar or liquid crystal phases. The increased rigidity of these lecithin microemulsion systems could thus be responsible for the larger solubilization capacity experienced by these systems (37,59), since both can be related to the length of the surfactant tail.

Conclusions

Lecithin microemulsions were formulated using sorbitol monoleate as lipophilic linker and hexyl polyglucoside as hydrophilic linker. This formulation was able to produce alcohol-free single-phase microemulsions with isopropyl myristate (IPM) at lectihin concentration levels lower than alcohol-based systems reported in the literature. The properties of the formulated microemulsion are also comparable to systems reported in the literature, with our linker-based systems having slightly smaller droplet size and viscosity. Also increasing temperature, electrolyte concentration, pH or ratio of lecithin to sorbitol monoleate all produced a phase transition of Type II-III-I. Furthermore, it was possible to formulate microemulsions with a wide range of oils while achieving solubilization levels twice or higher than linker-based microemulsions formulated using

alkyl sulfosuccinate surfactants. Finally it was proposed that the greater solubilization capacity of lecithin microemulsion is due to the longer tail of the lecithin isomers and to the relatively high rigidity of lecithin microemulsions. Finally, there is a number of potential applications for these kind of formulations, but a successful application will involve a careful consideration of the series of conditions at which the formulation will be exposed, especially those concerning dilution, temperature and pH changes.

Acknowledgments

This work was supported in part by the Institute for Applied Surfactant Research of the University of Oklahoma and in part by EPA grant no. 083090301.

Literature

[1] P. Kumar and K.L. Mittal, Editors. Handbook of Microemulsion Science and Technology. Marcel Dekker, Inc., New York, 1999.

[2] Bourrel, M. and Schecter R. Microemulsions and related systems. Marcell Dekker Inc. New York, 1988.

[3] Knox, R. C.; Shau, B.; Sabatini, D. A.; Harwell, J. H. Field demonstration studies of surfactant-enhanced solubilization and mobilization at Hill Air Force Base, Utah. ACS Symp. Ser. (1999), 725, 49-63

[4] Paul, B. K.; Moulik, S. P. Uses and applications of microemulsions. *Current Science* **2001**, 80(8), 990-1001.

[5] Chhabra, V.; Free, M. L.; Kang, P. K.; Truesdail, S. E.; Shah, D. O. Microemulsions as an emerging technology. From petroleum recovery to nanoparticle synthesis of magnetic materials and superconductors. *Tenside.* **1997**, 34(3), 156-168.

[6] Doerfler, H. D.; Grosse, A. Applications of microemulsions with different compositions in detergents technique. *Prog. Colloids. Polymer Sci.* **1996**, 101, 113-115.

[7] Nalecz-Jawecki, G.; Grabinska-Sota, E.; Narkiewicz, P. The toxicity of cationic surfactants in four bioassays. *Ecotoxicology and Environ. Safety.* **2003**, 54(1), 87-91.

[8] Drobeck, H. P. Current topics on the toxicity of cationic surfactants. Surfactant Science Series Volume 53. Marcell Dekker, 1994, pp. 61-94.

[9] Garcia, M. T.; Ribosa, I.; Leal, J. Sanchez; Vives, J. J. Effect of the hydrophobic moiety of quaternary ammonium based surfactants on their ecological properties. Proceedings of the 4th World Surfactants Congress, Barcelona, June 3-7, 1996, pp. 373-377.

[10] Cserhati, T.; Forgacs, E.; Oros, G. Biological activity and environmental impact of anionic surfactants. *Environment International.* **2002**, 28(5), 337-348.

[11] Ghirardini, A. V.; Novelli, A. A.; Likar, B.; Pojana, G.; Ghetti, P. F.; Marcomini, A. Sperm cell toxicity test using sea urchin Paracentrotus lividus Lamarck (Echinodermata: Echinoidea): sensitivity and discriminatory ability toward anionic and nonionic surfactants. *Environmental Toxicology and Chemistry.* **2001**, 20(3), 644-651.

[12] Lundahl, P.; Cabridenc, R. Molecular structure-biological properties relationships in anionic surface-active agents. *Water Research.* **1978**, 12(1), 25-30.

[13] Gloxhuber, C.; Editor. Surfactant Science Series, Vol. 10: Anionic Surfactants - Biochemistry, Toxicology, Dermatology. (1980), 456 pp.

[14] Elworthy, P. H.; Treon, J. F. Physiological activity of nonionic surfactants. Nonionic Surfactants. 1967 (1967), pp. 923-70

[15] Yoshimura, K. Biodegradation and fish toxicity of nonionic surfactants. *J. Am. Oil Chem. Soc.* **1986**, 63(12), 1590-6.

[16] Treon, J. F.; Gongwer, L. E.; Nelson, M. F.; Kirschman, J. C. Physiologic and metabolic patterns of nonionic surfactants. Chem. Phys. Appl. Surface Active Subst., Proc. Int. Congr., 4th (1967), Meeting Date 1964, 3 381-95

[17] Rosen, M.J. Surfactants and interfacial phenomena. 2nd. Ed. John Wiley & Sons, New York, 1989, pp 431.

[18] Floyd, D. T.; Schunicht, C.; Gruening, B. Zwitterionic and amphoteric surfactants. Handbook of Applied Surface and Colloid Chemistry (2002), 1 349-372.

[19] Dyson, R. D. Essentials of Cell Biology. 2nd Edition . Allyn and Bacon, Inc. 1978, 433pp.

[20] Sim, J. S. New extraction and fractionation method for lecithin and neutral oil from egg yolk. Egg Uses and Processing Technologies (1994), 128-38.

[21] Malmsten, M. "Microemulsions in Pharmaceuticals" in Handbook of Microemulsion Science and Technology. Editor: P. Kumar. Marcell Dekker, Inc. 1999, p. 755-772

[22] Engstroem, S. and Larsson, K. "Microemulsions in Foods" in Handbook of Microemulsion Science and Technology. Editor: P. Kumar. Marcell Dekker, Inc. 1999, p. 789-796

[23] El-Nokaly, M.; Cornell, D.; Editors. Microemulsions and Emulsions in Foods. ACS Symposium Series 448. 1991, 268 pp.

[24] Tenjarla, S. Microemulsions: an overview and pharmaceutical applications. *Critical Reviews in Therapeutic Drug Carrier Systems.* **1999**, 16(5), 461-521.

[25] Lawrence M. J. and Rees, G. D. "Microemulsion-based media as novel drug delivery systems". *Adv. drug delivery rev.* **2000**, 45, 89-121

[26] Paolino, D.; Ventura, C. A.; Nistico, S.; Puglisi, G.; Fresta, M. Lecithin microemulsions for the topical administration of ketoprofen: percutaneous adsorption through human skin and in vivo human skin tolerability. *Int. J. Pharm.* **2002**, 244(1-2), 21-31.

[27] Shinoda, K.; Shibata, Y.; Lindman, B. Interfacial tensions for lecithin microemulsions including the effect of surfactant and polymer addition. *Langmuir.* **1993**, 9(5), 1254-7.

[28] Aboofazeli, R.; Lawrence, M. J. Investigations into the formation and characterization of phospholipid microemulsions. I. Pseudo-ternary phase diagrams of systems containing water-lecithin-alcohol-isopropyl myristate. *Int. J. Pharm.* **1993**, 93(1-3), 161-75.

[29] Von Corswant, C.; Olsson, C.; Soederman, O. Microemulsions Based on Soybean Phosphatidylcholine and Isopropylmyristate - Effect of Addition of Hydrophilic Surfactants. *Langmuir.* **1998**, 14(24), 6864-6870.

[30] Von Corswant, C.; Soederman, O. Effect of Adding Isopropyl Myristate to Microemulsions Based on Soybean Phosphatidylcholine and Triglycerides. *Langmuir* **1998**, 14(13), 3506-3511.

[31] Trotta, M.; Pattarino, F.; Grosa, G. Formation of lecithin-based microemulsions containing n-alkanol phosphocholines. *Int. J. Pharm.* **1998**, 174(1-2), 253-259.

[32] Ruth, H. S.; Attwood, D.; Ktistis, G.; Taylor, C. J. Phase studies and particle size analysis of oil-in-water phospholipid microemulsions. *Int. J. Pharm.* **1995**, 116(2), 253-61.

[33] Graciaa, A.; Lachaise, J.; Cucuphat, C.; Bourrel, M.; Salager, J. L. Improving solubilization in microemulsions with additives. 1. The lipophilic linker role. *Langmuir*. **1993**, 9(3), 669-72

[34] Graciaa, A.; Lachaise, J.; Cucuphat, C.; Bourrel, M.; Salager, J. L. Improving solubilization in microemulsions with additives. 2. Long chain alcohols as lipophilic linkers. *Langmuir*. **1993**, 9(12), 3371-4.

[35] Salager, J. L.; Graciaa, A.; Lachaise, J. Improving solubilization in microemulsions with additives. Part III: lipophilic linker optimization. *J. Surfactants Deterg.* **1998**, 1(3), 403-406

[36] Uchiyama, H.; Acosta, E.; Tran, S.; Sabatini, D. A.; Harwell, J. H. Supersolubilization in Chlorinated Hydrocarbon Microemulsions: Solubilization Enhancement by Lipophilic and Hydrophilic Linkers. *Ind. Eng. Chem. Res.* **2000**, 39(8), 2704-2708

[37] Acosta, E. J.; Le, M. A.; Harwell, J. H.; Sabatini, David A. Coalescence and Solubilization Kinetics in Linker-Modified Microemulsions and Related Systems. *Langmuir*. **2003**, 19(3), 566-574.

[38] Sabatini, D. A.; Acosta, E.; Harwell, J. H. Linker molecules in surfactant mixtures. *Curr. Opin. Colloid Interface Sci.* **2003**, 8(4-5), 316-326

[39] Acosta, E.; Tran, S.; Uchiyama, H.; Sabatini, D. A.; Harwell, J. H. Formulating Chlorinated Hydrocarbon Microemulsions Using Linker Molecules. *Environ. Sci. Technol.* **2002**, 36(21), 4618-4624.

[40] Acosta, E.; Mai, P. D.; Harwell, J. H.; Sabatini, D. A. Linker-modified microemulsions for a variety of oils and surfactants. *J. Surfactants Detergents* **2003**, 6(4), 353-363.

[41] Tongcumpou, C.; Acosta, E. J.; Quencer, L. B.; Joseph, A. F.; Scamehorn, J. F.; Sabatini, D. A.; Chavadej, S.; Yanumet, N. Microemulsion formation and detergency with oily soils: I. Phase behavior and interfacial tension. *J. Surfactants Detergents*. **2003**, 6(3), 191-203

[42] Acosta, E.; Uchiyama, H.; Sabatini, D. A.; Harwell, J. H. The role of hydrophilic linkers. *J. Surfactants Detergents*. **2002**, 5(2), 151-157

[43] Arleth, L.; Bauer, R.; Ogendal, L.H.; Egelhaaf, S.U.; Schurtenberger, P.; Pedersen, J.S. Growth Behavior of Mixed Wormlike Micelles: a Small-Angle Scattering Study of the Lecithin-Bile Salt System. *Langmuir*. **2003**, 19, 4096-4104.

[44] Tanford, C. The hydrophobic effect: Formation of micelles and biological membranes; John Wiley & Sons: New York, 1980.

[45] Angelico, R.; Ceglie,A.; Olsson, U.; Palazzo G. Phase Diagram and Phase Properties of the System Lecithin-Water-Cyclohexane. *Langmuir*. **2000**, 16, 2124-2132.

[46] Akzo Nobel bulletin on Household and Industrial Cleaners. December 2003 http://surface.akzonobelusa.com/bulletins.cfm

[47] Peltonen, L.; Hirvonen, J.; Yliruusi, J. The Behavior of Sorbitan Surfactants at the Water–Oil Interface: Straight-Chained Hydrocarbons from Pentane to Dodecane as an Oil Phase. *J. Colloid Interface Sci.* **2001**, 240, 272-276.

[48] Salager, J.L.; Morgan ,J.; Schechter, R.S.; Wade ,W.H. and Vasquez E. Optimum Formulation of Surfactant/Water/Oil Systems for Minimum Interfacial Tension or Phase Behavior, *Soc. Petrol. Eng. J.* **1979**, 19, 107

[49] Salager, J.L.; Morgan ,J.; Schechter, R.S.; Wade ,W.H. Mixing Rules for Optimum Phase Behavior Formulations of Surfactants/Water/Oil Systems. *Soc. Petrol. Eng. J.* **1979**, 19, 271

[50] Lide, D. R. Editor. CRC handbook of chemistry and physics. 75th. Edition, CRC Press (1994) pp. 10-300, 301

[51] Soderman, O.; Johansson, I. Polyhydroxyl-based surfactants and their physico-chemical properties and applications. *Curr. Opin. Colloid Interface Sci.* **2000**, 4(6), 391

[52] Ryan, L. D.; Kaler, E. W. Alkyl polyglucoside microemulsion phase behavior. *Colloid Surfaces A.* **2001**, 176(1), 69-83

[53] Shiau, B.; Sabatini, D. A.; Harwell, J. H.; Vu, D. Q. Microemulsion of Mixed Chlorinated Solvents Using Food Grade (Edible) Surfactants. *Environ. Sci. Technol.* **1996**, 30(1), 97-103.

[54] Acosta, E.; Szekeres, E.; Sabatini, D. A.; Harwell, J. H. Net-Average Curvature Model for Solubilization and Supersolubilization in Surfactant Microemulsions. *Langmuir.* **2003**, 19(1), 186-195.

[55] Moreno, M. A.; Ballesteros, P.; Frutos, P. Lecithin-Based Oil-in-Water Microemulsions for Parenteral Use: Pseudoternary Phase Diagrams, Characterization and Toxicity Studies. *J. Pharm. Sci.* **2003**, 92(7), 1428-1437

[56] Gradzielski, M; Hoffman, H. "Rheological properties of microemulsions" in Handbook of Microemulsion Sci. and Technol. Ed. P. Kumar. Marcell Dekker, Inc. 1999, p.357-386

[57] Sabet, V. M.; Zourab, S. M.; Said, W. Interaction of surface active agents with lecithin at the xylene/water interface and its effect on the stability of the resulting emulsion. *Colloids Surfaces.* **1982**, 4(4), 359-66.

[58] Price, C. W.; Lewis, W. C. M. Electrophoretic behavior of lecithin and certain fats. *Trans. Faraday Soc.* **1933**, 29 775-87.

[59] De Gennes, P. G.; Taupin, C. Microemulsions and the flexibility of oil/water interfaces. *J. Phys. Chem.* **1982**, 86(13), 2294-304.

[60] Graciaa, A.; Lachaise, J.; Cucuphat, C.; Bourrel, M.; Salager, J. L. Interfacial segregation of an ethyl oleate/hexadecane oil mixture in microemulsion systems. *Langmuir.* **1993**, 9(6), 1473-8

CHAPTER 8

CONCLUSIONS

The purpose of this section is to summarize the knowledge gained in the individual sections of this work and highlight some of the overall principles and the most relevant issues resulting from the collective work. The implications and potential uses of these principles are also discussed. The overall purpose of this work was to investigate how surfactant membrane properties are affected by formulation conditions and the presence of linker molecules, and also how these linkers participate in the surfactant membrane.

In Chapter 2 the net-average curvature model was introduced to scale the net-curvature of the surfactant membrane using the surfactant affinity difference equation as an expression for the difference in chemical potential of the surfactant membrane at a given curvature versus the flat or net-zero curvature point which occurs in an optimum formulation (where equal amounts of oil and water are solubilized). The scaling constant (L or later referred to as ξ°) was found to be proportional to the extended length of the surfactant and independent of temperature, type of oil solubilized, presence of cosurfactants and, to a great extent, independent of the presence of linkers. The average curvature component of the model was used to account for the average size of the aggregates in bicontinuos phases. The size of the aggregates should be equivalent to the characteristic length of the system (ξ^{*}) which indicates the maximum radius where the aggregates can grow and still maintain a dynamic equilibrium.

Using this approach it was possible to reproduce the phase volumes, phase transitions and solubilization of microemulsion systems. In Chapter 2 a disparity was observed between the droplet size calculated using the net-average curvature model and the droplet size obtained from the diffusion studies. This difference is also evident when comparing the droplet sizes obtained by small angle neutron scattering (SANS) and dynamic light scattering (DLS) in Chapter 3. In Type I and II microemulsions the net-average curvature model underestimated the size of the droplets, but it was consistent with the characteristic length obtained from Type III systems. From this it was inferred that the main limitation of the net-average curvature model in predicting droplet sizes was that it assumed a constant area per molecule of the surfactant, for all types of microemulsions. Further analysis of the scattering curves reveals that the area per molecule of the surfactant decreased by as much as one half in droplet microemulsions (Type I and II) when compared to bicontinuous systems. A simple correction of the areas showed a close correspondence between the model and SANS and DLS measurements.

Interfacial tension is another important property predicted by the net-average curvature model. This property was predicted using the droplet size estimated by the net-average curvature model and a interfacial rigidity equation proposed to relate droplet size and interfacial tension. The concept of interfacial rigidity (E_r) was introduced as the energy provided by the surfactant membrane to maintain the dynamic equilibrium of the aggregates of the solubilized phase (oil or water).

Chapter 4 studied how addition of the hydrophilic linker sodium mono and dimethyl naphthalene sulfonate (SMDNS) and the lipophilic linker dodecanol affected

the characteristic length and interfacial rigidity of trichloroethylene microemulsions and how it affected the kinetics of coalescence and solubilization. It was found that the addition of the lipophilic linker (dodecanol) increased the characteristic length and interfacial rigidity of sodium dihexyl sulfosuccinate (SDHS) membranes. The addition of hydrophilic linker showed the opposite effect to the lipophilic linkers. The co-addition of lipophilic and hydrophilic linkers had an intermediate effect. It was discussed that, in the case of lipophilic linkers, the increase in rigidity was due to the accumulation of dodecanol molecules near the surfactant tails that restricted the mobility of the surfactant molecules, thus increasing the rigidity of the surfactant membrane. On the other hand, since the hydrophilic linker had such a small tail, its co-adsorption with the surfactant left space between surfactant tails that provided additional mobility of the surfactant molecules. Another important finding in Chapter 4 is that the interfacial rigidity is closely related to the activation energy of coalescence and solubilization. Thus the addition of linker molecules influences not only the equilibrium but also the dynamics of microemulsion formation.

In Chapter 5 a wider range of oils is studied, and the more hydrophobic surfactant AOT is used to formulate linker-based microemulsions. The first important result coming out of this work is that, when formulating SDHS-alone microemulsion systems, the most hydrophobic oil that can be formulated was octane, which shows very limited solubilization. Introducing linker molecules, it was possible to formulate microemulsions with oils as hydrophobic as hexadecane. When SDHS was replaced by AOT, it was possible to formulate microemulsions with oils as hydrophobic as motor oil and squalene.

An important result anticipated in Chapter 2, and becomes even more evident in Chapter 7; that while linker molecules can improve the solubilization capacity and modify the kinetics aspects of microemulsions, the main properties of the systems are dictated by the surfactant and not the linkers. A simple corollary that is deduced from these results is that in linker systems, the best formulation (for hydrophobic large molecular weight oils) uses a surfactant with a long hydrophobe (which leads to a larger ξ^{o}).

Chapter 6 reports on investigations of how hydrophilic and lipophilic linkers self-assemble in microemulsion systems. The first stage of that work led to the identification of the critical microemulsion concentration of the systems without linkers. This is the minimum surfactant concentration required to form the first droplet of bicontinuous microemulsion, as deduced from interfacial tension measurements. It was later found that linker molecules could not form middle phase microemulsion by themselves, and that the surfactant concentration needs to exceed a minimum value before they self-assembly to form middle phase microemulsions could occur. The nature of the interactions between hydrophilic and lipophilic linkers that makes them behave as a pseudo-surfactant is still not clear and future research is needed to investigate these interactions.

Chapter 7 applies the concept of linker microemulsions to formulate non-toxic and biocompatible microemulsions for drug, food and cosmetic delivery applications. The surfactant used in this case was lecithin, the hydrophilic linker was hexyl glucoside and sorbitan monoleate was used as the lipophilic linker. The formulations presented in this chapter could be considered the most advanced linker formulations to date, not only for their biocompatible character but because of the large solubilization experienced by

these systems, and because it was possible to form microemulsions with oils as hydrophobic as squalene using low electrolyte concentration. The main limitation of this and other linker-based microemulsions, as realized in Chapter 5, is that not all the linkers segregate at the oil/water interface, and that the partition effects reduce the effectiveness of the system.

The results of this dissertation can be used in several ways. The net-average curvature model can be used as a framework for characterizing future formulation studies. If enough systems are analyzed, a database of constants could be accumulated and used in predicting the phase behavior of microemulsion even without the need to perform laboratory studies. In the near term, this model could be used in flow simulators, such as UTCHEM, for predicting the displacement of crude oil and oily contaminants from porous media. This model can help estimate the capillary forces which results from interfacial tension, density and viscosity of the surfactant/microemulsion phases formed. Both density and viscosity could be obtained from the composition data generated by the model.

Relative to linker molecules, this formulation technique has opened a new door to formulate microemulsions, giving a whole new set of tools for the colloid chemists to formulate surfactant mixtures. From the theoretical point of view, the origin of the interaction between hydrophilic and lipophilic linkers is still unknown and current research is underway to study this phenomenon using certain spectroscopic techniques.

APENDIX 1

Modeling Microemulsion Solubilization and Interfacial Tension: The Net-average Curvature Model[†]

Abstract:

Microemulsions are nano-structured fluids that can be of three types. Type I microemulsions consist of micelles or swollen micelles of 1 to 100 nm filled with oil dispersed in continuous aqueous media. The curvature of the surfactant membrane at the oil/water interface in type I microemulsion is concave towards the oil (positive). Type II microemulsions consist of reverse micelles filled with water dispersed in oil as the continuous phase, and the curvature is convex towards oil (negative). Type III microemulsions are bicontinuous in oil and water with net curvatures close to zero. We describe the thermodynamic relevance of the interfacial curvature on the solubilization capacity by means of scaling laws and the "surfactant affinity difference" of microemulsions. In addition we introduce a droplet coexistence model to account for bicontinuity in Type III microemulsions. By combining these elements in a simple model having one adjustable length parameter, we were able to reproduce solubilization curves and phase transitions for ionic microemulsions. This length parameter was found to scale to the extended length of the surfactant tail. We also propose a model for interfacial tension based on an "average" rigidity model for surfactant membranes. The potential of

[†] This appendix or portions thereof has been published previously under the title "Modeling microemulsion solubilization and interfacial tension. The net-average curvature model" in Annual Meeting Archive - *American Institute of Chemical Engineers, Indianapolis, IN, United States, Nov. 3-8, 2002* (2002), 49-58.

the model for simulating equilibrium properties of this type of nanostructured fluid in design applications is described.

Introduction

Microemulsion is a term that refers to emulsions of oil and water that are thermodynamically stable. Unfortunately the term does not reflect the nanostructure nature of this type of systems. The typical "droplet" size of microemulsion systems ranges between 1 to 100 nm (1-3).

Unlike their macro counterpart, microemulsions phase behavior is dictated by the thermodynamic conditions at which they are prepared. Despite the previous fact, it is very difficult to understand and predict the interrelation between the different thermodynamic variables involved (2).

Microemulsion are used as a nanoparticle synthesis media, nanolatex synthesis, drug delivery, Food additives, detergent, cleaners and cosmetic formulation (1). The most widespread use of microemulsions is as an oil solubilization/displacement media for enhanced oil recovery and surfactant enhanced aquifer remediation (4). There are two main properties of microemulsion systems that influence the performance of the formulation: solubilization capacity and interfacial tension. There are other important properties such as viscosity, thermal stability, and interfacial rigidity/flexibility that also affect the performance in particular applications (1,2,4).

To understand microemulsion thermodynamics is necessary to identify the different types of microemulsions. According to Winsor, there are three types of microemulsions. Type I microemulsions correspond to oil droplets dispersed in

continuous aqueous media. Type II microemulsions correspond to water droplets dispersed in continuous oil media. Type III microemulsions correspond to bicontinuous network of oil and water channels (2).

Several authors have attempted to formulate equations that predict the thermodynamic equilibrium of microemulsions. Nagarajan and Ruckenstein have produced a molecular thermodynamic model based on the energy of transfer of each of the components from the bulk phases to the interfacial phase (5). Huh also generated a model for optimum microemulsion systems (Type III microemulsions with equal amount of oil and water) based on the conformational energy (Van der Walls and electrostatic forces) of alternative layers of oil and water (6). Safran and DeGennes among others have promoted microscopic models of microemulsions where the phase behavior is obtained by scaling methods and by applying membrane mechanic concepts to simulate the interface behavior (7,8).

Most thermodynamic models mentioned above are either too complicated or use parameters not readily available to formulators. Our objective is design a set of equations easy to solve and accurate enough to reproduce the phase behavior of actual microemulsion systems.

Our hypothesis to formulate this set of equations is that the curvature of the interface dictates the phase transition between the different types of microemulsions. Type I microemulsions have a concave curvature from the oil perspective (we assume a positive value). Type II microemulsions have a convex curvature from the oil perspective (negative curvature). Type III microemulsions have a near zero (flat) curvature.

Model development

Some authors have attempted to use critical scaling theory to reproduce the changes in oil radius (type I microemulsions) (2):

$$\xi = \frac{\xi_o}{|(\Delta\mu^*_s)|^n} \qquad \text{Eq. 1}$$

where ξ is a length parameter related to the radius of the oil solubilized in type I microemulsions, ξ_0 is a length constant, n is the scaling exponent. $\Delta\mu^*_S$ is the difference on chemical potential between the actual thermodynamic state and the "critical" point.

The key to use the critical scaling theory is to select the appropriate thermodynamic variables involved in the process (ξ, $\Delta\mu^*_S$ and n). According to our hypothesis the important variable that defines the thermodynamic transition is the curvature of the interface. The problem is that we can define two curvatures, either based on the oil or on the water present in the microemulsion, as follow:

Oil curvature $$H_O = \frac{1}{R_O} = \frac{As}{3*V_o} \qquad \text{Eq. 2}$$

Water curvature $$H_W = \frac{1}{R_W} = \frac{As}{3*V_W} \qquad \text{Eq. 3}$$

where "As" refers to the interfacial area provided by the adsorption of the surfactant and cosurfactant at the oil/water interface. V_O and V_W are the volume of oil and water present in the microemulsion system respectively. R_O and R_W are the equivalent radius of oil and water droplets. The interfacial area can be obtained using the expression:

$$As = \sum_i Cs_i * V * N_a * as_i * \phi_i \qquad \text{Eq.4}$$

where Cs_i is the initial concentration of the surfactant or cosurfactant "i" , V is the volume of the initial surfactant solution, N_a is the Avogrado's number, as_i is the area per molecule of the surfactant/cosurfactant "i" and ϕ_i is the fraction of the initial surfactant that is present in the microemulsion phase.

It seems natural for a type I microemulsion to think in terms of oil curvature and similarly for type II microemulsions to think in terms of water curvature. For systems close to type III microemulsions or type III microemulsions it makes sense to ask which curvature to use in the scaling model. Previous models have chosen either one of the curvatures, either choice resulted inappropriate to reproduce the behavior near type III microemulsions.

We propose a statistical description of the curvature through two additional curvatures:

Net curvature $$H_N = |H_O| - |H_W| \qquad \text{Eq. 5}$$

Average curvature $$H_{AVE} = \frac{|H_O| + |H_W|}{2} \qquad \text{Eq. 6}$$

The net curvature describes the curvature of the surfactant membrane. In other words, at optimum formulation ($V_O = V_W$) the curvature of the surfactant membrane is, in average, flat because it result from the coexistence of local concave and convex zones. If the curvature of the membrane only considers one of the initial curvatures, the radius of oil or water droplets would be infinite to achieve flat curvature, which is not true. In fact, the size of the aggregates of water and oil of type III microemulsions is finite. The

average curvature it actually gives the mean size of the aggregates for bicontinuous systems.

If we replace equation 2 and 3 in equation 6 we obtain:

$$\xi_c = \frac{1}{H_{AVE}} = \frac{6 * \varphi_o \varphi_w V_M}{As} \qquad \text{Eq. 7}$$

where ξ_c is the characteristic length of the microemulsion system as defined by DeGennes (8). This characteristic length can be compared to the "correlation length" that DeGennes defined for polymer systems. The correlation length is a thermodynamic property of the system that indicates the maximum distance that two polymer chains can be separated and still maintain significant interaction. Similarly, for microemulsion, as the curvature of the surfactant membrane goes to zero (due to added electrolyte or change in temperature or other thermodynamic variable), it seems easy for the droplet of oil or water to grow indefinitely. The true is that there is a certain cutoff length beyond which the thermal mixing (entropy) prevents a molecule from being "correlated" to the surfactant at the interface. This discussion lead to one of the model's constrain:

$$\xi_c = \frac{1}{H_{AVE}} \leq \xi^* \qquad \text{Eq. 8}$$

where ξ^* is the characteristic length at optimum formulation (the maximum characteristic length of the system) that we propose to be equivalent to the correlation length of the system.

According to the hypothesis we will use the inverse net curvature instead of oil or water radius in equation 1 ($\xi=1/H_N$). To solve equation 1, we need an expression for

($\Delta\mu^*_S$). Nagarajan and Ruckenstein, Chun Huh, Miller and others have developed these kind of expressions but most of them are difficult to solve and they have been developed under very particular restrictions so that the parameters are not general or easy to obtain (5-7,9).

Salager et al. have developed an empirical expression for $\Delta\mu^*_S$ called the surfactant affinity difference (SAD) equation that related the free energy change for transfer the surfactant molecule from the oil to the water phase (10):

For ionic surfactants:

$$\frac{SAD}{RT} = \frac{\mu_W^S - \mu_O^S}{RT} = \ln(S) - K(ACN) - f(A) + \sigma - a_T \Delta T \qquad \text{Eq.9}$$

For nonionic surfactants:

$$\frac{SAD}{RT} = \frac{\mu_W^S - \mu_O^S}{RT} = \alpha - EON + bS - K(ACN) - \phi(A) + c_T \Delta T \qquad \text{Eq.10}$$

where R is the gas constant, S is the electrolyte concentration, ACN is the alkane carbon number of the oil, K is a constant that depend on the surfactant, but generally has a value between 0.1 and 0.2 , f(A) and ϕ(A) are functions of the alcohol type and concentration, α and σ are parameters particular of the surfactant. "a_T, c_T" are the temperature coefficients. The SAD equation takes a value of zero at optimum formulation (V_O=V_W).

If we introduce these changes into equation 1:

$$\frac{1}{H_N} = \frac{L}{\left(-\frac{SAD}{RT}\right)^n} \qquad \text{Eq. 11}$$

where L is a length parameter. The value of the exponent "n" have been reported between 0.75 to 1.2 (2,11,12). We choose an exponent n=1, based on the Kelvin equation, where the droplet curvature is proportional to the excess chemical potential. The negative sign is adjusted to follow the curvature signs assigned to the curvatures.

We also propose a model to estimate the interfacial tension of the oil and water droplets. Lets consider a microemulsion droplet of oil in water of radius R_o ($1/H_O$) that with the presence of the surfactant shows an interfacial tension $\gamma_{o,s}$. In order to be in equilibrium, the overall excess energy of the droplet has to be zero. Therefore the surfactant self-assembly has to provide the energy to neutralize this excess energy. Here we call this energy the interfacial rigidity or E_r:

$$4\pi R^2 \gamma_s = E_r \qquad \text{Eq. 12}$$

By comparing this equations with previous equation presented in the literature (5), Er = 1 K_BT (K_B is the Boltzman constant) for most systems that have liquid-like membranes. The values of Er can also be different from 1 K_BT depending on the packing of the surfactant membrane. R and γ_s can be either oil or water. Next we will show several example applications of the model.

Model Example Applications

System 1: 4% (0.103 M) sodium dihexyl sulfosuccinate + limonene + varying NaCl @ 27°C, W/O = 1/1.

a_i = 100 $Å^2$/molecule (13), ϕ_i=0.99 (measured)

L = 10 Å (fitted)

S* (electrolyte at optimum formulation, SAD = 0): 6.4 % NaCl (from phase behavior)

ξ^* = 44 Å (calculated with eq. 7 and data from phase behavior)

E_r = 1 K_BT (fitted)

For SAD = 0

$$-\ln(S^*) = -K(ACN) - f(A) + \sigma - a_T \Delta T \qquad \text{Eq. 13}$$

Introducing this expression into eq. 9 and rearranging:

$$-\frac{SAD}{RT} = \ln\left(\frac{S^*}{S}\right) \qquad \text{Eq. 14}$$

The net curvature equation is:

$$H_N = |H_O| - |H_W| = \frac{1}{R_O} - \frac{1}{R_w} = \frac{\ln\left(\frac{S^*}{S}\right)}{L} = \frac{\left(-\frac{SAD}{RT}\right)}{L} \qquad \text{Eq. 15}$$

The average curvature equation is:

$$\frac{1}{H_{AVE}} = 2\frac{R_O R_W}{R_O + R_W} \leq \xi^* \qquad \text{Eq. 16}$$

For type I microemulsions, we know the volume of water (initial) and the amount of surfactant, therefore we can calculate R_W using equation 3. Using equation 15 we can calculate the radius of oil (R_O) for a given electrolyte concentration (S). We can then check for the characteristic length restriction (equation 16) and if the value is higher than the correlation length, then equations 15 and 16 have to be solved simultaneously for R_O and R_W, this would correspond to a type III microemulsion. For type II microemulsion R_O

is known and we solve for R_W. The interfacial tension can be calculated using equation 12 with the values of R_O and R_W.

The phase volumes can be predicted using the model by converting the radius of the droplets to volumes using equations 2 and 3. The volumes can also be converted into solubilization values using the density of oil or water accordingly.

Figure 1a shows the phase volume diagram for limonene including data and model prediction. Figure 1 b shows the interfacial tension curves of the system as a function of the electrolyte concentration.

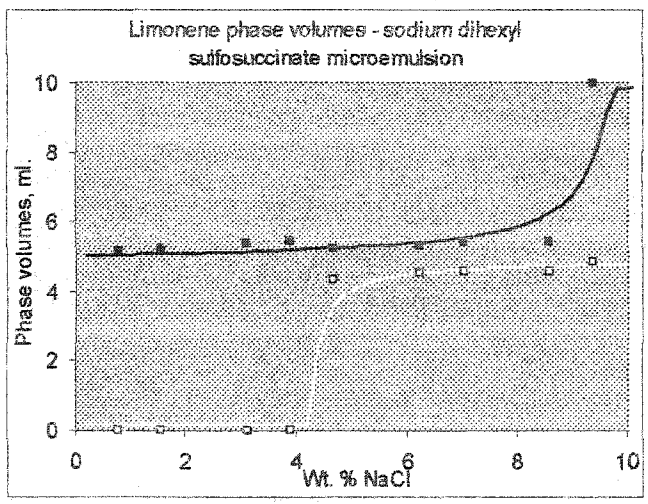

Figure 1a. Phase volumes for limonene-AMA

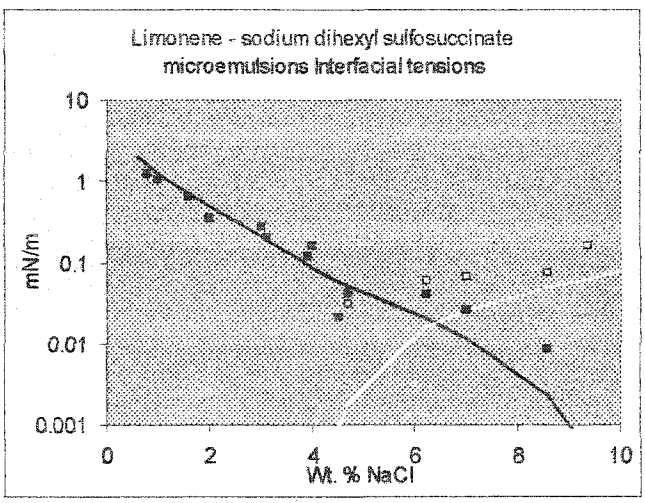

Figure 1b. Interfacial tension for limonene-AMA

The model reproduces the phase volumes and interfacial tension data for this limonene system.

System 2: 8% (0.206 M) sodium dihexyl sulfosuccinate + 4% isopropanol + TCE + varying NaCl @ 12°C and 32°C, W/O = 1/1. (14)

a_{AMA}= 100 Å^2/molecule (13),

ϕ_i=1 (assumed)

$a_{isopropanol}$=30 Å^2/molecule (13),

ϕ_i=1 (assumed)

L = 10 Å (fitted)

Normalized formulation, S/S*

ξ^* = 51 Å (calculated)

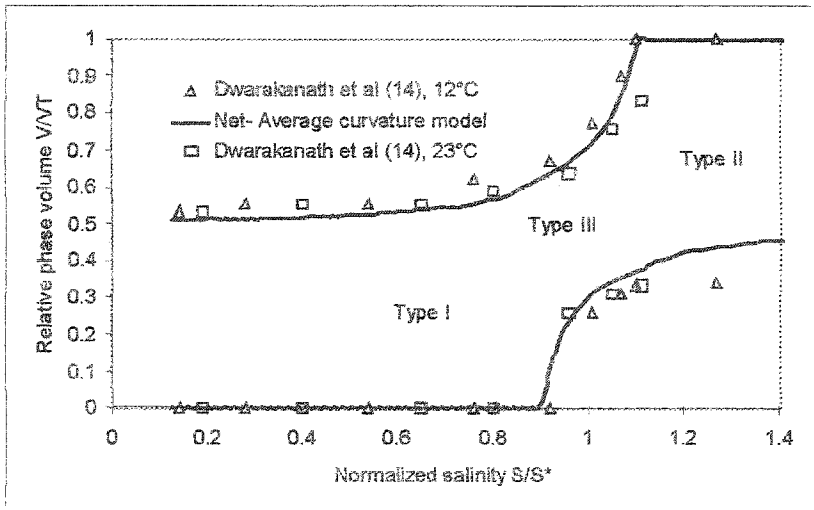

Figure 2. Phase volume for TCE-AMA-isopropanol with normalized salinity system

Figure 2 shows that the model reproduces well the phase volume for this chlorinated polar hydrocarbon (EACN ~ -3.8) at this two temperatures. Note that for this system we keep the same length parameter as used for limonene.

System 3: 1.6% wt. sodium dodecyl sulfate + 2.4% wt. pentanol – hexane (15)

a_{SDS}= 60 Å^2/molecule (13)

ϕ_i=1 (assumed)

$a_{pentanol}$=30 Å^2/molecule (13)

ϕ_i=1 (assumed)

L = 20 Å (fitted)

S*=5.65 % NaCl

ξ^* = 415 Å (calculated)

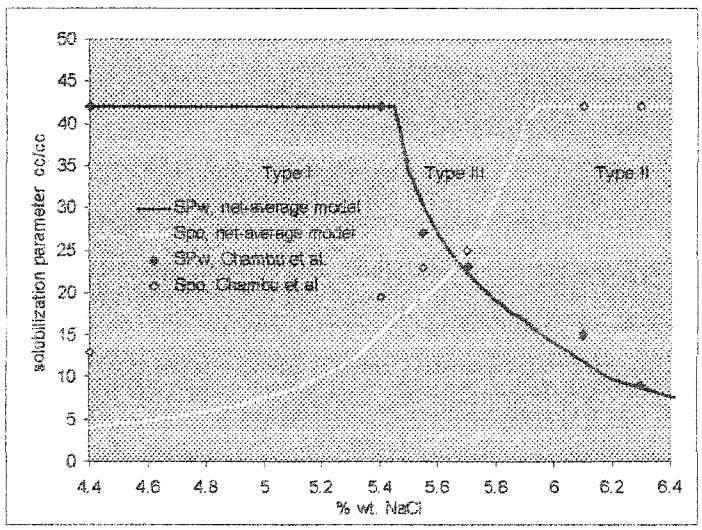

Figure 3. Solubilization curves for a hexane-SDS-pentanol-brine system.

For the SDS system, the surfactant has the same number of carbon in the hydrophobe as AMA (12 carbons). In AMA the tail length is approximately 9Å and for SDS 18Å. The length parameter "L" seems to scale with the extended length of the surfactant tail. This result is supported by Miller et al.. Next we will show how to solve the system for a nonionic system.

System 4: 0.7% wt. C10E4 – octane (16)

a_{C10E4}= 50 Å^2/molecule (13)

L = 20 Å (fitted); PIT= 25°C (16); $\xi^* = 232$ Å (16); $E_r = 3\ K_BT$ (fitted); $c_T = 0.054$ (2)

Note: PIT or phase inversion temperature is considered at the middle of the type III region.

$$H_N = \frac{1}{R_O} - \frac{1}{R_w} = \frac{c_T(PIT - T)}{L} = \frac{\left(-\frac{SAD}{RT}\right)}{L}$$

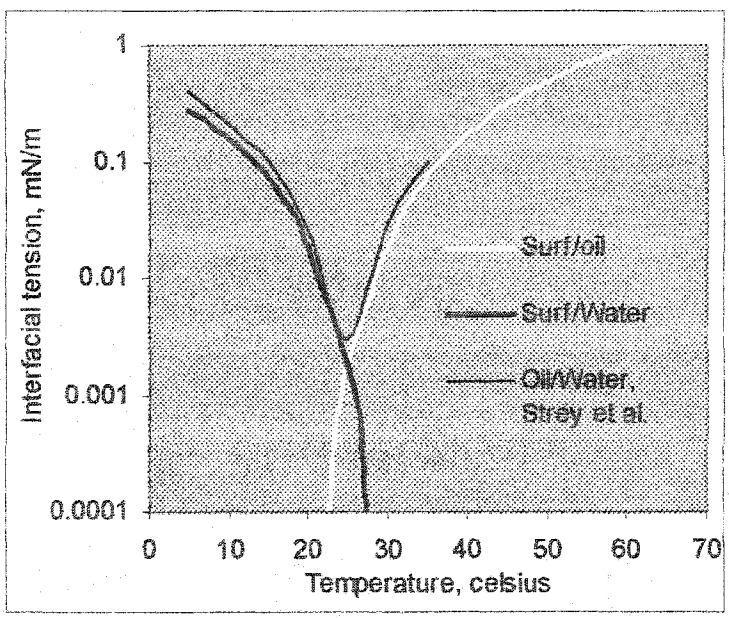

Figure 4. Interfacial tension curves for C10E4-octane system.

Figure 4 shows that the net-average curvature method can also be used to reproduce the behavior of nonionic surfactants. The length parameter L resulted higher than expected (17Å) probably due to partial adsorption of the first ethoxy group on the oil side of the interface.

Summary

The neat-average curvature model presented in this work was able to reproduce the solubilization and interfacial tension of real microemulsion systems (ionic and nonionics). The only fitted parameter used by the model is a length scale (L) that is proportional to the extended length of the surfactant tail.

The other important parameters, the correlation length (ξ^*) and the formulation variables are obtained by experimental methods. Many of these parameters are already available in the literature or can be deduced from published phase behavior systems.

The interfacial rigidity, also adjusted in these studies, is a parameter very difficult to measure and that often shows a large standard deviation. The fitting method used here may be the most simple and significant for these kind of systems.

There are certain simplifications used in this method such as neglecting the volume of the surfactant itself, the presence of a palisade layer for polar oils which exists in addition to the core solubilization calculated by the radius of oil and water (it is included in more advances versions of the model). And maybe one of the most important simplifications is neglecting the changes in curvature due to liquid crystalline or sponge phases, where the net curvature can be flat but there is little or no solubilization of oil.

The simplicity of the model makes it suitable for use in hydrodynamic models for surfactant flooding, performance analysis of potential formulations, molecular design of surfactants for particular application (optimum L, S*, PIT, etc), prediction of the average size of nanoscale aggregates (R_O,R_W), etc

Literature

1. Promod Kumar and K.L. Mittal, Editors. *Handbook of Microemulsion Science and Technology*. Marcel Dekker, Inc., New York, 1999.
2. Bourrel, M. and Schecter R. *Microemulsions and related systems*. Marcell Dekker Inc. New York, 1988.
3. Binks, Bernard P. *Modern Aspects of Emulsion Science*. Royal Society of Chemistry (publisher), Cambridge, UK 1998, 1-55
4. Harwell, J.H. and Sabatini, D.A. Editors. *Surfactant-Enhanced Subsurface Remediation*. ACS Symposium Series 594, Washington, DC, 1995.
5. Nagarajan, R.; Ruckenstein, E. *Langmuir* **2000**, 16(16), 6400.
6. Huh, Chun. *J. Colloid Interface Sci.* **1979**, 71(2), 408-26.
7. Gelbart, W. M., Ben-Shaul, A. and Roux, D. Editors. *Micelles, Membranes, Microemulsions and Monolayers*..; Springer-Verlag, New York, 1994.
8. De Gennes, P.G. and Taupin C. *J. Chem Phys.* **1982**, 86, 2284.
9. Hwan, Rei-Nan; Miller C.A.; Fort, T. *J. Colloid Interface Sci.* **1979**, 68(2), 221-234.
10. Salager, J. L. in *Encyclopedia of Emulsion Technology*. Becher, P. Editor. Marcel Dekker, New York, 1988, Vol 3, Chap. 3.
11. Huang, John S.; Kim, Mahn Won. *Soc. Pet. Eng. J.* **1984**, 24(2), 197-202.
12. Dorshow, R.; Briggs, J.; Bunton, C. A.; Nicoli, D. F. *J. Phys. Chem.* **1982**, 86(13), 2388-95.

13. Rosen, M.J. *Surfactants and interfacial phenomena*. 2nd. Ed. John Wiley & Sons, New York, 1989, pp 431

14. Dwarakanath, V.; Pope, Gary A. *Environ. Sci. Technol.* **2000**, 34, 4842

15. Bourrel, M. and Chambu, C. *J. Soc. Pet. Eng.* **1983**, 23, 327.

16. Sottmann, T. and Strey, R. J. Chem. Phys. **1997**, 106(20), 8606

APPENDIX 2

Turbidity curves used to determine the kinetics of coalescence in linker microemulsions (Chapter 4).

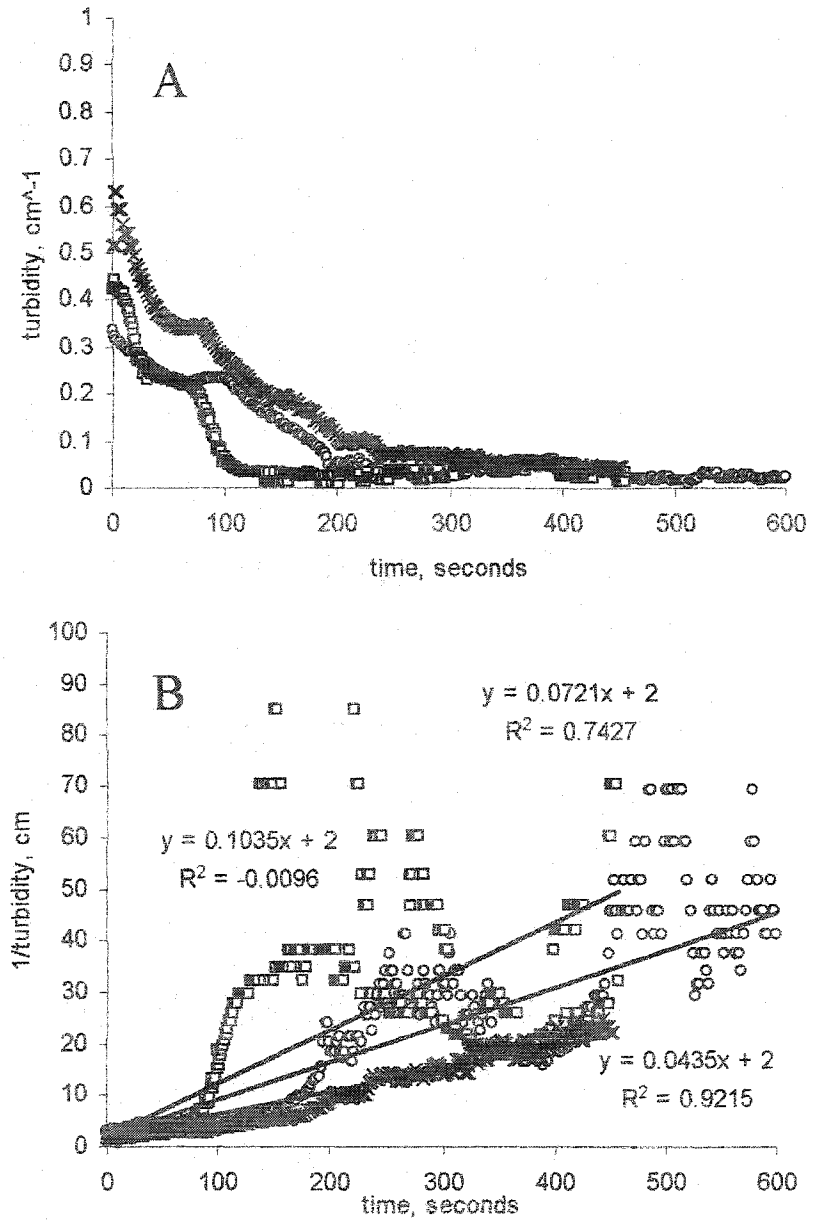

Figure 1. Turbidity curves (triplicates) for the system: 0.103M sodium dihexyl sulfosuccinate (SDHS) - TCE. Coalescence kinetic constant: 0.07 +/- 0.03 cm/s

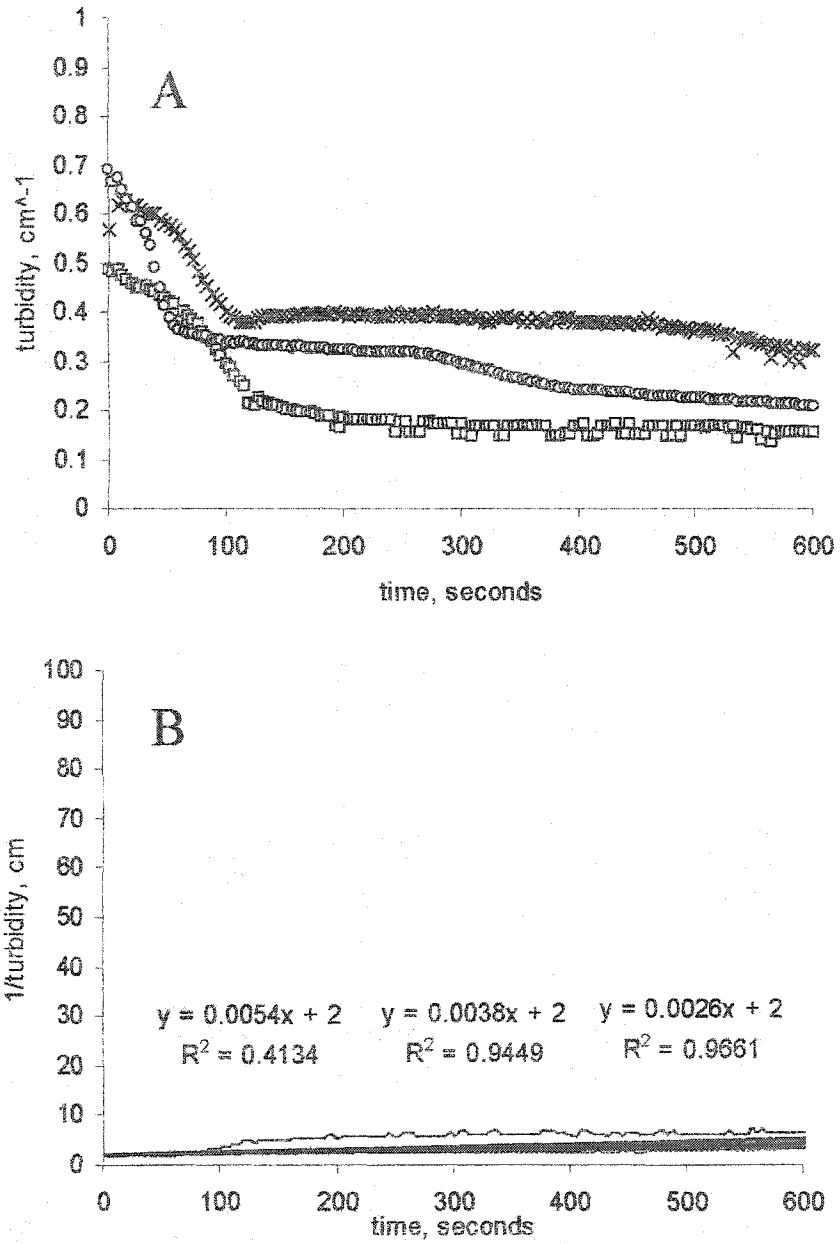

Figure 2. Turbidity curves (triplicates) for the system: 0.103M sodium dihexyl sulfosuccinate (SDHS), 0.09M dodecanol - TCE. Coalescence kinetic constant: 0.0028 +/- 0.0008 cm/s

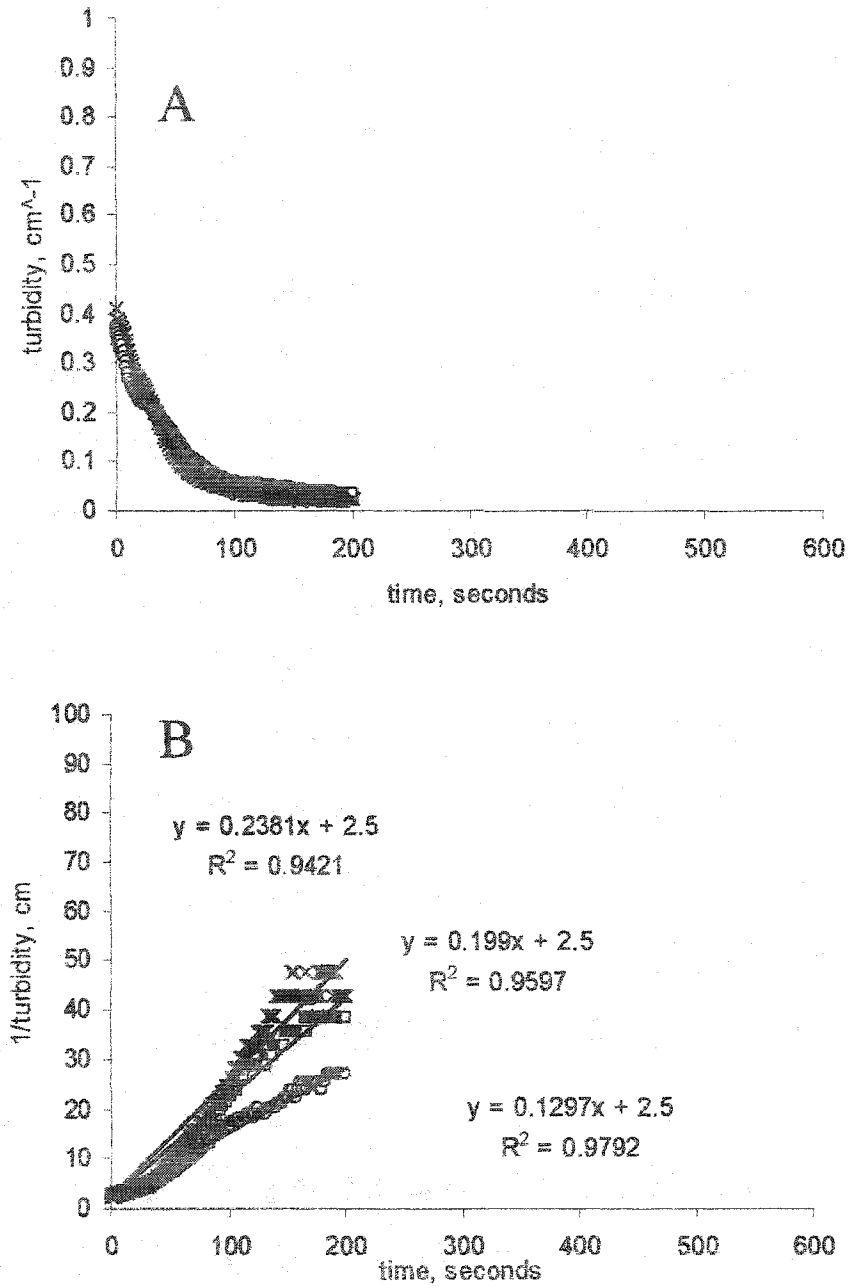

Figure 3. Turbidity curves (triplicates) for the system: 0.103M sodium dihexyl sulfosuccinate (SDHS), 0.09M sodium mono and dimethyl naphthalene sulfonate (SMDNS) - TCE. Coalescence kinetic constant: 0.18 +/- 0.06 cm/s

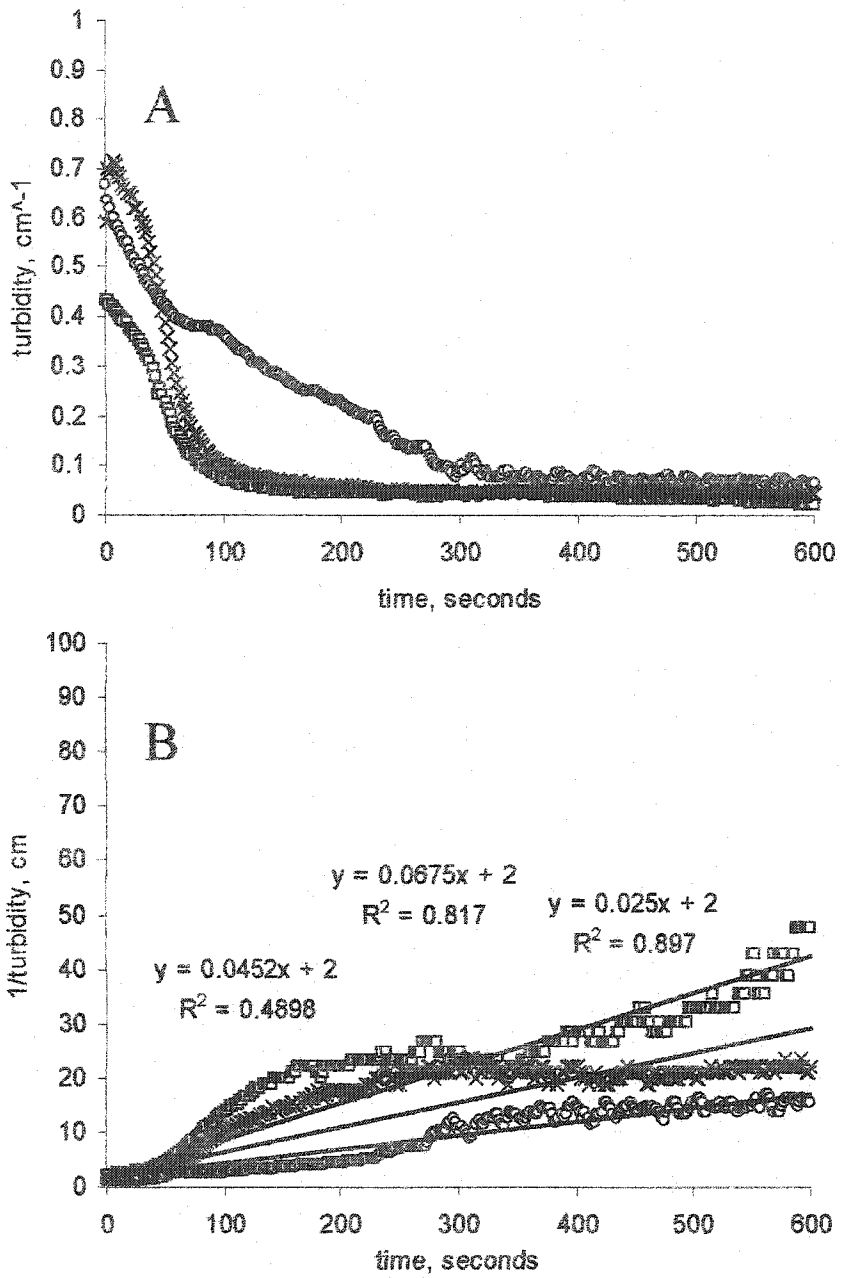

Figure 4. Turbidity curves (triplicates) for the system: 0.103M sodium dihexyl sulfosuccinate (SDHS), 0.09M dodecanol, 0.09M sodium mono and dimethyl naphthalene sulfonate (SMDNS) - TCE. Coalescence kinetic constant: 0.045 +/- 0.02 cm/s

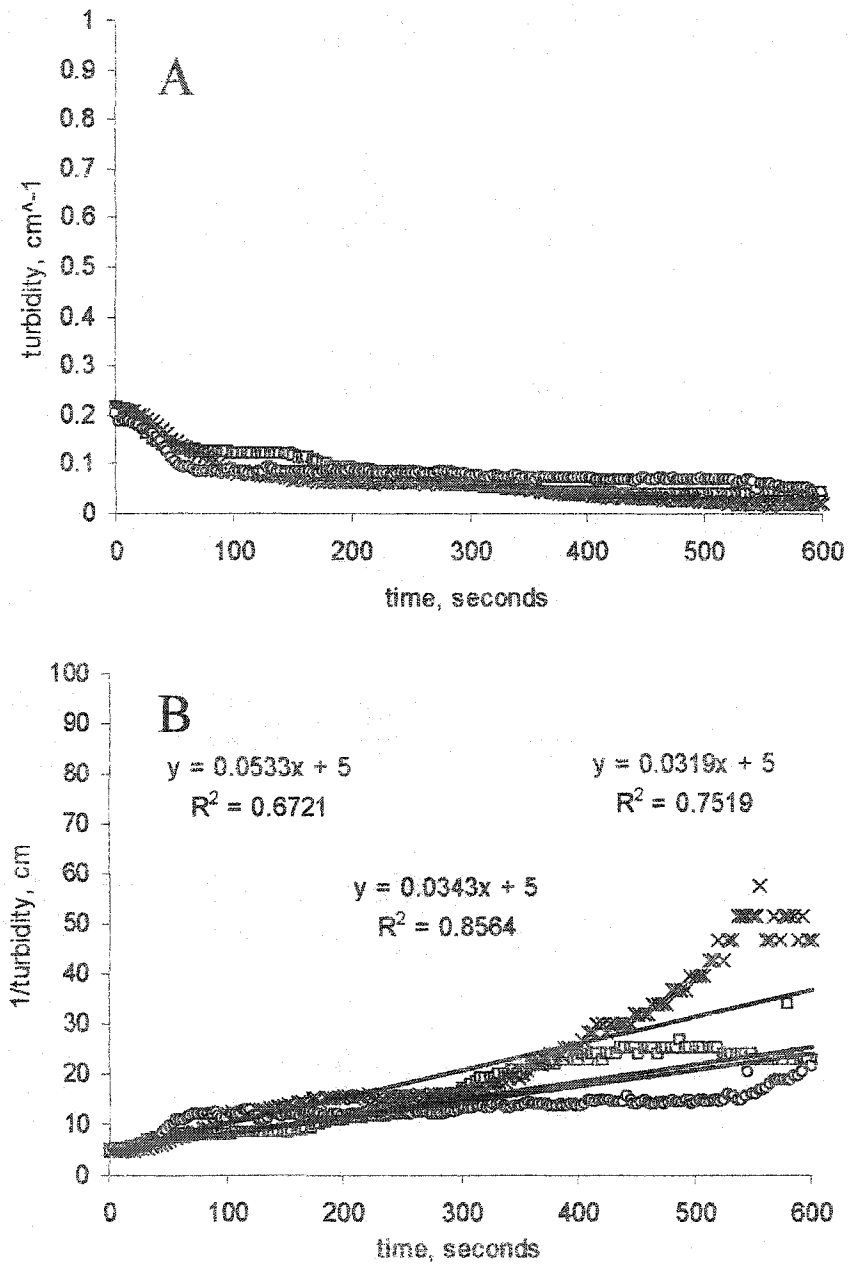

Figure 5. Turbidity curves (triplicates) for the system: 0.103M sodium dihexyl sulfosuccinate (SDHS), 0.045M dodecanol - TCE. Coalescence kinetic constant: 0.042 +/- 0.01 cm/s

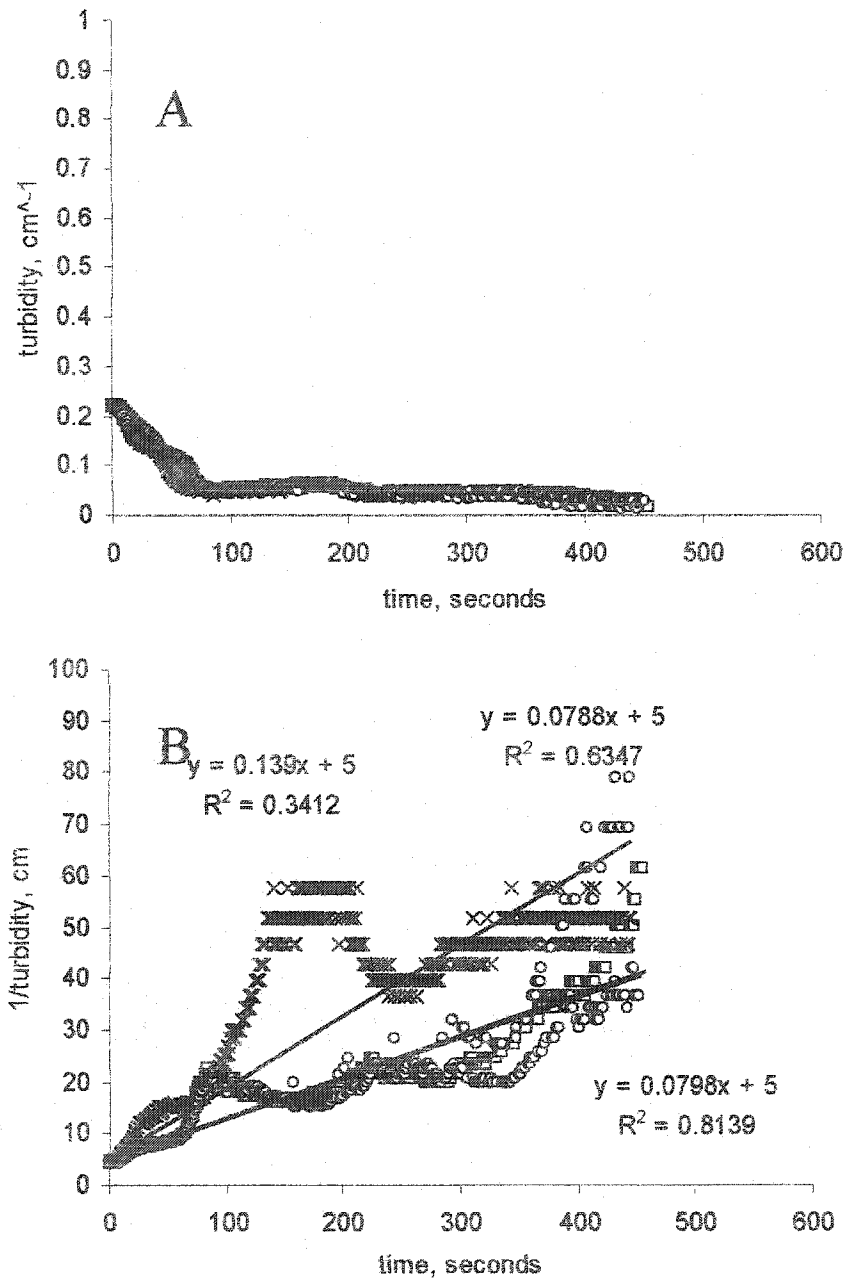

Figure 6. Turbidity curves (triplicates) for the system: 0.103M sodium dihexyl sulfosuccinate (SDHS), 0.045M SMDNS - TCE. Coalescence kinetic constant: 0.10 +/- 0.03 cm/s

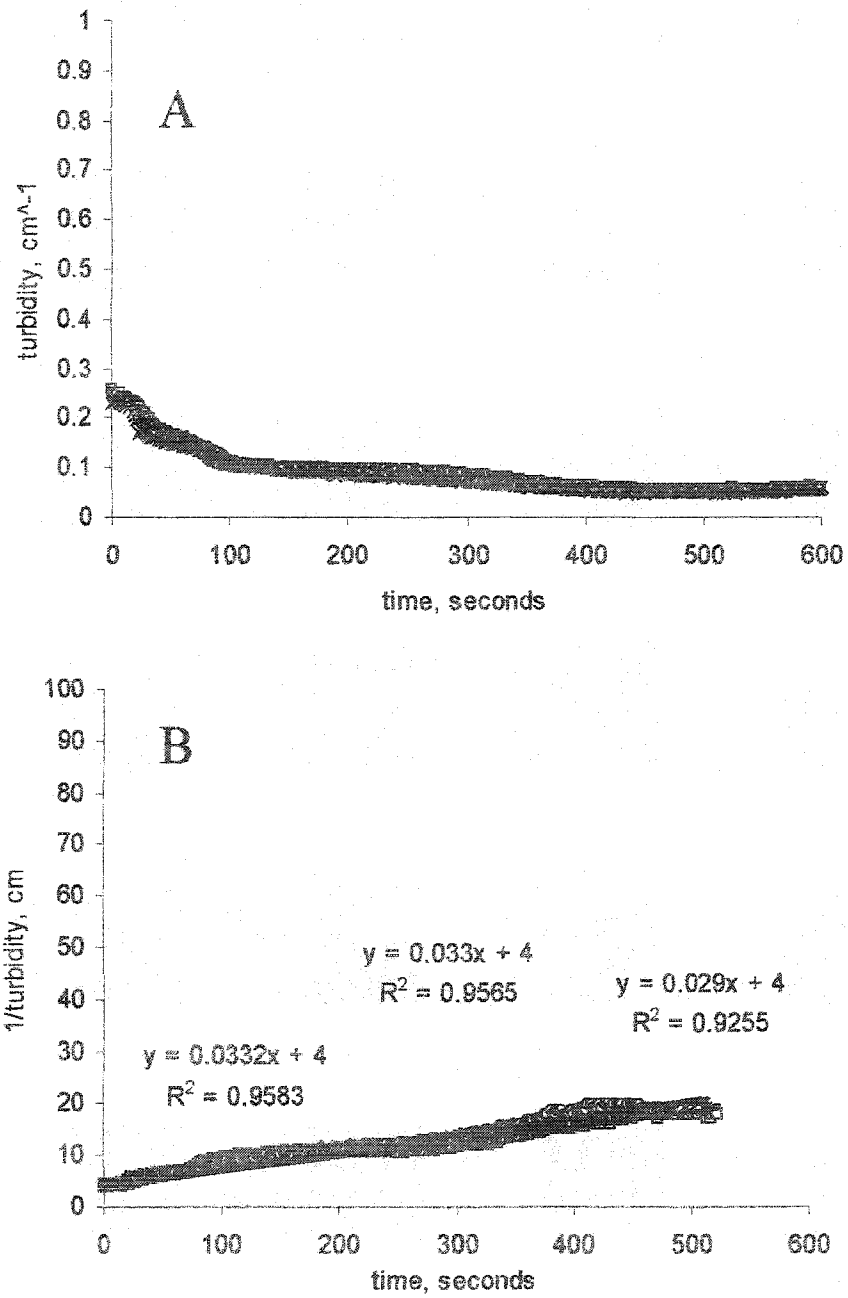

Figure 7. Turbidity curves (triplicates) for the system: 0.103M sodium dihexyl sulfosuccinate (SDHS), 0.045M SMDNS, 0.045M dodecanol - TCE. Coalescence kinetic constant: 0.031 +/- 0.003 *cm/s*

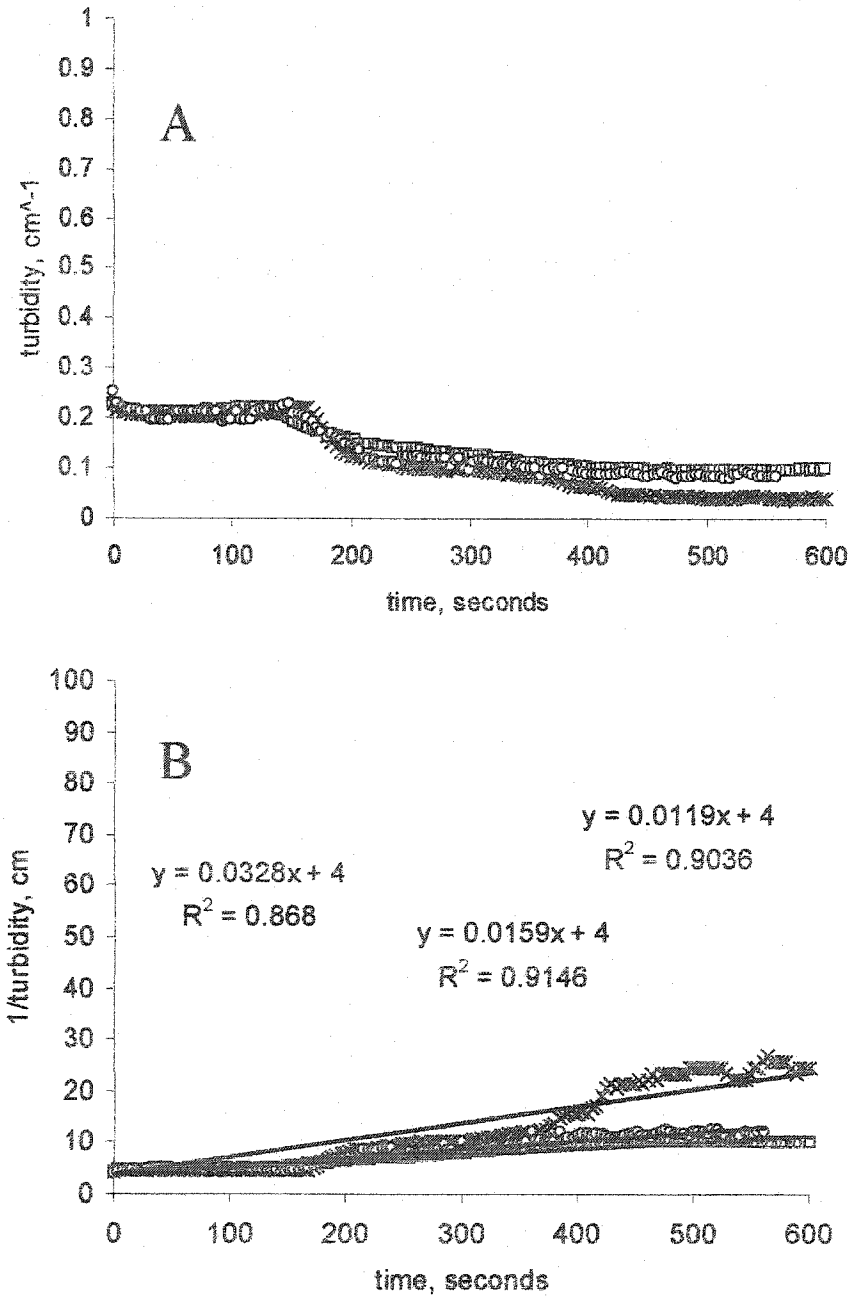

Figure 8. Turbidity curves (triplicates) for the system: 0.103M sodium dihexyl sulfosuccinate (SDHS), 0135M dodecanol - TCE. Coalescence kinetic constant: 0.022 +/- 0.01 cm/s

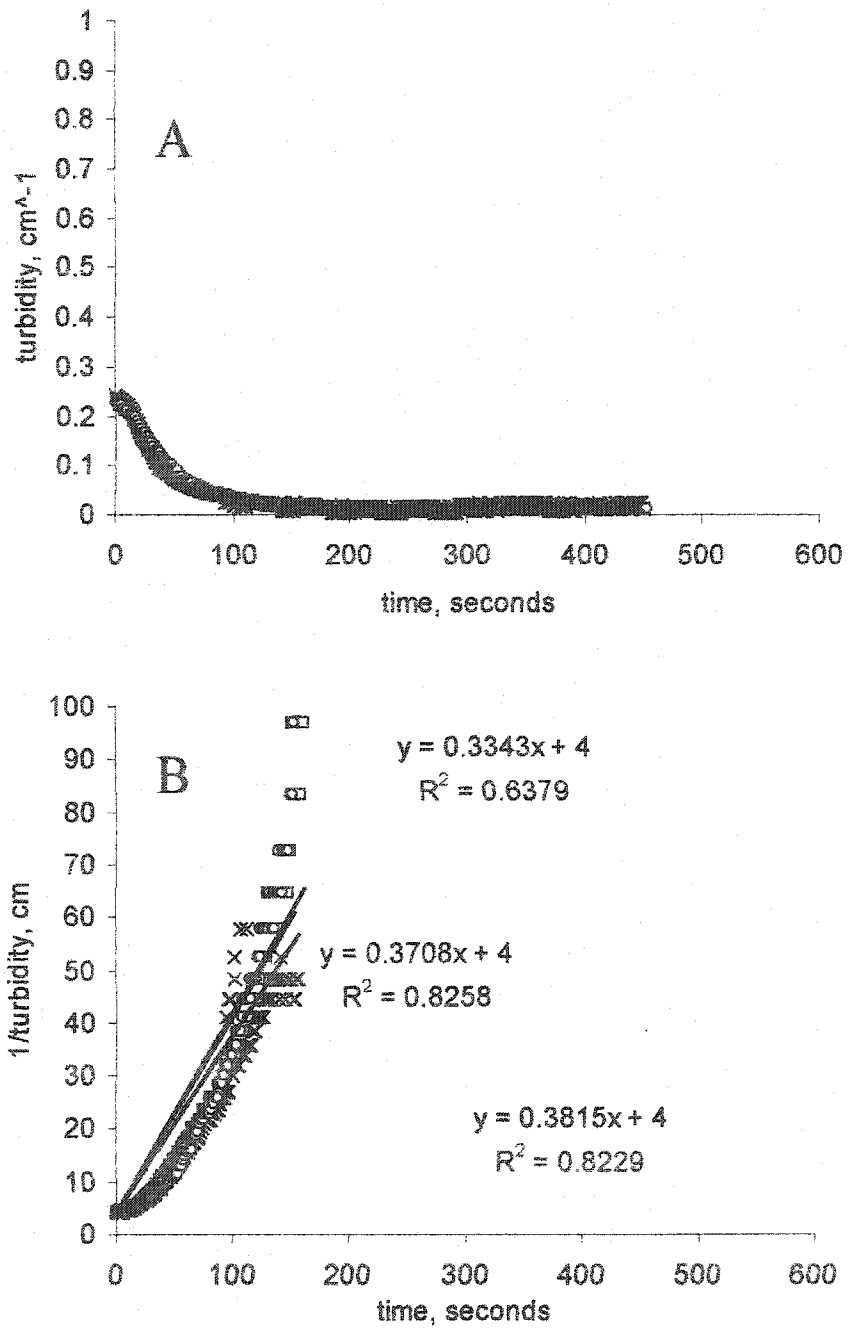

Figure 9. Turbidity curves (triplicates) for the system: 0.103M sodium dihexyl sulfosuccinate (SDHS), 0135M SMDNS - TCE. Coalescence kinetic constant: 0.36 +/- 0.03 cm/s

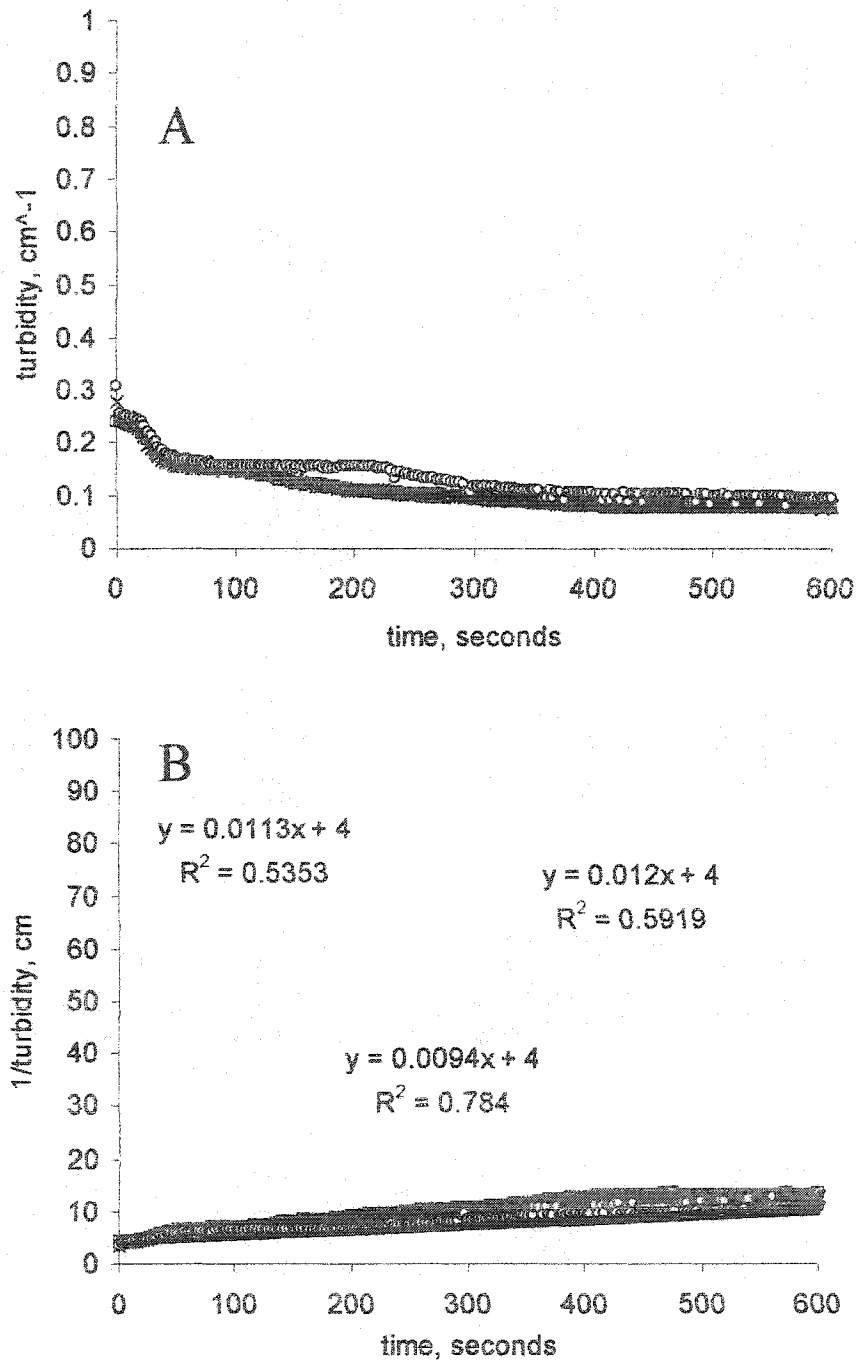

Figure 10. Turbidity curves (triplicates) for the system: 0.103M sodium dihexyl sulfosuccinate (SDHS), 0135M SMDNS, 0.135M dodecanol - TCE. Coalescence kinetic constant: 0.011 +/- 0.001 cm/s

APPENDIX 3

Small Angle Neutron Scattering Studies of Linker-Modified Toluene Microemulsions.

Summary

Here middle phase microemulsions formulated with sodium dihexyl sulfosuccinate (SDHS), containing equal amounts of toluene and water (optimum formulation) and varying concentrations of lipophilic linker dodecanol and hydrophilic linker sodium mono and dimethyl naphthalene sulfonate (SMDNS) where studied using small angle neutron scattering (SANS). The characteristic length of these linker microemulsions was obtained after adjusting SANS scattering curves obtained using a bulk contrast technique. This contrast was obtained by matching the neutron scattering length density of the surfactant membrane with that of the oil phase and using deuterated water to contrast the water domains. The results show that adding lipophilic linkers increase the characteristic length of the microemulsion system, adding hydrophilic linkers reduce the characteristic length and combinations of both linkers produces an intermediate value of this parameter, similar to that of the original surfactant microemulsion. These results confirm earlier values of characteristic length calculated based on solubilization values obtained in linker microemulsions, which supports the schematic of the linker effect proposed in Chapters 4 through 7 of this dissertation. The thickness of the surfactant film was also studied using the film contrast technique where the neutron scattering length density of water and toluene are matched by mixing the

appropriate proportions of hydrogenated and deuterated species of toluene and water. Adding hydrophilic linker SMDNS significantly reduced the thickness of the surfactant membrane, adding lipophilic linker dodecanol showed a slight increment of the thickness although the magnitude of the increment was not statistically significant. The SANS measurements of characteristic length and thickness of the surfactant membrane were consistent with the current model of linker segregation at near the oil/water interface and also validate the use of solubilization values to estimate the characteristic length of these systems.

Introduction

The general objective of this study is to characterize linker-based microemulsions, with special attention to the characteristic length and thickness of the surfactant membrane upon addition of linker molecules. Thus far the value of characteristic length in linker-based microemulsion has been obtained using the characteristic length expression based on solubilization initially proposed by DeGennes et al (1,2):

$$\xi = \frac{6 * \phi_o * \phi_w * V_m}{As} \qquad \text{Eq.1}$$

where ϕ_o , ϕ_w are the volume fractions of oil and water in the middle phase microemulsion, respectively, V_m is the total volume of the middle phase microemulsion (in $Å^3$), and As is the interfacial area making up the surfactant membrane by the surfactant, cosurfactant and hydrophilic linkers (in $Å^2$). The interfacial area can be calculated as:

$$As = \sum_i Cs_i * V_w * \varphi_i * 6.023 * 10^{23} * a_i \qquad \text{Eq.2}$$

where Cs_i is the initial concentration of the surfactant "i" in the aqueous solution, V_w is the initial volume of the aqueous solution in the system, φ_i is the fraction of surfactant, cosurfactant or hydrophilic linker in the middle phase microemulsion (with respect to the total surfactant concentration) and a_i is the area per molecule of the surfactant "i".

When Equation 1 was applied to linker-based microemulsion systems it was found that adding lipophilic linkers increased the characteristic length, while adding hydrophilic linker reduce this value and a combination of hydrophilic and lipophilic linkers produced an intermediate effect (3,4). These calculations where made based on assumptions that the hydrophilic linker coadsorbed with the surfactant at the oil/water interface thus increasing the interfacial area As, but since adding hydrophilic linker does not contribute to increase oil solubilization (5) it was anticipated the characteristic length to decrease in these systems. Another important assumption regarding the segregation of the lipophilic linker is that it segregates near the surfactant tails but that it does not coadsorb at the oil/water interface and thus it does not contribute to the interfacial area As. Since the addition of lipophilic linker increases the solubilization of oil (5) but not the interfacial area, it was expected that adding lipophilic linkers would increase the characteristic length of microemulsions.

There were good reasons for the assumptions made above, such as the effect of lipophilic and hydrophilic linkers on the formulation variables, and the partition of these additives into the different phases (6,7,8). Despite these compelling reasons, there were

no confirmation of such phenomena with spectroscopic techniques that would test such conformation of these molecules at the oil/water interface.

Based on the assumptions for linker segregation described above, it is also expected that the addition of linker molecules would impact the thickness of surfactant membrane. Specifically, since hydrophilic linker is assumed to coadsorb with the surfactant at the oil/water interface and having a short length (8), it is expected that the surfactant membrane would shorten upon addition of hydrophilic linkers. In contrast, since lipophilic linkers have been found to segregate near the oil/water interface in a Langmuirian style, it has been calculated that in the case of dodecanol in tetrachloroethylene microemulsions, segregation values as high as 1 molecule/nm^2 have been found, which corresponds to an average increase in surfactant membrane thickness of 1.7 Å (9). Based on this calculation, it is expected a slight increase of the surfactant membrane thickness when using lipophilic linkers.

The hypothesis of this work is that such assumptions regarding the segregation of hydrophilic and lipophilic linker molecules are valid and that the characteristic length and surfactant membrane thickness determined using SANS scattering curves would reflect the predicted trends described above.

In SANS a neutron beam of wavelength λ is passed through the sample and the intensity of neutron scattering I(q) is obtained as a function of the magnitude of the scattering vector (q), where $q=[4\pi\sin(\theta/2)]/\lambda$ and θ is the scattering angle[‡]. The

---

[‡] In this work, scattering was isotropic. The discussion and analysis assumes this convention

relationship between I(q) versus q has two main contributions: scattering due to interference between aggregates, the structure factor (S(q)), and scattering due to the size and shape of the individual aggregates, the form factor (P(q)). The overall scattering pattern can be written as I(q)=P(q)*S(q) (10). The appropriate expressions for a number of structures and form factors can be found elsewhere (11).

Experimental Section

Microemulsion phase behavior studies.

Microemulsion systems were formulated using sodium dihexyl sulfosuccinate (SDHS) (Fluka brand, 80% aqueous solution), toluene in either its hydrogenated form (Adrich brand, 99+%) or in its deuterated form (Aldrich brand, 99+%), nanopure water (18 MΩ/cm, Barnstead Nanopure® Infinity Base system) and/or deuterated water (Aldrich brand, 99+%), hydrophilic linker sodium mono and dimethyl naphthalene sulfonate (SMDNS) (Witco, 95+%) and lipophilic linker dodecanol (Aldrich brand, 98%). The SDHS concentration was kept constant at 4% w/v (0.10M). Sodium chloride (Fisher brand, 99.9+%) was added in increasing amounts to obtain the phase transition between microemulsion phases Type I-III-II for each series containing various combinations of surfactant and linkers. The oil to aqueous volume ratio was kept at 1/1 by adding 5 ml of aqueous solution containing the prescribed surfactant and electrolyte concentration to 5 ml of toluene in a 15-ml flat bottom test tube sealed with a Teflon-lined screwed cap. After mixing, the systems were kept at room temperature (300K) and left to equilibrate for two weeks before analysis. The surfactant (SDHS) and hydrophilic

linker (SMDNS) concentrations in the microemulsion phase was measured using a Dionex 500 ionic chromatographic system, the toluene concentration was obtained using a UV-VIS Hewlett Packard model 8452 diode array spectrophotometer set at a wavelength of 260 nm. The concentration of dodecanol was determined by gas chromatography using a direct injection Varian 3300 system equipped with a hydrophobic capillary column SPB20 (30m * 0.5 mm) and FID detector. The phase volumes of the bicontinuous systems were obtained by measuring the heights of the separated phases. Additional experimental details can be found elsewhere (3,4,8).

Table 1 summarizes the formulation of optimum middle-phase microemulsions.

Table 1. Summary of optimum formulation of SDHS-toluene microemulsions with varying amounts of hydrophilic linker SMDNS and lipophilic linker dodecanol.

NaCl, g/100ml of aqueous solution	Linker [SMDNS] molar	Linker [C12OH] molar	Contrast	Surfactant SDHS % volume fraction in microemulsion phase	Hydrophilic linker SMDNS % volume fraction in microemulsion phase	Lipophilic linker C12OH % volume fraction in microemulsion phase	Volume of microemulsion (ml)
2.8	0	0	DW/O	99	N.A.	N.A.	1.93
4.4	0.045	0	DW/O	98	50	N.A.	2.00
6.7	0.09	0	DW/O	99	48	N.A.	2.29
10.4	0.135	0	DW/O	98	49	N.A.	2.58
2.15	0	0.045	DW/O	99	N.A.	T.B.D.	1.69
1.7	0	0.09	DW/O	98	N.A.	T.B.D.	1.86
1.3	0	0.135	DW/O	100	N.A.	T.B.D.	1.93
3.4	0.045	0.045	DW/O	99	57	T.B.D.	1.71
4.15	0.09	0.09	DW/O	97	54	T.B.D.	2.07
5.1	0.135	0.135	DW/O	99	56	T.B.D.	2.57
8.15	0.135	0.045	DW/O	98	59	T.B.D.	2.00
6.45	0.135	0.09	DW/O	100	58	T.B.D.	2.14
4	0.135	0.18	DW/O	99	55	T.B.D.	2.79
2.3	0	0	DW/DO	100	N.A.	N.A.	2.3
2.8	0	0	DW/DO	99	N.A.	N.A.	1.93
3.3	0	0	DW/DO	100	N.A.	N.A.	2.4
6.7	0.09	0	DW/DO	98	50	N.A.	2.30
1.5	0	0.09	DW/DO	100	N.A.	T.B.D.	1.88
4.1	0.09	0.09	DW/DO	99	55	T.B.D.	2.10

Neutron scattering experiments.

Neutron scattering experiments were performed at the National Institute of Standards and Technology (NIST) Center for Neutron Research (NCNR, Gaithersburg, MD) NG7-30m SANS instrument using a neutron beam with λ = 6Å with the detector positioned at three different distances (1m, 4m and 15m) to give a combined q-range between 0.004 to 0.5 $Å^{-1}$. The two dimensional scattering data obtained at the three different distances were normalized, masked, and integrated to an I vs. q form for each distance, and later combined into a single I vs. q curve for each sample using the SANS data reduction software available through the NCNR website (11). The combined I vs. q data was later modified by subtracting the scattering background inherent to the amount of water and toluene present in each system. The measurements were made at room temperature with 1-mm cell path length titanium cells assembled using Teflon o-rings to prevent leakage of the toluene-containing samples.

Two types of contrast techniques where used in these experiments: water-oil contrast (noted as DW/O in Table 1) and film contrast (noted as DW/DO in Table 1).
To achieve the oil-water contrast, only 100% deuterated water with a neutron scattering length density of SLD= 6.3E-6 $Å^{-2}$ was used; toluene, SDHS, SMDNS and dodecanol were used in its hydrogenated form. The SLD of surfactants, linkers and toluene were close (within 5% deviation) to a value of SLD ~ 0.8 E-6 $Å^{-2}$. The absolute contrast in DW/O experiments was ΔSLD = (6.3 - 0.8) E-6 $Å^{-2}$ = 5.5 E-6 $Å^{-2}$. In the case of film contrast experiments a mixture of 90% deuterated water (SLD= 6.3E-6 $Å^{-2}$) and 10% hydrogenated water (SLD= -0.56E-6 $Å^{-2}$) was used to match the neutron scattering of

100% deuterated toluene (SLD= 5.6E-6 $Å^{-2}$) used in this set of experiments, in which case the scattering length density of SDHS, SMDNS and dodecanol is approximate 0.8 E-6 $Å^{-2}$.

The scattering curves obtained using the water-oil contrast were analyzed using the Treubner-Strey model (12,13):

$$I(q) = \frac{1}{a_2 + c_1 q^2 + c_2 q^4} \qquad \text{Eq. 3}$$

where a_2 , c_1 and c_2 are the fitting constants which are used to calculate the characteristic length (ξ) of the bicontinuous microemulsion:

$$\xi = \left[\frac{1}{2}\left(\frac{a_2}{c_2}\right)^{1/2} + \frac{1}{4}\frac{c_1}{c_2} \right]^{-1/2} \qquad \text{Eq.4}$$

The other parameter obtained from Equation 3 is the periodicity parameter d':

$$d' = 2\pi \left[\frac{1}{2}\left(\frac{a_2}{c_2}\right)^{1/2} - \frac{1}{4}\frac{c_1}{c_2} \right]^{-1/2} \qquad \text{Eq.5}$$

In the case of film contrast studies, the most important information regarding the thickness of the surfactant membrane can be obtained from the scattering profile at high q values (14). Here we use the expression proposed by Strey et al. for monolayer sponge phases and microemulsions studied using film contrast (15):

$$I(q) = 2\pi\phi_s \frac{v_s}{a_s} \frac{\Delta n^2}{q^2} e^{-q^2 t^2} \qquad \text{Eq. 6}$$

where ϕ_s is the volume fraction of the surfactant, v_s is the molecular volume of the surfactant (~650 $Å^3$/molecule for SDHS), a_s is the area per molecule of the surfactant, Δn

is the SLD contrast (~ 4.8 E-6 $Å^{-2}$), $t=d/(2\pi)^{0.5}$ where d is the thickness of the surfactant film.

Results and Discussions

Table 2 summarizes the morphological parameters obtained for the series presented in Table 1 after fitting the scattering curves to the appropriate models described above.

Table 2. Small angle neutron scattering (SANS) morphology for the system SDHS - SMDNS - dodecanol - toluene systems.

NaCl, g/100 ml	[SMDNS]	[C12OH]	Contrast	Model	Morphology parameters
2.8	0	0	DW/O	Teubner - Strey	ξ = 69 Å , d'= 236 Å
4.4	0.045	0	DW/O	Teubner - Strey	ξ = 69 Å , d'= 206 Å
6.7	0.09	0	DW/O	Teubner - Strey	ξ = 64 Å , d'= 198 Å
10.4	0.135	0	DW/O	Teubner - Strey	ξ = 55 Å , d'= 196 Å
2.15	0	0.045	DW/O	Teubner - Strey	ξ = 92 Å , d'= 300 Å
1.7	0	0.09	DW/O	Teubner - Strey	ξ = 92 Å , d'= 269 Å
1.3	0	0.135	DW/O	Teubner - Strey	ξ = 101 Å , d'= 347 Å
3.4	0.045	0.045	DW/O	Teubner - Strey	ξ = 66 Å , d'= 257 Å
4.15	0.09	0.09	DW/O	Teubner - Strey	ξ = 70 Å , d'= 293 Å
5.1	0.135	0.135	DW/O	Teubner - Strey	ξ = 73 Å , d'= 243 Å
8.15	0.135	0.045	DW/O	Teubner - Strey	ξ = 66 Å , d'= 230 Å
6.45	0.135	0.09	DW/O	Teubner - Strey	ξ = 72 Å , d'= 255 Å
4	0.135	0.18	DW/O	Teubner - Strey	ξ = 72 Å , d'= 226 Å
2.3	0	0	DW/DO	Strey - Winkler - Magid	d = 7.0 Å, a_s = 91 $Å^2$/mol
2.8	0	0	DW/DO	Strey - Winkler - Magid	d = 6.6 Å, a_s = 116 $Å^2$/mol
3.3	0	0	DW/DO	Strey - Winkler - Magid	d = 6.5 Å, a_s = 99 $Å^2$/mol
6.7	0.09	0	DW/DO	Strey - Winkler - Magid	d = 5.8 Å, a_s = 88 $Å^2$/mol
1.5	0	0.09	DW/DO	Strey - Winkler - Magid	d = 7.0 Å, a_s = 105 $Å^2$/mol
4.1	0.09	0.09	DW/DO	Strey - Winkler - Magid	d = 6.7 Å, a_s = 110 $Å^2$/mol

ξ correlation length of bicontinuous microemulsions, d': is the periodicity of the bicontinuos domain size, a_s: area per molecule of the surfactant.

Figures 1 through 5 present the scattering curves corresponding to the selected systems presented in Table 2

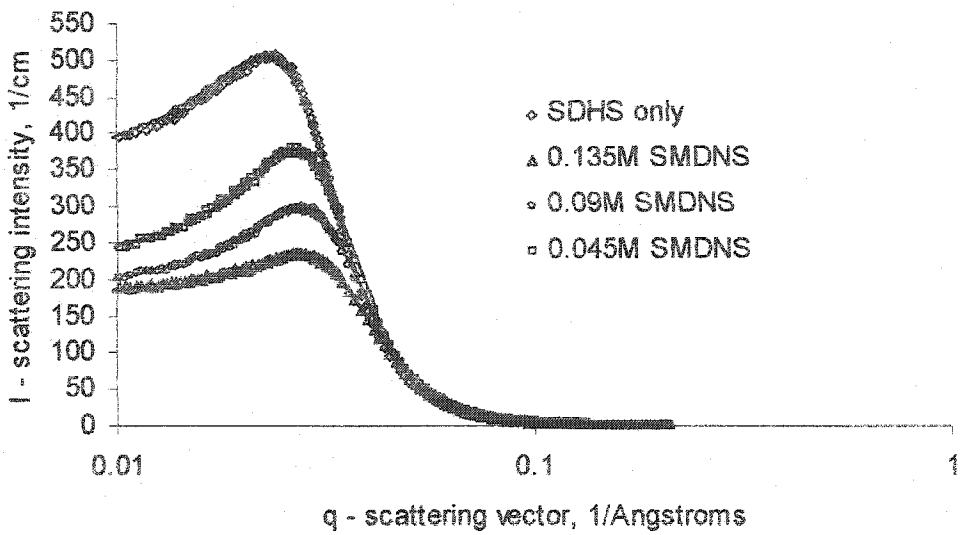

Figure 1. Scattering curves for the system 0.1M SDHS and varying concentration of hydrophilic linker SMDNS using oil-water contrast.

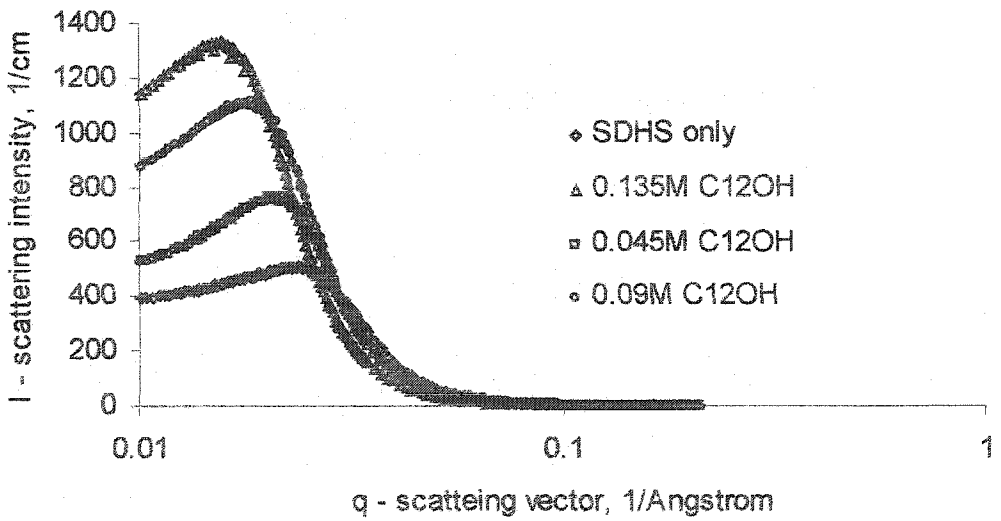

Figure 2. Scattering curves for the system 0.1M SDHS and varying concentration of lipophilic linker dodecanol using oil-water contrast.

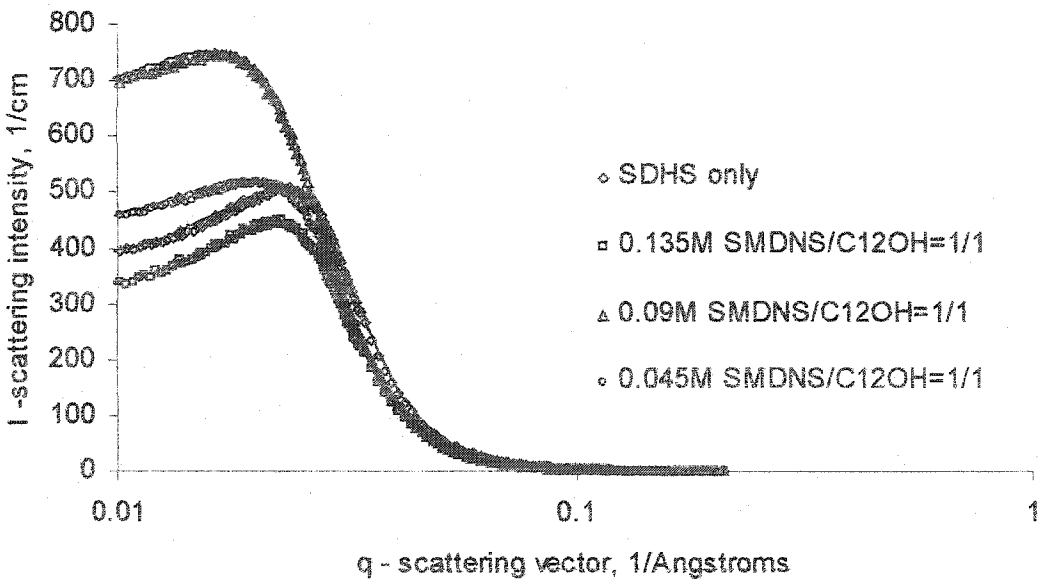

Figure 3. Scattering curves for the system 0.1M SDHS and varying concentration of lipophilic and hydrophilic linkers added in equimolar ratio using oil-water contrast.

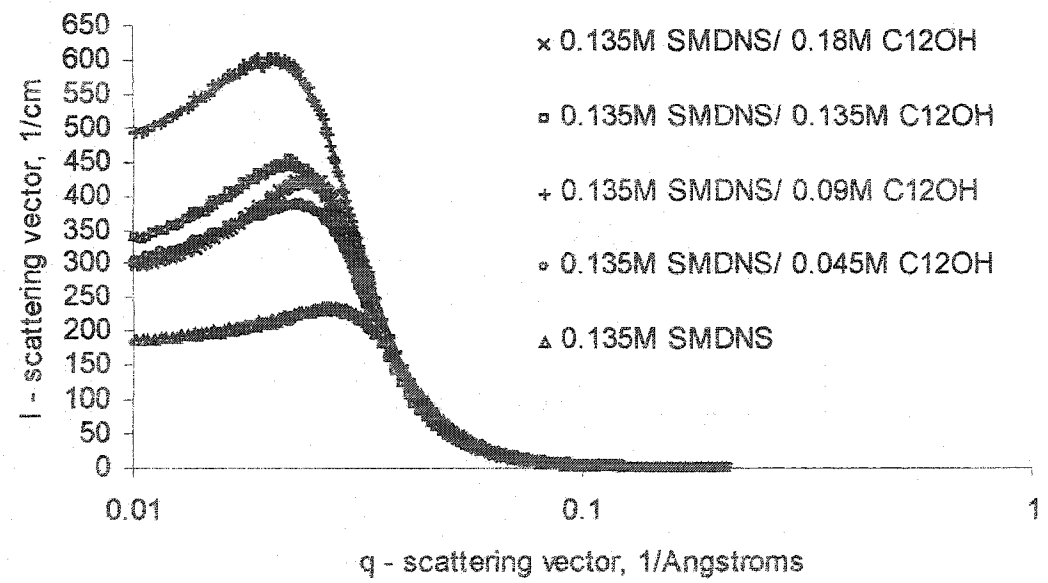

Figure 4. Scattering curves for the system 0.1M SDHS, 0.135M SMDNS and varying concentration of lipophilic linker dodecanol using oil-water contrast.

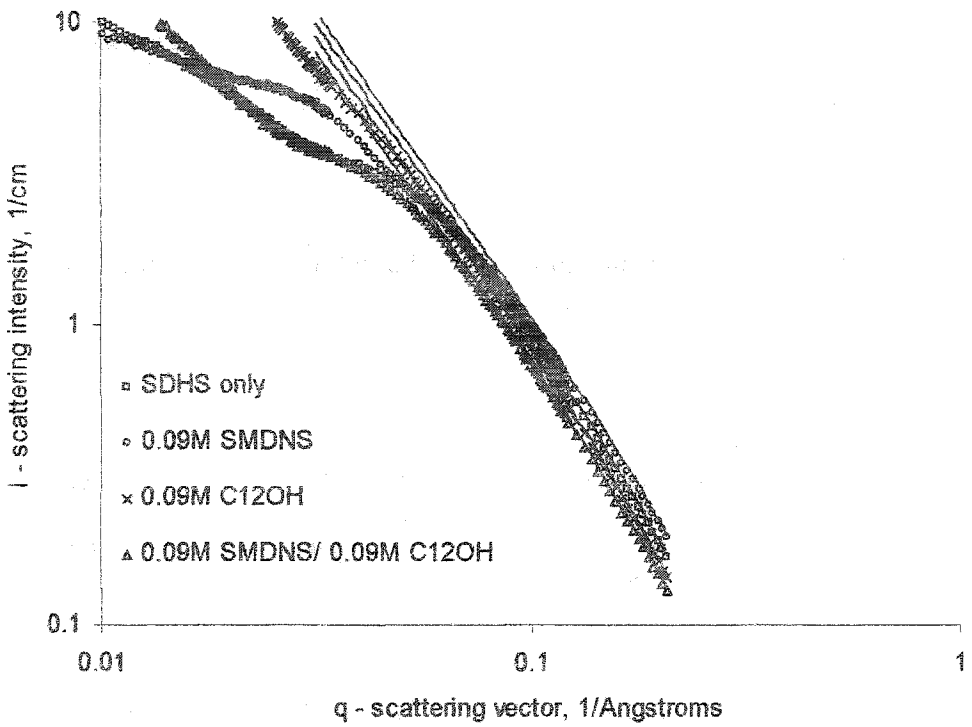

Figure 5. Scattering curves for the system 0.1M SDHS, and varying concentration of lipophilic linker dodecanol and hydrophilic linker SMDNS using film contrast.

Figures 1 through 4 were adjusted using the Treubner-Strey model and plotted as a thin solid line, which becomes indistinguishable among the scattering data points. Figure 5 shows the fit of the sponge phase model at large q.

The characteristic length values in Table 2 confirm the hypothesis initially stated for this project that hydrophilic linkers coadsorb with the main surfactant but lacking of interaction with the oil, produce a reduction of the characteristic length of the microemulsion. Lipophilic linkers segregate near the surfactant tails (without adsorbing at the oil/water interface), serving as an extension of the surfactant into the oil phase, thus increasing the characteristic length of the microemulsions. The combination of linkers

produced an intermediate characteristic length very similar to that of the surfactant-only microemulsion system.

Figure 6 compares the values of characteristic length obtained using Equation 1 and the solubilization data in Table 1 and the characteristic length values obtained after fitting the Treubner-Strey model to the scattering curves in Figures 1 through 4.

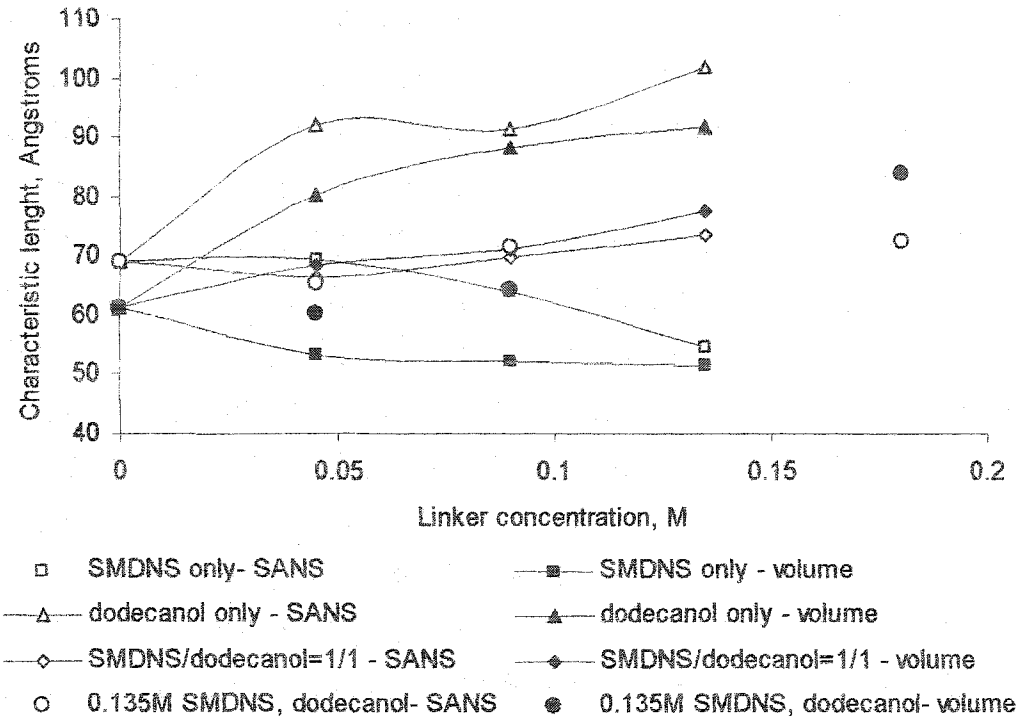

Figure 6. Characteristic length of linker microemulsions obtained using solubilization data (labeled as volume series) and small angle neutron scattering (SANS).

Figure 6 help to corroborate the close correspondence between the characteristic length calculated based on solubilization data and Equation 1, and the characteristic length values obtained from SANS profiles. While the values obtained using solubilization data seem to be consistently lower than SANS values, this could be due to

the area per molecule of SDHS used in Equation 1 (100Å^2/molecule, see reference 3), which according to the area per molecules in Table 2 could be as low as 90 Å^2/molecule.

In terms of the thickness of the surfactant membrane obtained using the film contrast experiments, the values for SDHS-toluene system offer an average thickness of 6.7 Å with a standard deviation of 0.26 Å. The system containing 0.09M of SMDNS shows a significantly shorter membrane thickness (5.8 Å), which is consistent with the initial hypothesis of hydrophilic linker coadsorption. The system containing 0.09M of dodecanol had a membrane thickness of 7.0 Å, which is almost within one standard deviation of the original membrane thickness and thus can't be claimed as significantly larger membrane thickness although the trend can be noted. While the claim of increased membrane thickness can't be made, it is important to highlight that this was a somewhat predicted outcome. The membrane thickness calculated on the basis of dodecanol segregation suggested an increase in thickness that at best would be slightly larger than 1 Å. An increase of 0.3 Å is within the expected value, but with the disadvantage that is also of the same magnitude of one standard deviation of the original membrane thickness.

Additional studies on dynamic light scattering and NMR self difussion studies will be performed to gain a better understanding of the nature of the interaction between linkers and surfactant. These SANS studies have helped clarify some of the aspects relating the segregation or adsorption of linker molecules but still the nature of the interactions taking place remain mostly unknown.

Literature

[1] De Gennes, P. G.; Taupin, C. Microemulsions and the flexibility of oil/water interfaces. *J. Phys. Chem.* **1982**, 86(13), 2294-304.

[2] Acosta, E.; Szekeres, E.; Sabatini, D. A.; Harwell, J. H. Net-Average Curvature Model for Solubilization and Supersolubilization in Surfactant Microemulsions. *Langmuir.* **2003**, 19(1), 186-195.

[3] Acosta, E. J.; Le, M. A.; Harwell, J. H.; Sabatini, David A. Coalescence and Solubilization Kinetics in Linker-Modified Microemulsions and Related Systems. *Langmuir.* **2003**, 19(3), 566-574.

[4] Acosta, E.; Mai, P. D.; Harwell, J. H.; Sabatini, D. A. Linker-modified microemulsions for a variety of oils and surfactants. *J. Surfactants Detergents* **2003**, 6(4), 353-363.

[5] Uchiyama, H.; Acosta, E.; Tran, S.; Sabatini, D. A.; Harwell, J. H. Supersolubilization in Chlorinated Hydrocarbon Microemulsions: Solubilization Enhancement by Lipophilic and Hydrophilic Linkers. *Ind. Eng. Chem. Res.* **2000**, 39(8), 2704-2708

[6] Graciaa, A.; Lachaise, J.; Cucuphat, C.; Bourrel, M.; Salager, J. L. Improving solubilization in microemulsions with additives. 1. The lipophilic linker role. *Langmuir.* **1993**, 9(3), 669-72

[7] Graciaa, A.; Lachaise, J.; Cucuphat, C.; Bourrel, M.; Salager, J. L. Improving solubilization in microemulsions with additives. 2. Long chain alcohols as lipophilic linkers. *Langmuir.* **1993**, 9(12), 3371-4.

[8] Acosta, E.; Uchiyama, H.; Sabatini, D. A.; Harwell, J. H. The role of hydrophilic linkers. *J. Surfactants Detergents.* **2002**, 5(2), 151-157

[9] Acosta, E. J. ; Harwell, J. H.; Sabatini, D.A. Self-Assembly in Linker-Modified Microemulsions. Submitted to: Journal of Colloid and Interface Science. Date: July 22, 2003

[10] Auvray, L. The structure of microemulsions: experiments. In *Micelles, Membrane, Microemulsions and Monolayers*. William Gelbart, Avinoam Ben-Shaul and Didier Roux Editors. Springer-Verlag. New York, 1994., pp. 347-393.

[11] http://www.ncnr.nist.gov/programs/sans/manuals/red_anal.html

[12] Teubner, M and Strey, R. Origin of the scattering peak in microemulsions. *J. Chem. Phys.* **1987**, 87(5), 3195-3199.

[13] Schubert, K.V. ; Strey R.; Kline, S. R. and Kaler E. W. Small angle neutron scattering near Lifshitz lines: Transition from weakly structured mixtures to microemulsions. *J. Chem. Phys.* **1994**, 101(6), 5343-5355.

[14] Acosta, E.J.; Szekeres, E.; Harwell, J.H.; Grady, B. P. and Sabatini, D.A. Net-average curvature model of microemulsions: predictions and measurements using small angle neutron scattering, dynamic light scattering and NMR techniques. Submitted to Langmuir, January 2004.

[15] Strey, R; Winkler, J. and Magid, L. Small Angle Neutron Scattering from Diffuse Interfaces 1. Mono- and Bilayers in the Water-Octane-$C_{12}E_5$ System. *J. Phys. Chem.* **1991**, 95, 7502-7507